



**THE DEVELOPMENT OF DYNAMIC MODELS FOR A DENSE  
MEDIUM SEPARATION CIRCUIT IN COAL BENEFICIATION**

by

**Ewald Jonathan Meyer**

Submitted in partial fulfillment of the requirements for the degree

Master of Engineering (Electronic Engineering)

in the

Faculty of Engineering, the Built Environment and Information Technology

UNIVERSITY OF PRETORIA

July 2010

## SUMMARY

### SUMMARY IN ENGLISH

Dense medium separation (DMS) plants are typically used to beneficiate run-of-mine (ROM) coal in coal metallurgy. These plants normally make use of a dense medium cyclone as the primary processing unit. Because of the deviations in the ROM quality, the production yield and quality become difficult to maintain. A control system could benefit such operations to maintain and increase product throughput and quality.

There are many different methods for developing a control system in a metallurgical operation; however, what is most fundamental is the use of a mathematical model to design a controller. For this reason, a first principle dynamic mathematical model has been developed for a DMS circuit. Each unit operation is modelled individually, then integrated together to form the complete system. The developed DMS circuit dynamic model is then used to simulate the process. It is also found that most models developed for DMS operations typically make use of steady-state analysis and that very little literature is available on dynamic models of this kind.

Difficulties that arise when validating a model in metallurgical processes are insufficient measurement points or the challenges in measuring certain variables, such as physical properties (e.g. particle size) or chemical components (e.g. ash percentage). This paper also explains how the Runge-Kutta approximation can be used in simulating DMS unit processes with intermediate online measurements that may be available. This can ultimately assist in verifying the accuracy of the simulation.

One of the other problems that can occur when developing models from first principles is the estimation of model parameters. Specifically when non-linear state-space relationships are developed, one must ensure that there is a unique solution for the parameters in question. A method employing parameter identifiability is also presented in this dissertation to illustrate its use. In addition the process of estimating parameters is explained and illustrated.

Keywords: dense medium separation; coal beneficiation; dynamic modelling; process control; simulation; parameter identifiability.

## OPSOMMING IN AFRIKAANS

Digte medium-skeiding- (DMS) aanlegte word gebruik om benefisiëring van loop-van-myn- (LVM) steenkool te bewerkstellig. Hierdie aanlegte gebruik normaalweg 'n digte medium sikloon as die primêre proses van verwerking. As gevolg van die kwaliteit-afwykings in die LVM van die produksie-opbrengs, word dit baie keer moeilik om die aanleg te beheer. 'n Beheerstelsel kan sulke bedrywighede hanteer en steenkoolproduksie en-kwaliteit verhoog.

Daar is baie verskillende metodes vir die ontwikkeling van sulke beheerstelsels in metallurgiese operasies, maar almal gebruik wiskundige modelle vir die ontwerp van die beheerstelsel. Om hierdie rede is 'n dinamiese wiskundige model ontwikkel vir 'n DMS-aanleg en die model is gebaseer op fundamentele metallurgiese beginsels. Elke eenheid-operasie word individueel gemodelleer en kan dan geïntegreer word om 'n geheel te vorm. Die ontwikkelde DMS-model kan dan gebruik word om die proses te simuleer. Daar is ook bevind dat die meeste modelle wat tot dusver ontwikkel is vir DMS-bedrywighede gewoonlik gebruik maak van ewewigbepalings en dat baie min literatuur beskikbaar is oor dinamiese modelle.

Die geldigheid van 'n model in 'n metallurgiese proses word bepaal deur onvoldoende inligting oor die meting van sekere veranderlikes in die proses. Voorbeelde daarvan is die steenkool LVM-deeltjiegrootte en die chemiese samestelling van die produkte. Hierdie verhandeling verduidelik hoe die Runge-Kutta wiskundige benadering 'n DMS-proses simuleer met die aanlynmetings wat beskikbaar is. Dit kan ook help met die bevestiging van die akkuraatheid van die simulاسies.

Een van die ander probleme wat kan voorkom in sulke wiskundige modelle is die by-benadering van die modelriglyne. Wanneer nie-liniêre modelle ontwikkel word, moet unieke oplossings vir die riglyne van die model bepaal word. Hierdie verhandeling illustreer ook die gebruik van die begrip van modelriglyn-identifiseerbaarheid.

Sleutelwoorde: digte medium-skeiding, steenkool-benefisiëring; dinamiese modellering; prosesbeheer; simulاسie; riglyn-identifiseerbaarheid.



## ACKNOWLEDGEMENT

I would like to thank my study leader Prof. I.K. Craig and my external examiner Prof. T.J. Napier-Munn for their assistance and valuable input for this work. Thanks go to Exxaro Resources for allowing me to conduct my studies at their Leeuwan Colliery. Special thanks go to Leeuwan operations management and their laboratory for assisting me with the collection and analysis of samples and plant data during the industrial experiment that was conducted at Leeuwan.



## LIST OF ABBREVIATIONS

CFD:	Computational Fluid Dynamics
DMC:	Dense Medium Cyclone
DMS:	Dense Medium Separation
H/C:	Hydrogen/Carbon
LV:	Low Volatile
MV:	Medium Volatile
O/C:	Oxygen/Carbon
ROM:	Run-of-mine
SAG:	Semi-autogenous Grinding
U/O:	Overflow and Underflow

## NOMENCLATURE

+	Metallurgical term used to indicate that a particle size is greater than a specific size
–	Metallurgical term used to indicate that a particle size is less than a specific size
$\alpha$	Overflow and underflow proportionality constant
$\alpha_c$	Percentage of mass split on the bottom deck (subscript $c$ ) for mass component $i$ of a double-deck screen
$\alpha_f$	Percentage of mass split for mass component $i$ for a fines (subscript $f$ ) material screen
$\alpha_o$	Percentage of mass split on the top deck (subscript $o$ ) for mass component $i$ of a double-deck screen
$\chi$	Distance between a detector and source
$\Delta p$	Pressure drop over a valve for water addition (subscript $p$ )
$\Delta P_v$	Pressure drop across a valve (subscript $v$ )
$\delta_{scr}$	Nominal screen (subscript $scr$ ) aperture
$\ell(\cdot)$	A positive scalar-valued function
$\ell_p$	Valve position for water addition (subscript $p$ )
$\epsilon(t, \theta_*)$	Prediction error for parameter estimates $\theta_*$
$\eta$	Medium viscosity
$\hat{\theta}_N$	A parameter estimate
$\hat{y}$	Estimated model output
$\mathcal{M}$	A model structure
$\mathcal{M}^*$	A set of models
$\mu$	Measure of the mass absorption coefficient
$\mu'$	Low energy gamma-ray source
$\mu''$	High energy gamma-ray source
$\mu_y$	Mean of a plant output $y$
$\Phi$	A meromorphic function

- $\rho$  Density
- $\rho(t)$  Instantaneous relative density of material
- $\rho_f$  Relative Density of a fluid (subscript  $f$ )
- $\rho_j$  Relative density fraction  $j$
- $\rho_m$  Medium (subscript  $m$ ) relative density
- $\rho_p$  Relative density of a particle (subscript  $p$ )
- $\rho_t$  Density of the corrected medium from the corrected medium tank (subscript  $t$ )
- $\rho_w$  Density of water (subscript  $w$ )
- $\rho_{50}$  or  $SG_{50}$  Separation cutpoint with a partition factor of 50% (subscript 50)
- $\rho_{c,ash}, \rho_{c,S}, \rho_{c,H_2O}, \rho_{c,vol}, \rho_{c,C}$  Ash (subscript  $ash$ ), sulphur (subscript  $S$ ), water (subscript  $H_2O$ ), volatiles (subscript  $vol$ ) and fixed carbon (subscript  $C$ ) densities for a DMC (subscript  $c$ )
- $\rho_{c,i,med}$  Density of the magnetite medium (subscript  $med$ ) in the feed (subscript  $i$ ) mix to a DMC (subscript  $c$ )
- $\rho_{c,i}$  Density of the feed (subscript  $i$ ) mix to a DMC (subscript  $c$ )
- $\rho_{c,o,med}$  Density of the magnetite medium (subscript  $med$ ) in the overflow (subscript  $o$ ) from a DMC (subscript  $c$ )
- $\rho_{c,o}$  Density of the overflow (subscript  $o$ ) from a DMC (subscript  $c$ )
- $\rho_{c,u,med}$  Density of the magnetite medium (subscript  $med$ ) in the underflow (subscript  $u$ ) from a DMC (subscript  $c$ )
- $\rho_{c,u}$  Density of the underflow (subscript  $u$ ) from a DMC (subscript  $c$ )
- $\rho_{coal}$  Relative density of coal (subscript  $coal$ )
- $\rho_{mb,med}$  Density of corrected magnetite medium (subscript  $med$ ) fed to a mixing box (subscript  $mb$ )
- $\rho_{mb}$  Density of mix within a mixing box (subscript  $mb$ )
- $\rho_{p,i}$  Density of recovered magnetite medium feed (subscript  $i$ ) for water addition (subscript  $p$ )
- $\rho_{p,med}$  Density of corrected magnetite medium (subscript  $med$ ) after water addition (subscript  $p$ )
- $\rho_s$  Relative density of a slurry (subscript  $s$ )

$\rho_{t,dis}$	Density of the magnetite make-up medium disturbance (subscript <i>dis</i> ) fed into the corrected medium tank (subscript <i>t</i> )
$\rho_{t,med}$	Density of the magnetite medium (subscript <i>med</i> ) recovered fed into the corrected medium tank (subscript <i>t</i> )
$\sigma$	Standard deviation
$\Sigma_{\theta}$	A non-linear system with parameters $\theta$
$\tau_c$	Time taken for ore to be transported over the bottom deck (subscript <i>c</i> ) screen component <i>i</i> for a double-deck screen
$\tau_f$	Time taken for ore to be transported over a fines (subscript <i>f</i> ) material screen component <i>i</i>
$\tau_o$	Time taken for ore to be transported over the top deck (subscript <i>o</i> ) screen component <i>i</i> for a double-deck screen
$\tau_{c,fc}$	Time taken for ore to be transported through (subscript <i>fc</i> ) the bottom deck (subscript <i>c</i> ) screen component <i>i</i> for a double-deck screen
$\tau_{f,uf}$	Time taken for ore to be transported through a fines (subscript <i>f</i> ) material screen component <i>i</i>
$\tau_{o,co}$	Time taken for ore to be transported through (subscript <i>co</i> ) the top deck (subscript <i>o</i> ) screen component <i>i</i> for a double-deck screen
$\theta$	Parameter variables for a system
$\theta_{msep}$	Angle of the separation zone for a magnetic separator (subscript <i>msep</i> )
$A$	Area of each screen for a double-deck screen
$A_c$	Area of the inlet for a DMC (subscript <i>c</i> )
$A_f$	Area of a fines (subscript <i>f</i> ) material screen
$A_t$	Effective area of the corrected medium tank (subscript <i>t</i> )
$A_{drm}$ and $B_{drm}$	Constants used to describe the partition factor for a drum (subscript <i>drm</i> ) separator
$a_{drm}$ and $b_{drm}$	Constants used to describe type of flow within a drum (subscript <i>drm</i> ) separator
$a_{pc}$	Relative density fraction in clean coal in the development of a partition curve (subscript <i>pc</i> )
$A_{scr}(\delta_{scr})$	Constant dependent on nominal screen (subscript <i>scr</i> ) aperture

- $b_{pc}$  Relative density fraction of total clean coal in the development of a partition curve (subscript  $pc$ )
- $C_A$  Concentration of chemical component  $A$
- $C_v$  Valve (subscript  $v$ ) coefficient
- $C_{ash}$  Concentration of ash (subscript  $ash$ )
- $c_{pc}$  Relative density fraction in discard in the development of a partition curve (subscript  $pc$ )
- $c_{vsc}$  Constant reflecting effects of particle shape on settling to incorporate effects of viscosity (subscript  $vsc$ )
- $D$  Diameter of a DMC
- $d$  Particle size
- $D_c$  Eddy diffusion coefficient (subscript  $c$ )
- $d_c$  Average particle size within a DMC (subscript  $c$ )
- $d_i$  Particle size  $i$
- $D_l$  Relative density of liquid (subscript  $l$ ) displaced by a particle
- $D_{msep}$  Diameter of the drum for a magnetic separator (subscript  $msep$ )
- $d_{pc}$  Relative density fraction of total discard in the development of a partition curve (subscript  $pc$ )
- $D_{pulp}$  Relative density of ROM pulp (subscript  $pulp$ )
- $E$  Apparent activation energy for a reaction process
- $e_{pc}$  Relative density fraction reconstructed feed in the development of a partition curve (subscript  $pc$ )
- $E_{pi}$  Separation efficiency of particle (subscript  $p$ ) size  $i$
- $F$  Feed rate of feed ore
- $f(\rho_{coal})$  Parametric equation as a function of relative density of coal (subscript  $coal$ )
- $f(x, \theta, u)$  Non-linear function describing a non-linear system in terms of its states ( $x$ ), parameters ( $\theta$ ) and inputs ( $u$ )
- $F_c$  Feed rate of cleaned coal (subscript  $c$ )
- $F_r$  Resultant (subscript  $r$ ) force acting on a particle suspended in a liquid

- $f_v(l_v)$  Valve (subscript  $v$ ) positioner function
- $f_{ij}$  Partition coefficient for size fraction  $i$  and density fraction  $j$
- $F_{scr,o}$  Screen (subscript  $scr$ ) feed rate of oversized (subscript  $o$ ) ore
- $g$  Gravitational force as given by Newton's second law ( $9.8 \text{ m/s}^2$ )
- $h$  Position of a particle within a DMC
- $h(x, \theta, u)$  Function describing the output of a system in terms of its states ( $x$ ), parameters ( $\theta$ ) and inputs ( $u$ )
- $h_t$  Height of the magnetite medium in the corrected medium tank (subscript  $t$ )
- $h_{t,max}$  Maximum (subscript  $max$ ) height of the magnetite medium in the corrected medium tank (subscript  $t$ )
- $I_i$  Intensity of radiation passing into (subscript  $i$ ) a pipe or slurry
- $I_o$  Intensity of radiation passing out (subscript  $o$ ) of a pipe or slurry
- $K$  Constant used in describing performance of separation
- $k$  and  $c$  Constants used to describe instantaneous relative density of material
- $k_0$  Proportionality constant for the Arrhenius equation
- $K_{c,o,ash}$  Proportionality constant for the ash (subscript  $ash$ ) overflow (subscript  $o$ ) of a DMC (subscript  $c$ )
- $K_{c,o,C}$  Proportionality constant for the fixed carbon (subscript  $C$ ) overflow (subscript  $o$ ) of a DMC (subscript  $c$ )
- $K_{c,o,H_2O}$  Proportionality constant for the moisture (subscript  $H_2O$ ) overflow (subscript  $H_2O$ ) of a DMC (subscript  $c$ )
- $K_{c,o,med}$  Proportionality constant for the magnetite medium (subscript  $med$ ) overflow (subscript  $o$ ) of a DMC (subscript  $c$ )
- $K_{c,o,S}$  Proportionality constant for the sulphur (subscript  $S$ ) overflow (subscript  $o$ ) of a DMC (subscript  $c$ )
- $K_{c,o,vol}$  Proportionality constant for the volatile (subscript  $vol$ ) overflow (subscript  $o$  of a DMC (subscript  $c$ ))
- $K_{c,o}$  Proportionality constant for the overflow (subscript  $o$ ) of a DMC (subscript  $c$ )
- $K_{c,u,ash}$  Proportionality constant for the ash (subscript  $ash$ ) underflow (subscript  $u$ ) of a DMC (subscript  $c$ )

- $K_{c,u,C}$  Proportionality constant for the fixed carbon (subscript  $C$ ) underflow (subscript  $u$ ) of a DMC (subscript  $c$ )
- $K_{c,u,H_2O}$  Proportionality constant for the moisture (subscript  $H_2O$ ) underflow (subscript  $u$ ) of a DMC (subscript  $c$ )
- $K_{c,u,med}$  Proportionality constant for the magnetite medium (subscript  $med$ ) underflow (subscript  $u$ ) of a DMC (subscript  $c$ )
- $K_{c,u,S}$  Proportionality constant for the sulphur (subscript  $S$ ) underflow (subscript  $u$ ) of a DMC (subscript  $c$ )
- $K_{c,u,vol}$  Proportionality constant for the volatile (subscript  $vol$ ) underflow (subscript  $u$ ) of a DMC (subscript  $c$ )
- $K_{c,u}$  Proportionality constant for the underflow (subscript  $u$ ) of a DMC (subscript  $c$ )
- $K_{drm}$  Machine constant for a drum (subscript  $drm$ ) separator
- $k_{Ep}$  Constant for the separation efficiency (subscript  $Ep$ ) model
- $L_1$  Length (subscript 1) of each screen for a double-deck screen
- $L_2$  Width (subscript 2) of each screen for a double-deck screen
- $l_v$  Lift of a valve (subscript  $v$ )
- $L_{1,f}$  Length (subscript 1) of a fines (subscript  $f$ ) material screen
- $L_{2,f}$  Width (subscript 2) of a fines (subscript  $f$ ) material screen
- $L_{msep}$  Fractional loss of magnetics for a magnetic separator (subscript  $msep$ )
- $M_c$  Mass of ore on the lower (subscript  $c$ ) deck of a double-deck screen
- $M_f$  Mass of ore on the top deck of a fines (subscript  $f$ ) material screen
- $M_l$  Mass of liquid (subscript  $l$ ) displaced by a particle
- $M_o$  Mass of ore on the upper (subscript  $o$ ) deck of a double-deck screen
- $m_p$  Mass of a particle (subscript  $p$ )
- $M_w$  Total mass of water (subscript  $w$ ) in ROM pulp
- $M_{c,i}$  Mass of ore on the bottom deck (subscript  $c$ ) for mass component  $i$  of a double-deck screen
- $M_{coal}$  Total mass of coal (subscript  $coal$ ) in ROM pulp
- $M_{f,i}$  Mass of ore for mass component  $i$  for a fines (subscript  $f$ ) material screen

- $M_{H_2O,ore}$  Total moisture (subscript  $H_2O$ ) content of ROM ore (subscript  $ore$ )
- $M_{o,i}$  Mass of ore on the top deck (subscript  $o$ ) for mass component  $i$  of a double-deck screen
- $n_{Ep}$  Hydrodynamic constant for the separation efficiency (subscript  $Ep$ ) model
- $p$  and  $q$  Parameters accounting for turbulence and viscous forces within a DMC
- $Q$  Slurry split
- $Q_t$  Volumetric flow rate of the corrected medium from the corrected medium tank (subscript  $t$ )
- $q_v$  Flow rate of a fluid after a valve (subscript  $v$ )
- $Q_w$  Volumetric flow rate of water (subscript  $w$ ) addition
- $Q_{c,i,med}$  Volumetric flow rate of the magnetite medium (subscript  $med$ ) in the feed (subscript  $i$ ) mix to a DMC (subscript  $c$ )
- $Q_{c,i}$  Volumetric flow rate of the feed (subscript  $i$ ) mix to a DMC (subscript  $c$ )
- $Q_{c,o}$  Volumetric flow rate of the overflow (subscript  $o$ ) from a DMC (subscript  $c$ )
- $Q_{c,u}$  Volumetric flow rate of the underflow (subscript  $u$ ) from a DMC (subscript  $c$ )
- $Q_{mb,med}$  Volumetric flow rate of corrected magnetite medium (subscript  $med$ ) fed to a mixing box (subscript  $mb$ )
- $Q_{mb}$  Volumetric flow rate of mix from a mixing box (subscript  $mb$ )
- $Q_{msep,f}$  Volumetric feed (subscript  $f$ ) rate per unit length for a magnetic separator (subscript  $msep$ )
- $Q_{p,i}$  Volumetric flow rate of recovered magnetite medium feed (subscript  $i$ ) for water addition (subscript  $p$ )
- $Q_{p,med}$  Volumetric flow rate of corrected magnetite medium (subscript  $med$ ) after water addition (subscript  $p$ )
- $Q_{pulp}$  Volumetric flow rate of ROM pulp (subscript  $pulp$ )
- $Q_{t,dis}$  Volumetric flow rate of the magnetite make-up medium disturbance (subscript  $dis$ ) fed into the corrected medium tank (subscript  $t$ )
- $Q_{t,med}$  Volumetric flow rate of the magnetite medium (subscript  $med$ ) recovered fed into the corrected medium tank (subscript  $t$ )
- $R$  Gas constant ( $8.314 \text{ J mol}^{-1} \text{ K}^{-1}$ )

$r_A$	Chemical reaction rate of chemical component $A$
$R_c$	Radius of a DMC (subscript $c$ )
$R_p$	The resistance to the relative motion of a particle (subscript $p$ ) in a liquid
$R_v$	Valve (subscript $v$ ) design parameter
$R_{c,eff}$	Effective (subscript $eff$ ) radius at which separation takes place near the spigot for a DMC (subscript $c$ )
$S$	A quantity which can be total mass, mass of individual components, total energy or momentum
$S_c$	Partition relative density for coal (subscript $c$ )
$S_m$	Medium (subscript $m$ ) relative density
$S_{cf}$	Correction factor (subscript $cf$ ) for weigh feeder or belt scale
$S_{scr}$	Screen (subscript $scr$ ) partition coefficient
$T$	Absolute temperature
$t$	Time
$t_1$ and $t_2$	Constants used to describe the upper and lower tails of a partition curve
$u$	Input variable for a system
$v$	Linear velocity of ore at each deck of a double-deck screen
$V_c$	Volume of the material within the cyclone (subscript $c$ )
$v_f$	Linear velocity of the ore transported over a fines (subscript $f$ ) material screen
$V_l$	Volume of liquid (subscript $l$ ) displaced by a particle
$v_l$	Drift velocity due to liquid (subscript $l$ ) flow
$V_N$	Scalar-valued norm
$V_p$	Volume required until solution is perfectly mixed for an in-line mixer (subscript $p$ )
$v_p$	Volume of a particle (subscript $p$ )
$V_r$	Random (subscript $r$ ) velocity with zero mean and variance $\sigma^2$
$v_s$	Particle settling (subscript $s$ ) velocity
$V_t$	Volume of the magnetite medium in the corrected medium tank (subscript $t$ ) or minimum acceptable degree of accuracy for a scalar-valued norm $V_N$

- $v_{100}$  Terminal velocity of a particle in a medium which allows for sinks to be recovered 100% (subscript 100)
- $v_{c,i}$  Linear velocity of the feed (subscript  $i$ ) mix in the DMC (subscript  $c$ )
- $V_{c,o}$  Volume split of the overflow (subscript  $o$ ) within the DMC (subscript  $c$ )
- $V_{c,u}$  Volume split of the underflow (subscript  $u$ ) within the DMC (subscript  $c$ )
- $V_{mb}$  Fixed volume of mixing box (subscript  $mb$ )
- $v_{t,p}$  Tangential (subscript  $t$ ) velocity of a particle (subscript  $p$ )
- $W_c$  Mass feed rate of coarse (subscript  $c$ ) sized ore begin transported on the lower deck of a double-deck screen
- $W_i$  Mass feed rate of ore fed into (subscript  $i$ ) a double-deck screen
- $W_o$  Mass feed rate of oversized (subscript  $o$ ) ore being transported on the upper deck of a double-deck screen
- $W_{c,i}$  Mass feed rate of the undersized ore exiting mass component  $i$  from the top deck (subscript  $c$ ) of a double-deck screen or mass feed rate of the feed (subscript  $i$ ) mix to a DMC (subscript  $c$ )
- $W_{c,o,ore}$  Mass feed rate of the ore (subscript  $ore$ ) overflow (subscript  $o$ ) from a DMC (subscript  $c$ )
- $W_{c,o}$  Mass feed rate of the overflow (subscript  $o$ ) from a DMC (subscript  $c$ )
- $W_{c,u,ore}$  Mass feed rate of the ore (subscript  $ore$ ) underflow (subscript  $u$ ) from a DMC (subscript  $c$ )
- $W_{c,u}$  Mass feed rate of the underflow (subscript  $u$ ) from a DMC (subscript  $c$ )
- $W_{f,i-1}$  Mass feed rate of the ore fed into component  $i$  for a fines (subscript  $f$ ) material screen
- $W_{f,i}$  Mass feed rate of the ore overflow exiting mass component  $i$  for a fines (subscript  $f$ ) material screen or mass feed rate of the undersized ore (subscript  $f$ ) exiting mass component  $i$  from the bottom deck of a double-deck screen
- $W_{i,f}$  Mass feed rate of the ore fed into (subscript  $i$ ) a fines (subscript  $f$ ) material screen
- $W_{o,f}$  Mass feed rate of the ore transported over (subscript  $o$ ) a fines (subscript  $f$ ) material screen
- $W_{o,i-1}$  Mass feed rate of the ore fed into component  $i$  on the top (subscript  $o$ ) deck of a double-deck screen

- $W_{o,i}$  Mass feed rate of the ore overflow exiting mass component  $i$  on the top deck (subscript  $o$ ) of a double-deck screen
- $W_{ore}$  Feed rate of coal ore (subscript  $ore$ )
- $W_{t,med}$  Mass feed rate of the magnetite medium (subscript  $med$ ) recovered into the corrected medium tank (subscript  $t$ )
- $W_{tc,i-1}$  Mass feed rate of the ore fed into component  $i$  (subscript  $tc$ ) on the bottom deck of a double-deck screen
- $W_{tc,i}$  Mass feed rate of the ore overflow exiting mass component  $i$  (subscript  $tc$ ) on the bottom deck of a double-deck screen
- $W_{u,f}$  Mass feed rate of the ore transported through (subscript  $u$ ) a fines (subscript  $f$ ) material screen
- $W_{u,f,f}$  Mass feed rate of the fine-sized (subscript  $f$ ) ore being transported through the underflow (subscript  $uf$ ) of a double-deck screen
- $W_{u,f,i}$  Mass feed rate of the ore underflow (subscript  $uf$ ) exiting mass component  $i$  for a fines material screen
- $x$  State variable for a system
- $x_i$  Particle size fraction  $i$
- $x_{c,i,ash}, x_{c,i,S}, x_{c,i,H_2O}, x_{c,i,vol}, x_{c,i,C}$  Percentage ash (subscript  $ash$ ), sulphur (subscript  $S$ ), water (subscript  $H_2O$ ), volatiles (subscript  $vol$ ) and fixed carbon (subscript  $C$ ) in the feed (subscript  $i$ ) mix in a DMC (subscript  $c$ )
- $x_{c,i,med}$  Percentage magnetite medium (subscript  $med$ ) in the feed (subscript  $i$ ) mix to a DMC (subscript  $c$ )
- $x_{c,o,ash}, x_{c,o,S}, x_{c,o,H_2O}, x_{c,o,vol}, x_{c,o,C}$  Percentage ash (subscript  $ash$ ), sulphur (subscript  $S$ ), water (subscript  $H_2O$ ), volatiles (subscript  $vol$ ) and fixed carbon (subscript  $C$ ) in the overflow (subscript  $o$ ) from a DMC (subscript  $c$ )
- $x_{c,o,med}$  Percentage magnetite medium (subscript  $med$ ) in the overflow (subscript  $o$ ) from a DMC (subscript  $c$ )
- $x_{c,u,ash}, x_{c,u,S}, x_{c,u,H_2O}, x_{c,u,vol}, x_{c,u,C}$  Percentage ash (subscript  $ash$ ), sulphur (subscript  $S$ ), water (subscript  $H_2O$ ), volatiles (subscript  $vol$ ) and fixed carbon (subscript  $C$ ) in the underflow (subscript  $u$ ) from a DMC (subscript  $c$ )
- $x_{c,u,med}$  Percentage magnetite medium (subscript  $med$ ) in the underflow (subscript  $u$ ) from a DMC (subscript  $c$ )



- $x_{msep,p}$  Pick-up (subscript  $p$ ) gap for a magnetic separator (subscript  $msep$ )
- $Y$  Partition factor
- $y$  Output variable for a system
- $Y_p$  and  $\rho_p$  Coordinates of the pivot point (subscript  $p$ ) for a size-by-size partition curve
- $Y_{ij}$  Partition number at particle size  $i$  and density  $j$
- $y_{pc}$  Yield for clean coal in the development of a partition curve (subscript  $pc$ )
- $W'_c$  Estimated output feed rate for the coarse (subscript  $c$ ) material
- $W'_f$  Estimated output feed rate for the fine (subscript  $f$ ) material
- a and b Mass absorption coefficient
- EPM or  $E_p$  Écart probable moyen or separation efficiency

## TABLE OF CONTENTS

Summary	i
Acknowledgement	ii
List of Abbreviations	iv
Nomenclature	v
Table of Contents	xvi
<b>1 Chapter 1: Introduction</b>	<b>1</b>
1.1 Background and Motivation . . . . .	1
1.2 Contribution . . . . .	2
1.3 Organisation . . . . .	4
<b>2 Chapter 2: Coal Beneficiation</b>	<b>5</b>
2.1 Introduction . . . . .	5
2.2 Coal Geology . . . . .	6
2.3 Coal Marketing . . . . .	7
2.3.1 Leeuwpans marketing . . . . .	7
2.4 Coal Beneficiation Principles . . . . .	9
2.4.1 Gravity separation . . . . .	10
2.4.2 Float and sink analysis . . . . .	12
2.4.2.1 Partition curves . . . . .	13
2.4.2.2 Washability curves . . . . .	15
2.4.2.3 Organic efficiency . . . . .	17
2.4.2.4 Near-dense material . . . . .	17
2.4.3 Dense medium separation . . . . .	18
2.4.3.1 The dense medium cyclone . . . . .	18
2.4.3.2 Dense medium cyclone analysis . . . . .	20
2.4.4 Dense medium separation circuits and process units . . . . .	27
2.4.4.1 Screens . . . . .	29
2.4.4.2 Drum separators . . . . .	31
2.4.4.3 Dense medium cyclones . . . . .	32
2.4.4.4 Magnetic separators . . . . .	32
2.4.4.5 Instrumentation and field devices . . . . .	35
2.4.5 Mathematical modelling and computer simulations . . . . .	43
2.4.5.1 Dense medium separators . . . . .	43
2.4.5.2 Screens . . . . .	47
2.4.5.3 Magnetic separators . . . . .	47
2.5 Conclusion . . . . .	48
<b>3 Chapter 3: Modelling for Feedback Control</b>	<b>50</b>
3.1 Introduction . . . . .	50
3.2 Steady-state and Dynamic Modelling . . . . .	51
3.3 System Identification . . . . .	53
3.4 Mathematical Representation of Processes . . . . .	54
3.4.1 Model-based Control in Mineral Engineering . . . . .	55
3.5 Financial Benefits of Using Automatic Control . . . . .	59
3.6 Conclusion . . . . .	61

<b>4</b>	<b>Chapter 4: Mathematical Modelling</b>	<b>62</b>
4.1	Introduction . . . . .	62
4.2	Model Development . . . . .	62
4.2.1	Screen model . . . . .	62
4.2.1.1	Single-deck screen model . . . . .	62
4.2.1.2	Double-deck screen model . . . . .	65
4.2.2	Magnetite medium water addition model . . . . .	68
4.2.3	Mixing box model . . . . .	70
4.2.4	DMC model . . . . .	71
4.2.5	Magnetite make-up corrected medium model . . . . .	79
4.3	DMS Plant Simulation Model . . . . .	80
4.4	Discussion . . . . .	81
4.5	Conclusion . . . . .	83
<b>5</b>	<b>Chapter 5: Parameter Identification and Estimation</b>	<b>84</b>
5.1	Introduction . . . . .	84
5.2	Parameter Identifiability Theory and Process . . . . .	84
5.3	Parameter Identifiability . . . . .	86
5.3.1	DMC model . . . . .	86
5.4	Parameter Estimation Process . . . . .	89
5.5	Statistical analysis of results . . . . .	91
5.6	Parameter Estimation . . . . .	92
5.6.1	Single-deck screen model . . . . .	93
5.6.2	Double-deck screen model . . . . .	93
5.6.3	Magnetite water-addition model . . . . .	95
5.6.4	Mixing box model . . . . .	95
5.6.5	DMC model . . . . .	95
5.6.6	Magnetite make-up corrected medium tank model . . . . .	97
5.7	Discussion . . . . .	97
5.8	Conclusion . . . . .	97
<b>6</b>	<b>Chapter 6: Model Validation</b>	<b>99</b>
6.1	Introduction . . . . .	99
6.2	Leeuwpan operation analysis and industrial experiment . . . . .	99
6.2.1	Leeuwpan DMS plant operation and analysis . . . . .	99
6.2.2	Industrial Experiment Test Case . . . . .	106
6.3	Model Simulations . . . . .	108
6.3.1	Single- and double-deck screen models . . . . .	108
6.3.2	Magnetite water-addition model . . . . .	115
6.3.3	Mixing box model . . . . .	116
6.3.4	DMC model . . . . .	119
6.3.5	Magnetite make-up corrected medium model . . . . .	134
6.4	Model Simulation . . . . .	137
6.5	Discussion . . . . .	137
6.6	Conclusion . . . . .	149
<b>7</b>	<b>Chapter 7: Conclusion</b>	<b>151</b>
7.1	Introduction . . . . .	151
7.2	Discussion . . . . .	151
7.3	Recommendation for Further Work . . . . .	152



References	154
Addendum A: Washability tables and curves for blocks OD, OH and OM for seam 2	160
Addendum B: Process and instrumentation diagrams for Leeuwpan DMS plant	164
Addendum C: Pea and duff product qualities for October 2008	171
Addendum D: Leeuwpan pump and fine cyclone equipment efficiencies	182
Addendum E: Matlab source code for DMS plant simulation	184
List of Tables	236
List of Figures	237

## CHAPTER 1: INTRODUCTION

### 1.1 BACKGROUND AND MOTIVATION

The coal seams that were formed in South Africa have existed for over 200 million years. It has been estimated that the coal reserves contain over 194 000 million tons and are typically found in the eastern half of South Africa. Coal can be used for metallurgical purposes such as reductants in steel processing or for generation of thermal energy that may be used in electricity generation.

Raw coal that is mined contains a number of impurities and is typically processed to improve its overall quality. The mineral processing of this coal from the run-of-mine (ROM) involves a complicated and sophisticated operation including comminution, classification and separation. These separation processes normally make use of particle classification on the basis of density. Coal, typically being lighter, is separated from the heavier gangue by utilising the difference in specific gravity. These processes can make use of mediums that are made to specific relative densities to ensure the separation of coal from gangue. A dense medium separation (DMS) circuit is typically used for efficient beneficiation.

Implementing a control system can provide a means of understanding a plant or process dynamics to enable improvement of the plant in terms of stability and performance. This enables the reduction of plant upsets due to disturbances and ensures a plant keeps to its desired setpoints. It is often required that a plant runs at a desired specification. Control systems assist in reducing the deviation that occurs between the desired specifications and actual measurements. Since control systems typically make use of a model that incorporates plant dynamics, they usually ensure that a plant reaches its steady state in the fastest time possible after start-up or process setpoint changes.

Control systems can be applied to any process or plant and are used in a number of industries, such as mining, manufacturing, aerospace, transportation, power systems, robotics, appliances and many others. The benefits mentioned earlier relate to the economic improvement of a process and give that process a competitive edge. Control systems theory has advanced a great deal over the past 40 years and allows for exciting new applications in minerals processing and coal beneficiation.

This research will assist in improving the current understanding of process control in DMS for coal beneficiation. The Leeuwpan coal mine will be used to conduct an industrial experiment so that data can be collected and analysed. Leeuwpan is

an open-pit coal mine that produces 3 Mtpa metallurgical and power station coal near the town of Delmas, Mpumalanga. If the results of this research allow for the implementation of a process controller at Leeuwpan coal mine, improvements should be realised in production performance and stability and therefore overall financial improvement.

By analysing product yield and product quality data from the Leeuwpan DMS plant, it is possible to determine whether or not there is room for improvement or optimisation for the process by making use of process control. If variations or oscillations in product yield and quality due to disturbances or changes in setpoints are found, it can be argued that control could possibly be used to eliminate or reduce such deviations. It can then be assumed that a reduction in such variations will result in improved product throughput and quality.

From the analysis in section 6.2.1 it is found that disturbances or oscillations in the yield and product qualities indicate that there is an opportunity for process improvement at Leeuwpan. Process control can be used to provide this improvement by ensuring the plant runs closer to steady state and also ensuring setpoint changes are tracked properly. An improvement to the process, such as improvement in average yield or ash content, can be related to a monetary value. In order for this to be determined, certain marketing data are required.

Based on the Leeuwpan industrial experiment, other DMS plants that experience similar variations in yield and qualities can also benefit from process control. This research aims in developing a model that can be used for the development of a process controller in DMS plants.

## 1.2 CONTRIBUTION

In process control, it is often necessary to develop a model for the process that is simple enough to be used for a controller but sophisticated enough to ensure simulation of plant dynamics and accurate predictions. Once a model has been developed, a range of controller designs can be employed to improve process performance and stability and therefore ensure economic benefits.

In order to solve this problem in a manner that allows coal beneficiation to be improved by process control, a number of research questions need to be asked with regard to mathematical modelling. These are formulated as follows:

1. What is the current knowledge of DMS and coal beneficiation?

2. Does a dynamic model exist for coal beneficiation through DMS and has it been validated?
3. What benefits are there if a model of the process is developed and a controller is ultimately designed?

The above questions will be answered by this research and this will therefore answer the research problem, whereby a model for a DMS circuit will be developed. This model will be validated according to actual production data. The ultimate goal is to develop a controller to improve overall production stability and performance to create financial gain.

This study is therefore limited to the modelling of DMS in coal beneficiation. The fines coal beneficiation plant at Leeuwan will be used for this study and all process information will be obtained from that plant. Dynamic models that are developed will be fitted to the Leeuwan DMS circuit. This study will make use of knowledge from the domains of coal beneficiation and mathematical modelling and identification.

The layout of this research is expressed such that the research problem and questions can be answered for the following objectives and goals:

1. Develop a dynamic model of a coal DMS circuit that can be used in a model-based controller.
2. Validate the model through simulations such that it can be implemented to benefit the coal industry.

The approach to the problem and specific steps to be followed are the initial step-by-step design procedures for control system design, according to Skogestad and Postlethwaite (2005:1). However, the controller design will be omitted for the purposes of this research.

1. A study of the DMS system will be conducted and initial information about the control objectives will be obtained.
2. A model of the system will be developed and then simplified, if necessary. Parameters will be estimated.
3. The resulting model will then be analysed and its properties will be determined.
4. It will be determined which variables must be controlled.

### 1.3 ORGANISATION

For this research dissertation, the layout of the chapters will assist in answering the research problem and questions as described earlier. A motivation and background for conducting this study are addressed in this chapter.

Initially the knowledge that is available on coal beneficiation, relating specifically to DMS, will be studied. This literature study will be conducted in chapter 2 of this research. Similarly, the information available in literature on modelling for feedback control will be discussed. This theory and its application to minerals processing will be presented in chapter 3.

After the literature study, chapter 4 will describe the development of the dynamic models used to simulate the process and its equipment. Once the mathematical models have been derived, the parameters describing the models will be identified and estimated in chapter 5. This chapter will also explain the techniques used in model validation and parameter identification. Chapter 6 will describe the Leeuwan process analysis and industrial experiment performed. It will also illustrate the model simulations and model validation results.

Certain recommendations, discussions and conclusions from the research will be described in chapter 7.

## CHAPTER 2: COAL BENEFICIATION

### 2.1 INTRODUCTION

Coal can be used as a source of energy for electrical power stations, synthetics and in the production of metals. It is classified as an organic material, as it originates from the decomposition of plants. Owing to the variety of organic matter and formations of marshes and swamps, each coal deposit can have a large range of physical and chemical properties.

Hayes (2003:25–28) describes coal as being a heterogeneous material that is made up of primarily carbon, hydrogen and oxygen, with smaller amounts of sulphur and nitrogen. Owing to the different conditions that may occur when plant matter changes to coal, various maceral types have been identified. The varying geological conditions of hydrogen/carbon (H/C) and oxygen/carbon (O/C) ratios give rise to a number of coal types, as illustrated in figure 2.1.

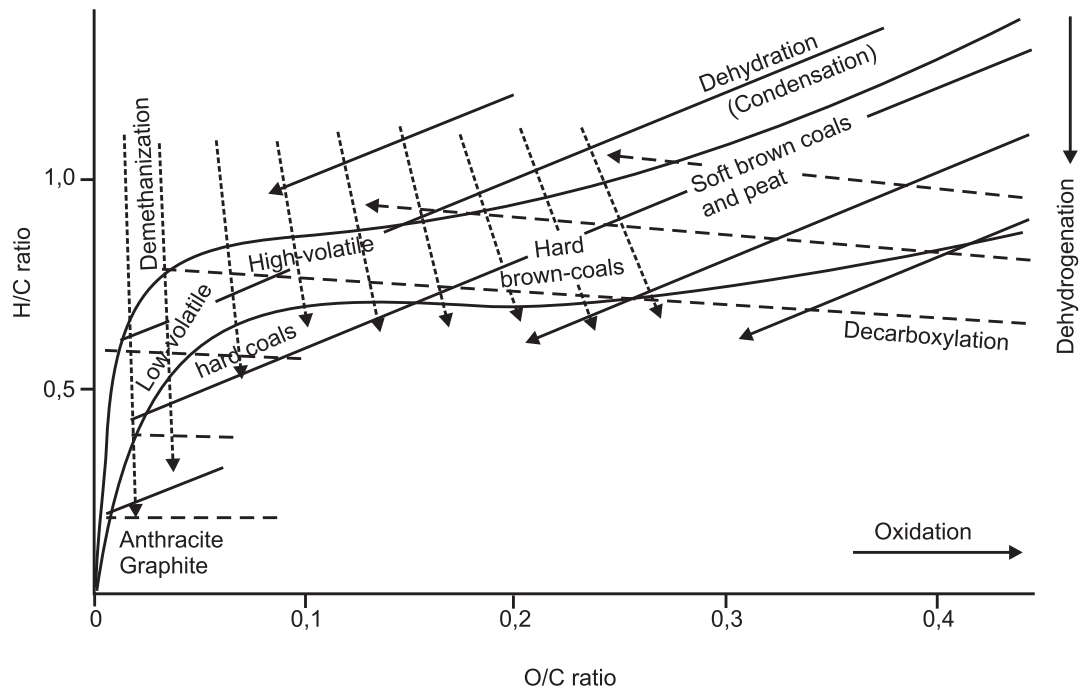


Figure 2.1: The influence of oxygen and hydrogen in coal transformation (Hayes, 2003:27).

Because of the heterogeneous nature of the material, the chemical analysis of coal provides some information to describe its behaviour and properties. Various measurements have been developed to describe coal for further properties, such as ash content and volatile matter. More properties are described by Hayes (2003:28) in table 2.1.



Table 2.1: Measurements used to describe coal (Hayes, 2003:28).

Property Measurements	Empirical Tests
Total analysis	Swelling
Fixed carbon	Reactivity
Volatile matter	Mechanical strength
Moisture content	Abrasion
Specific energy	Slagging/fouling indices
Sulphur	
Ash content	
Maceral analysis	
Size	

The value of coal is referred to as the grade of the coal. This is measured particularly in terms of the usefulness of the coal in a specific application and the economic worth is determined by unique properties or by empirical tests as given in table 2.1.

## 2.2 COAL GEOLOGY

In Mpumalanga, South Africa (England, Hand, Michael, Falcon and Yell, 2002:1–13) the coal seams were formed in the Ecca beds of the Karoo system over 200 million years ago. The formation of these seams started off as what is called peat formation. This is where plants grew in marshes and over time were biochemically altered through decay.

For the peat to become coal, water with layers of clay, silt and sand had to be deposited on top. Through time as more and more of these layers built up, the peat seams were exposed to pressures and temperatures. These physical changes resulted in decay stopping, the water contained within the coal decreasing and the oxygen content being reduced.

The coal seams consist of different strata, namely coal, shale and sandstone. Dwyka tillite can also be found as the floor or sometimes the ceiling of a bottom seam of coal.

When coal is combusted there is usually some inert material that remains behind, which is typically referred to as ash. This is due to the mixing of clay in the original vegetation of the coal. The objective of coal beneficiation is to reduce the amount of ash such that the grade of the coal is of high economic worth and can be used in downstream processes. Other types of mineral matter can also occur in coal, such as pyrite and calcite (seen as white veins in the coal joints).

Botha (2008:16–20) describes the general geology of the Leeuwpan coal mine

where coal seams are divided into two zones, namely top and bottom coal. The bottom coal contains seam 1 and seam 2 of the Witbank coalfield. The top coal is not part of the Witbank coalfields but is divided into four upper and four lower seams and seam 5 separated by shales. (Botha, 2008:40) concludes that the ash distribution throughout seam 2 approximates a normal distribution for the different blocks that are mined (Blocks OD, OH and OM in table 2.2).

Table 2.2: Leeuwpaan normal ash distributions per block (taken from Botha (2008:40)).

Block	Mean Ash %	Standard Deviation
OD	10.92	3.49
OH	11.36	3.67
OM	11.98	3.51

Botha (2008:95–98) also indicates the wash tables and washability curves for each mine block. This information has been used in addendum A of this dissertation.

## 2.3 COAL MARKETING

In the mining industry the main strategy is to run a sustainable operation to the benefit of the clients, employees and community. The marketing of Leeuwpaan coal is used as a typical example for the industry.

### 2.3.1 Leeuwpaan marketing

In the case of Leeuwpaan the products that are made vary between customers. A description of the different product specifications made by Leeuwpaan can be found in figures 2.2, 2.3, 2.4, 2.5 and 2.6.

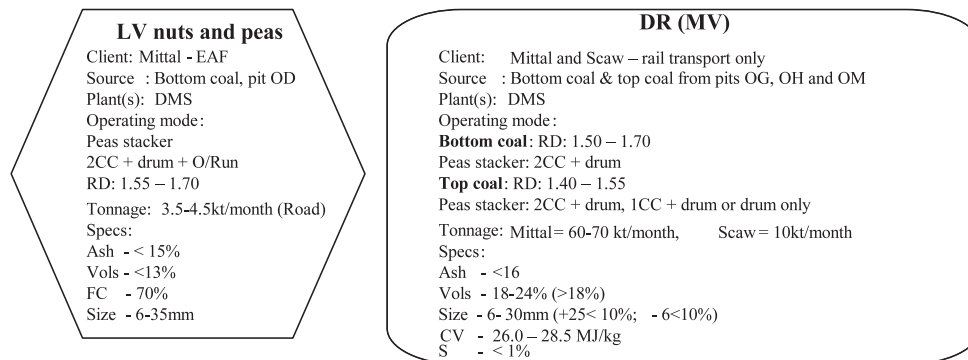


Figure 2.2: Low volatile and medium volatile nuts and peas product specifications.

Figure 2.2 illustrates the product specifications for the nuts and peas products that Leeuwpaan produces. There is a low volatile (LV) and medium volatile (MV)

product specification. LV has less than 13% volatiles in the product while MV has between 18% and 24% volatiles in the product. Both products have an ash percentage less than 16% and particle size specification of +6 mm and –35 mm or –30 mm. These products are derived from the bottom coal of the pits and are beneficiated by the DMS plant.

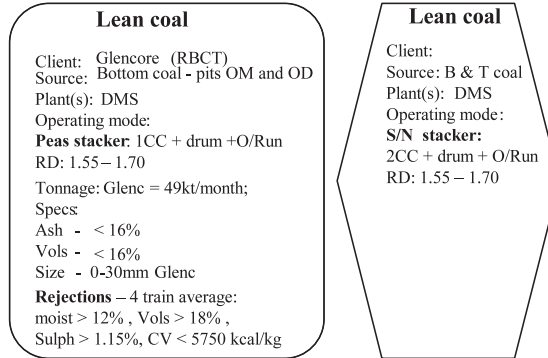


Figure 2.3: Lean coal product specifications.

Figure 2.3 illustrates the product specifications for lean coal. This product must have an ash content of less than 16% and it must have less than 16% volatiles. Particle sizes can vary between 0 mm and 30 mm. This product is mined from the bottom coal in the pits and is beneficiated using the DMS plant.

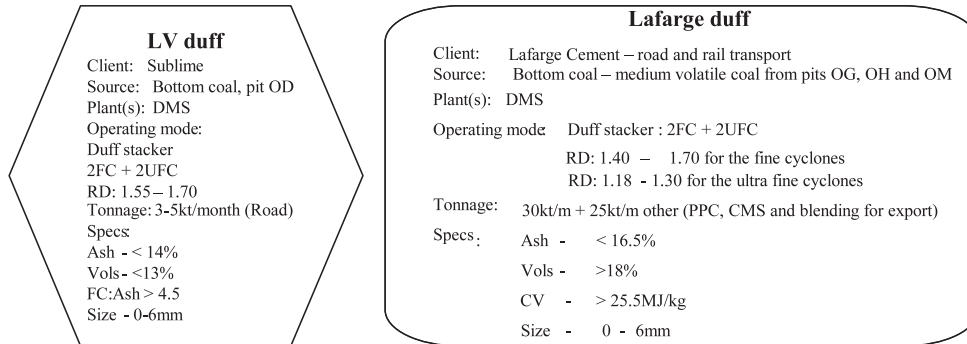


Figure 2.4: LV and MV duff product specifications.

Figure 2.4 illustrates the product specifications for the duff that is produced at Leeuwan. Different volatile products are produced where an LV product of less than 13% is made and an MV product of greater than 18% is produced. Duff has a size specification of +0 mm to –6 mm. This product is mined from bottom coal and processed through the DMS plant.

Figure 2.5 illustrates the specifications for the nuts product produced at Leeuwan. This product consists of the overrun, which means the product size specification would typically be +25 mm to –45 mm. This product can consist of both bottom and top coal and is beneficiated in the DMS plant.



can be determined in the data collected by de Korte (2003b) that 98% of the 53 coal-preparation plants in South Africa are making use of the DMC as their beneficiating unit.

### 2.4.1 Gravity separation

The principle of coal washing is based on the differences in relative density between coal and discard particles (England *et al.*, 2002:103). A process that helps one to understand this is known as settling theory. It is understood since particles fall as a result of gravitational force when suspended in a liquid.

To follow this principle in more detail, a free body diagram, figure 2.7, can be used to show the various forces acting on a particle within a liquid.

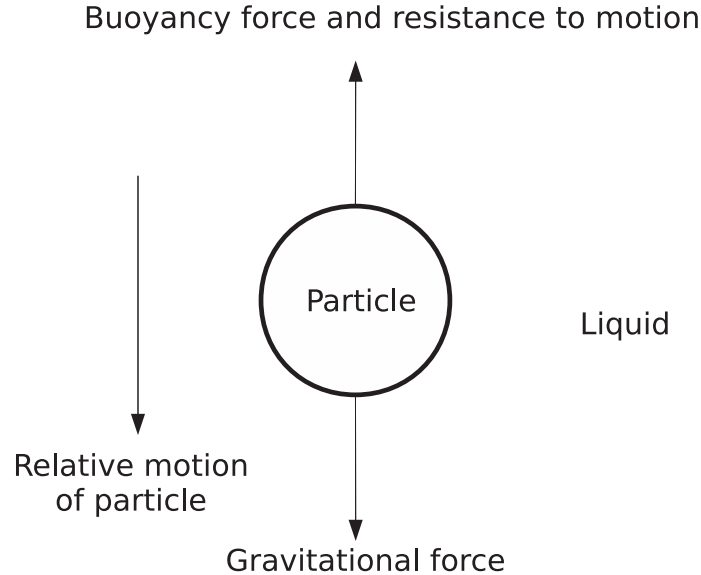


Figure 2.7: Free body diagram illustrating the different forces acting on a particle moving in a relative motion in a liquid.

England *et al.* (2002:103–109) describe settling theory as follows. The viscosity of a liquid determines the difficulty or extent to which it will resist or hold the movement of particles in it. This viscosity is termed the resistance ( $R_p$ ) which can be represented as a force opposite to the relative motion of a particle in a liquid. Using the relationship  $m_p = \rho_p v_p$  where  $m_p$  is the mass of the particle,  $\rho_p$  is the relative density of the particle and  $v_p$  is the volume of the particle, it is possible to determine the force pulling the particle down as  $g\rho_p v_p$ , where  $g$  is the gravitational force as given by Newton's second law.

Similarly, the buoyancy force can be determined by using the mass ( $M_l$ ) of liquid



displaced by the particle, the volume ( $V_l$ ) displaced and the relative density ( $D_l$ ) of the liquid as  $gD_lV_l$ . The volume of the liquid displaced is the same as the particle volume,  $V_l = v_p$ . The buoyancy force can therefore be rewritten as  $gD_lv_p$ . Table 2.3 summarises these various forces that have been described.

Table 2.3: Various forces acting on a particle in motion through a liquid.

Gravitational force	$g\rho_p v_p$
Buoyancy force	$gD_lv_p$
Resistance to motion	$R_p$

The resultant force  $F_r$  acting on the particle is the difference between the gravitational force and the remaining buoyancy and resistance force,

$$F_r = gv_p(\rho_p - D_l) - R_p. \quad (2.1)$$

Since the speed or velocity of the particle is proportional to the resultant force  $F_r$  it can be seen that an increase in the particle relative density  $\rho_p$  or size  $v_p$  will increase its speed. This is assuming gravity  $g$  and the liquid relative density ( $D_l$ ) are kept constant. The particle shape has a negative influence on its resistance to motion in the liquid with increased surface area. This means that the particle velocity will decrease if the particle becomes flatter.

If one understands this principle, it is possible to apply it to a large number of coal and discard particles in a liquid. It is noted that the movement of these particles is difficult to describe mathematically because of the complexity of the process. However, these equations describe general behaviour for particle motion. If all particles are of similar size and shape, the differentiating factor will be their difference in relative densities, which in turn means a difference in falling velocities. Since discard has a larger relative density than coal, it can fall approximately 26 (England *et al.*, 2002:108) times faster than the particles of coal, given specific conditions. This principle can be used to separate particles on the basis of relative density and allows classification according to ash content. This is because the ash content is regarded as discard. A particle such as coal, having a smaller density than the medium it is suspended in ( $\rho_p < D_l$ ), will result in a negative resultant force ( $F_r$ ) which will cause it to float. Ash, having a larger density than the medium it is suspended in ( $\rho_p > D_l$ ), will result in a positive resultant force ( $F_r$ ) which will cause it to sink.

Some examples of equipment that make use of gravity separation are the barrel washer and the upward current washers. More efficient coal-washing equipment has been developed to make use of the principles described above, but in a different fashion, such as float and sink separation. The mathematical description

of the principle is similar to that described above; however, the relative density of the liquid or medium is made a variable.

### 2.4.2 Float and sink analysis

Float and sink analysis is a technique used to determine properties of coal. Coal samples are separated into two or more relative density fractions using similar principles as in gravity separation. However, liquids are made up of different relative densities between that of the discarded material or ash and pure coal.

England *et al.* (2002:47–59) describe the process of float and sink analysis and their description is summarised in this section. By separating a sample using a liquid with a high relative density, the float can be recovered and each float can be immersed consecutively thereafter into a series of liquids of different relative densities in decreasing order (Figure 2.8). Typical relative density ranges are from 1.30 to 1.70, with typical step intervals of 0.05. Each fraction must be given sufficient time such that complete separation of sinks and floats occurs. These times can vary from two minutes for large coal sizes to ten minutes for  $-5$  mm and  $+0.5$  mm sized coal. Smaller sized coal requires centrifugal separation. It is important to note that this analysis is performed when the system is at steady state owing to this long time taken for settling.

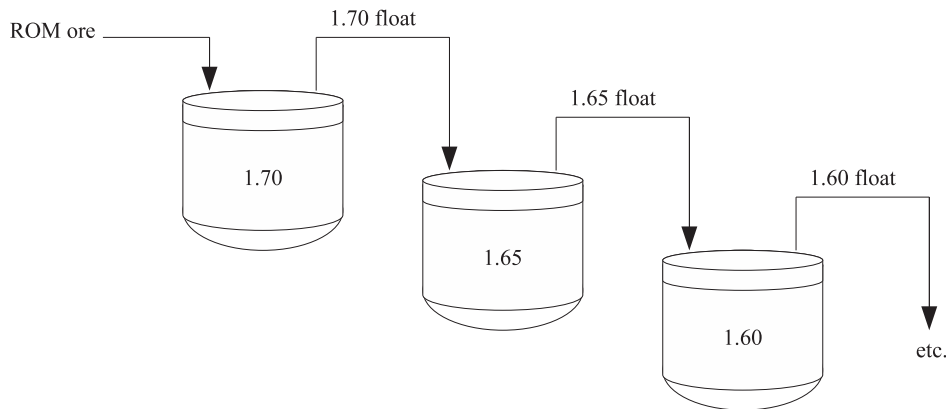


Figure 2.8: Float and sink analysis illustration.

After the coal fractions have settled, the sinks are dried, weighed and analysed in terms of ash content. From these data, a number of techniques can be used to analyse the information to determine partition curves, washability curves (densimetric curves and ash curves) and organic efficiency.



### 2.4.2.1 Partition curves

A partition curve (also known as a Tromp curve) for density separation allows the degree of separation and efficiency for a plant to be illustrated. By using the yield of clean coal from a plant and the float and sink analysis of the product and discard it is possible to determine the partition factor (ratio of the total clean coal to the feed) per relative density fraction. Table 2.4 shows an example of the data and necessary calculations required to derive a partition curve. This is based on a yield of 41.6% for clean coal.

Table 2.4: Example of details and calculations required for a partition curve (England *et al.*, 2002:51).

Relative Density Fraction	Clean Coal ( $y_{pc} = 0.416$ )		Discard ( $1 - y_{pc} = 0.584$ )		Reconst. Feed $b_{pc} + d_{pc} = e_{pc}$	Partition Factor $b_{pc}/e_{pc} \times 100$
	Fract. Yield % ( $a_{pc}$ )	Fract. of Total $a_{pc} \times y_{pc} = b_{pc}$	Fract. Yield % ( $c_{pc}$ )	Fract. of Total Coal $c_{pc}(1 - y_{pc}) = d_{pc}$		
F1.3	43.69	18.18	0.79	0.46	18.64	97.5
1.3 1.32	25.82	10.74	0.71	0.41	11.15	96.3
1.32 1.34	14.23	5.92	1.29	0.75	6.67	88.8
1.34 1.36	11.59	4.82	3.93	2.30	7.12	67.7
1.35 1.38	3.97	1.65	8.93	5.22	6.87	24.0
1.38 1.40	0.40	0.17	10.36	6.05	6.22	2.7
1.40 1.42	0.10	0.04	9.29	5.43	5.47	0.7
1.42 1.44	0.07	0.03	8.58	5.01	5.04	0.6
1.44 1.46	0.03	0.01	8.58	5.01	5.02	0.2
1.46 1.48	0.03	0.01	7.86	4.59	4.60	0.2
1.48 1.50	0.03	0.01	6.43	3.76	3.77	0.3
S1.50	0.03	0.01	33.24	19.41	19.42	0.05
Whole Coal	99.99	41.59	99.99	58.40	99.99	—

Figure 2.9 illustrates an example of a partition curve where the partition factor of a plant is shown with respect to relative density of the liquid. This figure also shows the relative density that will allow for the plant to have a partition factor of 50%.

The value at 50%, also known as the separation cutpoint ( $\rho_{50}$  or  $SG_{50}$ ), is the specific relative density of a particle having an equal chance of reporting to a float or sink (partition factor). From the above table the separation cutpoint is 1.354 for the data given. Another parameter that can be used to describe this curve is the écart probable moyen (EPM or  $E_p$ ), which describes the sharpness of the curve. This value is also known as the separation efficiency and is calculated as follows:

$$E_p = \frac{\rho_{25} - \rho_{75}}{2}, \quad (2.2)$$

where  $\rho_{25}$  is the relative density at 25% and  $\rho_{75}$  is the relative density at 75%.

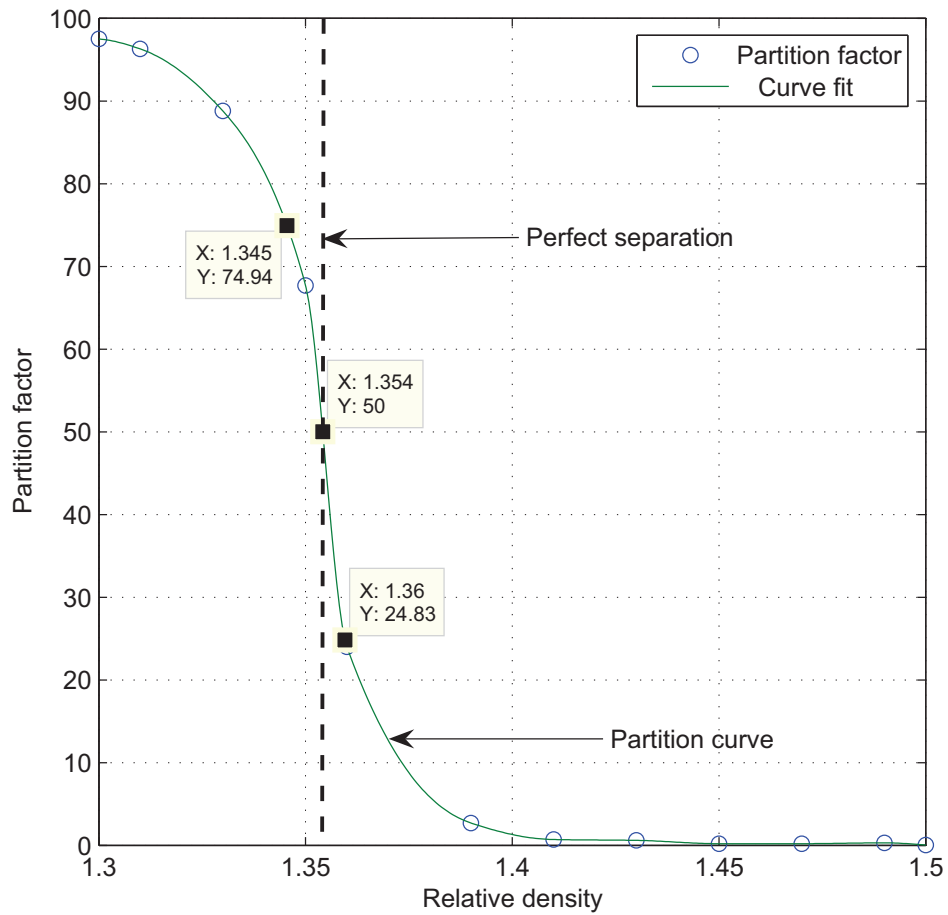


Figure 2.9: Example of a partition curve plotted from table 2.4.



Figure 2.9 also illustrates what the curve would look like for perfect separation. This would have an EPM of zero. A plant having a low EPM value means that it will have very good separation through density separation. Note that a plant can also refer to a specific piece of equipment.

The partition curve is dependent on particle size of the coal that is processed and the relative density of separation as described by de Korte (2008:74–75). It is possible to normalise a partition curve by dividing the relative density intervals by the  $\rho_{50}$  such that a general model for the equipment can be derived. A similar expression exists where the EPM can be made independent of  $\rho_{50}$ . This is termed imperfection (de Korte, 2008:74). The particle size of the coal will cause the efficiency of the partition curve to decrease as size decreases. This is because smaller particles take a longer time to settle and are affected more by the viscosity of the medium.

Other variables that can influence the partition curve are feed rate, maintenance of equipment and operating variables such as pressure, amount of magnetite used and contaminants in the medium (de Korte, 2008:77–78).

#### 2.4.2.2 Washability curves

ROM coal contains varying degrees of characteristics with respect to relative density. A washability curve allows the properties of coal ore to be analysed such that the best possible way to beneficiate it can be achieved while ensuring a profit is still made. Particles that have a higher relative density will generally have a higher ash content. A particle with a higher ash content will then have a lower calorific value. This information can be obtained by performing float and sink analysis on the coal.

Initially the yield of clean coal that floats is determined with respect to the relative density fraction. This allows a densimetric curve to be plotted where the cumulative floats or yield is graphed against relative density. Figure 2.10 illustrates an example of this plot showing relative density/yield (taken from de Korte [2006:16]). The ash content of each float can also be determined and then plotted against its relative density fraction. This is also illustrated in figure 2.10 and is known as an ash curve. The combination of the two curves creates a washability curve, which illustrates the relationship between cumulative yield and quality of the coal (ash content).

In some operations, the discard might also be saleable. In this case the ash

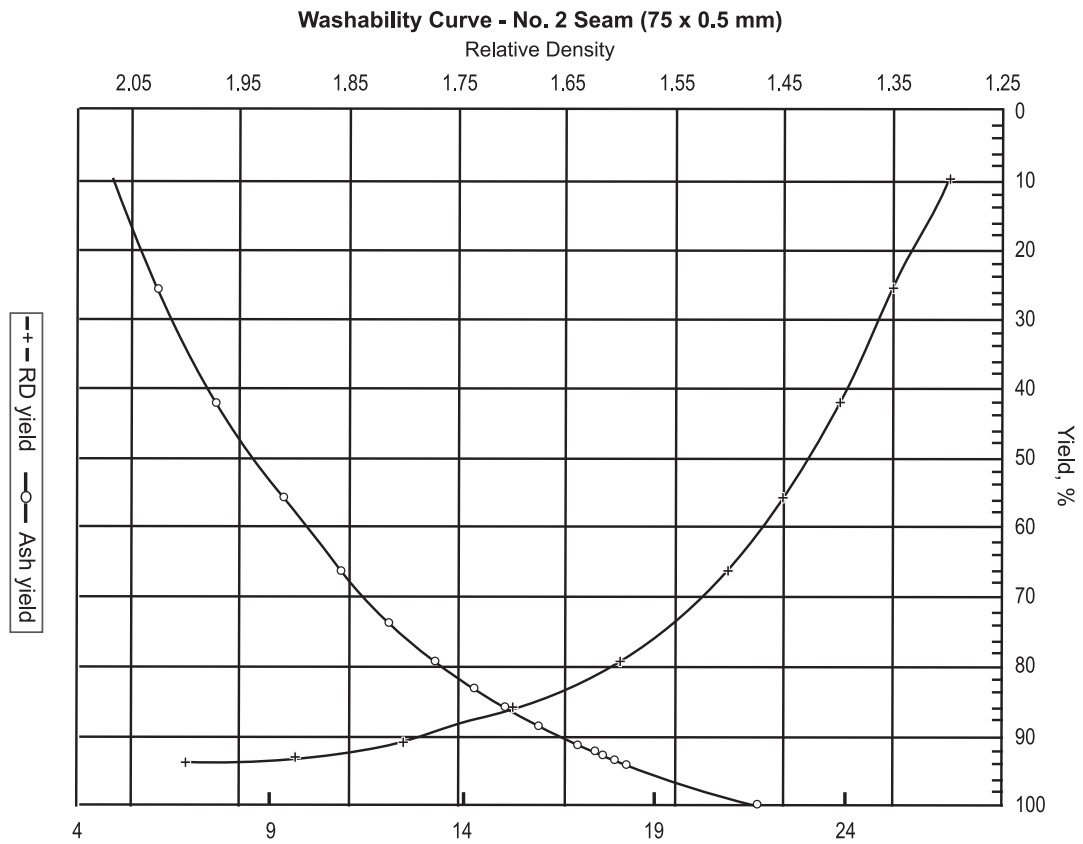


Figure 2.10: Example of a washability curve (de Korte, 2006:16).



content of the sinks can also be determined and plotted. Because the results of a float and sink analysis occur at steady state, perfect separation is assumed. This means that a washability curve illustrates the yield and ash content of the coal for perfect separation. These theoretical values are not normally achieved owing to inefficiencies in operational equipment.

The partition curve can be used to determine how plant efficiency will affect the ROM coal based on the washability analysis. Napier-Munn (1991:333) explains that this method can be used to simulate the characteristics of the product based on different parameters. This can be very useful when designing a plant flowsheet and selecting equipment.

### **2.4.2.3 Organic efficiency**

Organic efficiency is another parameter that can be determined from a float and sink analysis. It is the ratio between the actual yield achieved in an operation and the theoretical yield obtained from the washability curve.

### **2.4.2.4 Near-dense material**

Near-dense or near gravity material is a material in which the impurities and coal are inadequately liberated. Near-gravity material is material close to the separating density of the DMS unit. In the case of Leeuwpan, the ore that is mined is typically near-dense material.

As explained by de Korte (2008:69), near-dense material makes it very difficult to separate the coal from the ash since settling occurs very slowly. When a float and sink analysis is done on near-dense material, it is found that most of the material lies within 0.1 relative density units of the cutpoint (de Korte, 2008:86). This means that the probability of material that should report to the floats, but reporting incorrectly to the sinks, will increase. It is indicated (de Korte, 2008:79) that coal ore having a near-dense material of above 7% becomes increasingly difficult to wash. In the case of Leeuwpan, the ore contains 60 – 70% near-dense material. This indicates that the ore at Leeuwpan is very difficult to wash.

### 2.4.3 Dense medium separation

DMS makes use of the same principles as float and sink analysis except that a liquid or medium is selected that has a relative density greater than a coal particle so that the particle will float. Similarly, if a discard particle has a relative density greater than the liquid, it will sink. This will therefore separate the coal from the discard by selecting the appropriate liquid or medium relative density. The DMC makes use of centrifugal separation implying that particles undergo a greater force than that of gravity. England *et al.* (2002:149–177) describe DMS well as summarised in this section.

#### 2.4.3.1 The dense medium cyclone

The medium that is typically used in DMC separation is magnetite ( $\text{Fe}_3\text{O}_4$ ). Magnetite is used because it forms a stable suspension in water over a wide range of relative densities and can be reused when it is recovered. It is a ferrimagnetic mineral with a relative density of approximately 5. It has a typical particle size of  $-45 \mu\text{m}$  and contains more than 90% magnetics. For coarse material at Leeuwpán, magnetite with more than 85% magnetics is used while for fine material,  $\text{Fe}_3\text{O}_4$  is used with more than 95% magnetics in the magnetite.

Figure 2.11 illustrates the typical cyclone geometry and configuration according to Magwai and Bosman (2007:95). The cyclone is the equipment used in the DMC to create the centrifugal separation. Crushed and screened ROM coal mixed with medium is pumped into the cyclone inlet. This feed follows a spiral flow pattern similar to what is illustrated in figure 2.12. The heavy discard is forced towards the outer edge and exits the spigot while the lighter clean coal is forced towards the centre, creating an inward migration to reverse its vertical velocity, and discharges at the vortex finder.

Gupta and Yan (2006:533–535) describe the principle of the DMC operation as being similar to gravity separation as described in section 2.4.1 of this chapter. Similar forces are applicable in the DMC, however, with the acceleration due to gravity substituted by centrifugal acceleration  $\frac{v_{t,p}^2}{R_c}$ . The tangential velocity of the particle is represented by  $v_{t,p}$  and the radius of the DMC is  $R_c$ . By making use of a centrifugal force, it is possible to ensure that a DMC causes particles to undergo forces far greater than the effects of gravity.

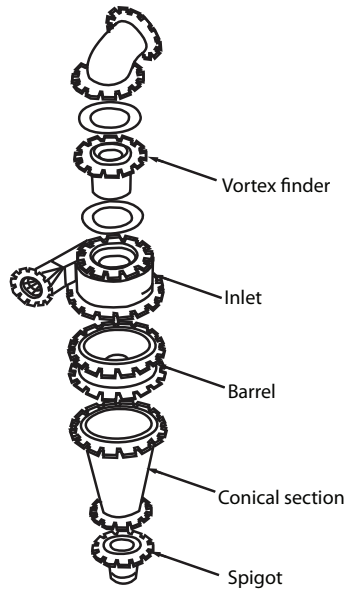
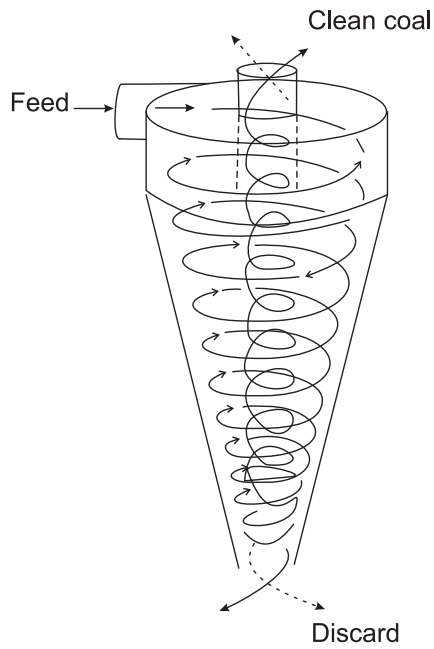


Figure 2.11: Diagram illustrating the geometry of a cyclone (Magwai and Bosman, 2007:95).



The spiral flow in the cyclone

Figure 2.12: Spiral flow within a cyclone (England *et al.*, 2002:165).



### 2.4.3.2 Dense medium cyclone analysis

Gupta and Yan (2006:534) explain that particles at the inlet of a cyclone typically experience forces 20 times greater than that of gravity. At the apex of a cyclone, acceleration will increase to over 200 times that of gravity. In view of the increase in forces that separate the particles in a DMC, a higher capacity of coal can be beneficiated while allowing for separation of smaller-sized particles.

Gupta and Yan (2006:535) explain that with the reduction in radius near the apex of the DMC, and therefore much larger centrifugal force, the concentration of medium particles is higher than that which is mixed with the feed. This is considered the main reason why separation in the cyclone occurs at a slightly higher specific gravity (SG) than the SG of the feed medium. He and Laskowski (1994:214) have conducted tests on four different magnetite mediums and determined the cyclone overflow and underflow relative densities with respect to variations in the feed medium relative density. Figure 2.13 illustrates the results that were obtained from a small 150 mm DMC. Note that the relative density differential between the underflow and overflow may be used to characterise the medium stability. This figure indicates that, depending on the magnetite properties such as magnetite particle size, there is a certain maximum relative density differential at a specific medium relative density. At high and low medium relative densities the relative density differential becomes smaller.

The density offset can be predicted from the simple equilibrium orbit hypothesis model of the cyclone (equation 2.1) where the density difference between solid and medium is determined (Bradley, 1965). The prediction of overflow and underflow medium density from a DMC is also mentioned in Wood, Davis and Lyman (1987) and Davis and Napier-Munn (1987).

The DMC is typically installed at an angle to the horizontal to allow for sufficient drainage during a shutdown. The typical angle of inclination that is used is 20° (Gupta and Yan, 2006:535). At high feed rates and pressures, this angle does not influence the DMC performance significantly.

A feed pressure of approximately 140 kPa is typically used in industry. Gupta and Yan (2006:535) also describe that the operation of a DMC for coal can make use of a head tank (5 m to 6 m above the cyclone inlet) where medium and ore are added. Both pump and gravity fed coal-washing DMCs generally operate at a head of around  $9D$  where  $D$  is the cyclone diameter. In this particular case, a 5 m to 6 m head will only apply to a cyclone of 550 mm to 650 mm. Mukherjee, Sripriya, Rao and Das (2003:261–265) describe the relationship between the effect of increasing

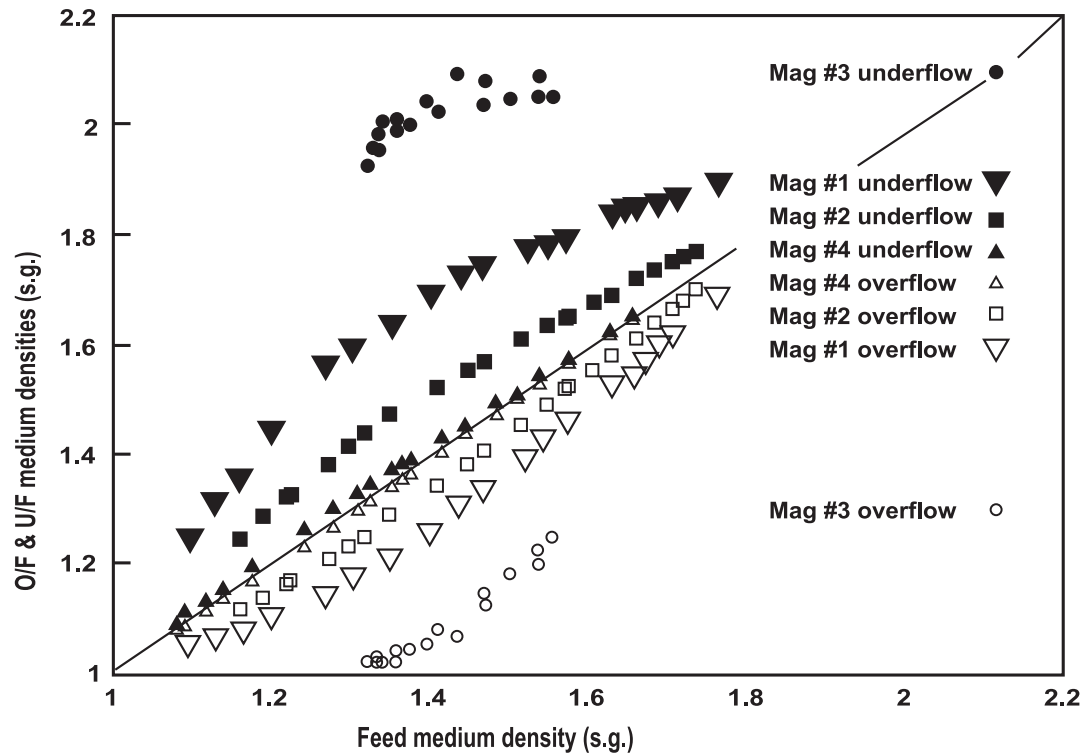


Figure 2.13: Overflow and underflow medium relative density versus feed medium relative density (He and Laskowski, 1994:214).

the inlet pressure of a small 100 mm DMC from 59.5 kPa to 125.7 kPa with a measurement of separation efficiency<sup>1</sup>. This separation efficiency calculation makes use of the combustible and incombustible percentage of coal in the feed and the percentage of combustible coal in the product and discard.

Figure 2.14 illustrates how an increase in feed inlet pressure can result in improved separation efficiency. It must be ensured that the correct spigot size is used to achieve best results. This can be seen in figure 2.14 where a 15 mm spigot diameter has a far lower separation efficiency than a 10 mm spigot diameter.

Figure 2.15 illustrates the effect of feed pressure on the magnetite medium relative density differential between the overflow and underflow. This indicates that an increase in feed pressure will increase the relative density differential of magnetite. This will cause changes in product yield and ash content and must be monitored. Mukherjee *et al.* (2003:267–273) indicate that if pressure is increased in a DMC, the vortex finder and spigot diameter must be increased appropriately, to allow for the increase in feed rate. This will also ensure better separation and possibly improved product yield.

<sup>1</sup>Note that this separation efficiency differs from the DMC EPM separation efficiency.

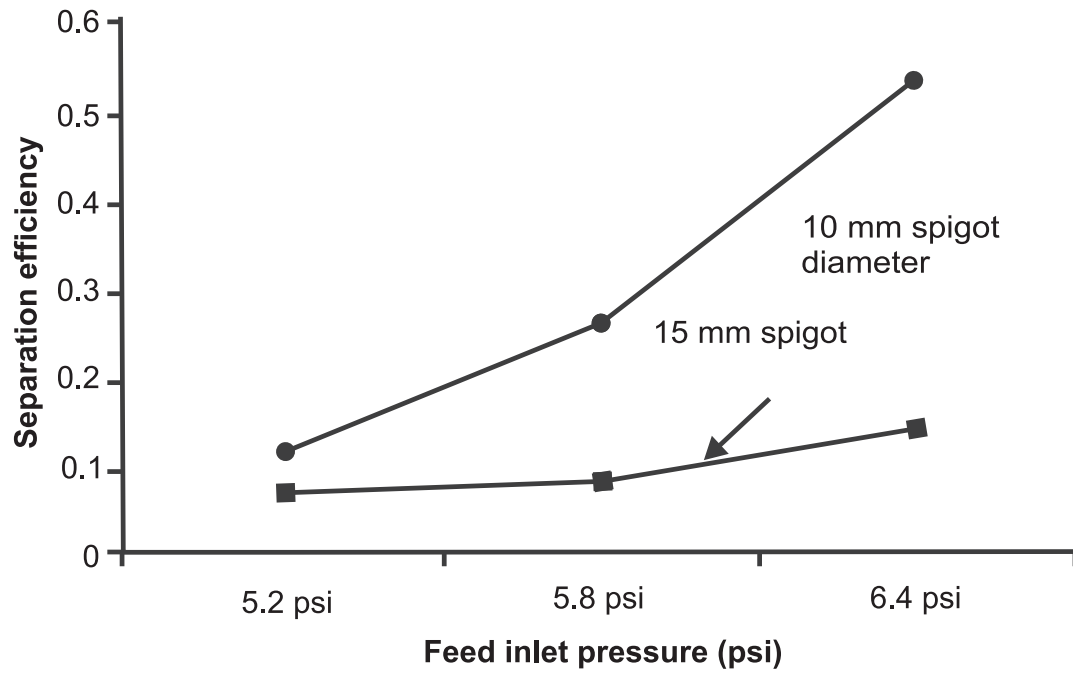


Figure 2.14: Effect of feed inlet pressure on separation efficiency in a DMC (Mukherjee *et al.*, 2003:265).

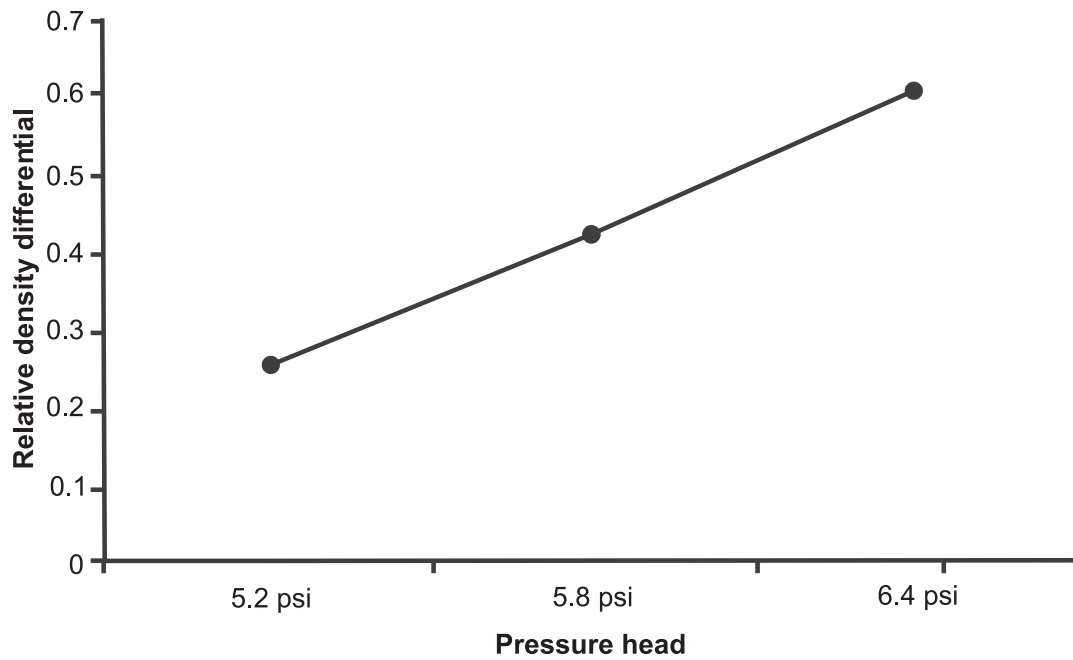


Figure 2.15: Effect of feed pressure on magnetite relative density differential between the overflow and underflow (Mukherjee *et al.*, 2003:267).

Because of the vortex finder and spigot diameter being increased as a result of increased feed pressure and feed rate, the resulting overflow and underflow flow rate will also increase. He and Laskowski (1994:212) indicate that the overflow and underflow flow rate ratio (O/U ratio) is one of the most important operating parameters that affect the DMC performance. They also indicate that an adjustment in this variable requires the spigot and vortex diameters to be adjusted accordingly and will therefore affect the DMC performance indirectly.

Figure 2.16 illustrates how the O/U ratio influences the separation efficiency and cutpoint shift (the difference between the partition relative density and the magnetite medium relative density) of a DMC. This test makes use of a small 150 mm diameter DMC and two different magnetite medium particle sizes. It can be seen that an increase in O/U ratio improves the separation efficiency. He and Laskowski (1994:212) suggest that an O/U ratio of 2 be used as an optimum for coal beneficiation, but this will depend on the coal properties of the ore. If the O/U ratio is made too high, the feed will cause roping and jamming of the cyclone.

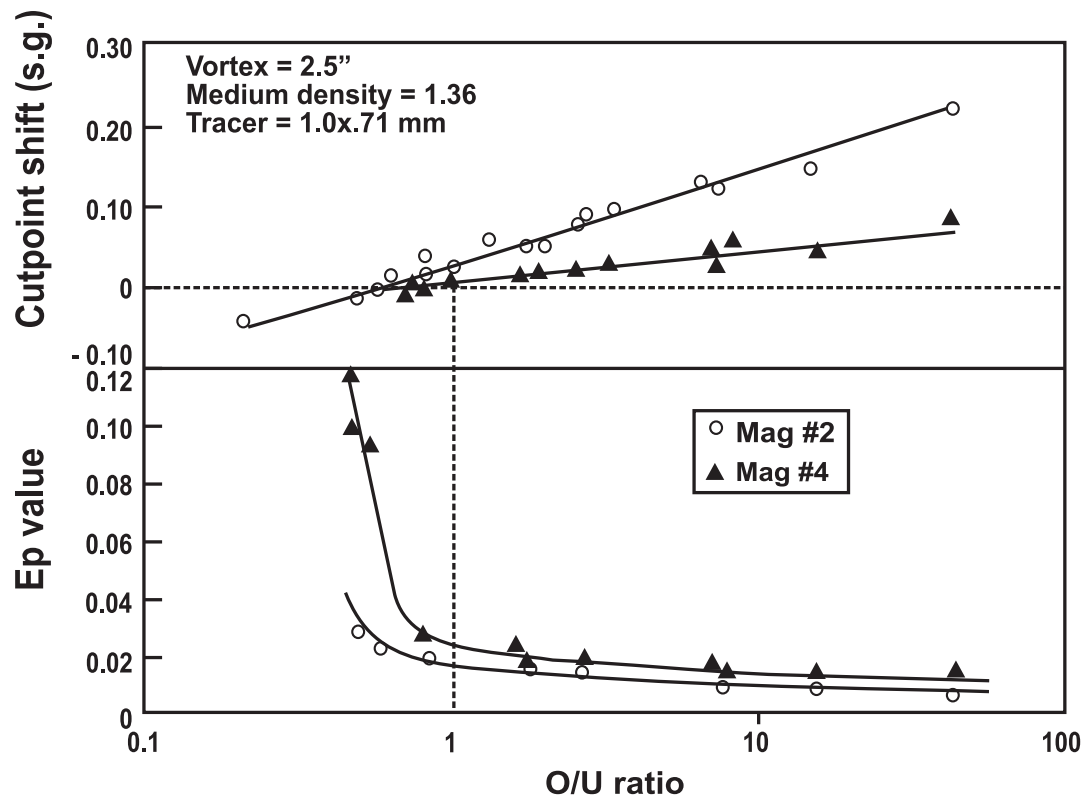


Figure 2.16: Feed overflow to underflow flow rate ratio and its effect on separation efficiency and cutpoint shift (He and Laskowski, 1994:213).

Another test that He and Laskowski (1994:213) performed was to determine the effect of changing the medium relative density with respect to medium flow rate

and the O/U ratio while ensuring a constant inlet pressure. Figure 2.17 illustrates that with a constant feed pressure, the medium flow rate is kept constant (this reaffirms the relationship between inlet feed rate and inlet pressure). It also indicates that changes in medium relative density do not influence the inlet feed rate (owing to inlet pressure being kept constant) and the O/U ratio. By making use of four different particle sizes for the magnetite medium, it can be illustrated that magnetite particle size also has very little or no influence on these parameters.

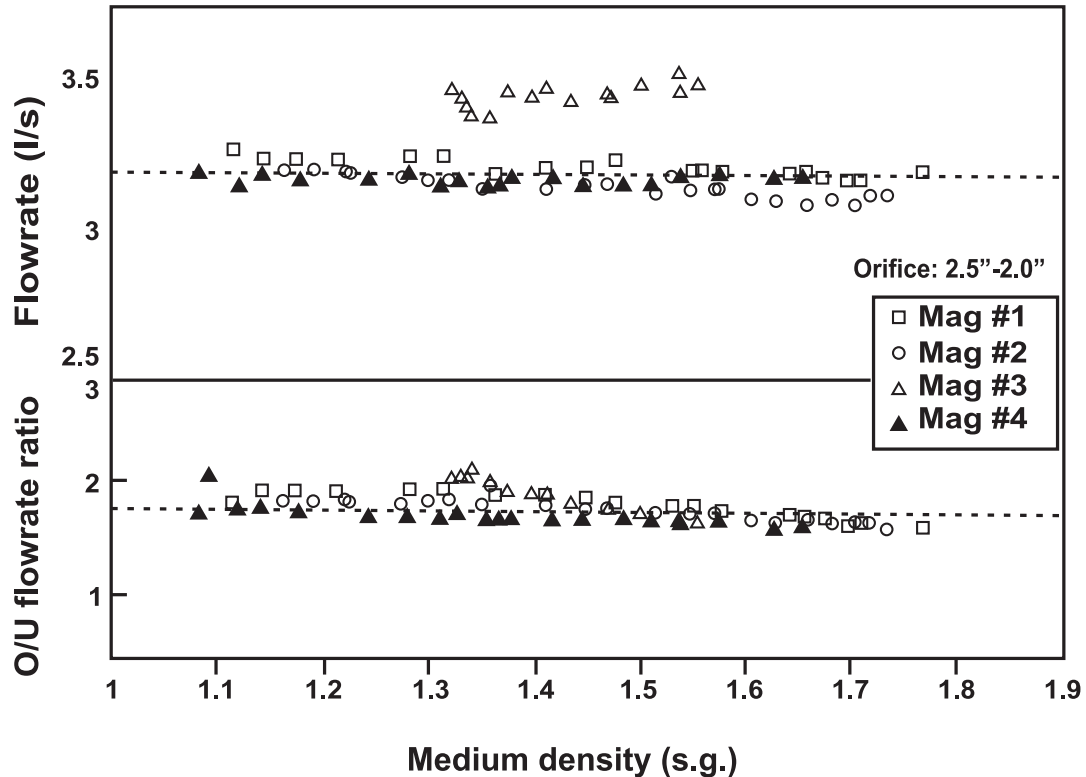


Figure 2.17: Medium relative density and its effect on medium flow rate and overflow to underflow flow rate ratio (He and Laskowski, 1994:213).

The typical medium-to-coal ratio that is used is 5:1 to allow for the greatest efficiency of separation, while a ratio of 3:1 or less will cause a decrease in operational performance (Gupta and Yan, 2006:535). King and Juckes (1984:151–153) indicate that the cutpoint shift ratio ( $\frac{S_c - S_m}{S_m - 1}$ ) increases significantly with a decrease in medium-to-coal ratio (Figure 2.18).  $S_c$  is the partition relative density and  $S_m$  is the medium relative density.

Cyclones can vary in sizes from 0.5 m to 1.2 m in diameter (Gupta and Yan, 2006:535). Preptech (2008:5) gives a number of examples of different cyclones that are available from Multotec. Table 2.5 indicates some of the DMCs that are available from a South African manufacturer. From this table it can be seen that an increase in cyclone diameter allows for an increase in cyclone capacity.



An increase in medium relative density also shows an improvement in cyclone capacity. England *et al.* (2002:164) provide a more detailed range of cyclone capacities that are available (Table 2.6).

Table 2.5: Different DMC equipment available from Multotec (Preptech, 2008:5).

DMC capacity at nine times the diameter pressure and 1,5 coal relative density			Capacity (t/h) at medium-to-coal ratio 4:1		
Cyclone model	Diameter (mm)	Inlet type	Medium relative density of 1.4	Medium relative density of 1.5	Medium relative density of 1.6
MA510-20-1	510	High capacity	75	79	83
MA660-20-1	660	High capacity	133	141	148
MA800-20-1	800	High capacity	206	218	230

Table 2.6: DMC capacity table (England *et al.*, 2002:164).

Cyclone diameter (mm)	Medium + coal capacity at nine times the diameter pressure (m <sup>3</sup> /h)	Maximum feed coal capacity (t/h)	Maximum top size (mm)	Maximum spigot solids (m <sup>3</sup> /h)
6.3	9.0	14.1	20.3	27.6
21	25	28	36	42
25	36	55	84	121
36.1	45.6	56.3	75.0	95.0
47	53	59	68	77
69	100	155	236	341
157	205	262	368	491
360	420	510	610	710
441	577	736	1035	1382
800	900	1000	1150	1300

Bosman and Engelbrecht (1999:5) conducted a study for Multotec Process Equipment Pty Ltd in which a number of cyclones with different diameters were analysed according to imperfection ( $\frac{E_p}{\rho_{50}}$ ) and ore particle size. Figure 2.19 illustrates these relationships. It can be seen that at each DMC diameter size (represented as horizontal lines) there is a breakaway point where the efficiency or imperfection deteriorates as ore particle sizes decrease. This breakaway point becomes smaller as the DMC diameter size is reduced. This diagram can serve as a good guideline when determining DMC characteristics based upon feed particle size. Bosman and Engelbrecht (1999:5) indicate that these values can change depending on factors such as medium viscosity and stability.

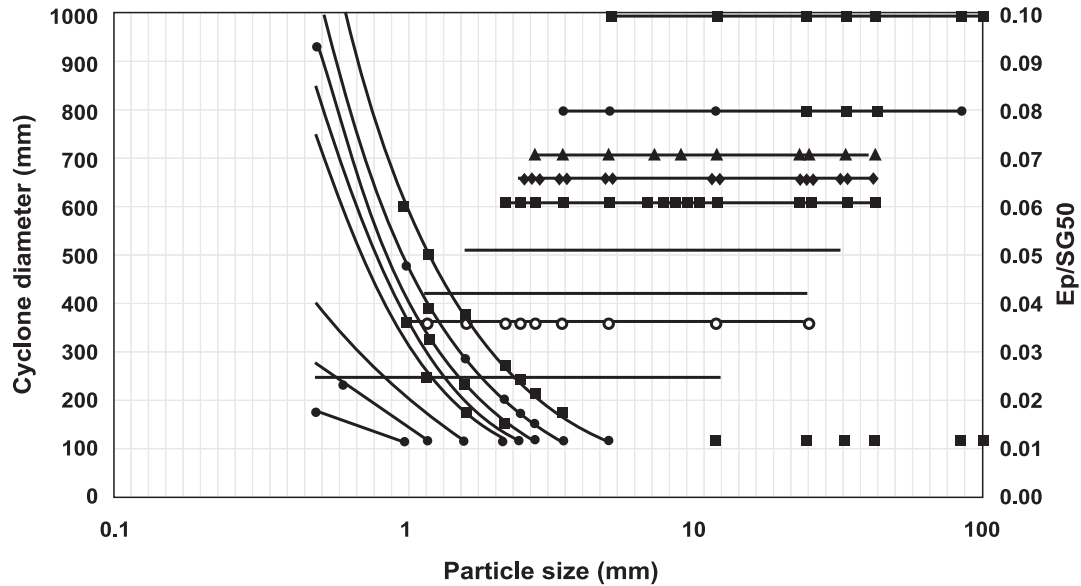


Figure 2.19: DMC diameter (represented as horizontal lines) and EPM versus ore particle size (Bosman and Engelbrecht, 1999:5).

#### 2.4.4 Dense medium separation circuits and process units

The process flow of coal washing plants is relatively simple when compared to other metallurgical operations (King, 1999:14–15). The process flow consists of relatively simple processing units and the performance of these units can be calculated to make the various combinations and simulations possible. These simulations can then be analysed to determine which combination is better suited to the type of coal being beneficiated. Figure 2.20 illustrates what a typical process flow diagram looks like for a variety of feed coal size fractions.

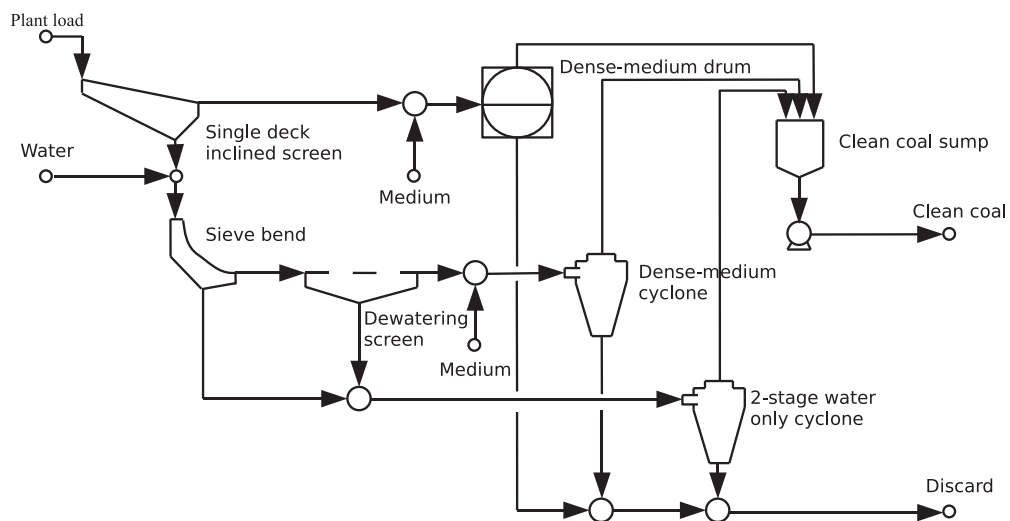


Figure 2.20: Typical modern process flow diagram to treat a variety of size-spectrum coal feeds (King, 1999:16).

After comminution and particle size classification have occurred at the mine, the ore is initially fed into a screen where very coarse material or overrun ore is washed in a dense medium drum. The intermediate-sized ore is beneficiated by DMCs and the fines can be washed by water-only cyclones. Process flow circuits for coal beneficiation can vary because of the different product specification requirements for the market.

England *et al.* (2002:166) indicate some differences from figure 2.20 in that a mixing box for the medium and the ore is used and some more detail in the density control is shown. They also describe the process flow of the magnetite recovery making use of a magnetic separator and demagnetising coil. Figure 2.20 does, however, describe the general objective of a coal-washing circuit.

Figure 2.21 is an illustration of a dense medium drum circuit. This diagram illustrates the typical circuit used for separation of large particle sizes by making use of the dense medium drum. The medium is recovered by making use of a magnetic separator. This medium is collected into a sump and a density controller is used to correct the density of the medium that is added to the crushed coal ore. The initial screen is used to classify the ore so that the smaller sized coal feed can be separated in the DMC circuit.

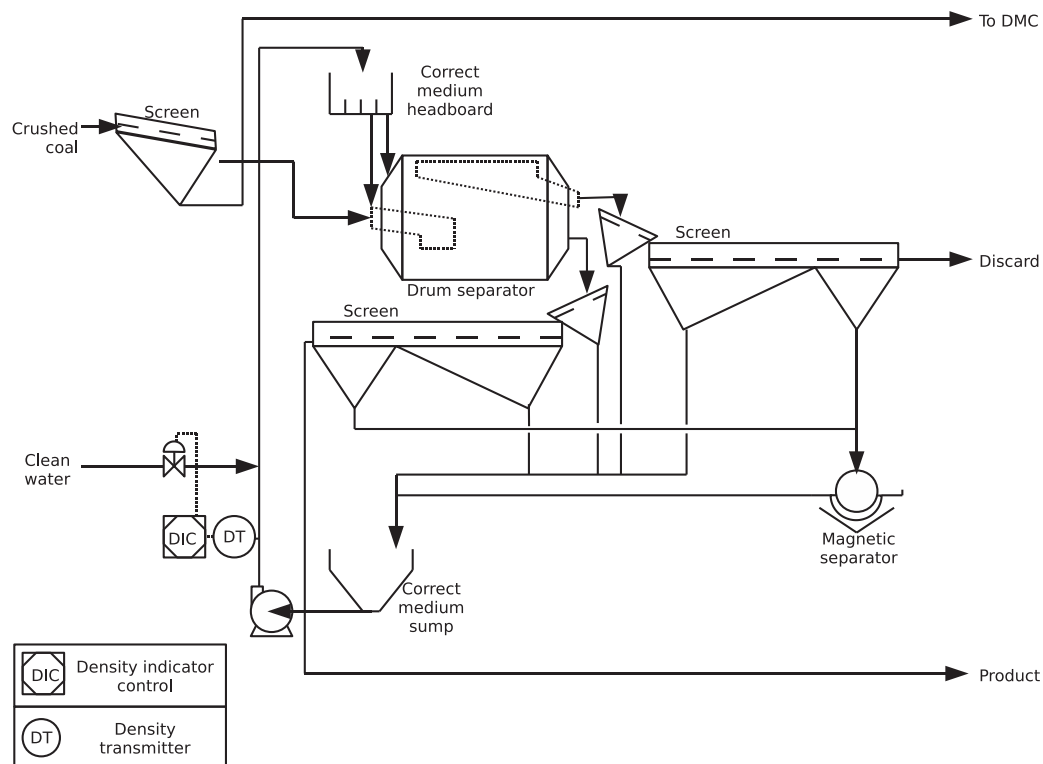


Figure 2.21: Dense medium drum with circulating medium circuit (Adapted from England *et al.* (2002:157)).

The DMC circuit (Figure 2.22) has a similar layout to the drum circuit, except that the drum has been replaced by a DMC with a mixing box and pump. Figure 2.22 also indicates the magnetite in closed circuit with a density controller. The undersized material from the DMC circuit consists of the fines. These fines can either be separated using froth flotation ( $-350 \mu\text{m}$  material) or water-only cyclones (Kalyani, Charan, Haldar, Sinah and Suresh, 2008:94–95); however, in the case of Leeuwpaan, the fines (called ultra-fines,  $+1 \mu\text{m}$  to  $-350 \mu\text{m}$ ) are beneficiated further using smaller DMC units. The ultra-fine cyclones at Leeuwpaan consist of 400 mm cyclones in series with 360 mm cyclones. This can be seen in the piping and instrument diagrams of Leeuwpaan in addendum B. At Leeuwpaan different-sized cyclones are used to produce coarse ( $+6 \text{ mm}$  to  $-25 \text{ mm}$ ) and fine ( $+1 \text{ mm}$  to  $-6 \text{ mm}$ ) material. The coarse cyclones have a diameter of 800 mm while the fine cyclones have a diameter of 710 mm.

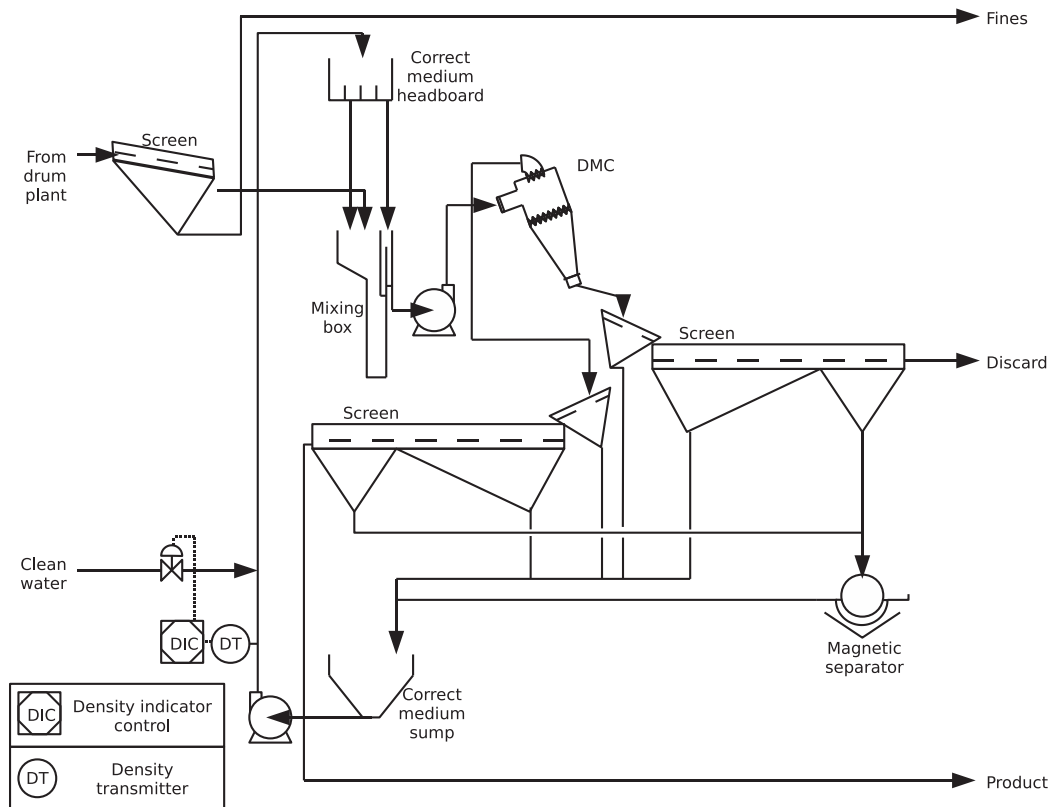


Figure 2.22: DMC with circulating medium circuit (Adapted from England *et al.* (2002:166)).

#### 2.4.4.1 Screens

Sizing and screening are typically used in DMS to ensure that initially the correctly sized ore is fed into the specifically sized separation circuit that has



been designed. Drain and rinse screening is also performed on the coal and discard products to remove and recover the medium that has been used in the process.

England *et al.* (2002:61–87) provide a detailed study on screening and its use in coal beneficiation. This section will make use of this reference to provide a brief overview of the equipment operation and basic principles.

Screening is the process where non-uniform particles of different sizes are separated by a surface opening that is designed for a specific size group. In other words, particles that are smaller than the size group will pass through the surface opening, while particles larger than the size group will not. The size opening of a screen is called the aperture size and can be made into different shapes, typically square, rectangular or round. The cut size of the screen is the actual diameter size of coal or ore that will pass through the screen. This value is typically 20% smaller than the aperture size and is dependent on the efficiency of the screen.

Screen efficiency can be measured as the ratio of undersized particles that have passed through the screen apertures to the actual amount of undersized particles in the original feed. The screen efficiency can also be calculated as the product of oversize and undersize displacements.

The screens that are used in coal beneficiation typically make use of vibration to move the feed across the surface or deck of the screen. This vibration is referred to as the throw or stroke of the screen and is measured as the distance that a particle is thrown away from the screen surface by the motion of a drive.

Some of the parameters that influence the operation of a screen are its slope, speed, particle shape, moisture in the feed and tonnage fed. If the slope of the screen is increased, more material will be allowed to move over the deck. This means that the capacity of the screen is increased; however, the efficiency of separation is reduced. This is because the openings in the screen are effectively reduced owing to the inclination. By increasing the speed of vibration of a screen, the throw of particles will be higher and particles will be allowed to separate even more in the bed. This will result in improved efficiency. Physical limitations prevent a screen from being operated at very high vibration speeds.

Moisture in the feed can cause blinding of the screen as fine particles stick to larger particles, thus preventing separation. Wet screening can overcome this and is typically used in coal beneficiation. High-pressure water sprays are used

to wash the feed on the screen deck.

The feed rate of the ore into a screen can influence the efficiency of a screen if it exceeds the designed capacity. Figure 2.23 illustrates what this relationship typically looks like.

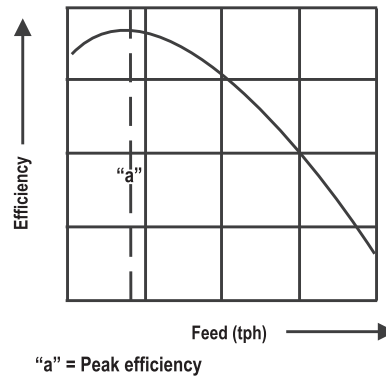


Figure 2.23: Relationship of screen efficiency and feed rate (England *et al.*, 2002:66).

In some cases, a screen can consist of more than one deck (double- or triple-deck screens). A double-deck screen will be able to separate ore by making use of two different aperture sizes. The larger aperture sized screen will be at the top, while the smaller sized screen will be below. This allows for separation of coarse, fine and ultra-fine particles and is used in the Leeuwpan DMS plant. The disadvantage of a double-deck screen is that the stroke is sized according to the upper deck and could result in the lower deck not operating efficiently. A stroke that is too small will cause the material to peg or blind, while a stroke that is too large will cause undesirable ore breakage.

#### 2.4.4.2 Drum separators

Hayes (2003:85) describes horizontal drums as being used for DMS of coarse material (+15 mm to -100 mm). The process operates on the principle of float and sink analysis where particles of different densities to the medium can either float or sink in the medium because of gravity. Feed is mixed with the medium and passed through a relatively static container. There is a wide range of equipment configurations for horizontal drums, two of which are described by England *et al.* (2002:159–161).

The Wemco drum separator as seen in figure 2.24 consists of a steel shell equipped with a tyre and collar construction (Wilkes, 2006:180). Rollers are engaged with

the tyres to support the drum shell and maintain the drum to operate in a longitudinal position. A drive chain and motor rotate the drum shell at a required operating speed. Medium is added to the feed chute and sinks launder. While the drum is rotating, sinks are collected by sink lifters and discharged into the sinks launder. The floats are carried through the lower exit.

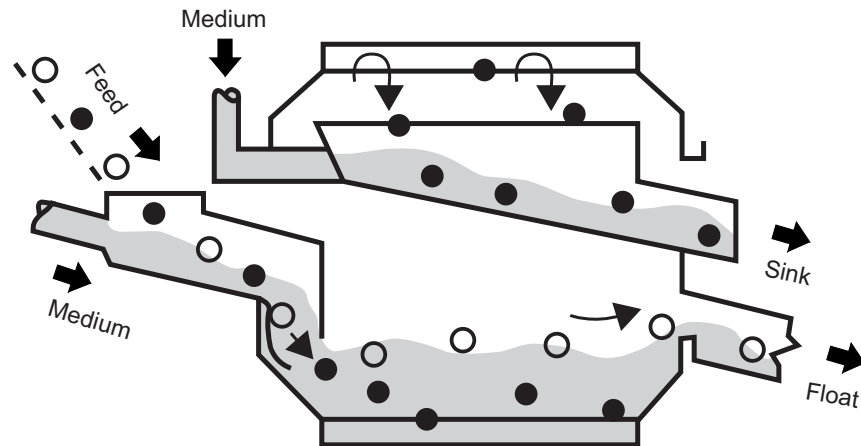


Figure 2.24: Typical operation of the Wemco drum (Wilkes, 2006:180).

The Teska drum or bath (England *et al.*, 2002:160) makes use of a bucket wheel that rotates around an open bottom tank filled with medium. The tank has an opening at the bottom to allow for discard to sink into the bucket wheel. The floats or clean coal exit the tank overflow while the sinks are drained and collected in a refuse launder. Medium is drained from the tank and collected and circulated by making use of a medium sump. This ensures a constant relative density throughout the system. Figure 2.25 illustrates this operation of the Teska drum.

#### 2.4.4.3 Dense medium cyclones

Hayes (2003:85) describes how cyclones are used for DMS of smaller material (+0.5 mm to -50 mm). They allow for a more efficient separation and a larger throughput. The DMC has been described in more detail in section 2.4.3.1 of this chapter.

#### 2.4.4.4 Magnetic separators

In the DMS process, medium is recovered in the drain and rinse screens (Figures 2.21 and 2.22) from the product and discard after the separation process. Magnetite is initially drained off the material to form the correct medium.

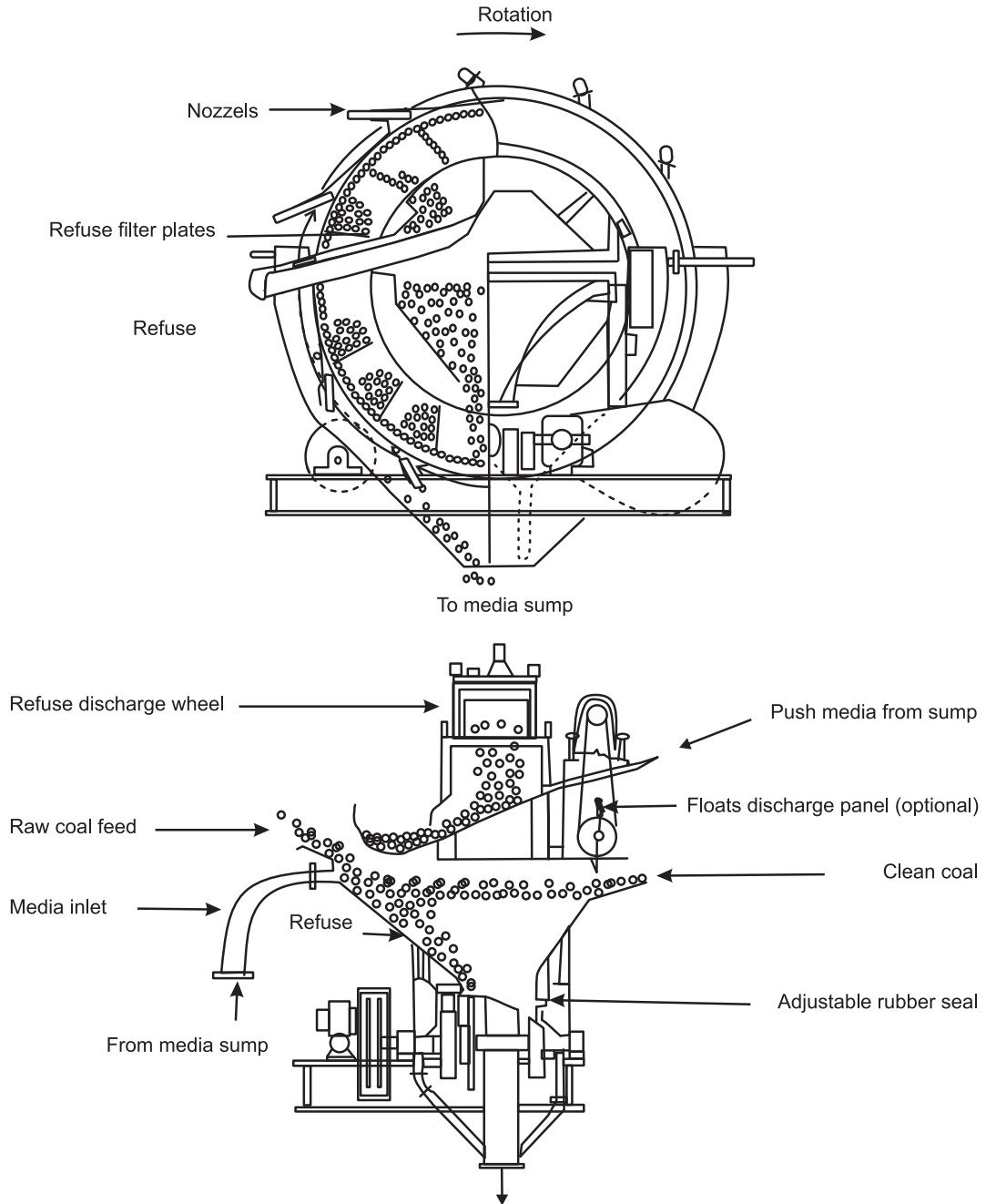


Figure 2.25: Illustration of a Teska drum (England *et al.*, 2002:161).

The medium particles that have adhered to the material are sprayed with high-pressure water. This forms a diluted medium that has to be cleaned and concentrated so that it can be recycled (England *et al.*, 2002:172–173).

Wet magnetic separators are typically used to clean and recover the dilute magnetite. Hayes (2003:92–95) describes the process as a low-intensity magnetic field that carries particles with magnetic properties by a drum separator. Wet drum separators can be configured as co-current, counter-rotating and counter-current. Figure 2.26 illustrates a typical magnetic separator where the feed slurry is sent into a trough. Since this figure illustrates a co-current separator, the feed moves in the same direction as the rotating drum. In a counter-rotating separator, the feed moves through the trough in the opposite direction to the drum rotation. The counter-current separator feeds the slurry in the same direction as the drum rotation. However, the tailings are fed back into the feed while the concentrate discharges at the end. This configuration can consist of a number of separators in series.

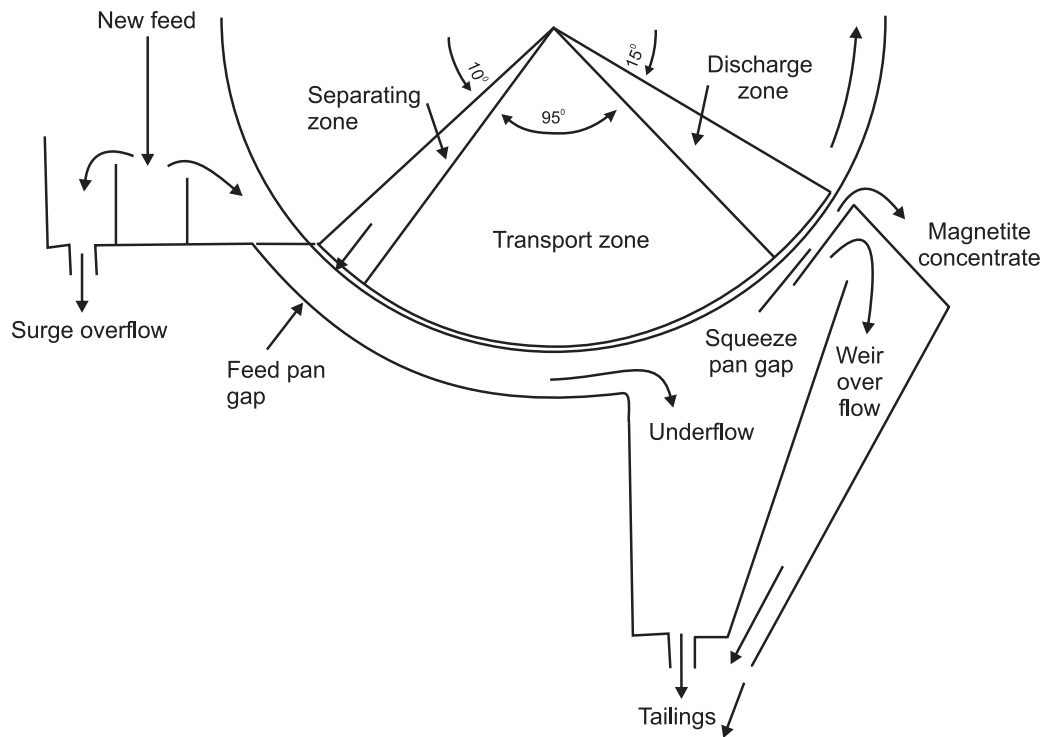


Figure 2.26: Wet drum magnetic separator operating in co-current configuration (Rayner and Napier-Munn, 2003:163).

England *et al.* (2002:174) indicate that the latest strontium-ferrite magnetic separators recover 99.98%. This can result in losses being as low as 0.06 kg/m<sup>3</sup> of magnetite in the dilute medium effluent or tailings. After the magnetite has been recovered, the particles can still retain their magnetic properties. It is necessary to

demagnetise the medium after it has been recovered, as this can result in medium instability in the DMC or dense medium drum (England *et al.*, 2002:177).

#### 2.4.4.5 Instrumentation and field devices

Figures 2.21 and 2.22 indicate density control of the magnetite used in the DMS process. Density measurement forms an integral part of this controller. Mikhail and Humeniuk (1980:391) describe a gauge or instrument that measures density by making use of gamma radiation (radioactive source Cesium 137).

This source passes gamma radiation through a pipe with slurry flowing through it (Figure 2.27). In this case, the slurry is the magnetite medium. The gauge measures the intensity of the absorption of gamma radiation. This is inversely proportional to the relative density of the slurry,

$$I_o = I_i e^{-\mu \rho_s \chi}, \quad (2.3)$$

where  $I_o$  is the intensity of radiation passing out of the pipe or slurry,  $I_i$  is the intensity of radiation passing into the pipe or slurry,  $\mu$  is a measure of the mass absorption coefficient,  $\rho_s$  is the relative density of the slurry and  $\chi$  is the distance between the detector and source.

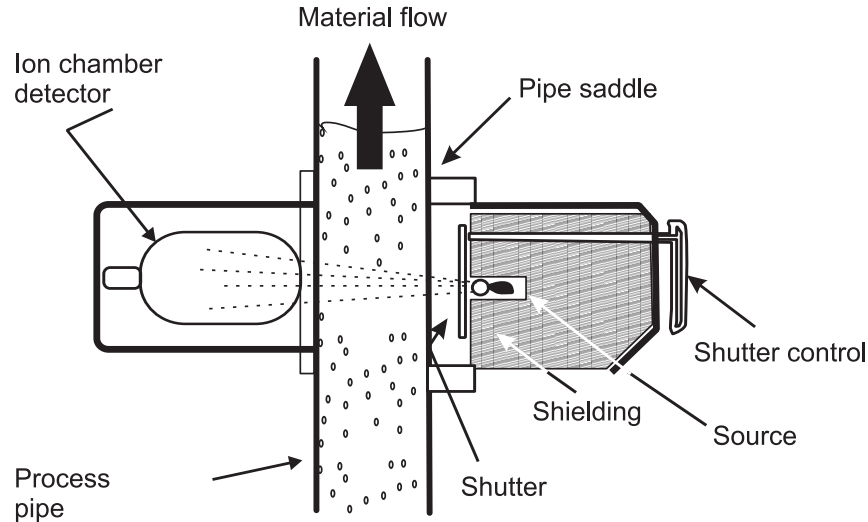


Figure 2.27: Illustration depicting the principle of density measurement by using gamma radiation (Lipták, 1995b:631).

In equation 2.3, it is assumed that the absorption coefficient ( $\mu$ ) and distance ( $\chi$ ) are constant. This results in the measured intensity ( $I_o$ ) being a function of the slurry relative density ( $\rho$ ) and therefore allowing the density measurement to be made available.

Figures 2.21 and 2.22 also indicate control valves being used to regulate the amount of clean water addition to the magnetite slurry for the density control. These valves are typically pneumatically driven. Seborg, Edgar and Mellichamp (1995:215–221) describe the principle and operation of a pneumatic valve as a final control element. The valve positioner forms an important part of the valve, as it controls the position of the stem, which is used for moving the valve plug to adjust the size of the area made available for fluid flowing through it. Figure 2.4 illustrates an example of a pneumatic control valve.

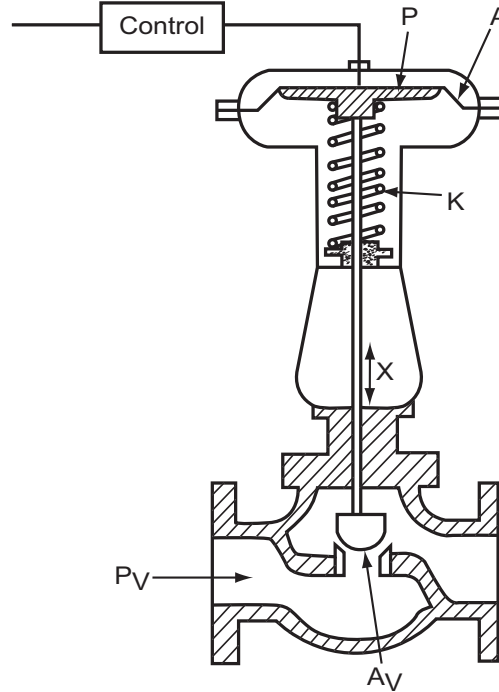


Figure 2.28: Example of a pneumatic control valve (Lipták, 1995a:422).

The flow rate ( $q_v$ ) of the fluid after the valve is proportional to the valve positioner function ( $f_v(l_v)$ ),

$$q_v = C_v f_v(l_v) \sqrt{\frac{\Delta P_v}{\rho_f}}, \quad (2.4)$$

where  $\Delta P_v$  is the pressure drop across the valve,  $\rho_f$  is the relative density of the fluid and  $C_v$  is the valve coefficient describing valve capacity and size. The positioner is a function of the lift ( $l_v$ ) describing the percentage opening of the valve. The positioner function is dependent on the valve type. A linear valve type ( $f_v(l_v) = l_v$ ) means that the positioner function has a linear relationship with the lift. A quick opening valve type ( $f_v(l_v) = \sqrt{l_v}$ ) has a square root relationship allowing more flow at lower percentage openings. An equal percentage valve type ( $f_v(l_v) = R_v^{l_v-1}$ ) allows for an equal percentage change in flow for each change in lift.  $R_v$  is a valve design parameter that is typically between 20 and 50.

A measurement that is typically used in DMCs is the pressure at which the feed is pumped into the inlet. (This is shown in the coarse and fine dense medium cyclones process and instrument diagrams of Leeuwpan in addendum B.) Seborg *et al.* (1995:211) indicate that differential pressure can be measured by using a strain gauge to measure a diaphragm deflection between two process pressures (Figure 2.29).

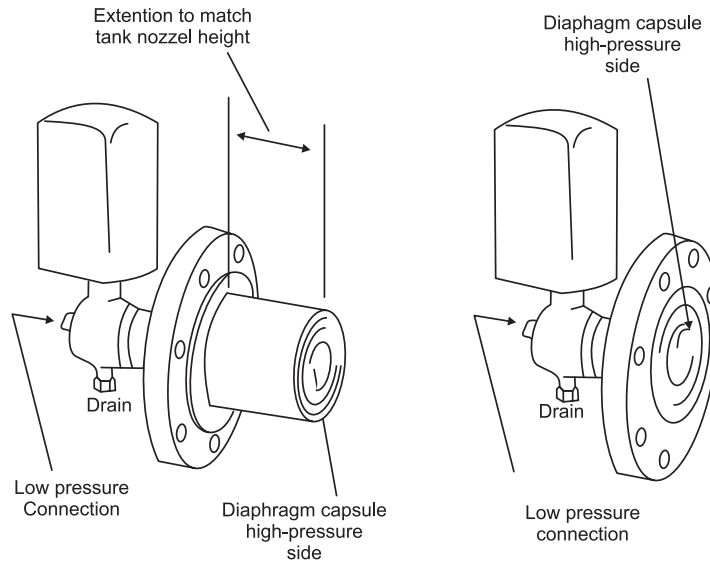


Figure 2.29: Graphical representation of a differential pressure cell (Lipták, 1995b:553).

Other measurements that are made available in DMS operations include feed rates and tank levels. Addendum B illustrates the feed rate measurement points on the ore fed into each module, the feed into the drum and the feed of the products. Belt scales are typically used to measure the feed rates of conveyor belts. The feed rates are typically controlled by varying the speed of the conveyor belt or the vibrating feeder of that specific production line. Variable speed drives can be used to accomplish this where the frequency of the electrical motor driving the conveyor or feeder can be varied. Level measurement is typically done on the magnetite make-up and recovery circuits with certain storage tanks.

Cierpisz, Mironowicz and Mirkowski (1980:375) describe some measuring devices that are used for measuring coal quality in automatic control. The parameters that are measured include ash, moisture, sulphur and calorific value. Figure 2.30 shows how some of these parameters can be measured on-line from a conveyor belt.

Ash content in coal can be measured by radiometric means or by using the relationship between bulk density of coal and ash content (Cierpisz *et al.*, 1980:376–378). The radiometric ash-meters measure ash content in coal

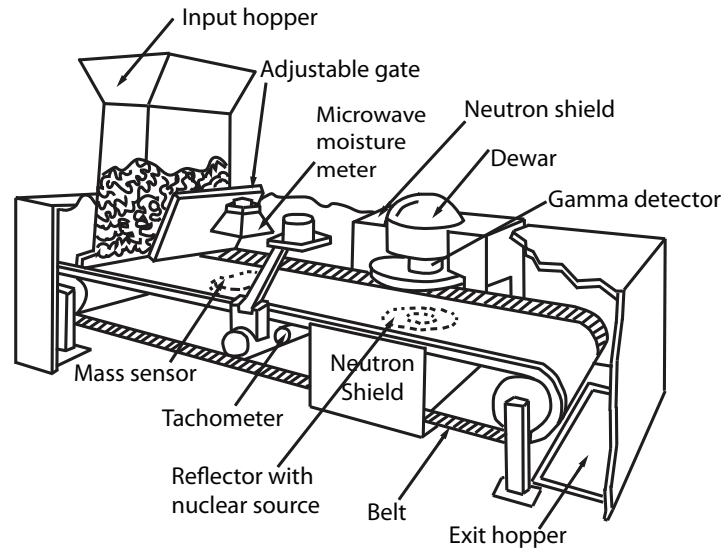


Figure 2.30: Illustration of on-line coal analysis (Lipták, 1995b:957).

continuously over a conveyor belt. Gamma radiation using a radioactive source is directed through the coal and conveyor belt. Systems can detect either the back-scattered gamma radiation or the attenuation of gamma radiation (Figure 2.31) through the coal. The intensity of the detection is calibrated to an ash content in the coal. Borsaru, Dixon, Rojc, Stehle and Jency (2001:408) mention that it is important to measure high- and low-energy regions of the back-scatter spectrum. This means that the instrument must be able to acquire spectrometric measurements across the whole back-scatter spectrum.

Watt and Sowerby (1983:266) describe the intensity calculation for the attenuation of gamma rays as being the same as equation 2.3 for the density gauge except that the mass absorption coefficient  $\mu$  varies while other variables are assumed constant. By using low ( $\mu'$ ) and high ( $\mu''$ ) energy gamma-ray sources, the concentration of ash ( $C_{ash}$ ) can be determined as

$$C_{ash} \approx \frac{a\mu'}{\mu'' + b}, \quad (2.5)$$

where  $a$  and  $b$  are constants that are determined as mass absorption coefficients.

Watt and Sowerby (1983:277) describe the pair production gauge (Figure 2.32) for back-scattered radiation. Very high energy gamma radiation is used to create positron-electron pairs, which are annihilated when interacting with the coal. Gamma-rays are generated in the opposite direction and their intensity is used to measure ash content.

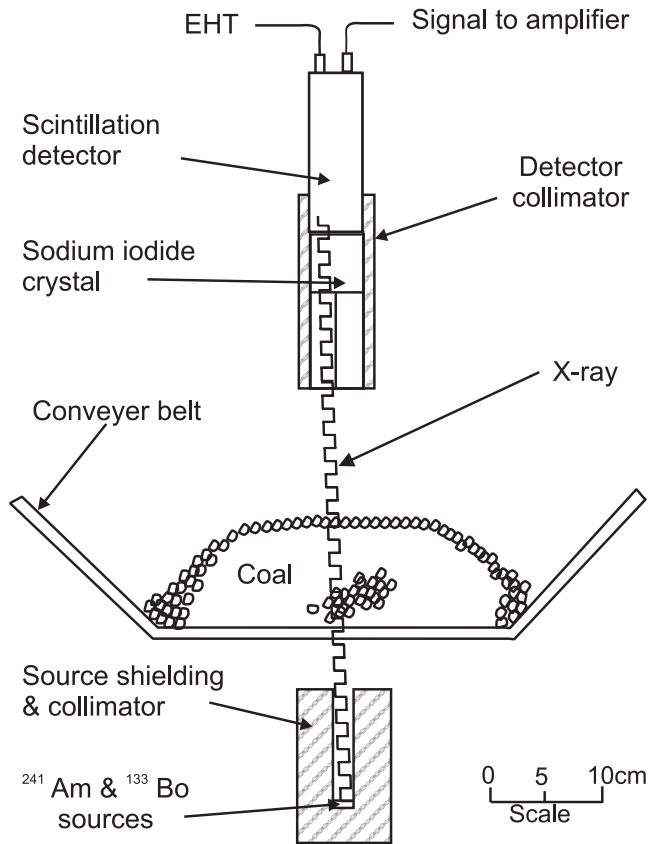


Figure 2.31: Low-energy gamma-based radiation directed through a conveyor belt to determine ash content in coal (Watt and Sowerby, 1983:265).

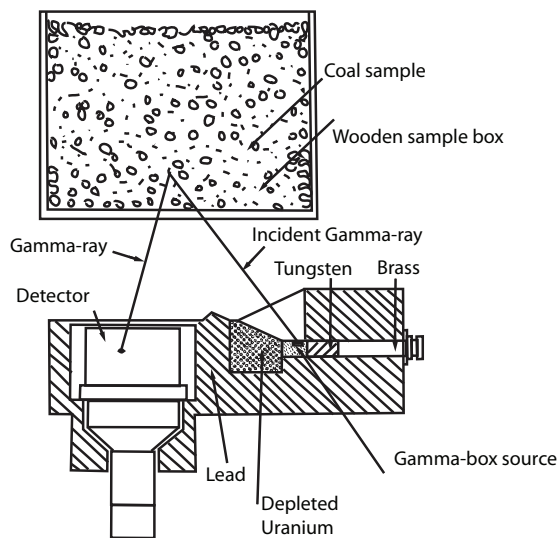


Figure 2.32: Illustration of a pair production gauge (Watt and Sowerby, 1983:278).

Several other methods are used to determine ash content based on x-rays and gamma-rays (Watt and Sowerby, 1983:264). A neutron technique can also be used to determine concentration of individual elements of the ash content and total ash. Figure 2.30 shows the configuration of a neutron ash analyser. Gu, Cheng, Yin, Qiao, Liu and Zhang (2005:23) describe the fundamentals and principles on which a neutron coal analyser operates and also indicate that this method of coal analysis is more accurate and effective than conventional techniques. Measuring the induced capture spectrum from the thermal neutrons that have bombarded the coal ore by a pulsed neutron beam, makes it possible to analyse the spectrum data and determine the elemental analysis of the coal ore. Gu *et al.* (2005:22) indicate that this technique can be used for measuring not only ash, but also carbon, oxygen, hydrogen, sulphur and water percentages. Figure 2.33 illustrates how the different elements can be detected based on different spectrum analysis.

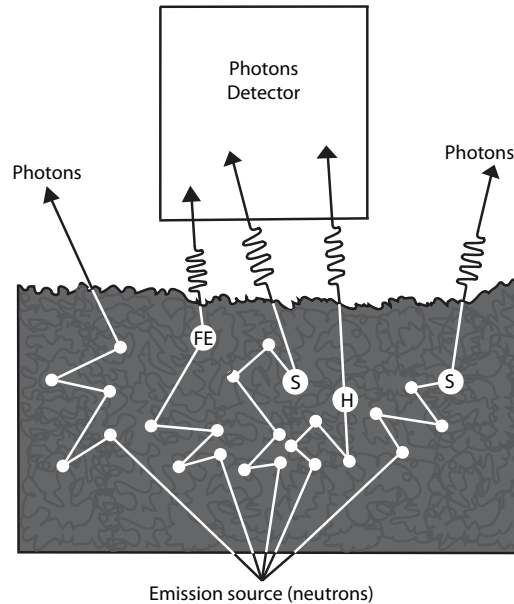


Figure 2.33: Principles of a neutron-based coal analyser (Lipták, 1995b:957).

Mikhail and Humeniuk (1980:390–392) describe the method through which ash content can be calculated by making use of a linear relationship between the relative density of a specific coal and its ash content between 5% and 50% ash. This linearisation is made on the assumption that there is little variation in the quality of the feed material. The calculation begins with determining the relative density of the coal ( $\rho_{coal}$ ),

$$\rho_{coal} = \frac{D_{pulp}M_{coal}}{M_{coal} + M_w(1 - D_{pulp})}, \quad (2.6)$$

based on the process flow diagram in figure 2.34.  $D_{pulp}$  is the relative density of the pulp,  $M_{coal}$  is the total mass of the coal in the pulp and  $M_w$  is the total mass

of water in the pulp.

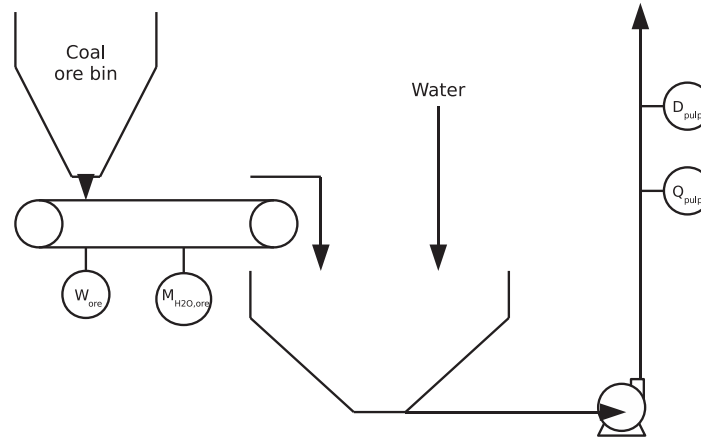


Figure 2.34: Measurement points for in-line ash monitor using a linear coal relative density to ash relationship (Mikhail and Humeniuk, 1980:398).

$M_s$  is calculated as follows:

$$M_s = \frac{(W_{ore} - S_{cf})(100 - M_{H_2O,ore})}{100}, \quad (2.7)$$

where  $W_{ore}$  is the feed rate of the coal ore,  $S_{cf}$  is a correction factor if the weigh feeder or belt scale has an offset error and  $M_{H_2O,ore}$  is the total moisture content of the ore.  $M_w$  is determined by

$$M_w = D_{pulp}Q_{pulp} - M_s, \quad (2.8)$$

where  $Q_{pulp}$  is the volumetric flow rate of the pulp.

After the relative density of the coal has been determined, it is possible to develop a parametric equation relating ash percentage to relative density of the coal through a float and sink analysis ( $C_{ash} = f(\rho_{coal})$ ).

The moisture measurement of coal can be determined either by electrical or microwave methods (Cierpisz *et al.*, 1980:379). Electrical parameters such as conductance (Figure 2.35) and permittivity can be related to moisture. Microwave techniques (Figure 2.36) measure changes in wave attenuation, phase or reflectivity to determine moisture content. These methods can be employed for continuous measurement on belt conveyors.

Sulphur can also be measured by making use of radiometric methods (Cierpisz *et al.*, 1980:381). The absorption of soft x-ray beams that penetrate the coal ore can give an indication of the sulphur content. This technique is similar to the way in which ash content can be measured, as described earlier.

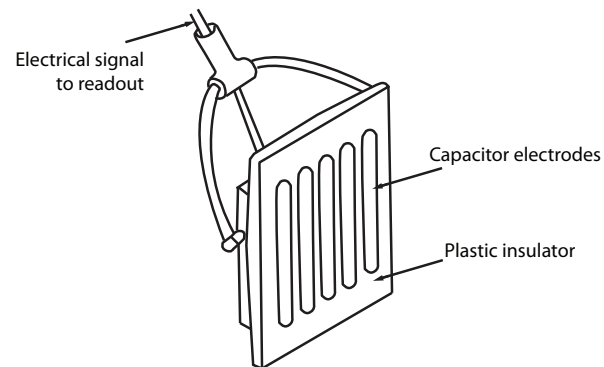


Figure 2.35: Head making use of capacitance to measure moisture in solids (Lipták, 1995b:1082).

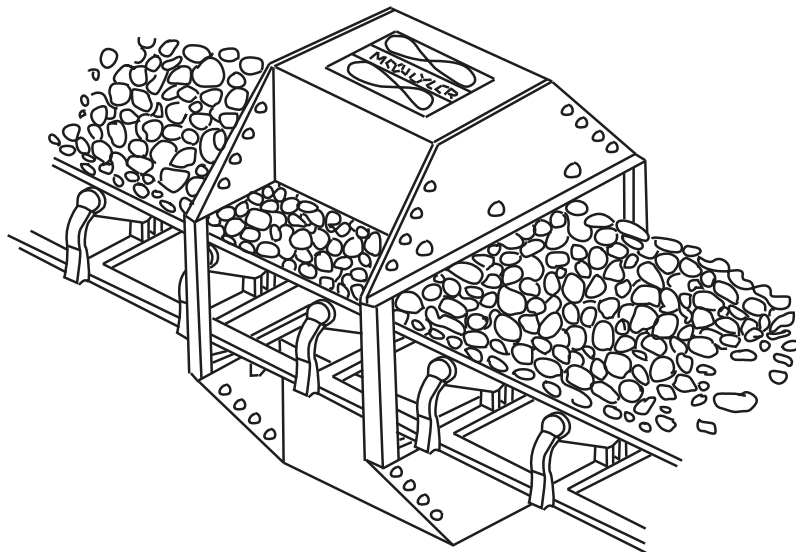


Figure 2.36: Moisture analyser using the microwave principle (Lipták, 1995b:1082).



Cierpisz *et al.* (1980:380) indicate that the calorific value of the coal is determined from the results of ash content and moisture content of the ore. A relationship between these parameters has to be determined beforehand.

## 2.4.5 Mathematical modelling and computer simulations

### 2.4.5.1 Dense medium separators

One of the main parameters which describes a DMC is its efficiency in separating coal from ash. Section 2.4.2.1 describes the use of a partition curve to make this analysis.

Erasmus (1973:2–3) has developed an equation which can be fitted to the partition curve by making use of an ideal washer in which no misplacement occurs. The instantaneous relative density of material ( $\rho(t)$ ) can be described according to

$$\rho(t) = \frac{\tan(t)}{k + c}, \quad (2.9)$$

where  $t$  is time and  $k$  and  $c$  are constants. By evaluating this cyclically with time (Napier-Munn, 1991:332), the imperfect performance can be simulated as

$$Y = \frac{t_2 - \arctan(k\rho - kc)}{t_2 - t_1}, \quad (2.10)$$

proposed by Erasmus (1973:3) where  $Y$  is the partition factor and  $t_1$  and  $t_2$  are constants that describe the upper and lower tails of the partition curve. Regression analysis must be used to fit equation 2.10 to sink and float data such that the constants can be determined.

Another mathematical model for a partition curve described by Napier-Munn (1991:332),

$$Y = \frac{1}{1 + e^{\frac{1.099(\rho_{50} - \rho)}{E_p}}}, \quad (2.11)$$

is derived by substituting equations from Lynch (1977), King and Jukes (1984:151) and King and Jukes (1988).

Napier-Munn (1991:340–341) also explains that each partition curve changes with respect to ore feed particle size. Scott and Napier-Munn (1992) noticed that each size-by-size partition curve intersects at one point (called the pivot point). This point occurs owing to the phenomenon where different-sized particles at the same density of the medium split proportionally to the medium since the particles experience no separating force. As a result, a regression similar to equation 2.11

can be expressed as

$$Y_{ij} = \frac{1}{1 + e^{\frac{\ln(Y_p^{-1}) + 1.099(\rho_p - \rho_{ij})}{E_{pj}}}}, \quad (2.12)$$

where  $Y_{ij}$  is the partition number at particle size  $i$  and density  $j$  and  $(Y_p, \rho_p)$  are the coordinates of the pivot point illustrated in figure 2.37. Scott and Napier-Munn (1992) have also expressed  $E_{pi}$ , the EPM or separation efficiency of particle size  $i$ , as an inverse function of particle size ( $d_i$ ). This is defined as

$$E_{pi} = k_{Ep} d_i^{n_{Ep}}, \quad (2.13)$$

where  $k_{Ep}$  is a constant for the model and  $n_{Ep}$  is a hydrodynamic constant.

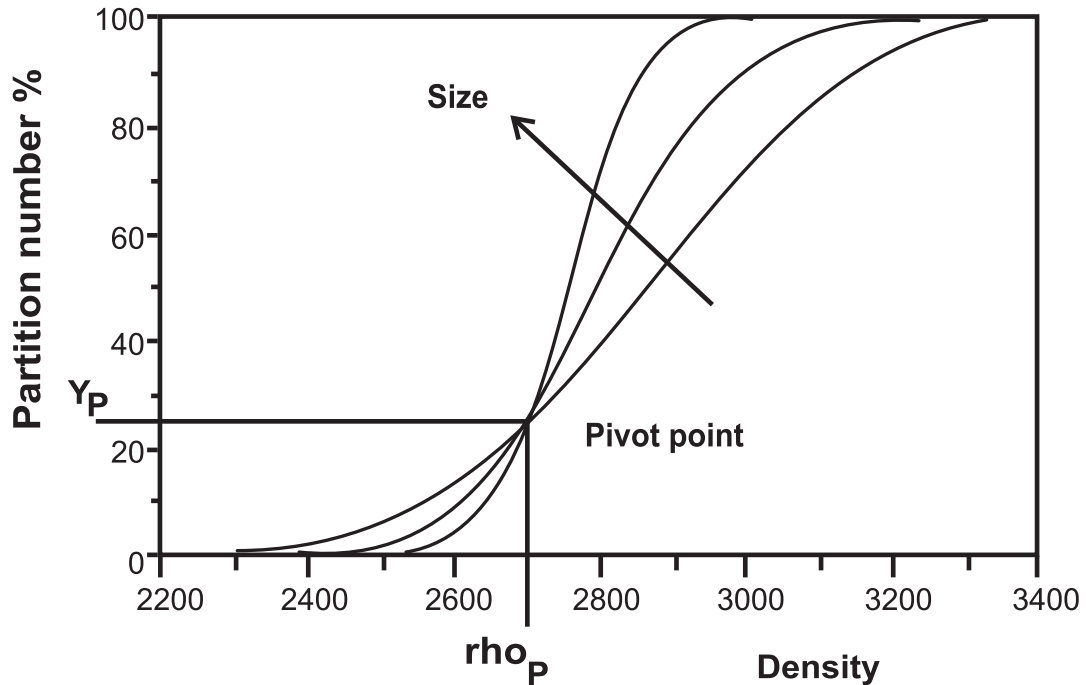


Figure 2.37: Example of a size-by-size partition curve for a DMC (Napier-Munn, 1991:341).

Another technique that has been used to model the size-density ( $d$ - $\rho$ ) partition surface of a DMC without the use of the pivot phenomena is stochastic modelling (Rao, Kapur and Konnur, 2003:447–448). The position of a particle ( $h$ ) within the DMC is modelled by making use of particle settling velocity ( $v_s$ ), drift velocity ( $v_l$ ) due to liquid flow and random velocity ( $V_r$  with zero mean and variance  $\sigma^2$ ). This gives rise to an instantaneous particle velocity,

$$\frac{dh}{dt} = v_s - v_l + V_r. \quad (2.14)$$

With  $V_r$  being normally distributed and  $v_s$  being expressed as a function of gravitational acceleration ( $g$ ), medium relative density ( $\rho_m$ ) and medium viscosity

( $\eta$ ),

$$v_s = \frac{gd^{c_{vsc}}(\rho - \rho_m)}{18\eta}, \quad (2.15)$$

the partition surface can be represented by

$$Y = 50 \left[ 1 - \operatorname{erf} \left( \frac{g}{18\sqrt{2}\eta\sigma d^{c_{vsc}}(\rho - \rho_m)} - \frac{v_l}{\sqrt{2}\sigma} \right) \right]. \quad (2.16)$$

The constant  $c_{vsc}$  could reflect the particle flow regime. Figure 2.38 shows an example of a DMC partition surface that has been generated by making use of a stochastic model by using equation 2.16.

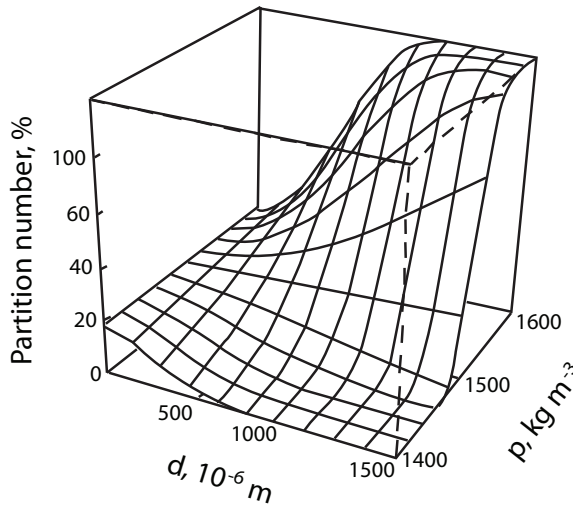


Figure 2.38: Example of a DMC partitioned surface (Rao *et al.*, 2003:444).

A computer simulation by Firth, Grice, Jenssen and Weale (1983:427–428) has been developed to simulate the efficiency of DMS processes. This technique requires a large number of partition coefficient data sets and feed composition data divided into several relative density fractions with respect to each size fraction. This means that sufficient information on the separation process and ore feed size distribution with washability data is required in order for the simulation to be accurate. The model describes the feed rate of the cleaned coal ( $F_c(\rho_{50})$ ) as a function of feed rate of the feed ore ( $F(x_i, \rho_j)$ ) and partition coefficient ( $f_{ij}(\rho_{50})$ ),

$$F_c = \sum_i \sum_i f_{ij}(\rho_{50}) F(x_i, \rho_j), \quad (2.17)$$

for relative density fraction  $\rho_j$  and particle size fraction  $x_i$ .

Another model, which incorporates both size and density partition, was developed by Rao (2004:953–954) using a Weibull function. This efficiency model makes



use of density that is size-dependent, as developed by Plitt (1971), and pivot coordinates. The result is a Weibull model,

$$Y = 1 - e^{\ln\left(\frac{1}{1-Y_p}\right)\left(\frac{\rho}{\rho_p}\right)^{pd^q}}, \quad (2.18)$$

where parameters  $p$  and  $q$  account for turbulence and viscous forces within the DMC. Rao (2004:955) gives a number of solutions for these parameters based on different separators.

The separation cutpoint ( $\rho_{50}$ ) of a DMS process is normally increased or decreased by manipulating the medium density set point ( $\rho_m$ ). Most of the models described above, other than the stochastic model, do not include a relationship between  $\rho_{50}$  and  $\rho_m$ . Napier-Munn (1991:337–340) gives a number of regression functions relating these two parameters based on experimental data. These regression functions vary as the particle size of the ore decreases. A model developed by Clarkson (1983) makes use of a force balance with turbulence to include more operating variables to simulate the performance of separation. The partition curve,

$$Y = \frac{e^{\frac{-Kd^2(\rho_p - \rho_m)}{D_c \eta Q}} - 1}{e^{\frac{-Kd^2(\rho_p - \rho_m)}{D_c \eta}} - 1}, \quad (2.19)$$

was developed to include slurry split ( $Q$ ), density differences between particle ( $\rho_p$ ) and medium ( $\rho_m$ ), particle size ( $d$ ), eddy diffusion coefficient ( $D_c$ ) and a constant ( $K$ ).

A number of hydrocyclone models have been developed and are described by Chen, Zydek and Parma (2000). These models, however, have been developed primarily for particle size classification and not particle separation due to density.

Other DMC models have been developed that make use of more sophisticated techniques, such as computational simulations using Eulerian models for the medium and Lagrangian models for the coal particles (Suasnabar and Fletcher, 1999:202–204). Brennan (2003:60) reports on an algebraic slip mixture model, which makes use of computational fluid dynamics (CFD) to solve the Reynolds averaged Navier Stokes equations. Cortés and Gil (2007:412) indicate that CFD modelling can become very costly owing to the turbulence modelling, making use of large eddy simulations or direct numerical simulations. This is because of the unsteady nature of the flow.

A model developed for dense medium baths or drums has been referenced by Napier-Munn (1991:334). This model, developed by Scott and Lyman (1987),

uses sedimentation theory to express the separation cutpoint as

$$\frac{\rho_{50} - \rho_m}{\rho_{50}} = K_{drm} \frac{\eta^{a_{drm}}}{d^{b_{drm}} \rho_m^{a_{drm}}}, \quad (2.20)$$

where  $K_{drm}$  is called the machine constant and  $a_{drm} = 1$ ,  $b_{drm} = 2$  for laminar flow while  $a_{drm} = 0$ ,  $b_{drm} = 1$  for turbulent flow within the drum. Baguley and Napier-Munn (1996) determined the partition factor for the drum separator as

$$Y = [1 - (v_{100} - v_t)^2] \left( \frac{A_{drm}}{d^2 + B_{drm}} \right), \quad (2.21)$$

where  $v_{100}$  is the terminal velocity, which allows for sinks to be recovered 100%,  $v_t$  is the terminal velocity of the particle and  $A_{drm}$  and  $B_{drm}$  are constants that need to be determined. This model for dense medium baths or drums was developed using an iron ore process and has not been tested for coal.

#### 2.4.5.2 Screens

A computer simulation for screens developed by Firth *et al.* (1983:424) makes use of a similar principle as equation 2.17. However, relative density is not included and the partition coefficient is made a function of nominal screen aperture ( $\delta_{scr}$ ). The model describes the feed rate of the oversized ore ( $F_{scr,o}(\delta_{scr})$ ) as a function of feed rate of the feed ore ( $F_{scr}(x_i)$ ) and partition coefficient ( $S_{scr}(x_i, \delta_{scr})$ ),

$$F_{scr,o} = \sum_i S_{scr}(x_i, \delta_{scr})(F_{scr}(x_i)), \quad (2.22)$$

for particle size fraction  $x_i$ . Firth *et al.* (1983:424) indicate that Gottfried (1973) has developed a generalised equation for wet screening, which can be used to evaluate the partition coefficients per particle size fraction. This equation is

$$S_{scr}(x_i, \delta_{scr}) = e^{-A_{scr} \delta_{scr} \left( \frac{1-x_i}{\delta_{scr}} \right)}, \quad (2.23)$$

where  $A_{scr}(\delta_{scr})$  is a constant dependent on the nominal screen aperture.

#### 2.4.5.3 Magnetic separators

Rayner and Napier-Munn (2003) have developed a model through which recovery of magnetics in a wet drum magnetic separator is determined. This model was based on a flocculation process where the proportion of unflocculated particles is



used as the fractional loss of magnetics ( $L_{msep}$ ). This loss is described as

$$L_{msep} = e^{\frac{-k_{msep}\theta_{msep}D_{msep}x_{msep,p}}{Q_{msep,f}}}, \quad (2.24)$$

where  $Q_{msep,f}$  is the volumetric feed rate per unit length,  $\theta_{msep}$  is the angle of the separation zone,  $D_{msep}$  is the diameter of the drum and  $x_{msep,p}$  is the pick-up gap.

## 2.5 CONCLUSION

In this chapter, the subject of coal and coal beneficiation was discussed. The initial formation of coal, its geology and the marketing of coal was briefly presented. The various coal products, specifically relating to Leeuwpan, were looked at. After the general overview of coal, its formation and marketing were explained and a more detailed study of its beneficiation was conducted by making use of the available literature.

The fundamental principle behind coal beneficiation is gravity separation. Gravity separation and the method of evaluating properties of coal ore by float and sink analysis provide a very useful means to determine a number of parameters involved in separation. The use of a dense medium to regulate the separation of coal from discard allows plant efficiencies to be determined by generating partition curves. This method can also be used to evaluate the properties of the coal ore itself. A washability curve indicates at what relative density the ore will separate such that a specific ash percentage is obtained. In conjunction with ash percentage, the associated yield can also be determined. These tools allow for the setpoints of a coal beneficiation plant to be determined while running at steady state.

After giving an understanding of the principles behind coal beneficiation, the practical equipment and processing units in a typical coal washing plant that makes use of density separation were discussed. Since most beneficiation plants in South Africa make use of the DMS method and DMC equipment for coal beneficiation, it was decided that the DMS process would be evaluated in more detail. Based on this and the initial problem to be solved in this research, it is necessary to understand the process very well in order to control it. As a result this literature study looked at the details behind the typical DMS plant and its equipment.

Instrumentation and field devices that are typically used to control such plants



were also investigated. An interesting study of online coal analysis was done and could prove to be very useful for real-time control. This will benefit a controller greatly, since otherwise it would instead have to make use of a coal quality estimate and update the estimate from laboratory results, which typically take a few hours to obtain. Finally, various mathematical models of DMS equipment available in literature were investigated and discussed. These models are typical steady-state models and require an in depth understanding of the complex principles behind the equipment and minerals processing. Many of the models make use of regression analysis and parametric equations to fit experimental data to a theoretical mathematical equation. These models give a good understanding of how a DMS plant operates and can prove to be very valuable in process control.

## CHAPTER 3: MODELLING FOR FEEDBACK CONTROL

### 3.1 INTRODUCTION

In general, a control system contains both a theoretical or mathematical aspect and a physical aspect. Craig and Henning (2000:770) illustrate this concept with the representation in figure 3.1.

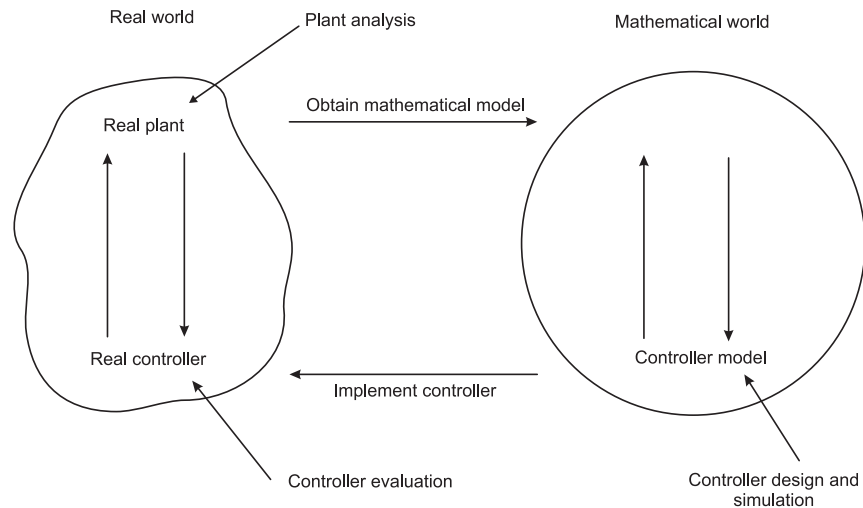


Figure 3.1: General control framework (Craig and Henning, 2000:770).

The real world is represented with uneven lines, which means that it is ill-defined and difficult to describe. By utilising mathematics the real world can be represented; however, this will never be a full description of it. 3.1 illustrates the framework required for implementing a control system. The steps involve initially obtaining a mathematical model of a real plant as accurately as required for control purposes. A control system is then designed for the model. Simulation of the controller and plant model is used to determine the improvements made to the process and their financial impact. If the controller proves to be financially successful, it would then be implemented.

Lipták (1995a:5) indicates that in order to control a process, it is necessary to understand it fully. The knowledge of a process can be described using mathematical modelling. Understanding of process dynamics allows a plant to be modelled for process control. These models can also be used in simulations to analyse a process in greater detail. Seborg *et al.* (1995:17) also indicate that dynamic models can be used for training purposes, development of control strategies and process optimisation. This chapter describes the various classes of models that are available for automatic feedback control. System identification and its application are also discussed.

A plant that is to be optimised by a control system will only require a model to be as complicated as the optimisation requirements. Process models can either be determined from first principles (theoretical models) or they can be obtained by experimental data and regression (empirical models). A combination of both methods will yield semi-empirical models (Seborg *et al.*, 1995:17). This chapter also outlines some of the model-based controller applications that have been developed for the minerals-processing industry. The economic benefits of automatic control are also discussed.

### 3.2 STEADY-STATE AND DYNAMIC MODELLING

It is possible to develop process models based on steady-state or static analysis. These models are typically used in chemical and metallurgical engineering for process design (Lipták, 1995a:70–72). Static models assist in allowing the understanding of process variable relationships and are typically used to determine the steady-state process gain for control system models. A steady-state model is usually determined by sampling and measuring a process through which small changes in a manipulated variable show changes in the controlled variable. Chapter 2 of this dissertation describes a number of steady-state models for coal beneficiation.

Dynamic modelling involves the use of differential equations to describe a system that is in transition to or from steady state or is in a state of oscillation based on initial conditions and process behaviour (Lipták, 1995a:73).

Brogan (1991:13) describes the different dynamic models that could possibly be used in control systems modelling. Figure 3.2 illustrates some of these models in a tree diagram. The models that branch into a dashed line mean that further branches may occur, but have not been illustrated. Models that incorporate both space and time are referred to as distributed parameter models. These models are represented by partial differential equations. Distributed parameter models are normally approximated by a number of lumped parameter models. Lumped parameter models are represented by ordinary differential equations (ODEs) or difference equations. This approximation can be achieved by using finite element methods, expansions of models or other approximation techniques.

Ljung (1987:7) describes different techniques for obtaining model sets using system identification. Models can be developed where formal properties are combined with a priori knowledge and engineering intuition. Other models can be developed from physical laws and other well-established relationships with

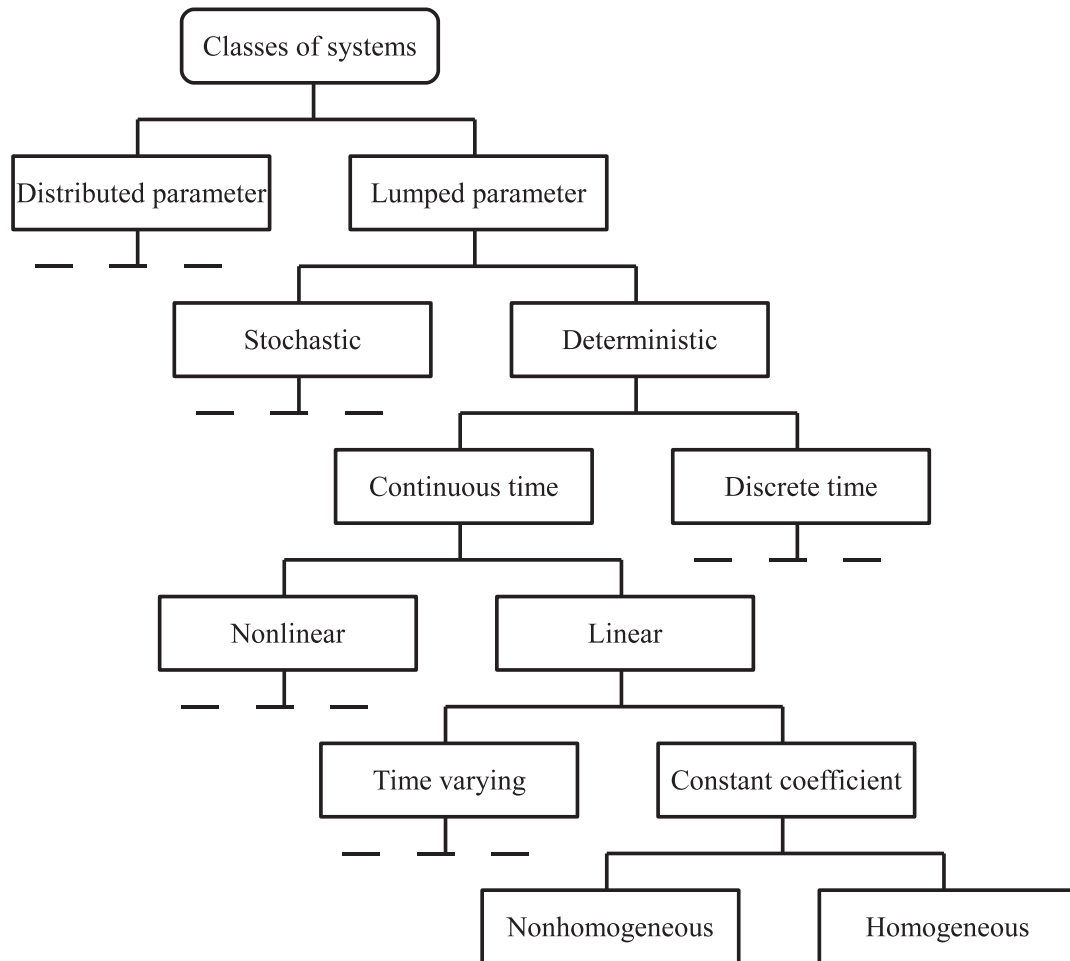


Figure 3.2: Classes of system equations used for modelling for control (Brogan, 1991:13).

certain unknown physical parameters. Models can also be developed by using standard linear models and not incorporating any reference to the physical world in the design. Models that have parameters to allow fitting of data and do not incorporate physical considerations are referred to as empirical models. Models that incorporate physical considerations and that have adjustable parameters are called semi-empirical models. These models' equation structures can be developed from first principles with uncertain parameters.

Controller design methods usually make use of linear time-invariant models. The reason for this is that a control system is normally designed from a model that is as complicated as the process requirements for enhancement. Complex models such as nonlinear models are normally linearised around an operating point (Skogestad and Postlethwaite, 2005:7–8).

### 3.3 SYSTEM IDENTIFICATION

Ljung (1987) presents a scientific method for building mathematical models of dynamic systems from observed data of those systems. The system identification procedure (Ljung, 1987:1–10) given in figure 3.3 involves the recording of data, obtaining a set of candidate models and a rule which allows the candidate models to be assessed with the data available.

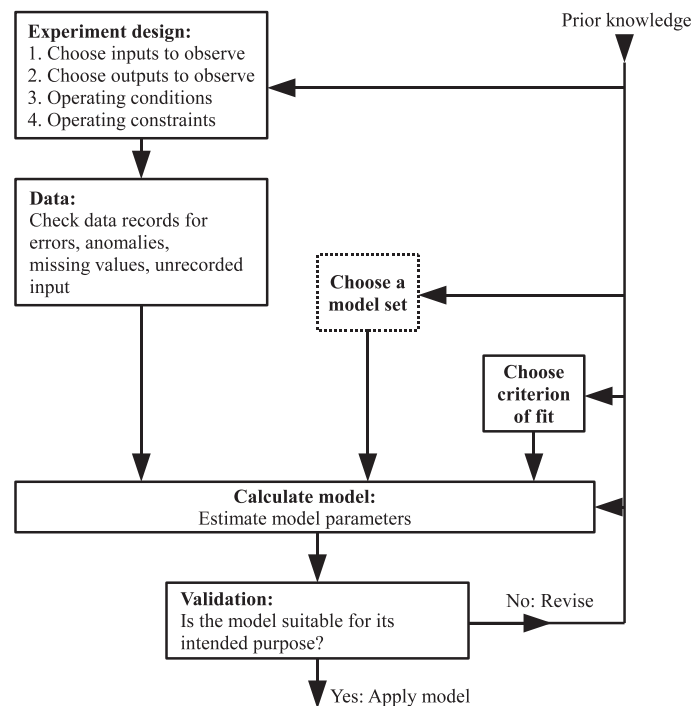


Figure 3.3: The system identification procedure (Ljung, 1987:9).

This dissertation makes use of an industrial experiment where data from a typical DMS process are collected. Dynamic models of the process will be developed by first principles. These first principle models will, however, contain parameters that are uncertain. As a result, the uncertain parameters form candidate models, which need to be assessed according to the experimental data that will be collected.

### 3.4 MATHEMATICAL REPRESENTATION OF PROCESSES

When deriving a mathematical representation of a process, it is important to identify the system by sketching the process and identifying the key variables that define the system. The boundaries of the system should also be considered (Marlin, 1995:56).

Marlin (1995:56) also indicates that a system can be modelled as a lumped parameter system if there is no spatial variation of important variables. If, however, there are significant changes in one or more directions the system must be modelled as a distributed-parameter system. It is also necessary to understand the assumptions that can be made for a particular model to allow for accurate prediction of the system. This is because the macroscopic behaviour of a process is normally sufficient to understand a dynamic process.

Data that are important for the modelling of a physiochemical system include heat capacities, reaction rates, densities and flow rates. These are all dependent on the type of process being modelled. Stephanopoulos (1984:48–49) indicates that the equations used to model a process are generally derived from the conservation principles that are obeyed by all physical systems. The principle of conservation of a quantity  $S$  can be described as

$$\begin{aligned}
 \frac{\left[ \begin{array}{c} \text{accumulation of } S \\ \text{within a system} \end{array} \right]}{\text{time period}} &= \frac{\left[ \begin{array}{c} \text{flow of } S \\ \text{into the system} \end{array} \right]}{\text{time period}} - \frac{\left[ \begin{array}{c} \text{flow of } S \\ \text{out of the system} \end{array} \right]}{\text{time period}} + \\
 &\quad \frac{\left[ \begin{array}{c} \text{amount of } S \\ \text{generated within} \\ \text{the system} \end{array} \right]}{\text{time period}} - \frac{\left[ \begin{array}{c} \text{amount of } S \\ \text{consumed within} \\ \text{the system} \end{array} \right]}{\text{time period}}, \tag{3.1}
 \end{aligned}$$

where  $S$  can have the following fundamental quantities:

- total mass,
- mass of individual components,
- total energy or
- momentum.

Marlin (1995:58) indicates that it is sometimes necessary to make use of constitutive equations to specify a processing system completely. Equations such as fluid flow (equation 2.4) and chemical reaction rates,

$$r_A = k_0 e^{E/RT} C_A, \quad (3.2)$$

can be used. Equation 3.2 makes use of the Arrhenius equation as explained in Hayes (2003:557), where  $k_0$  is a proportionality constant,  $R$  is the gas constant ( $8.314 \text{ J mol}^{-1} \text{ K}^{-1}$ ),  $E$  is the apparent activation energy for the reaction process and  $T$  is the absolute temperature (K).  $C_A$  is the concentration of chemical component  $A$ . This is, however, only applicable to chemical processes where reactions take place and are to be controlled.

### 3.4.1 Model-based Control in Mineral Engineering

As indicated in section 3.1, it is difficult to obtain an accurate model of a real plant. By using uncertainty, it is possible to make use of a class of plant models that are bounded within an acceptable uncertainty range (Skogestad and Postlethwaite, 2005:3). Goodwin, Seron and Mayne (2008:18) say that the major challenges in optimisation problems are those of modelling. For this reason, a summary of the literature that describe developments in mathematical models for control in minerals processing is given below.

Herbst, Pate and Oblad (1992) have written a paper in which model-based control strategies were developed for a semi-autogenous grinding (SAG) mill, a rod/ball mill grinding circuit and a flotation circuit. Figure 3.4 illustrates the nature of their control strategy where a process model, estimator and optimiser are used. The process model is developed to be simple enough for fast computations, but detailed enough to represent the plant dynamics. The estimator that was used was a Kalman filter to provide information on the state of the system at any time. The optimisation that took place typically made use of a performance index, which was to be minimised. When developing the process models, the conservation of mass, energy and momentum as described in section 3.4 were used to formulate state-space expressions.

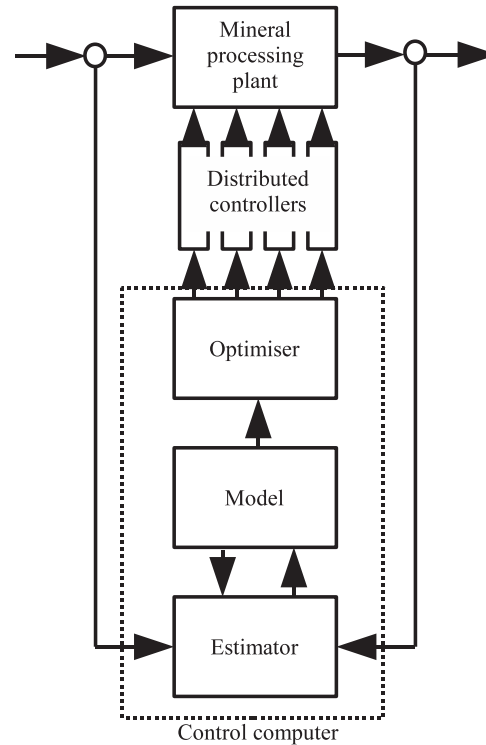


Figure 3.4: Model-based control strategy (Herbst *et al.*, 1992:22).

Galán, Barton and Romagnoli (2002) gave a solution for a robust controller for a SAG mill. They made use of a  $H_\infty$  controller to find an optimal controller and then reduced it to form a feedback plus feedforward control system. This was done to make the controller easy to implement.

Craig and MacLeod (1995) and Craig and MacLeod (1996) illustrate a robust controller that makes use of  $\mu$ -synthesis to develop a  $\mu$ -controller for a grinding mill plant model with uncertainty. This was applied and implemented on a closed-loop milling circuit.

Another control system shown in Chen, Li and Fei (2008) makes use of a model predictive controller (MPC) for a ball mill grinding process and utilises its advantage of having an inherent decoupling scheme. The MPC algorithm uses a constrained dynamic matrix control problem consisting of a predictive model, reference trajectory, feedback correction and rolling optimisation (minimisation of a quadratic objective function). This technique is illustrated in figure 3.5.

Chen *et al.* (2008:34) describe the dynamic matrix control algorithm as being able to determine the future set of control moves to move a predicted output as close as possible to the setpoint based on minimising an objective function at any time instant and by using a reasonably accurate predictive model. Further detail

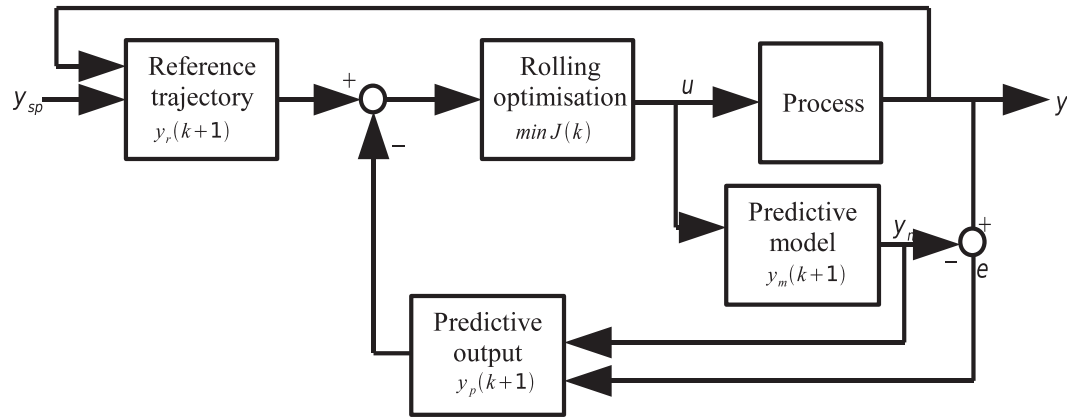


Figure 3.5: Illustration of the dynamic matrix control used by Chen *et al.* (2008:35).

on the dynamic matrix control algorithm is described in Marlin (1995:746–766).

Lyman, Denney, Wood, Askew and Brenchley (1983:291–283) show work where the feasibility of controlling the ash content of coal washed in dense medium cyclones using an on-line ash gauge is investigated. Their work on dynamic simulations of SG control relies on dynamic mathematical models of dense medium coal washing circuits developed in the conference proceeding from Lyman, Askew, Wood and Davis (1982). It is indicated that the simulation results, on a second-to-second basis, calculate the progress of coal, magnetite and water around the circuit (Lyman *et al.*, 1983:296–299). Detailed flow rates, SGs and sump levels were calculated as a function of time. Their simulation results, which show corrected medium SG, corrected medium sump volume, feed sump volume and overdense sump volume over time, were shown to provide a clear realistic representation of the plant operation. This work was conducted at West Cliff Collieries.

Similar simulations were conducted at Buchanan Borehole Collieries where an on-line control run was conducted with the intention to control the amount of ash in the product coal. The same control algorithm used at West Cliff Collieries was used for the on-line control at Buchanan Borehole Collieries. The algorithm used for the simple feedback ash control (Lyman *et al.*, 1983:305–308) made use of a linear regression where ash content is dependent on medium SG. This limitation arose during their control run as the anticipated slope of the average ash versus SG would be insufficient to cater for a wide range of SGs. However, the basic SG controller which maintained the SG set point was stable and had a good response time. Lyman *et al.* (1983:307–308) indicate that future control runs will incorporate the possibility of making the slope of the average ash versus SG a function of current circuit SG.

The work developed in Lyman *et al.* (1982) and Lyman *et al.* (1983) is relevant to this dissertation in that the objective of a dynamic model to be used for the control of product ash is the same. However, the work in this dissertation will develop dynamic equipment models from first principles. The cyclone product mass component (i.e. ash) model for this dissertation will differ from the model developed in Lyman *et al.* (1982) in that it will incorporate first principles when describing the mass of components in the cyclone overflow and underflow. Lyman *et al.* (1982) did not develop a dynamic model for the DMC as the residence time in the cyclone was negligible for their particular case. However, it is indicated that there is an advantage in developing a cyclone model with a feature where the overflow and underflow SGs and flow rates are determined when the cyclone throughput and feed medium SG are known. The DMC dynamic model developed for this dissertation will incorporate these features by making use of the conservation of mass.

Cierpisz (1998) has developed a computer simulation of the control system for a heavy media coal washing process. The control system that was implemented made use of an algorithm that applies on-off control signals with pulse width modulation proportional to the difference between measured and desired heavy media density values. The control algorithm also made use of an expert algorithm that applies parameters for discrete control equations for each channel of the process. The simulation model that was developed incorporated transfer functions to describe the heavy media tank levels, heavy media densities in vessels and media flows. Similar to the work in Cierpisz (1998), this dissertation will incorporate the concept of transfer functions for predicting process outputs such as density. However, they will be developed from first principles and the model will not only include the control of medium density. It will also include the modelling of the beneficiation of the ore.

Keast-Jones, Smitham, Horrocks and Ellison (1991) have presented a paper on DMC control for two sections of the washeries at Broken Hill Proprietary's slab and plate products division at Port Kembla. Their work primarily focuses on the development of control strategies for more accurate control of DMC separation densities in parallel DMC modules. Experimental results and relationships such as dependency of magnetite split on separation density, dependency of magnetics concentration in overflow on separation density, dependency of overflow density on separation density, variation of offset with separation density and effect of coal feed rate on separation density were investigated. Further work (Keast-Jones, Smitham, Horrocks and Ellison, 1993) shows that the implementation of such control strategies will improve the stability of separation density over time.

### 3.5 FINANCIAL BENEFITS OF USING AUTOMATIC CONTROL

Craig and Henning (2000:771–772) describe a framework that can be used to determine economic benefits by using advanced process control. They indicate that the primary objective of a control system in the process industry is to maximise profits while benefiting ore or raw materials. In order for this to be accomplished a control system must minimise downtime and reduce variations in the controlled variables of the process.

Craig and Henning (2000:771–772) indicate that control systems can only improve pseudo-downtime, which is when a plant is out of steady state, such as during start-up phase or after process disruptions or when a setpoint is changed by the operator. It is also indicated that unscheduled shutdowns can be prevented by using control methodologies such as MPC and fault detection. By using process control, it is possible to ensure that a plant reaches its steady state in the fastest possible time after a disruption. This will ultimately save money in a process. Craig and Henning (2000:771–772) also indicate that control systems will ensure that controlled variables have a reduced standard deviation, which can provide significant financial benefits.

Bauer and Craig (2008:3–10) have described a framework for performing an economic assessment of advanced process control (APC) systems. This framework begins with an initial base case identification where the current system's performance is analysed. A performance function is then developed where either a profit or loss is linked to the variance of a process variable. By computing the average performance of a process, a base case can be established. By implementing an APC system, it is possible to determine the benefits gained from the new controller. This framework is also reflected in figure 3.1. An industrial survey was conducted on the economic assessment of APC with APC experts, users and suppliers (Bauer and Craig, 2008:8). Figure 3.6 illustrates some of the results of the survey that was done.

The results from figure 3.6 indicate that the most important benefits achieved from APC are throughput increase (approximately 3-5% as described by Bauer and Craig [2008:8]), improvement in stability, energy conservation and improvement in product quality. Quality and throughput were indicated as being the factor contributing most to financial benefits for APC.

Bauer and Craig (2008:7) indicate that a higher quality product from a process will limit the throughput of the process (figure 3.7). APC typically improves a process in both quality and throughput (figure 3.7), which reflects the results

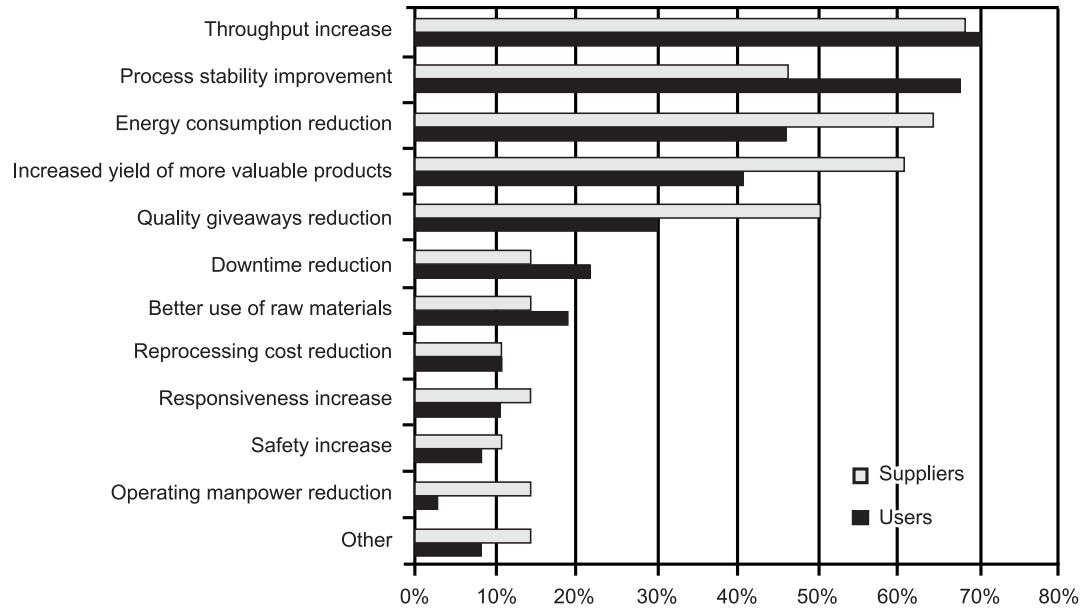


Figure 3.6: APC survey results indicating main profit contributors for APC (Bauer and Craig, 2008:8).

obtained from the survey.

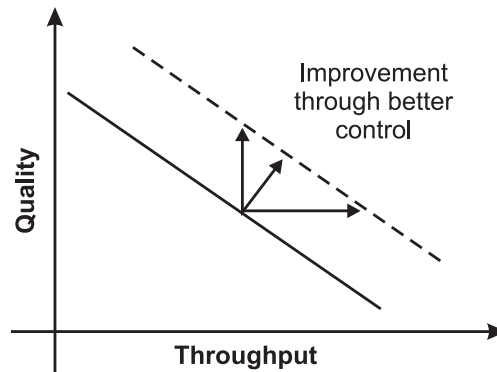


Figure 3.7: Effect of APC on throughput and quality (Bauer and Craig, 2008:8).

Craig and Henning (2000:773–779) show a case study where an advanced process controller was used on a gold flotation plant. It was proven, using statistical hypothesis testing, that a 1% improvement in gold recovery occurred when using the advanced controller. Process control will also ensure products are of the correct grade or quality and can assist operators in their understanding of the process.

### 3.6 CONCLUSION

In this chapter a literature study on modelling for control and its application to minerals processing was conducted. A control system will ensure that a plant or system reaches its desired specifications by automatically adjusting its manipulated variables to try and achieve the best possible response for that system. When one understands a plant in terms of its dynamic behaviour, it becomes easier to design a control system for best possible performance. For this reason, the concepts of steady-state modelling and dynamic modelling were discussed. The classes of systems that classify models and illustrate the process followed in model identification were also discussed.

In view of the nature of control systems, the mathematics of these models becomes part of their explanation and many tools, such as linear systems theory, are used and assumed to be known. Similar mathematics is used for describing the theory and principles behind control systems.

Many of the models used to describe physical or chemical processes make use of fundamental principles such as conservation of mass, energy and momentum. These principles were explained from the available literature.

Because of the requirement for a model for model-based control and by looking at the scope of this research, literature that was available for model-based controllers in minerals processing was found and discussed. Since it is realised that this research should add value to the industry, a section on the financial benefits of using automatic control was investigated. Based on this, it is evident that control systems can enhance an operation and improve financial returns by reducing the time taken for a plant to reach steady state, reducing the effects of disturbances in the process and ensuring less deviation in product specifications.

## CHAPTER 4: MATHEMATICAL MODELLING

### 4.1 INTRODUCTION

In this chapter the theoretical framework discussed in the literature study in chapters 2 and 3 will be applied to develop mathematical models for the screen, mixing box, magnetite water addition, the DMC and corrected medium magnetite make-up tanks from first principles. Process dynamics will be used where applicable in the model designs. Once the mathematical models have been developed, they will be compiled into a plant simulation model. Certain assumptions will be stated and made to enable the simulation of the plant model.

### 4.2 MODEL DEVELOPMENT

#### 4.2.1 Screen model

The screen is used in the DMS plant primarily to size the ore being separated by the differently sized dense medium cyclones as described in chapter 2. Water is normally used to assist the ore in its separation. This addition of water will not be modelled, as it is normally recovered and will only increase the moisture content of the ore slightly. Since the screens used in the Leeuwpan DMS plant are either single-deck or double-deck ones, two different models will be developed. These models can then be combined to enable the models to be used for the simulation of each particle size stream.

##### 4.2.1.1 Single-deck screen model

With the development of the single-deck screen model, the conservation of total mass is used for  $S$  in equation 3.1. A simplified illustration of a single-deck screen can be seen in figure 4.1. This representation, equation 3.1 and associated variables are used to develop a linear dynamic model of the ore passing over it.

The following is an explanation of the different variables used to describe the operation of the single-deck de-watering screen, as in figure 4.1,

- $W_{i,f}$  - Mass feed rate of the ore fed into the screen (kg/s),
- $W_{o,f}$  - Mass feed rate of the ore transported over the screen (kg/s),
- $W_{u,f}$  - Mass feed rate of the ore transported through the screen (kg/s),

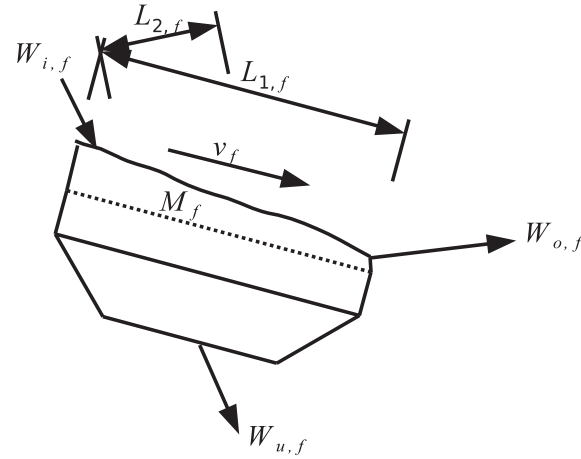


Figure 4.1: Simplified representation of a single-deck screen.

- $M_f$  - Mass of ore on the top deck (kg),
- $v_f$  - Linear velocity of the ore transported over the screen (m/s),
- $L_{1,f}$  - Length of the screen (m),
- $L_{2,f}$  - Width of the screen (m),
- $A_f = L_{1,f}L_{2,f}$  - Area of the screen (m<sup>2</sup>).

Since the profile of the mass on top of the deck varies with length and time from the inlet to the outlet, it can be modelled as a distributed parameter system. In order to simplify the model, it is necessary to break the modelling of the screen deck into a number of linear ODE components. This will form a lumped parameter system and allow the screen operation to be modelled to a sufficient degree of accuracy. The development of this distributed model is described in figure 4.2.

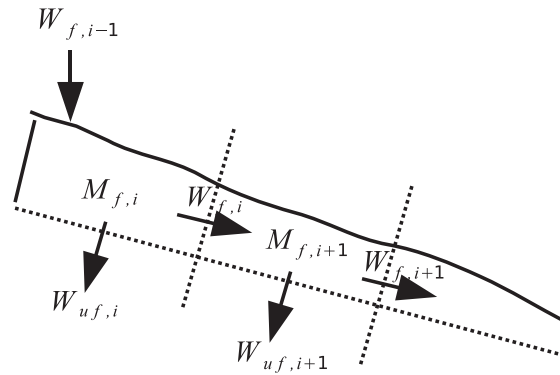


Figure 4.2: Simplified representation of the mass distribution for a single-deck screen.

The following is an explanation of the different variables used to describe  $n$  mass distributions across the single-deck de-watering screen for figure 4.2,

- $W_{f,i-1}$  - Mass feed rate of the ore fed into component  $i$  (kg/s),
- $W_{f,i}$  - Mass feed rate of the ore overflow exiting mass component  $i$  (kg/s),
- $W_{uf,i}$  - Mass feed rate of the ore underflow exiting mass component  $i$  (kg/s),
- $M_{f,i}$  - Mass of ore for mass component  $i$  (kg),
- $\alpha_f$  - Percentage of mass split for mass component  $i$ ,
- $\tau_f$  - Time taken for ore to be transported over screen component  $i$  (s),
- $\tau_{f,uf}$  - Time taken for ore to be transported through screen component  $i$  (s).

The following is a list of assumptions that have been made for the modelling of the single-deck screen:

- The screen is a distributed parameter system, but can be approximated with  $n$  first order lumped parameter systems or components.
- The overflow and underflow mass feed rates of each component is proportional to their mass on top of each component.
- The proportion of mass split for each component is dependent on the particle size distribution of the feed.

Using equation 3.1 and figure 4.2, it is possible to determine that the conservation of total mass for each component of the single-deck screen is as follows:

$$\frac{dM_{f,i}}{dt} = W_{f,i-1} - W_{f,i} - W_{uf,i}. \quad (4.1)$$

By using the assumption that the mass feed rates of the ore overflow and underflow exiting mass component  $i$  ( $W_{f,i}$  and  $W_{uf,i}$ ) are proportional to their mass state in terms of  $\alpha$ ,  $\tau_f$  and  $\tau_{f,uf}$ , it is possible to make the following simplification of equation 4.1,

$$\frac{dM_{f,i}}{dt} = W_{f,i-1} - \alpha_f \frac{M_{f,i}}{\tau_f} - (1 - \alpha_f) \frac{M_{f,i}}{\tau_{f,uf}}. \quad (4.2)$$

Modelling each mass component  $i$  of the single-deck screen for a maximum of  $n$  components will result in  $W_{f,0}$  being the initial feed into the screen ( $W_{i,f}$ )

and  $W_{f,n}$  being the final mass feed rate of the oversize material ( $W_{o,f}$ ). Since the initial feed is typically the fine material collected from the double-deck screen, it is necessary to combine this model with the fines output from a double-deck screen model (as described in the next section) simulation. The undersized material ( $W_{u,f}$ ) from the single-deck de-watering screen is collected and can be taken as the sum of all underflow mass components (i.e.  $W_{u,f} = \sum_1^n W_{u,f,i}$ ).

#### 4.2.1.2 Double-deck screen model

Similar to the development of the single-deck screen model, the conservation of total mass is used for  $S$  in equation 3.1. A simplified illustration of a double-deck screen can be found in figure 4.3. This representation, equation 3.1 and associated variables are used to develop a linear dynamic model of the ore being separated by it. The ore separated at the lower deck underflow forms the fines material and is collected into a chute or hopper and fed into the single-deck de-watering screen.

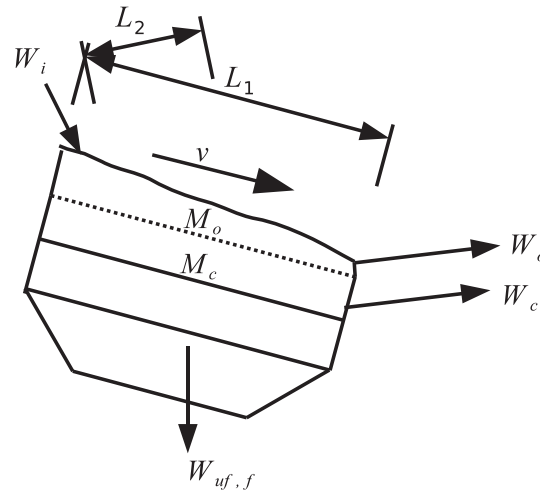


Figure 4.3: Simplified representation of a double-deck screen.

The following is an explanation of the different variables used to describe the operation of the double-deck screen,

- $W_i$  - Mass feed rate of the ore fed into the screen (kg/s),
- $W_o$  - Mass feed rate of the oversized ore being transported on the upper deck (kg/s),
- $W_c$  - Mass feed rate of the coarse sized ore begin transported on the lower deck (kg/s),

- $W_{uf,f}$  - Mass feed rate of the fine-sized ore being transported through the underflow (kg/s),
- $M_o$  - Mass of ore on the upper deck (kg),
- $M_c$  - Mass of ore on the lower deck (kg),
- $v$  - Linear velocity of the ore at each deck (m/s),
- $L_1$  - Length of the screen (m),
- $L_2$  - Width of the screen (m),
- $A = L_1L_2$  - Area of the screen (m<sup>2</sup>).

The following is an explanation of the different variables used to describe  $n$  mass distributions across each deck in the double-deck particle classification screen shown in figure 4.4:

- $W_{o,i-1}$  - Mass feed rate of the ore fed into component  $i$  on the top deck (kg/s),
- $W_{o,i}$  - Mass feed rate of the ore overflow exiting mass component  $i$  on the top deck (kg/s),
- $W_{c,i}$  - Mass feed rate of the undersized ore exiting mass component  $i$  from the top deck (kg/s),
- $M_{o,i}$  - Mass of ore on the top deck for mass component  $i$  (kg),
- $\alpha_o$  - Percentage of mass split on the top deck for mass component  $i$ ,
- $\tau_o$  - Time taken for ore to be transported over the top deck screen component  $i$  (s),
- $\tau_{o,co}$  - Time taken for ore to be transported through the top deck screen component  $i$  (s),
- $W_{tc,i-1}$  - Mass feed rate of the ore fed into component  $i$  on the bottom deck (kg/s),
- $W_{tc,i}$  - Mass feed rate of the ore overflow exiting mass component  $i$  on the bottom deck (kg/s),
- $W_{f,i}$  - Mass feed rate of the undersized ore exiting mass component  $i$  from the bottom deck (kg/s),
- $M_{c,i}$  - Mass of ore on the bottom deck for mass component  $i$  (kg),

- $\alpha_c$  - Percentage of mass split on the bottom deck for mass component  $i$ ,
- $\tau_c$  - Time taken for ore to be transported over the bottom deck screen component  $i$  (s),
- $\tau_{c,fc}$  - Time taken for ore to be transported through the bottom deck screen component  $i$  (s).

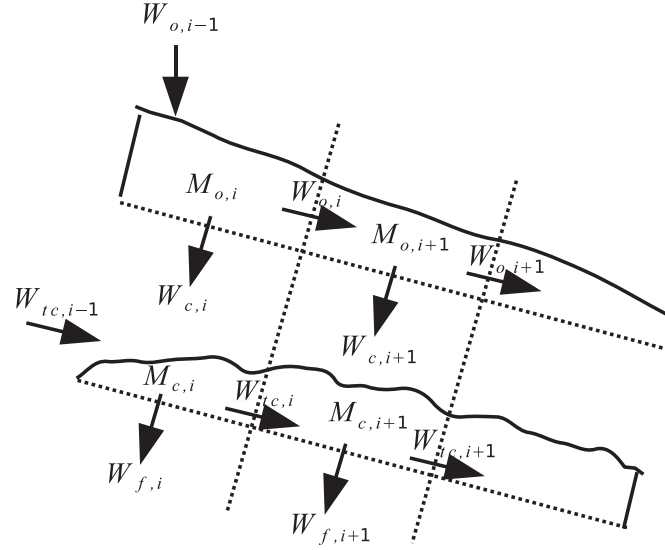


Figure 4.4: Simplified representation of the mass distribution for a double-deck screen.

The following is a list of assumptions that have been made for the modelling of the double-deck screen:

- Both decks of the screen are a distributed parameter system, but can be approximated with  $n$  first order lumped parameter systems or components.
- The overflow and underflow mass feed rates of each component are proportional to their mass on top of each component for both the top and bottom deck.
- The proportion of mass split for each component on the top and bottom deck is dependent on the particle size distribution of the feed.

Using equation 3.1 and figure 4.4, it is possible to determine that the conservation of total mass for each component of both the top and bottom deck screen is as follows:

$$\frac{dM_{o,i}}{dt} = W_{o,i-1} - W_{o,i} - W_{c,i}, \quad (4.3)$$

$$\frac{dM_{c,i}}{dt} = W_{tc,i-1} - W_{c,i} - W_{tc,i} - W_{f,i}. \quad (4.4)$$

By assuming the mass feed rate of the ore overflow and underflow exiting mass component  $i$  for both the top and bottom deck ( $W_{o,i}$  and  $W_{c,i}$  for the top deck and  $W_{tc,i}$  and  $W_{f,i}$  for the bottom deck) are proportional to their mass states in terms of  $\alpha_o$ ,  $\tau_o$  and  $\tau_{o,co}$  for the top deck and  $\alpha_c$ ,  $\tau_c$  and  $\tau_{c,fc}$  for the bottom deck, the following simplification can be made for equations 4.3 and 4.4:

$$\frac{dM_{o,i}}{dt} = W_{o,i-1} - \alpha_o \frac{M_{o,i}}{\tau_o} - (1 - \alpha_o) \frac{M_{o,i}}{\tau_{o,co}}, \quad (4.5)$$

$$\frac{dM_{c,i}}{dt} = W_{c,i-1} - \alpha_c \frac{M_{c,i}}{\tau_c} - (1 - \alpha_c) \frac{M_{c,i}}{\tau_{c,fc}}. \quad (4.6)$$

Modelling each mass component  $i$  for each deck with a maximum of  $n$  components will result in  $W_{o,0}$  being the initial feed into the double deck screen ( $W_i$ ),  $W_{o,n}$  being the final mass feed rate of the oversize material ( $W_o$ ) for the top deck and  $W_{tc,n}$  being the final mass feed rate of the oversize material ( $W_c$ ) for the bottom deck or coarse material. The undersized material ( $W_{u,f}$ ) from the bottom deck is collected in a chute or hopper and can be taken as the sum of all underflow mass components (i.e.  $W_{u,f} = \sum_1^n W_{f,i}$ ).

#### 4.2.2 Magnetite medium water addition model

Magnetite is used as the medium in the DMS plant as described in chapter 2. Medium that has been used in the DMC is normally recovered and collected so that it can be used again. Water is added in-line with this medium to correct the density before it is mixed with the ore. With the development of the magnetite-water mixing model, the conservation of total mass is used for  $S$  in equation 3.1. A simplified illustration of this process can be found in figure 4.5. This representation, equation 3.1 and associated variables are used to develop a dynamic model of the in-line mixing of water and recovered magnetite medium.

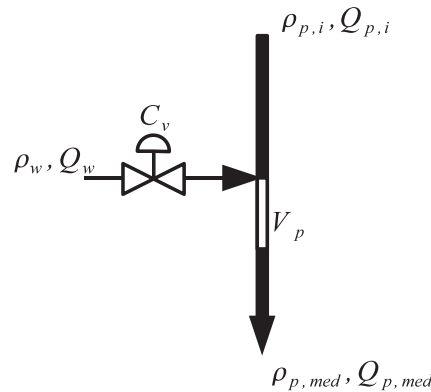


Figure 4.5: Simplified representation of water-magnetite in-line mixing.

The following is a description of the variables used to model the mixing process:

- $\rho_w = 1000$  - Density of water ( $\text{kg}/\text{m}^3$ ),
- $Q_w$  - Volumetric flow rate of the water ( $\text{m}^3/\text{s}$ ),
- $C_v$  - Valve coefficient ( $\text{m}^2$ ),
- $\ell_p$  - Valve position (%),
- $\Delta p$  - Pressure drop over the valve (kPa),
- $\rho_{p,i}$  - Density of the recovered magnetite medium ( $\text{kg}/\text{m}^3$ ),
- $Q_{p,i}$  - Volumetric flow rate of the recovered magnetite medium ( $\text{m}^3/\text{s}$ ),
- $\rho_{p,med}$  - Density of the corrected magnetite medium ( $\text{kg}/\text{m}^3$ ),
- $Q_{p,med}$  - Volumetric flow rate of the corrected magnetite medium ( $\text{m}^3/\text{s}$ ),
- $V_p$  - Volume required until solution is perfectly mixed ( $\text{m}^3$ ).

The following is a list of assumptions that have been made for the modelling of the magnetite medium addition of water:

- In-line mixing takes place between the added water ( $Q_w$ ) and medium ( $Q_{p,i}$ ). The effluent is well-mixed within a constant volume  $V_p$  of the pipe.
- The valve is linear with a constant pressure drop  $\Delta p$ .
- The volumetric flow rates of the recovered ( $Q_{p,i}$ ) and corrected medium ( $Q_{p,med}$ ) is instantaneous before and after a step is introduced in the valve position  $\ell_p$  (i.e. no valve dynamics).

Using equation 3.1 (assuming the volume  $V_p$  is constant) and equation 2.4 (where  $Q_w = C_v \frac{\ell_p}{100} \sqrt{\frac{\Delta p}{1000}}$ ) and assuming a linear valve, it is possible to determine that the conservation of total mass for the in-line mixing is as follows,

$$\frac{d\rho_{p,med}}{dt} = \frac{-Q_{p,med}}{V_p} \rho_{p,med} + \frac{1000K_p}{V_p} \frac{\ell}{100} + \frac{Q_{p,i}}{V_p} \rho_{p,i}, \quad (4.7)$$

where  $K_p = C_v \sqrt{\frac{\Delta p}{1000}}$ .

### 4.2.3 Mixing box model

The corrected medium is mixed with the screened ore before it is pumped to the DMC as described in chapter 2. With the development of the mixing box model, the conservation of total mass is used for  $S$  in equation 3.1. A simplified illustration of this mixing process can be found in figure 4.6. This representation, equation 3.1 and associated variables are used to develop a dynamic model of the mixing box for ore and corrected magnetite.

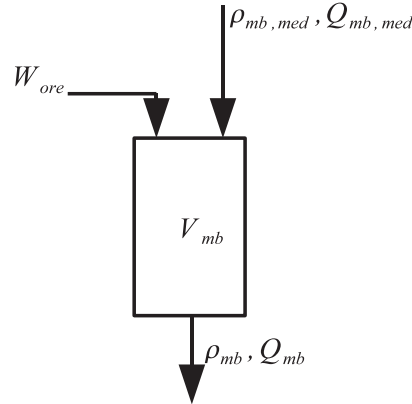


Figure 4.6: Simplified representation of a mixing box.

The following is a description of the variables used to model the mixing box:

- $W_{ore}$  - Mass feed rate of the ore (kg/s),
- $\rho_{mb,med}$  - Density of the corrected magnetite medium (kg/m<sup>3</sup>),
- $Q_{mb,med}$  - Volumetric flow rate of the corrected magnetite medium (m<sup>3</sup>/s),
- $\rho_{mb}$  - Density of the mix (kg/m<sup>3</sup>),
- $Q_{mb}$  - Volumetric flow rate of the mix (m<sup>3</sup>/s),
- $V_{mb}$  - Fixed volume of mixing box (m<sup>3</sup>).

The following is a list of assumptions that have been made for the modelling of the mixing box:

- The medium and ore is well-mixed within a constant volume  $V_{mb}$ .
- The volumetric flow rates of the corrected medium and mix ( $Q_{mb,med}$  and  $Q_{mb}$ ) are instantaneous before and after a step is introduced in the medium density ( $\rho_{mb,med}$ ) or mass feed rate of the ore ( $W_{ore}$ ). The fixed-speed pumping of material and constant mixing box volume result in no rate of change of volume.

Using equation 3.1 (assuming the volume  $V$  is constant), the conservation of total mass for the mixing box can be determined as follows,

$$\frac{d\rho_{mb}}{dt} = \frac{-Q_{mb}}{V_{mb}}\rho_{mb} + \frac{Q_{mb,med}}{V_{mb}}\rho_{mb,med} + \frac{1}{V_{mb}}W_{ore}. \quad (4.8)$$

#### 4.2.4 DMC model

The mixed ore is separated by using gravity separation in the DMC as described in chapter 2. With the development of the DMC model, the conservation of total mass and of individual components is used for  $S$  in equation 3.1. Since it is assumed that no chemical reaction takes place in this minerals-processing unit, no additional mass of a component is generated. A simplified illustration of the DMC can be found in figure 4.7. This representation, equation 3.1 (with  $S$  as the conservation of total mass and mass of individual components) and associated variables are used to develop a dynamic model for the DMC.

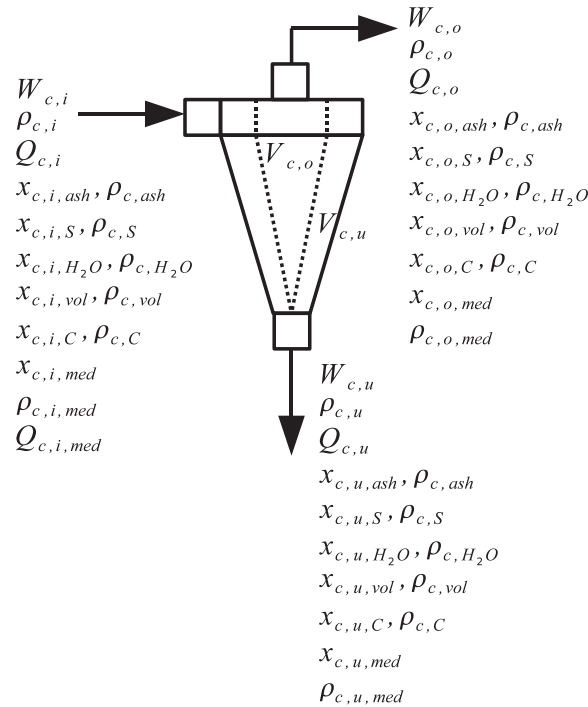


Figure 4.7: Simplified representation of a DMC.

The overall conservation of mass is used to model the throughput of the DMC. In order to model the quality of the coal product dynamically it is necessary to ensure conservation of mass of components is used. The following is a description of the variables used to model the DMC:

- $W_{c,i}$  - Mass feed rate of the feed mix (kg/s),

- $\rho_{c,i}$  - Density of the feed mix ( $\text{kg}/\text{m}^3$ ),
- $Q_{c,i}$  - Volumetric flow rate of the feed mix ( $\text{m}^3/\text{s}$ ),
- $v_{c,i}$  - Linear velocity of the feed mix ( $\text{m}/\text{s}$ ),
- $V_c = V_{c,o} + V_{c,u}$  - Volume of the material within the cyclone ( $\text{m}^3$ ),
- $\alpha$  - Overflow and underflow proportionality constant,
- $A_c$  - Area of the inlet ( $\text{m}^2$ ),
- $R_{c,eff}$  - Effective radius at which separation takes place near the spigot (m),
- $d_c$  - Average particle size (m),
- $x_{c,i,ash}, x_{c,i,S}, x_{c,i,H_2O}, x_{c,i,vol}, x_{c,i,C}$  - Percentage ash, sulphur, water, volatiles and fixed carbon in the feed mix,
- $\rho_{c,ash}, \rho_{c,S}, \rho_{c,H_2O}, \rho_{c,vol}, \rho_{c,C}$  - Ash, sulphur, water, volatiles and fixed carbon densities ( $\text{kg}/\text{m}^3$ ),
- $x_{c,i,med}$  - Percentage magnetite in the feed mix,
- $\rho_{c,i,med}$  - Density of the magnetite medium in the feed mix ( $\text{kg}/\text{m}^3$ ),
- $Q_{c,i,med}$  - Volumetric flow rate of the magnetite medium in the feed mix ( $\text{m}^3/\text{s}$ ),
- $W_{c,o}$  - Mass feed rate of the overflow ( $\text{kg}/\text{s}$ ),
- $\rho_{c,o}$  - Density of the overflow ( $\text{kg}/\text{m}^3$ ),
- $Q_{c,o}$  - Volumetric flow rate of the overflow ( $\text{m}^3/\text{s}$ ),
- $V_{c,o}$  - Volume split of the overflow within the DMC ( $\text{m}^3$ ),
- $x_{c,o,ash}, x_{c,o,S}, x_{c,o,H_2O}, x_{c,o,vol}, x_{c,o,C}$  - Percentage ash, sulphur, water, volatiles and fixed carbon in the overflow,
- $x_{c,o,med}$  - Percentage magnetite medium in the overflow,
- $\rho_{c,o,med}$  - Density of the magnetite medium in the overflow ( $\text{kg}/\text{m}^3$ ),
- $W_{c,u}$  - Mass feed rate of the underflow ( $\text{kg}/\text{s}$ ),
- $\rho_{c,u}$  - Density of the underflow ( $\text{kg}/\text{m}^3$ ),
- $Q_{c,u}$  - Volumetric flow rate of the underflow ( $\text{m}^3/\text{s}$ ),
- $V_{c,u}$  - Volume split of the underflow within the DMC ( $\text{m}^3$ ),
- $x_{c,u,ash}, x_{c,u,S}, x_{c,u,H_2O}, x_{c,u,vol}, x_{c,u,C}$  - Percentage ash, sulphur, water, volatiles and fixed carbon in the underflow,

- $x_{c,u,med}$  - Percentage magnetite medium in the underflow,
- $\rho_{c,u,med}$  - Density of the magnetite medium in the underflow ( $\text{kg}/\text{m}^3$ ),
- $K_{c,o}$  - Proportionality constant for the overflow ( $\text{m}^3/\text{s}$ ),
- $K_{c,u}$  - Proportionality constant for the underflow ( $\text{m}^3/\text{s}$ ),
- $K_{c,o,ash}$  - Proportionality constant for the ash overflow ( $\text{m}^3/(\text{kg}\cdot\text{s})$ ),
- $K_{c,u,ash}$  - Proportionality constant for the ash underflow ( $\text{m}^3/(\text{kg}\cdot\text{s})$ ),
- $K_{c,o,S}$  - Proportionality constant for the sulphur overflow ( $\text{m}^3/(\text{kg}\cdot\text{s})$ ),
- $K_{c,u,S}$  - Proportionality constant for the sulphur underflow ( $\text{m}^3/(\text{kg}\cdot\text{s})$ ),
- $K_{c,o,H_2O}$  - Proportionality constant for the moisture overflow ( $\text{m}^3/(\text{kg}\cdot\text{s})$ ),
- $K_{c,u,H_2O}$  - Proportionality constant for the moisture underflow ( $\text{m}^3/(\text{kg}\cdot\text{s})$ ),
- $K_{c,o,vol}$  - Proportionality constant for the volatile overflow ( $\text{m}^3/(\text{kg}\cdot\text{s})$ ),
- $K_{c,u,vol}$  - Proportionality constant for the volatile underflow ( $\text{m}^3/(\text{kg}\cdot\text{s})$ ),
- $K_{c,o,med}$  - Proportionality constant for the magnetite medium overflow ( $\text{m}^3/(\text{kg}\cdot\text{s})$ ),
- $K_{c,u,med}$  - Proportionality constant for the magnetite medium underflow ( $\text{m}^3/(\text{kg}\cdot\text{s})$ ),
- $K_{c,o,C}$  - Proportionality constant for the fixed carbon overflow ( $\text{m}^3/(\text{kg}\cdot\text{s})$ ),
- $K_{c,u,C}$  - Proportionality constant for the fixed carbon underflow ( $\text{m}^3/(\text{kg}\cdot\text{s})$ ).

The following is a list defining the subscripts used in the variables for the DMC model:

- $c$  - DMC,
- $i$  - Input,
- $o$  - Overflow,
- $u$  - Underflow,
- $eff$  - Effective,
- $ash$  - Ash,
- $S$  - Sulphur,
- $H_2O$  - Moisture,

- *vol* - Volatile,
- *C* - Fixed carbon,
- *med* - Magnetite medium.

The following is a list of assumptions that have been made for the modelling of the DMC:

- The volume of the mix in the cyclone ( $V_c$ ) is constant.
- The volumes of the overflow ( $V_{c,o}$ ) and underflow ( $V_{c,u}$ ) mix in the cyclone and are split at a constant ratio  $\alpha$ .
- The volumetric flow rates of the feed ( $Q_{c,i}$ ), overflow ( $Q_{c,o}$ ) and underflow ( $Q_{c,u}$ ) are constant before and after a step is introduced in the medium density ( $\rho_{c,i}$ ) or feed rate of the ore ( $W_{c,i}$ ).
- The volumetric flow rates of the overflow ( $Q_{c,o}$ ) and underflow ( $Q_{c,u}$ ) are split at a constant ratio  $\alpha$ .
- Only ash, sulphur, moisture, volatile, medium and fixed carbon components will be considered for the conservation of mass of components in the feed (i.e.  $x_{c,i,ash} + x_{c,i,S} + x_{c,i,H_2O} + x_{c,i,vol} + x_{c,i,med} + x_{c,i,C} = 1$ ), overflow (i.e.  $x_{c,o,ash} + x_{c,o,S} + x_{c,o,H_2O} + x_{c,o,vol} + x_{c,o,med} + x_{c,o,C} = 1$ ) and underflow (i.e.  $x_{c,u,ash} + x_{c,u,S} + x_{c,u,H_2O} + x_{c,u,vol} + x_{c,u,med} + x_{c,u,C} = 1$ ).
- The rates of change in mass for the overflow ( $\frac{dW_{c,o}}{dt}$ ) and underflow ( $\frac{dW_{c,u}}{dt}$ ) are proportional to the difference in their densities ( $\rho_{c,o}$  and  $\rho_{c,u}$ ) to the magnetite medium density ( $\rho_{c,i,med}$ ), the acceleration due to a centrifugal force ( $\frac{v_{c,i}^2}{R_{c,eff}}$ ) and the percentage of either ash or carbon in the feed ( $x_{c,i,ash}$  or  $x_{c,i,C}$ ).
- The rates of change in percentages of components to the overflow ( $\frac{dx_{c,o,ash}}{dt}$ ,  $\frac{dx_{c,o,S}}{dt}$ ,  $\frac{dx_{c,o,H_2O}}{dt}$ ,  $\frac{dx_{c,o,vol}}{dt}$  and  $\frac{dx_{c,o,C}}{dt}$ ) and underflow ( $\frac{dx_{c,u,ash}}{dt}$ ,  $\frac{dx_{c,u,S}}{dt}$ ,  $\frac{dx_{c,u,H_2O}}{dt}$ ,  $\frac{dx_{c,u,vol}}{dt}$  and  $\frac{dx_{c,u,C}}{dt}$ ) are proportional to the difference in their component densities ( $\rho_{c,ash}$ ,  $\rho_{c,S}$ ,  $\rho_{c,H_2O}$ ,  $\rho_{c,vol}$  and  $\rho_{c,C}$ ) to the magnetite medium density ( $\rho_{c,i,med}$ ), the difference in their component percentages ( $x_{c,o,ash}$ ,  $x_{c,o,S}$ ,  $x_{c,o,H_2O}$ ,  $x_{c,o,vol}$ ,  $x_{c,o,C}$ ,  $x_{c,u,ash}$ ,  $x_{c,u,S}$ ,  $x_{c,u,H_2O}$ ,  $x_{c,u,vol}$  and  $x_{c,u,C}$ ) to their corresponding feed percentages ( $x_{c,i,ash}$ ,  $x_{c,i,S}$ ,  $x_{c,i,H_2O}$ ,  $x_{c,i,vol}$  and  $x_{c,i,C}$ ), the acceleration due to a centrifugal force ( $\frac{v_{c,i}^2}{R_{c,eff}}$ ) and inversely proportional to the average particle size of the ore ( $d_c$ ).

In order to simplify the model, it is assumed that volumetric flow is in the steady state (i.e.  $Q_{c,i} = Q_{c,o} + Q_{c,u}$ ) and that the overflow and underflow are split by a

proportion  $\alpha$ . This means that  $Q_{c,o} = \alpha Q_{c,u}$  (i.e.  $Q_{c,o} = \frac{\alpha Q_{c,i}}{1+\alpha}$  and  $Q_{c,u} = \frac{Q_{c,i}}{1+\alpha}$ ) as described in section 2.4.3.2 of this dissertation. Similarly, it is assumed that the cyclone volume  $V_c$  is separated according to the same split proportion  $\alpha$  as in the volumetric feed flow (i.e.  $V_{c,o} = \frac{\alpha V_c}{1+\alpha}$  and  $V_{c,u} = \frac{V_c}{1+\alpha}$ ).

Using equation 3.1 (assuming the volumes  $V_o$  and  $V_u$  are constant) it is possible to determine that the conservation of total mass for the DMC is as follows:

$$V_{c,o} \frac{d\rho_{c,o}}{dt} + V_{c,u} \frac{d\rho_{c,u}}{dt} = W_{c,i} - Q_{c,o}\rho_{c,o} - Q_{c,u}\rho_{c,u}. \quad (4.9)$$

By using the assumption that the rates of change in mass to the overflow and underflow are proportional to the difference in their densities to the magnetite medium density, the acceleration due to centrifugal force and the percentage of either ash or carbon will yield the following relationships,

$$V_{c,o} \frac{d\rho_{c,o}}{dt} = K_{c,o}(\rho_{c,i,med} - \rho_{c,o})x_{c,i,C}, \quad (4.10)$$

$$V_{c,u} \frac{d\rho_{c,u}}{dt} = K_{c,u}(\rho_{c,i,med} - \rho_{c,u})x_{c,i,ash}, \quad (4.11)$$

where  $\frac{v_{c,i}^2}{R_{c,eff}} = \frac{Q_{c,i}^2}{A_c^2 R_{c,eff}}$  is the centrifugal acceleration (where  $A_c$  is the cross-sectional area of the inlet and  $R_{c,eff}$  is the effective radius of the cyclone near the spigot where most of the separation takes place) taken into the coefficients  $K_{c,o}$  and  $K_{c,u}$ .

Using equation 3.1 (assuming the volumes  $V_{c,o}$  and  $V_{c,u}$  are constant), the conservation of mass of individual components for the DMC can be determined

as follows,

$$\begin{aligned} V_{c,o}\rho_{c,o}\frac{dx_{c,o,ash}}{dt} + V_{c,o}x_{c,o,ash}\frac{d\rho_{c,o}}{dt} + V_{c,u}\rho_{c,u}\frac{dx_{c,u,ash}}{dt} + V_{c,u}x_{c,u,ash}\frac{d\rho_{c,u}}{dt} \\ = W_{c,i}x_{c,i,ash} - Q_{c,o}\rho_{c,o}x_{c,o,ash} - Q_{c,u}\rho_{c,u}x_{c,u,ash}, \end{aligned} \quad (4.12)$$

$$\begin{aligned} V_{c,o}\rho_{c,o}\frac{dx_{c,o,S}}{dt} + V_{c,o}x_{c,o,S}\frac{d\rho_{c,o}}{dt} + V_{c,u}\rho_{c,u}\frac{dx_{c,u,S}}{dt} + V_{c,u}x_{c,u,S}\frac{d\rho_{c,u}}{dt} \\ = W_{c,i}x_{c,i,S} - Q_{c,o}\rho_{c,o}x_{c,o,S} - Q_{c,u}\rho_{c,u}x_{c,u,S}, \end{aligned} \quad (4.13)$$

$$\begin{aligned} V_{c,o}\rho_{c,o}\frac{dx_{c,o,H_2O}}{dt} + V_{c,o}x_{c,o,H_2O}\frac{d\rho_{c,o}}{dt} + V_{c,u}\rho_{c,u}\frac{dx_{c,u,H_2O}}{dt} + V_{c,u}x_{c,u,H_2O}\frac{d\rho_{c,u}}{dt} \\ = W_{c,i}x_{c,i,H_2O} - Q_{c,o}\rho_{c,o}x_{c,o,H_2O} - Q_{c,u}\rho_{c,u}x_{c,u,H_2O}, \end{aligned} \quad (4.14)$$

$$\begin{aligned} V_{c,o}\rho_{c,o}\frac{dx_{c,o,vol}}{dt} + V_{c,o}x_{c,o,vol}\frac{d\rho_{c,o}}{dt} + V_{c,u}\rho_{c,u}\frac{dx_{c,u,vol}}{dt} + V_{c,u}x_{c,u,vol}\frac{d\rho_{c,u}}{dt} \\ = W_{c,i}x_{c,i,vol} - Q_{c,o}\rho_{c,o}x_{c,o,vol} - Q_{c,u}\rho_{c,u}x_{c,u,vol}, \end{aligned} \quad (4.15)$$

$$\begin{aligned} V_{c,o}\rho_{c,o}\frac{dx_{c,o,med}}{dt} + V_{c,o}x_{c,o,med}\frac{d\rho_{c,o}}{dt} + V_{c,u}\rho_{c,u}\frac{dx_{c,u,med}}{dt} + V_{c,u}x_{c,u,med}\frac{d\rho_{c,u}}{dt} \\ = W_{c,i}x_{c,i,med} - Q_{c,o}\rho_{c,o}x_{c,o,med} - Q_{c,u}\rho_{c,u}x_{c,u,med}, \end{aligned} \quad (4.16)$$

$$\begin{aligned} V_{c,o}\rho_{c,o}\frac{dx_{c,o,C}}{dt} + V_{c,o}x_{c,o,C}\frac{d\rho_{c,o}}{dt} + V_{c,u}\rho_{c,u}\frac{dx_{c,u,C}}{dt} + V_{c,u}x_{c,u,C}\frac{d\rho_{c,u}}{dt} \\ = W_{c,i}x_{c,i,C} - Q_{c,o}\rho_{c,o}x_{c,o,C} - Q_{c,u}\rho_{c,u}x_{c,u,C}. \end{aligned} \quad (4.17)$$

Using the assumption that the rates of change in percentages of components to the overflow and underflow are proportional to the difference in their component densities to the magnetite medium density, the difference in their component percentages to their corresponding feed percentages, the acceleration due to centrifugal force  $\frac{v_{c,i}^2}{R_{c,eff}}$  and being inversely proportional to the average particle

size  $d_c$  of the ore will yield the following relationships:

$$\frac{dx_{c,o,ash}}{dt} = K_{c,o,ash}(\rho_{c,i,med} - \rho_{ash})(x_{c,i,ash} - x_{c,o,ash}), \quad (4.18)$$

$$\frac{dx_{c,u,ash}}{dt} = K_{c,u,ash}(\rho_{ash} - \rho_{c,i,med})(x_{c,i,ash} - x_{c,u,ash}), \quad (4.19)$$

$$\frac{dx_{c,o,S}}{dt} = K_{c,o,S}(\rho_{c,i,med} - \rho_S)(x_{c,i,S} - x_{c,o,S}), \quad (4.20)$$

$$\frac{dx_{c,u,S}}{dt} = K_{c,u,S}(\rho_S - \rho_{c,i,med})(x_{c,i,S} - x_{c,u,S}), \quad (4.21)$$

$$\frac{dx_{c,o,H_2O}}{dt} = K_{c,o,H_2O}(\rho_{c,i,med} - \rho_{H_2O})(x_{c,i,H_2O} - x_{c,o,H_2O}), \quad (4.22)$$

$$\frac{dx_{c,u,H_2O}}{dt} = K_{c,u,H_2O}(\rho_{H_2O} - \rho_{c,i,med})(x_{c,i,H_2O} - x_{c,u,H_2O}), \quad (4.23)$$

$$\frac{dx_{c,o,vol}}{dt} = K_{c,o,vol}(\rho_{c,i,med} - \rho_{vol})(x_{c,i,vol} - x_{c,o,vol}), \quad (4.24)$$

$$\frac{dx_{c,u,vol}}{dt} = K_{c,u,vol}(\rho_{vol} - \rho_{c,i,med})(x_{c,i,vol} - x_{c,u,vol}), \quad (4.25)$$

$$\frac{dx_{c,o,med}}{dt} = K_{c,o,med}(\rho_{c,i,med} - \rho_{c,o,med})(x_{c,i,med} - x_{c,o,med}), \quad (4.26)$$

$$\frac{dx_{c,u,med}}{dt} = K_{c,u,med}(\rho_{c,u,med} - \rho_{c,i,med})(x_{c,i,med} - x_{c,u,med}), \quad (4.27)$$

$$\frac{dx_{c,o,C}}{dt} = K_{c,o,C}(\rho_{c,i,med} - \rho_C)(x_{c,i,C} - x_{c,o,C}), \quad (4.28)$$

$$\frac{dx_{c,u,C}}{dt} = K_{c,u,C}(\rho_C - \rho_{c,i,med})(x_{c,i,C} - x_{c,u,C}). \quad (4.29)$$

In the case of the percentage of magnetite medium in equations 4.26 and 4.27, the difference between overflow and underflow medium density and the feed medium density is used. This is based on the fact that the density of the medium changes owing to the centrifugal forces within the DMC (this process is described in more detail in section 2.4.3.2 of this dissertation). The proportionality constants absorb the  $\frac{v_{c,i}^2}{R_{c,eff}d_c}$  term.

By using equations from this section, a non-linear state-space representation of the DMC can be derived. This will result in a non-linear model with each state equation having a non-linear function  $\dot{\mathbf{x}} = f(\mathbf{x}, \theta, \mathbf{u})$  where  $\mathbf{x}$  represents the densities ( $\rho_{c,o}$  and  $\rho_{c,u}$ ) and mass component percentages ( $x_{c,o,ash}$ ,  $x_{c,o,S}$ ,  $x_{c,o,H_2O}$ ,  $x_{c,o,vol}$ ,  $x_{c,o,med}$ ,  $x_{c,o,C}$ ,  $x_{c,u,ash}$ ,  $x_{c,u,S}$ ,  $x_{c,u,H_2O}$ ,  $x_{c,u,vol}$ ,  $x_{c,u,med}$  and  $x_{c,u,C}$ ) of the overflow and underflow.  $\theta$  represents the proportionality constants and  $\mathbf{u}$  represents the manipulated variables ( $W_{c,i}$  and  $\rho_{c,i,med}$ ).

Since the dynamic model of the DMC is derived from comprehensive dynamic mass balances, it is possible to determine a steady-state model which can be used to predict the partitioning behavior of the DMC similar to section 2.4.2.1. By

substituting equation 4.10 into equation 4.9, it is possible to obtain the density response of the underflow of the DMC. Similarly by substituting equation 4.11 into equation 4.9, it is possible to obtain the density response of the overflow of the DMC. By taking the derivatives of these two density responses to zero, a steady-state solution for the overflow and underflow densities can be found. Using the same principle with the percentage of medium in the overflow and underflow responses (i.e. substituting equation 4.26, equation 4.10 and equation 4.11 into equation 4.16 to obtain a percentage medium response in the underflow and substituting equation 4.27, equation 4.10 and equation 4.11 into equation 4.16 to obtain a percentage medium response in the overflow), it is possible to obtain steady-state solutions for the percentage of medium in the overflow and underflow (i.e. taking the derivatives of the two percentage medium responses to zero).

By simulating a float and sink analysis similar to the approach in section 2.4.2, it is possible to calculate the fractional yield percentages for different density fractions for the clean coal and discard. Using the yield, it is possible to obtain the reconstructed feed and compute the partition factor similar to what has been done in table 2.4. The partition factor can then be determined as follows:

$$Y = \frac{W_{c,o,ore}y_{pc}}{W_{c,o,ore}y_{pc} + W_{c,u,ore}(1 - y_{pc})}, \quad (4.30)$$

where  $W_{c,o,ore} = Q_{c,o}\rho_{c,o}(1 - x_{c,o,med})$ ,  $W_{c,u,ore} = Q_{c,u}\rho_{c,u}(1 - x_{c,u,med})$  and  $y_{pc} = \frac{W_{c,o,ore}}{W_{c,o,ore} + W_{c,u,ore}}$  is the yield. From this partition factor equation, it is possible to obtain an efficiency curve similar to that in figure 2.9 for a particular set of conditions, based on the predicted mass distributions to float and sink products of the different densities in the feed ( $\rho_{c,i}$ ). It must be noted that for increasing density fractions, the mass feed for consecutive density fractions is the mass rate from the sink of the previous density fraction. The mass rate for each float is computed using the steady-state equations while the mass rate for the sink is computed as the difference between float and the feed. Similarly, for decreasing density fractions, the mass feed for consecutive density fractions is the mass rate from the float of the previous density fraction. The mass rate for each sink is computed using the steady-state equations, while the mass rate for the float is computed as the difference between sink and the feed. The partition factor is calculated for each density fraction until the remaining mass rate is zero.

#### 4.2.5 Magnetite make-up corrected medium model

The magnetite medium is screened and washed out of the overflow and underflow products in the DMC. Section 2.4.4 illustrates how the dense medium is washed from the DMC product and discard and is kept in closed circuit and collected in a medium sump or tank. The product and discard are washed further to recover more magnetite. The water from this diluted solution is recovered by making use of a magnetic separator. To simplify this model, only the solution collected in the medium tank will be modelled. It is also assumed that perfect mixing occurs. A simplified illustration of the corrected medium tank can be found in figure 4.8.

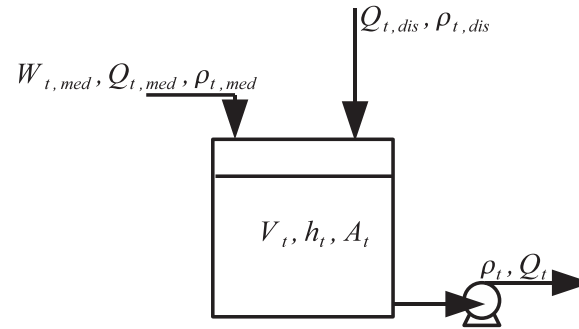


Figure 4.8: Simplified representation of a corrected medium make-up tank.

The following is a description of the variables used to model the corrected medium tank:

- $W_{t,med}$  - Mass feed rate of the magnetite medium recovered (kg/s),
- $\rho_{t,med}$  - Density of the magnetite medium recovered (kg/m<sup>3</sup>),
- $Q_{t,med}$  - Volumetric flow rate of the magnetite medium recovered (m<sup>3</sup>/s),
- $\rho_{t,dis}$  - Density of the magnetite make-up medium disturbance (kg/m<sup>3</sup>),
- $Q_{t,dis}$  - Volumetric flow rate of the magnetite make-up medium disturbance (m<sup>3</sup>/s),
- $\rho_t$  - Density of the corrected medium (kg/m<sup>3</sup>),
- $Q_t$  - Volumetric flow rate of the corrected medium (m<sup>3</sup>/s),
- $V_t$  - Volume of the magnetite medium in the corrected medium tank (m<sup>3</sup>),
- $h_t$  - Height of the magnetite medium in the corrected medium tank (m),
- $h_{t,max}$  - Maximum height of the magnetite medium in the corrected medium tank (m),
- $A_t$  - Effective area of the corrected medium tank (m<sup>2</sup>).

The following is a list of assumptions that have been made for the modelling of the corrected medium tank:

- The volumetric flow rates of the recovered medium ( $Q_{t,med}$ ), make-up medium ( $Q_{t,dis}$ ) and corrected medium ( $Q_t$ ) are instantaneous before and after a step is introduced in the recovered medium density ( $\rho_{t,med}$ ) or make-up medium density ( $\rho_{t,dis}$ ).
- The effective area of the corrected medium tank ( $A_t$ ) does not change with a change in height of the medium ( $h_t$ ) in the corrected medium tank.

Using equation 3.1 (as indicated by Stephanopoulos [1984:50], however, assuming the density is not constant), the conservation of total mass for the corrected medium tank can be determined as follows:

$$A_t h_t \frac{d\rho_t}{dt} + A_t \rho_t \frac{dh_t}{dt} = Q_{t,med} \rho_{t,med} + Q_{t,dis} \rho_{t,dis} - Q_t \rho_t, \quad (4.31)$$

where the rate of change in height of solution in the tank can be expressed using a similar expression as equation 3.1; however, only to include conservation of volumetric flow,

$$A_t \frac{dh_t}{dt} = Q_{t,med} + Q_{t,dis} - Q_t. \quad (4.32)$$

By substituting equation 4.32 into equation 4.31, using the height  $h_t$  as a measurement of that state, and by approximating the solution to the state equation using the fourth-order Runge-Kutta approximation, it is possible to model and simulate this system. For a tank that has a conical base, the surface area  $A_t$  can be expressed as a function of height. Since many level transmitters return their readings as a percentage of height, the maximum tank height  $h_{t,max}$  is required to compute the volume  $V_t$ .

### 4.3 DMS PLANT SIMULATION MODEL

This section describes how the models defined in section 4.2 are arranged and connected together. Only module one fines circuit of the Leeuwpan DMS plant will be modelled. However, module two can also be developed, as it is an exact duplicate of the module one plant. Only the plant tag names will differ between modules.

Figure 4.9 illustrates the typical configuration and interconnection of the different equipment models. This figure only shows the configuration for the fines section

of module one for the DMS plant at Leeuwpán. The tag names used can be found in the piping and instrument diagrams of Leeuwpán in addendum B.

Table 4.1 indicates the descriptions used for the tag names describing measurement information from the Leeuwpán DMS plant.

Table 4.1: Table indicating the description of the tag names taken from the production supervisory control and data acquisition system used for Leeuwpán DMS plant measurements.

Tag name	Description
L120-LT-1210	Module one circulating medium cyclone sump ultrasonic level transmitter
L120-PT-1206	Module one fine cyclone pressure
L100-WT-1002	Plant feed conveyor one belt scale
L140-WT-0300	Drum feed conveyor belt scale
L140-WT-0305B	Combined discard conveyor belt scale
L140-WT-4300	Stacker conveyor belt scale
L120-DY-1203	Circulating medium fine cyclone module one current-to-pressure converter
L120-DT-1203	Module one circulating medium density

It must be noted that the model that was developed only indicates the fines section of module one at the Leeuwpán DMS plant. This model can be expanded to the coarse and ultrafine section of the plant and ultimately include module two.

#### 4.4 DISCUSSION

The development of dynamic models can prove to be challenging and become very complex. These models can only be developed by understanding the intimate details of the equipment or process being modelled. This is achieved by conducting a detailed literature study of the process and its equipment.

By using fundamental equations describing the first principles of operation of processes in equipment, and combining these dynamic equations with specific assumptions, accurate relationships of the dynamics can be created. These dynamic equations formulate the system responses. These systems usually have a number of parameters, which can be used to match simulated responses to the actual process. The parameters are a result of the relationships developed.

Once each individual piece of equipment in the process has been modelled, they can be combined into an integrated model. This integrated model can be used to simulate the entire process being studied.



## 4.5 CONCLUSION

In this chapter, the various equipment models for the fine cyclone DMS plant were developed. Each equipment model contains a detailed explanation of the variables that make up the model and an explanation of the development of the process dynamics. As a result, a system model is developed for each piece of equipment. Finally, an integrated model is given to show how a combination of all individual equipment models can form a model for the fine cyclone DMS plant. This can then be expanded to other cyclones, such as the coarse and ultrafine section.

## CHAPTER 5: PARAMETER IDENTIFICATION AND ESTIMATION

### 5.1 INTRODUCTION

In this chapter the parameters defined for the various equipment models in chapter 4 are identified and estimated. The technique of algebraic identifiability as described by Xia and Moog (2003:331–332) will be applied to the non-linear equipment model developed for the DMC (section 4.2.4). The definition of algebraic identifiability will also be described in this chapter.

Once the parameters for each model have been identified and estimated from the input-output data that are available, it might be necessary to improve the estimation of the parameters by using an iterative process through which the plant and model outputs are compared and the parameter(s) are adjusted accordingly until a minimum acceptable scalar-valued norm is achieved. Ljung (1987) has documented and described these requirements and the scientific method of parameter estimation and model validation that will be used in this chapter in greater detail.

A section on correlations and scatterplots is presented because a scatterplot is used to illustrate a number of linear relationships for the top deck mass split ratio of the double deck screen.

### 5.2 PARAMETER IDENTIFIABILITY THEORY AND PROCESS

Before the parameters for the non-linear model that has been developed can be estimated, it is necessary to prove that the input and output data sets can be mapped uniquely to the parameters defining the system. This will then allow the minimal number of measurements of the input and output variables to be determined so that the parameters can be computed as described by Xia and Moog (2003:330).

In order to estimate the parameters required to define the model that will be developed, the technique and examples shown by Xia and Moog (2003:330–336) will be used. Xia and Moog (2003:331) consider a non-linear system

$$\Sigma_{\theta} : \left\{ \begin{array}{l} \dot{x} = f(x, \theta, u), x(0, \theta) = x_0, \\ y = h(x, \theta, u) \end{array} \right\}, \quad (5.1)$$

where  $x \in R^n$ ,  $u \in R^m$ ,  $y \in R^p$  are the state, input and output variables of the

system. Assuming that

$$\text{rank} \frac{\partial h(x, \theta, u)}{\partial x} = p, \quad (5.2)$$

means that the measurements of the various inputs and outputs are linearly independent where  $\theta$  is the parameter to be identified and  $x_0$  is independent of  $\theta$ .

A system is algebraically identifiable when its parameters can be estimated using the input and output information. Xia and Moog (2003:331–332) have provided definitions 3 and 4 to describe algebraic identifiability for the system in equation 5.1. These definitions are repeated below.

**Definition 1.** The system  $\Sigma_\theta$  is said to be algebraically identifiable if there exists a  $T > 0$ , a positive integer  $k$  and a meromorphic function  $\Phi: R^q \times R^{(k+1)m} \times R^{(k+1)p} \rightarrow R^q$  such that

$$\det \frac{\partial \Phi}{\partial \theta} \neq 0 \quad (5.3)$$

and

$$\Phi(\theta, u, \dot{u}, \dots, u^{(k)}, y, \dot{y}, \dots, y^{(k)}) = 0 \quad (5.4)$$

hold on  $[0, T] \forall (\theta, u, \dot{u}, \dots, u^{(k)}, y, \dot{y}, \dots, y^{(k)})$  where  $(\theta, x_0, u)$  belong to an open and dense subset of  $R^q \times R^q \times C_u^N[0, T]$ .  $C_u^N[0, T]$  denotes the set of all admissible inputs (on  $[0, T]$ ) that have continuous derivatives up to the order  $N$ .  $u, \dot{u}, \dots, u^{(k)}$  and  $y, \dot{y}, \dots, y^{(k)}$  are the derivatives of the input  $u(t)$  and output  $y(t, \theta, x_0, u)$ ;  $u(t) \in C^k[0, T]$ .

This enables the parameters to be computed by solving algebraic equations depending only on the information of the input and output data. If the initial conditions are known, this additional information can be used to determine the system parameters. The next definition describes this.

**Definition 2.** The system  $\Sigma_\theta$  is said to be identifiable with known initial conditions if there exists a positive integer  $k$  and a meromorphic function  $\Phi: R^q \times R^{(k+1)m} \times R^{(k+1)p} \rightarrow R^q$  such that  $\det \frac{\partial \Phi}{\partial \theta} \neq 0$  and

$$\Phi(\theta, x_0, u(0^+), u(\dot{0}^+), \dots, u^{(k)}(0^+), y(0^+), y(\dot{0}^+), \dots, y^{(k)}(0^+)) = 0 \quad (5.5)$$

hold for all  $(\theta, x_0, u(0^+), u(\dot{0}^+), \dots, u^{(k)}(0^+), y(0^+), y(\dot{0}^+), \dots, y^{(k)}(0^+))$ , where  $(\theta, x_0, u(0^+), u(\dot{0}^+), \dots, u^{(k)}(0^+))$  belong to an open and dense subset of  $R^q \times R^q \times R^{(k+1)m}$  and  $(y(0^+), y(\dot{0}^+), \dots, y^{(k)}(0^+))$  are the derivatives of the corresponding output  $y(t, \theta, x_0, u)$  evaluated at  $t = 0^+$ .

Rathaba (2004:58) indicates that definition 2 follows a similar procedure as

definition 1. He also explains that if the  $\text{rank} \frac{\partial h(x, \theta, u)}{\partial x} < p$  then some states cannot be estimated from the input-output data and therefore will require initial condition information.

The following steps will be used to ensure the parameters can be uniquely determined (shown by the example from Rathaba [2004:58–63]).

- Obtain the non-linear model in the form of equation 5.1.
- Determine the meromorphic function  $\Phi$  by taking the difference between the first time derivative of the output ( $\frac{\partial h}{\partial t}$ ) and the state derivative ( $\dot{x}$ ).
- Determine the Jacobian  $\frac{\partial \Phi}{\partial \theta}$  and its rank.
- The rank of the Jacobian determines the number of parameters that can be uniquely determined from measurements. If the rank equals the number of equations describing the states, the system is algebraically identifiable.

Once the non-linear system is proven to be algebraically identifiable, it is possible to determine the minimal number of measurements required from the input-output data to estimate the parameters. Xia and Moog (2003:334–335) illustrate this with an example of an HIV/AIDS model. In their example, higher order derivatives of the outputs are used to obtain unique solutions for their parameters. Each derivative requires an additional measurement. This can be used for the identification of the non-linear DMC model developed in chapter 4 to determine a unique solution for the parameters required.

## 5.3 PARAMETER IDENTIFIABILITY

### 5.3.1 DMC model

The parameters of the DMC model developed in section 4.2.4 can be identified by using the process described in section 5.2. In order to simplify the identification process, only the ash component will be used from the DMC model (equations 4.12, 4.18 and 4.19). The reason for this is that the equations representing the other components, such as sulphur, water, volatiles, magnetite medium and carbon, are similar to the ash equations. The conservation of overall mass for the DMC (equations 4.9, 4.10 and 4.11) will also be used for the parameter identifiability. The volumes,  $V_{c,o}$  and  $V_{c,u}$ , and volumetric flow rates,  $Q_{c,o}$  and  $Q_{c,u}$ , are expressed using the variables  $V_c$ ,  $Q_{c,i}$  and  $\alpha$  to simplify the parameter estimation.

For the identifiability study, the following parameters will initially be considered:

- $\alpha$  - Overflow and underflow volumetric proportionality split.
- $K_{c,u}$  - Proportionality constant for the underflow.
- $K_{c,u,ash}$  - Proportionality constant for the ash underflow.
- $x_{c,i,ash}$  - Percentage ash in the feed mix.
- $V_c$  - Volume of the cyclone.
- $Q_{c,i}$  - Volumetric flow rate of the feed mix.
- $A_c$  - Area of the inlet.
- $R_c$  - Effective radius at which separation takes place near the spigot.
- $\rho_{c,ash}$  - Ash density.
- $d_c$  - Average particle size.

The following state variables will also be considered for the identifiability study.

- $\rho_{c,o}$  - Density of the overflow.
- $\rho_{c,u}$  - Density of the underflow.
- $x_{c,o,ash}$  - Percentage ash in the overflow.
- $x_{c,u,ash}$  - Percentage ash in the underflow.

The following inputs will be considered for the identifiability study to follow.

- $W_{c,i}$  - Mass feed rate of the feed mix.
- $\rho_{c,i,med}$  - Density of the magnetite medium in the feed mix.

By assuming that all of the DMC model parameters are not fixed and by assigning

$$\text{the variables } \mathbf{x} = \begin{bmatrix} x_1 \\ x_2 \\ x_3 \\ x_4 \\ x_5 \\ x_6 \\ x_7 \\ x_8 \end{bmatrix} = \begin{bmatrix} \rho_{c,o} \\ \dot{x}_1 \\ \rho_{c,u} \\ \dot{x}_3 \\ x_{c,o,ash} \\ \dot{x}_5 \\ x_{c,u,ash} \\ \dot{x}_7 \end{bmatrix}, \theta = \begin{bmatrix} \alpha \\ K_{c,u} \\ K_{c,u,ash} \\ x_{c,i,ash} \\ V_c \\ Q_{c,i} \\ A_c \\ R_c \\ \rho_{c,ash} \\ d_c \end{bmatrix} \text{ and } \mathbf{u} = \begin{bmatrix} u_1 \\ u_2 \\ u_3 \\ u_4 \end{bmatrix} =$$

$$\begin{bmatrix} W_{c,i} \\ \dot{u}_1 \\ \rho_{c,i,med} \\ \dot{u}_3 \end{bmatrix}$$
 where  $\mathbf{x}$  represents the state variables,  $\theta$  represents the parameters

and  $\mathbf{u}$  represents the inputs for the system. This will yield a similar expression to the non-linear model in equation 5.1. Expressing the meromorphic function as  $\Phi = \mathbf{f}(\mathbf{t}, \mathbf{x}, \theta, \mathbf{u}) - \begin{bmatrix} \dot{y}_1 & \dot{y}_2 & \dot{y}_3 & \dot{y}_4 & \dot{y}_5 & \dot{y}_6 & \dot{y}_7 & \dot{y}_8 \end{bmatrix}^T$  where  $\dot{\mathbf{x}} = \mathbf{f}(\mathbf{t}, \mathbf{x}, \theta, \mathbf{u})$  and  $\mathbf{y} = \mathbf{h}(\mathbf{t}, \mathbf{x}, \theta, \mathbf{u})$  and with all states being measured in the output,  $\mathbf{h}(\mathbf{t}, \mathbf{x}, \theta, \mathbf{u}) =$

$$\begin{bmatrix} y_1 \\ y_2 \\ y_3 \\ y_4 \\ y_5 \\ y_6 \\ y_7 \\ y_8 \end{bmatrix} = \begin{bmatrix} x_1 \\ x_2 \\ x_3 \\ x_4 \\ x_5 \\ x_6 \\ x_7 \\ x_8 \end{bmatrix}, \text{ will ensure the properties required for algebraic identifiability}$$

hold. Since there are ten parameters and only eight state equations, it is not possible to identify this system. The derivatives of the inputs and outputs in the meromorphic function gives an indication of what will be the minimum number of measurements required to determine the system parameters. Further derivatives of the inputs and outputs could be used to express the meromorphic function; however, this will not be feasible because of the practical difficulty of taking many measurements of the overflow and underflow density and ash contents for the DMC.

Since most of the parameters describing the DMC model can be estimated, measured or calculated to a relatively high degree of accuracy, only the parameters  $\alpha$ ,  $K_{c,u}$ ,  $K_{c,u,ash}$  and  $x_{c,i,ash}$  need to be identified. The parameter  $x_{c,i,ash}$  is not used as an input in this study, as it is assumed constant. It can, however, be treated as an input for the model, which would be recommended when running the model online or using it in a control system. The volume  $V_c$  of the DMC can be measured or calculated very accurately. Since there is a fixed speed pump pumping the mix to the DMC, the volumetric flow rate  $Q_{c,i}$  can be estimated to a high degree of accuracy. It must be noted that there are other variables which affect flowrate, including the medium density and thus viscosity (a small effect), and wear in a pump over time. For the purposes of this dissertation, these affects are assumed negligible. The other parameters, such as the cross-sectional area of the feed inlet ( $A_c$ ) and effective radius at the spigot ( $R_c$ ), are known. The particle density (physical density) of ash ( $\rho_{c,ash}$ ) is a physical property and is known.

By assigning the variables from the DMC model as  $\mathbf{x} = \begin{bmatrix} x_1 \\ x_2 \\ x_3 \\ x_4 \end{bmatrix} = \begin{bmatrix} \rho_{c,o} \\ \rho_{c,u} \\ x_{c,o,ash} \\ x_{c,u,ash} \end{bmatrix}$ ,

$\theta = \begin{bmatrix} \alpha \\ K_{c,u} \\ K_{c,u,ash} \\ x_{c,i,ash} \end{bmatrix}$  and  $\mathbf{u} = \begin{bmatrix} u_1 \\ u_2 \end{bmatrix} = \begin{bmatrix} W_{c,i} \\ \rho_{c,i,med} \end{bmatrix}$  with all states being measured

in the output defined as  $\mathbf{y} = \mathbf{h}(\mathbf{t}, \mathbf{x}, \theta, \mathbf{u})$ . This gives the following state-space representation  $\dot{\mathbf{x}} = \mathbf{f}(\mathbf{t}, \mathbf{x}, \theta, \mathbf{u})$  as

$$\dot{x}_1 = \frac{1+\alpha}{\alpha V_c} u_1 - \frac{Q_{c,i}}{V_c} x_1 - \frac{Q_{c,i}}{\alpha V_c} x_2 - \frac{1+\alpha}{\alpha V_c} K_{c,u} (x_2 - u_2) \frac{Q_{c,i}^2}{A_c^2 R_c} x_{c,i,ash}, \quad (5.6)$$

$$\dot{x}_2 = \frac{1+\alpha}{V_c} K_{c,u} (x_2 - u_2) \frac{Q_{c,i}^2}{A_c^2 R_c} x_{c,i,ash}, \quad (5.7)$$

$$\begin{aligned} \dot{x}_3 = & \left( \frac{1}{x_3} \right) \left[ \frac{1+\alpha}{\alpha V_c} u_1 x_{c,i,ash} - \frac{Q_{c,i}}{V_c} x_1 x_3 - \frac{Q_{c,i}}{\alpha V_c} x_2 x_3 - \right. \\ & \left. x_3 \left( \frac{1+\alpha}{\alpha V_c} u_1 - \frac{Q_{c,i}}{V_c} x_1 - \frac{Q_{c,i}}{\alpha V_c} x_2 - \frac{1+\alpha}{\alpha V_c} K_{c,u} (x_2 - u_2) \frac{Q_{c,i}^2}{A_c^2 R_c} x_{c,i,ash} \right) - \right. \\ & \left. \frac{1}{\alpha} x_2 K_{c,u,ash} (\rho_{c,ash} - u_2) \frac{Q_{c,i}^2}{A_c^2 R_c d_c} (x_{c,i,ash} - x_4) - \right. \\ & \left. \frac{1}{\alpha} x_4 \left( \frac{1+\alpha}{V_c} K_{c,u} (x_2 - u_2) \frac{Q_{c,i}^2}{A_c^2 R_c} x_{c,i,ash} \right) \right], \quad (5.8) \end{aligned}$$

$$\dot{x}_4 = K_{c,u,ash} (\rho_{c,ash} - u_2) \frac{Q_{c,i}^2}{A_c^2 R_c d_c} (x_{c,i,ash} - x_4). \quad (5.9)$$

The Jacobian  $\frac{\partial \Phi}{\partial \theta}$  for this system has a rank of 4. This allows a unique solution for the parameters in  $\theta$  for the DMC to be determined. This can be achieved by using measurements from inputs and outputs based on the functions  $\rho_{c,o}$ ,  $\dot{\rho}_{c,o}$ ,  $\rho_{c,u}$ ,  $\dot{\rho}_{c,u}$ ,  $x_{c,o,ash}$ ,  $\dot{x}_{c,o,ash}$ ,  $x_{c,u,ash}$ ,  $\dot{x}_{c,u,ash}$ ,  $W_{c,i}$  and  $\rho_{c,i,med}$ . This means that the four parameters are algebraically identifiable and can therefore be estimated for unique solutions. In order to estimate these parameters, at least two measurements of each state (i.e.  $\rho_{c,o}$ ,  $\rho_{c,u}$ ,  $x_{c,o,ash}$  and  $x_{c,u,ash}$ ) will be required and at least one measurement of  $W_{c,i}$  and  $\rho_{c,i,med}$  will be necessary.

#### 5.4 PARAMETER ESTIMATION PROCESS

The system identification procedure described in section 3.3 indicates that once a set of candidate models is obtained, it is necessary to assess the candidate models using available data. Ljung (1987:169) supposes that a set of candidate models has been selected as a model structure  $\mathcal{M}$  and is parametrised with particular

models  $\mathcal{M}(\theta)$  using parameter vector  $\theta \in \mathbf{D}_{\mathcal{M}} \subset \mathbf{R}^d$ . This set of models is therefore defined as,

$$\mathcal{M}^* = \{\mathcal{M}(\theta) | \theta \in \mathbf{D}_{\mathcal{M}}\}. \quad (5.10)$$

Ljung (1987:170) describes a batch of data for the system as

$$\mathbf{Z}^N = [\mathbf{y}(\mathbf{1}), \mathbf{u}(\mathbf{1}), \mathbf{y}(\mathbf{2}), \mathbf{u}(\mathbf{2}), \dots, \mathbf{y}(\mathbf{N}), \mathbf{u}(\mathbf{N})], \quad (5.11)$$

and indicates that it is necessary to use the information in  $\mathbf{Z}^N$  to select a proper value  $\hat{\theta}_N$  of the parameter vector  $\theta$  to obtain a proper member  $\mathcal{M}(\hat{\theta}_N)$  in the set  $\mathcal{M}^*$ . The mapping of the data  $\mathbf{Z}^N$  to the set  $\mathbf{D}_{\mathcal{M}}$ ,

$$\mathbf{Z}^N \rightarrow \hat{\theta}_N \in \mathbf{D}_{\mathcal{M}}, \quad (5.12)$$

is known as a parameter estimation method.

In order for a model to predict a system output, a prediction error,

$$\epsilon(t, \theta_*) = y(t) - \hat{y}(t | \theta_*), \quad (5.13)$$

given by a certain model  $\mathcal{M}(\theta_*)$  must be computed for  $t = 1, 2, \dots, N$  for a known data set  $\mathbf{Z}^N$ . Parameter estimation is described as the process where  $\hat{\theta}_N$  is selected so that the prediction error (equation 5.13) becomes as small as possible (Ljung, 1987:171).

Ljung (1987:171) mentions two approaches to qualify the size of the prediction error. These are the scalar-valued norm approach and the approach that demands  $\epsilon(t, \hat{\theta}_N)$  is uncorrelated with a given data sequence. The scalar-valued norm that measures the size of  $\epsilon$  is used for the parameter estimation of the equipment models for this dissertation and is described in more detail below.

The norm,

$$V_N(\theta, \mathbf{Z}^N) = \frac{1}{N} \sum_{\mathbf{t}=1}^N \ell(\epsilon(\mathbf{t}, \theta)), \quad (5.14)$$

with  $\ell(\cdot)$  as a positive scalar-valued function, can be used to measure the validity of the model  $\mathcal{M}(\theta)$ . The minimisation of equation 5.14,

$$\hat{\theta}_N = \hat{\theta}_N(\mathbf{Z}^N) = \arg \min_{\theta \in \mathbf{D}_{\mathcal{M}}} \mathbf{V}_N(\theta, \mathbf{Z}^N), \quad (5.15)$$

allows the estimation of  $\hat{\theta}_N$ . The procedures used to estimate  $\theta$  are referred to as prediction-error identification methods (PEM). For this dissertation  $\ell(\cdot)$  is chosen

as the quadratic norm (Ljung, 1987:172),

$$\ell(\epsilon) = \frac{1}{2}\epsilon^2. \quad (5.16)$$

By applying equation 5.15 it is possible to obtain a PEM to estimate model parameters by iteration. Rathaba (2004:87–88) describes a process that can be used to ensure that the model parameters define the actual process to a certain degree of accuracy  $V_i$ . By computing the norm (equation 5.14) and iteratively changing the model parameters ( $\theta_N$ ), it is possible to find a model that fits the data to a specific accuracy. Figure 5.1 illustrates this process.

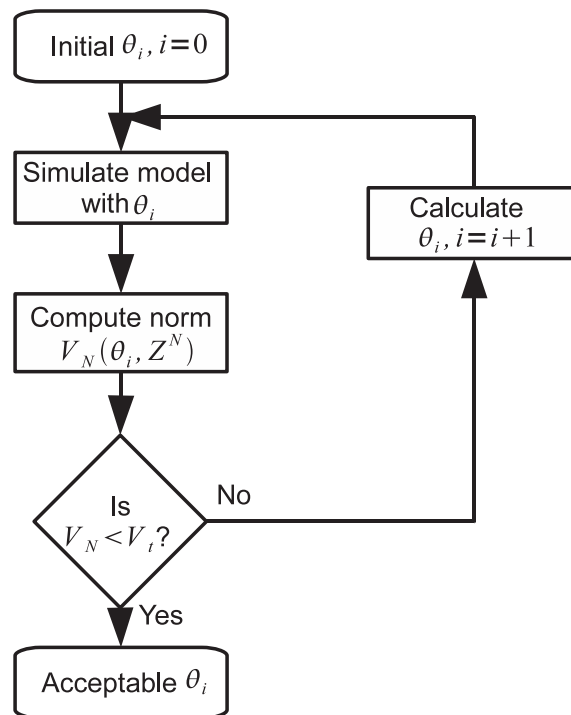


Figure 5.1: Parameter estimation iteration (Adapted from Rathaba (2004:88))

## 5.5 STATISTICAL ANALYSIS OF RESULTS

Performing an industrial experiment on the Leeuwpan DMS plant makes it possible to illustrate the accuracy of the models that have been developed by comparing the output of the models to the actual measured output of the plant in response to actual measured plant manipulated variables (Figure 5.2). The plant inputs and plant and model outputs and the resulting residuals can then be analysed to ascertain the quality of the model. The percentage fit between

the plant and model output is calculated as

$$\text{fit} = 100 \left[ \frac{1 - \sqrt{\sum |y - \hat{y}|^2}}{\sqrt{\sum |y - \mu_y|^2}} \right], \quad (5.17)$$

where  $y$  is the plant output,  $\hat{y}$  is the model output and  $\mu_y$  is the mean of  $y$  (Ljung, 2005:8:12). The percentage fit indicates the percentage of the output variation that is explained by the model. The definition of percentage fit allows for its value to be negative. A percentage fit of less than 0% indicates that the model does not explain the output variation.

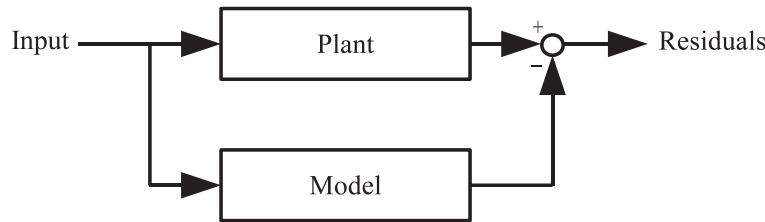


Figure 5.2: Comparison of a plant model to an actual plant output

The residual analysis consists of two tests (whiteness and independence test) as described by Ljung (2005:8:20). The whiteness test applies the autocorrelation function to the residual. If the autocorrelation result is inside the confidence interval, the residuals are uncorrelated. The independence test applies the cross correlation function to the residual and input. If the cross correlation result is outside the confidence interval, the model does not describe how part of the output relates to the corresponding input.

Another means of determining the relationship between two variables such as the simulation output and actual output or the cause-effect relationship between the dynamics of a state variable and output, a correlation can be performed on the two variables. Page and Meyer (2003:160–161) illustrate a graphical means of showing these relationships by making use of scatterplots in which each variable is plotted on an axis. A higher correlation between the variables will illustrate a linear plot of the data.

## 5.6 PARAMETER ESTIMATION

This section applies the principles and methods described in section 5.4 with the equipment models developed in section 4.2 to determine the model parameters.

### 5.6.1 Single-deck screen model

Table 5.1 indicates the values used for the single-deck screen model parameters. These values are used in the simulation of the model.

Table 5.1: Table showing single-deck screen parameter estimates.

Parameter	Estimate
$\alpha_f$	$\sqrt[10]{\frac{W'_f}{W_i}}$
$\tau_f$	0.7 (s)
$\tau_{f,uf}$	6.3 (s)

In order to simulate this model, the proportion of mass split ( $\alpha_f$ ) is estimated by utilising the measured input ( $W_i$ ) and output ( $W'_f$ ) feed rates. The reason for calculating  $\alpha_f$  is described in the section giving the parameters for the double deck screen (section 5.6.2). This means that  $\alpha_f$  is treated as a variable and not as a constant during the simulation.

### 5.6.2 Double-deck screen model

Table 5.2 indicates the values used for the double-deck screen model parameters. These values are used in the simulation of the model.

Table 5.2: Table showing double-deck screen parameter estimates.

Parameter	Estimate
$\alpha_o$	$\sqrt[10]{\frac{W_o}{W_i}}$
$\tau_o$	0.7 (s)
$\tau_{o,co}$	0.7 (s)
$\alpha_c$	$\sqrt[10]{\frac{W'_c}{W_i}}$
$\tau_c$	0.7(s)
$\tau_{c,fc}$	1.4 (s)

The parameter describing the proportion of mass split for the top ( $\alpha_o$ ) and bottom ( $\alpha_c$ ) deck is not constant over all feed rates. The mass split parameters vary because of the change in particle size distribution of the feed. The scatterplot in figure 5.3 illustrates this relationship over a number of shifts. The various linear relationships show the different particle distributions of the ore batches fed into the plant. Since the particle size distribution of the feed is not known, it is necessary to estimate the mass split based on measurements that are available from online belt scales. This means that  $\alpha_o$  and  $\alpha_c$  are treated as variables and not as constants for the simulation of the double deck screen.

The mass split on the top deck ( $\alpha_o$ ) can be estimated by taking the ratio between the belt scale measuring the oversized material conveyed to the drum ( $W_o$ ) and

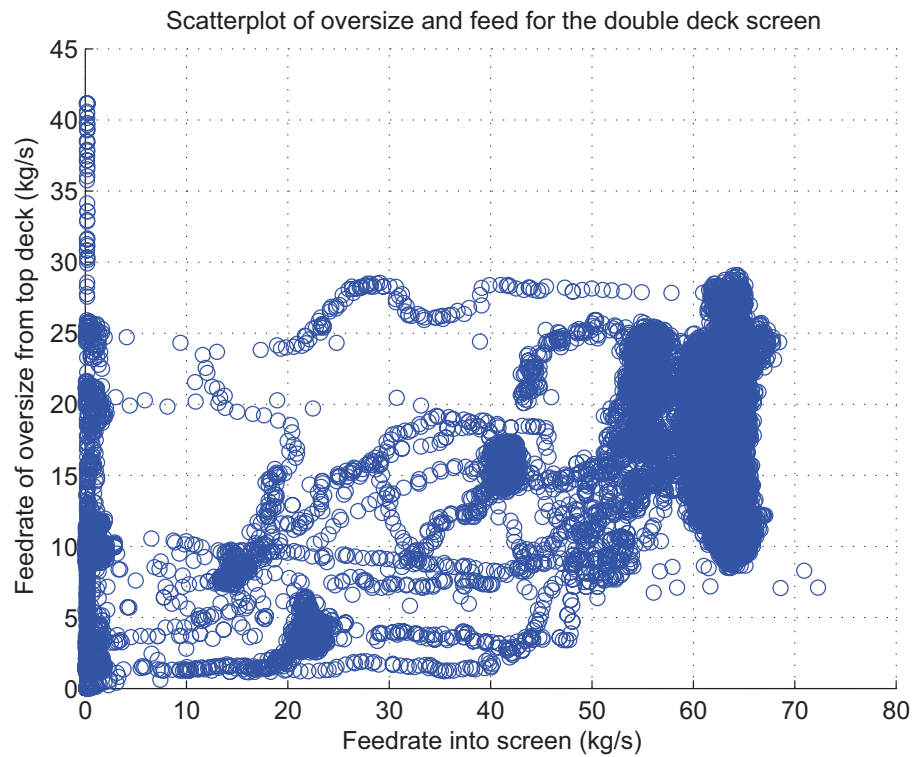


Figure 5.3: Scatterplot illustrating relationship between double-deck screen feed and oversized material.

the belt scale of the feed ( $W_i$ ). For the estimation of the mass split at the bottom deck ( $\alpha_c$ ), an estimate needs to be made of the coarse material throughput ( $W'_c$ ) as there is no mass throughput measurement made directly after this section of the screen. This estimate can be made by adding the discard and coarse material mass throughput measurements. By assuming that each screen deck can be modelled as 10 first-order linear system distributions in series, the 10<sup>th</sup> root of each mass split parameter is calculated. This calculation is required to ensure that the overall gain is maintained at  $\frac{W_o}{W_i}$  for the top deck and  $\frac{W'_c}{W_i}$  for the bottom deck.

### 5.6.3 Magnetite water-addition model

Table 5.3 indicates the values used for the magnetite water-addition model parameters. These values are used in the simulation of the model.

Table 5.3: Table showing magnetite water-addition parameter estimates.

Parameter	Estimate
$Q_{p,i}$	0.495 (m <sup>3</sup> /s)
$Q_{p,med}$	0.495 (m <sup>3</sup> /s)
$V_p$	3.53 (m <sup>3</sup> )
$K_p$	0.16E-3 (m <sup>2</sup> )

### 5.6.4 Mixing box model

Table 5.4 indicates the values used for the mixing box model parameters. These values are used in the simulation of the model.

Table 5.4: Table showing mixing box parameter estimates.

Parameter	Estimate
$Q_{mb}$	0.500 (m <sup>3</sup> /s)
$Q_{mb,med}$	0.495 (m <sup>3</sup> /s)
$V_{mb}$	0.16 (m <sup>3</sup> )

### 5.6.5 DMC model

Table 5.5 indicates the values used for the DMC model parameters. These values are used in the simulation of the model.

The parameter describing the volumetric flow rate to the DMC is estimated from the pump curve, which can be found in addendum D. The volume of the DMC is determined from estimated flow rates and residence time. The volumetric

Table 5.5: Table showing DMC parameter estimates.

Parameter	Estimate
$Q_{c,i}$	0.500 (m <sup>3</sup> /s)
$V_c$	0.38 (m <sup>3</sup> )
$\alpha$	2
$\rho_{c,ash}$	2000 (kg/m <sup>3</sup> )
$\rho_{c,S}$	1920 (kg/m <sup>3</sup> )
$\rho_{c,vol}$	1100 (kg/m <sup>3</sup> )
$\rho_{c,H_2O}$	1000 (kg/m <sup>3</sup> )
$\rho_{c,i,med} - \rho_{c,o,med}$	100 (kg/m <sup>3</sup> )
$\rho_{c,u,med} - \rho_{c,i,med}$	100 (kg/m <sup>3</sup> )
$Q_{c,i,med}$	0.495 (m <sup>3</sup> /s)
$K_{c,o}$	0.22 (m <sup>2</sup> s)
$K_{c,u}$	0.22 (m <sup>2</sup> s)
$K_{c,o,ash}$	200E-6 (m <sup>3</sup> s/kg)
$K_{c,u,ash}$	77E-6 (m <sup>3</sup> s/kg)
$K_{c,o,S}$	390E-6 (m <sup>3</sup> s/kg)
$K_{c,u,S}$	390E-6 (m <sup>3</sup> s/kg)
$K_{c,o,H_2O}$	150E-6 (m <sup>3</sup> s/kg)
$K_{c,u,H_2O}$	30E-6 (m <sup>3</sup> s/kg)
$K_{c,o,vol}$	890E-6 (m <sup>3</sup> s/kg)
$K_{c,u,vol}$	8.9E-6 (m <sup>3</sup> s/kg)
$K_{c,o,med}$	480E-6 (m <sup>3</sup> s/kg)
$K_{c,u,med}$	390E-6 (m <sup>3</sup> s/kg)

overflow and underflow split are estimated from the literature available in section 2.4.3.1. He and Laskowski (1994:213) performed a test to determine the effect of changing the medium relative density with respect to medium flow rate and the O/U ratio while ensuring a constant inlet pressure, and the DMC efficiency curves found in addendum D.

The densities of the various components such as ash, sulphur, volatiles and water have been taken from Hayes (2003). The difference in medium densities between feed and overflow and underflow is determined from the literature discussed in section 2.4.3.1 where He and Laskowski (1994:214) conducted tests on four different magnetite mediums, determined the cyclone overflow and underflow relative densities with respect to variations in the feed medium relative density. The magnetite medium flow rate is also determined from this section, where it is stated that the typical medium-to-ore ratio for coal beneficiation is 5:1. It is noted, however, that the ratio used both at Leeuwpan and the simulations are considerably larger than 5:1.

The parameters defining the proportionality constants can be estimated by making use of the parameter identifiability theory described in 5.2. However, because of the practical limitations of taking these measurements at Leeuwpan, they have been estimated by making use of simulation and iteration.

### 5.6.6 Magnetite make-up corrected medium tank model

Table 5.6 indicates the values used for the DMC model parameters. These values are used in the simulation of the model.

Table 5.6: Table showing magnetite make-up corrected medium parameter estimates.

Parameter	Estimate
$Q_{t,med}$	0.495 (m <sup>3</sup> /s)
$Q_t$	0.495 (m <sup>3</sup> /s)
$A_t$	0.28 (m <sup>2</sup> )
$h_{t,max}$	1.5 (m)

## 5.7 DISCUSSION

The parameters describing the dynamic systems that have been developed for the various equipment models are identified and estimated. Since the DMC model is non-linear, it has been proven to be algebraically identifiable.

The parameter identifiability of the DMC model can only be achieved by reducing the number of parameters to four and only considering the density and ash transfer functions. The remaining parameters need to be measured or must be known constants. If the feed mass components were to be considered as inputs instead of parameters, this would reduce the number of parameters to three, which would also ensure identifiability. Parameter identifiability is a very powerful tool when evaluating non-linear models, as it ensures model parameters can be uniquely matched to input and output data. It also gives an indication of how many measurements are required for the input-output data.

The estimation of the equipment parameters is an iterative process where the scalar-valued norm between the simulated output and actual measured output is determined. Each parameter is adjusted to reduce the scalar-valued norm. This estimation process can become time-consuming owing to the delays that occur as a result of the simulation time. The adjustment of the parameters is determined by knowing the processes involved and developing an intuitive knowledge of the systems.

## 5.8 CONCLUSION

This chapter describes the processes involved in identifying the parameters for the non-linear model of the DMC and then estimating all parameters for all

equipment models. The parameter estimates are described for each equipment model. The simulation results and model validations are described in the next chapter.

## CHAPTER 6: MODEL VALIDATION

### 6.1 INTRODUCTION

In this chapter the parameter estimates determined for the various equipment models in chapter 5 are used in conjunction with the mathematical models developed in chapter 4 to perform simulations in Matlab<sup>1</sup>. The models are simulated by either making use of the control systems toolbox available in Matlab or the fourth-order Runge-Kutta method (Mathews and Fink, 1999:458–460). The programming scripts used to generate the simulations can be found in addendum E. In order for the simulations to be conducted, the Leeuwpan DMS plant operation was analysed and a specific industrial test case was performed to illustrate the accuracy of the models and parameters.

### 6.2 LEEUWPAN OPERATION ANALYSIS AND INDUSTRIAL EXPERIMENT

#### 6.2.1 Leeuwpan DMS plant operation and analysis

A simplified process flow diagram representing the Leeuwpan DMS plant is given in figure 6.1. Data collected from Leeuwpan have been analysed and the findings will be given in this section. These data can be found in addendum C of this dissertation.

The yield for the DMS plant can be determined by computing the ratio of feed rates between the different products produced (peas, nuts and duff) and the ore fed into the plant. This yield is shown in figure 6.2 using a sample time of 60 s for the entire month of October 2008. It can be seen that the yield varies greatly during the month, possibly owing to instability or lack of control and changes in setpoints. It must be noted, however, that changes in setpoints will occur to enable the production team to produce various products of different ash contents based on the washability curve of the ore.

Using the yield curve in figure 6.2, it is possible to compute a Fast Fourier Transform (FFT), which can be found in figure 6.3. The larger spikes in the graph indicate prevalent oscillations having associated periods in the yield time-based curve. The average yield for October was 51.3%, with a standard deviation of 25.1%.

---

<sup>1</sup>Matlab is a technical computing system used for computation, visualisation and programming developed by The MathWorks, Inc. ([www.mathworks.com](http://www.mathworks.com)).

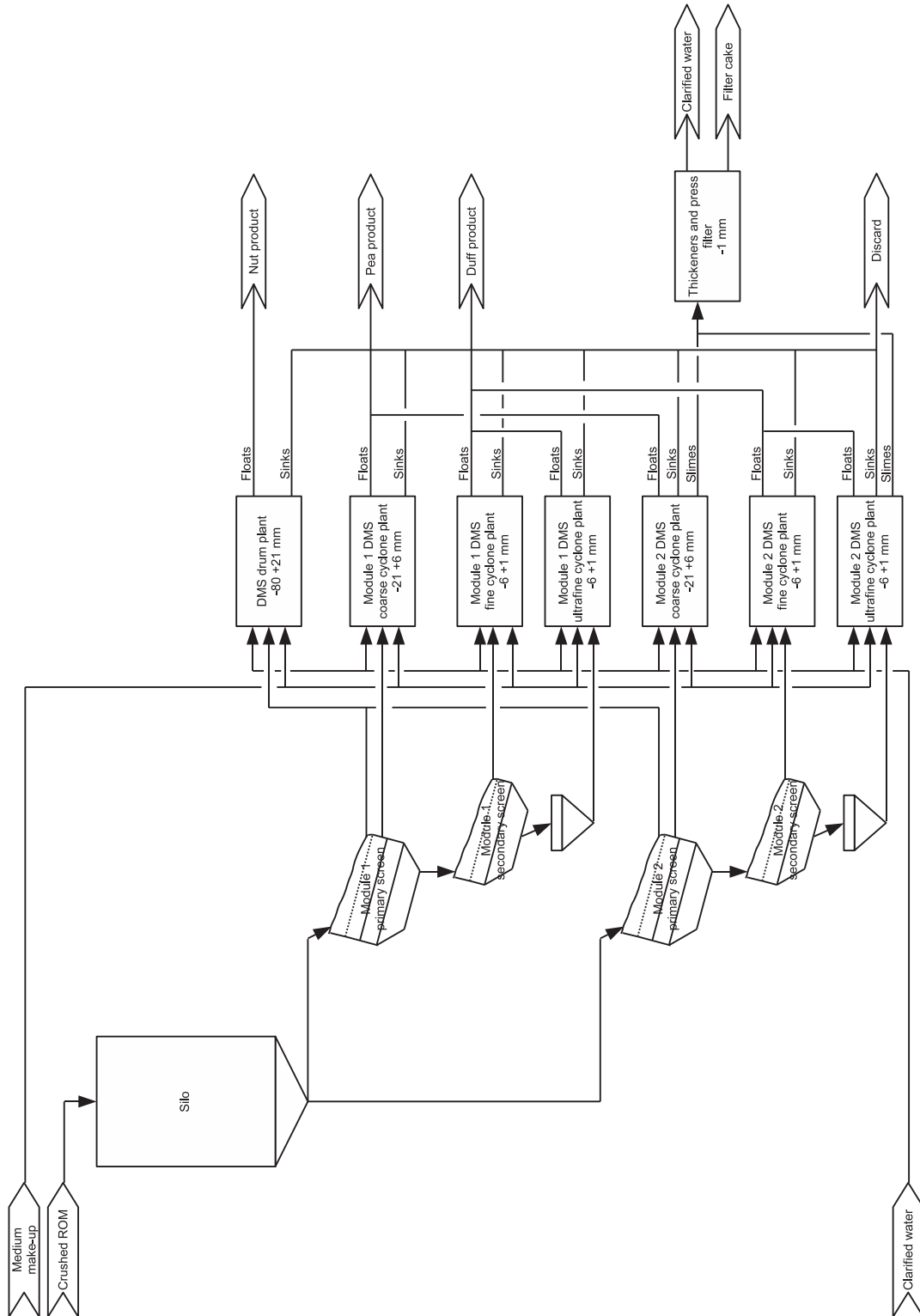


Figure 6.1: Leeuwan plant process flow diagram.

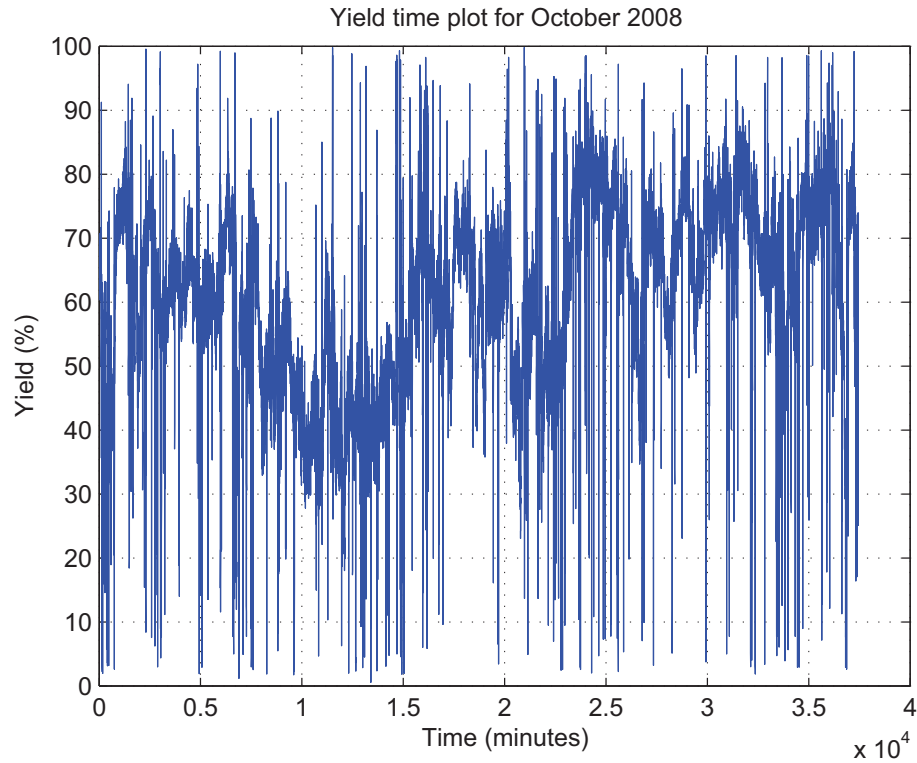


Figure 6.2: Yield over the month of October 2008.

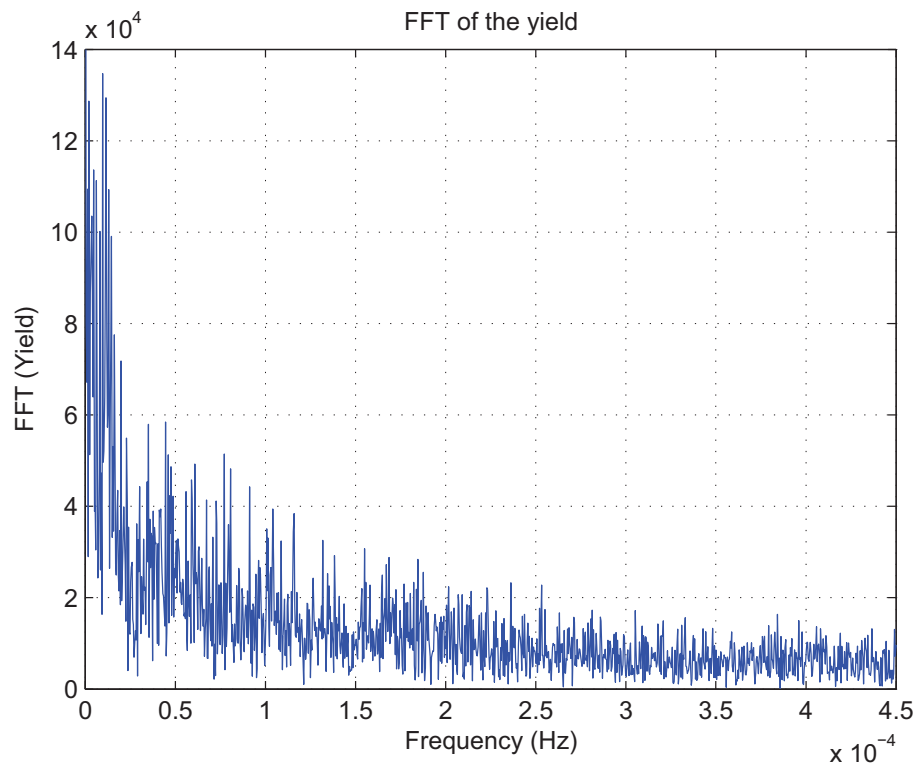


Figure 6.3: FFT of the yield for October 2008.

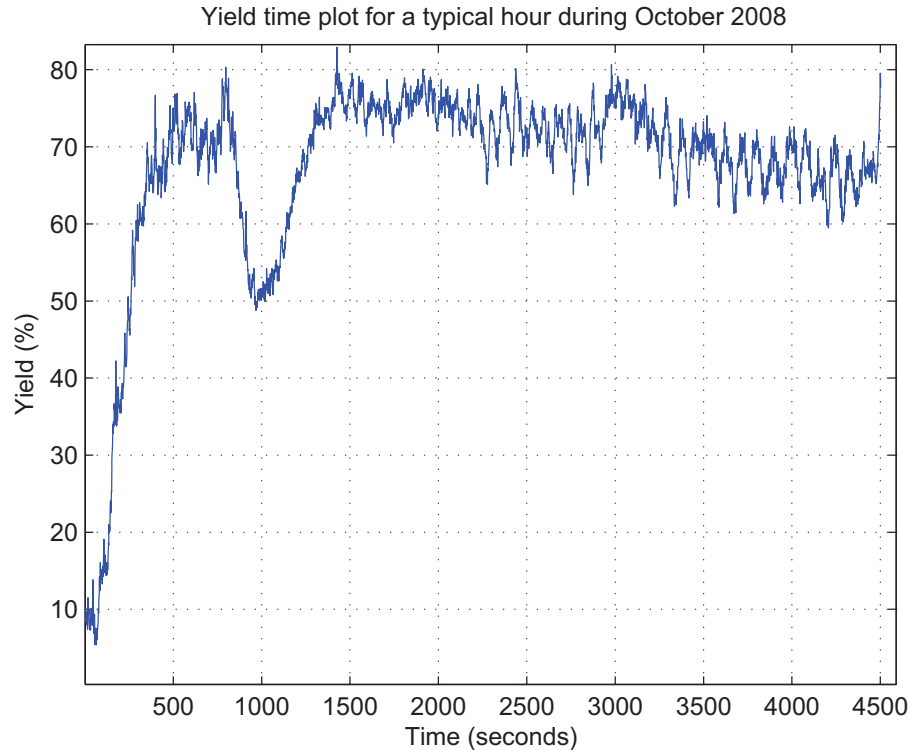


Figure 6.4: Yield for an hour during October 2008.

In order to examine some of these variations more closely, an hour of data sampled every 1 s was used. Figure 6.4 illustrates this curve for a typical plant start-up and operating mode. The FFT of this curve has also been computed (figure 6.5) to illustrate the oscillations for that hour in more detail. It can be seen that there are spikes, for example, at frequencies 1.1 mHz, 2.2 mHz, 3.1 mHz, 4.6 mHz and 11.8 mHz. This corresponds to oscillations in figure 6.4 having time periods of 15 minutes, 7.5 minutes, 5.4 minutes, 3.6 minutes and 1.4 minutes.

Figures 6.6 and 6.8 illustrate the ash percentages of the peas and duff products for the month of October 2008. The sampling period for this is 2 hours. It can be seen that product quality (i.e. ash content) varies significantly in the figures. The average ash content for the peas product during October 2008 is 15.4% with a standard deviation of 2%. The average ash content for the duff product during October 2008 is 15.9%, with a standard deviation of 2.1%. It is interesting to note that the correlation between the peas and duff ash content data is 68%. This indicates that the distribution of ash from the ore is fairly even between the two products measured.

The FFT for the peas and duff ash content curves has been computed and is illustrated in figures 6.7 and 6.9. It can be seen that there are spikes for the peas

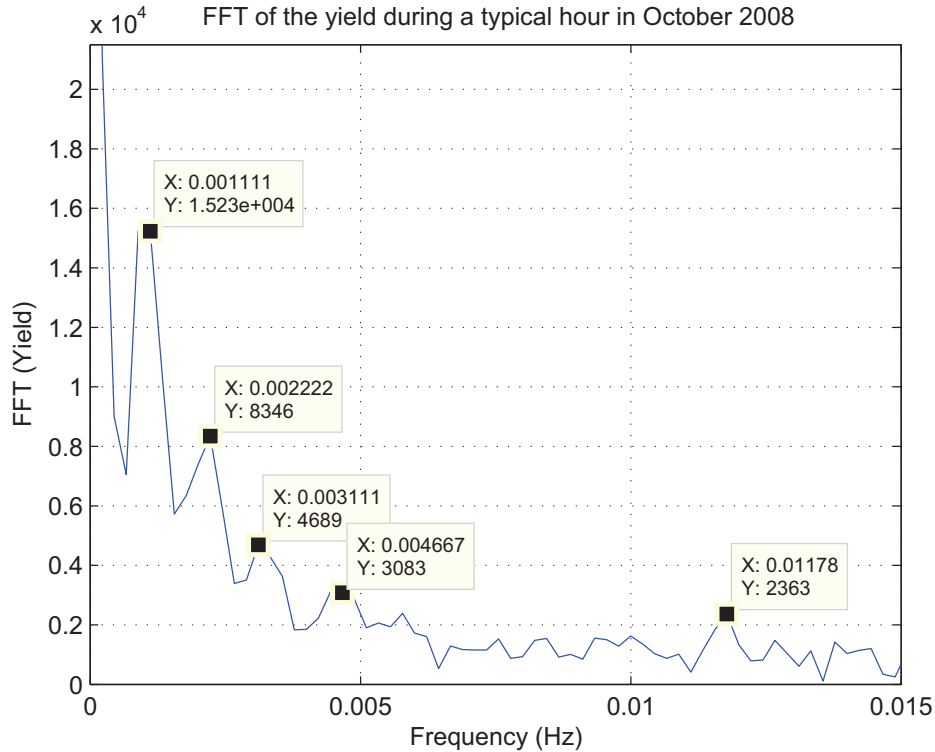


Figure 6.5: FFT of the yield for an hour during October 2008.

ash percentage at frequencies 1.3  $\mu\text{Hz}$ , 8.1  $\mu\text{Hz}$ , 10.0  $\mu\text{Hz}$  and 11.9  $\mu\text{Hz}$ . This corresponds to oscillations in figure 6.6 having time periods of 8.9 days, 1.4 days, 1.2 days and 23 hours. The spikes for the duff ash percentage are at frequencies 1.3  $\mu\text{Hz}$  and 8.1  $\mu\text{Hz}$ . This shows a similar response in oscillations to the peas ash percentage frequency response with 8.9 days and 1.4 days.

By reducing the frequency scale of figure 6.3 to be of a similar range to figures 6.7 and 6.9, it is possible compare the yield frequency response to the frequency response for ash percentages of peas and duff. Figure 6.10 illustrates the yield FFT over a smaller frequency range. It can be seen that there are spikes at frequencies 2.277  $\mu\text{Hz}$ , 9.866  $\mu\text{Hz}$  and 11.76  $\mu\text{Hz}$ . This corresponds to oscillations having time periods of 5.1 days, 1.2 days and 23.6 hours.

From the theory discussed in the literature study on washability curves in section 2.4.2.2, it is known that there is a relationship between yield and ash content at specific separation densities. From a comparison of the frequency responses of the yield (figure 6.10) and ash contents in peas (figure 6.7) and duff (figure 6.9), it can be assumed that variations or oscillations that occur in the yield result in similar disturbances in the ash content in the products.

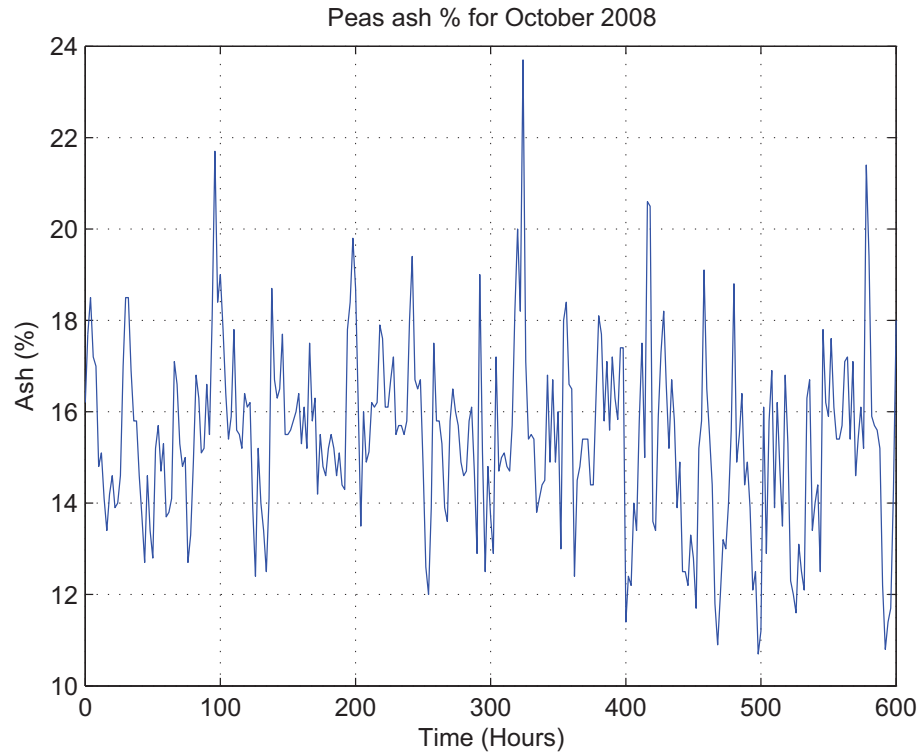


Figure 6.6: Ash percentage of the peas product during October 2008.

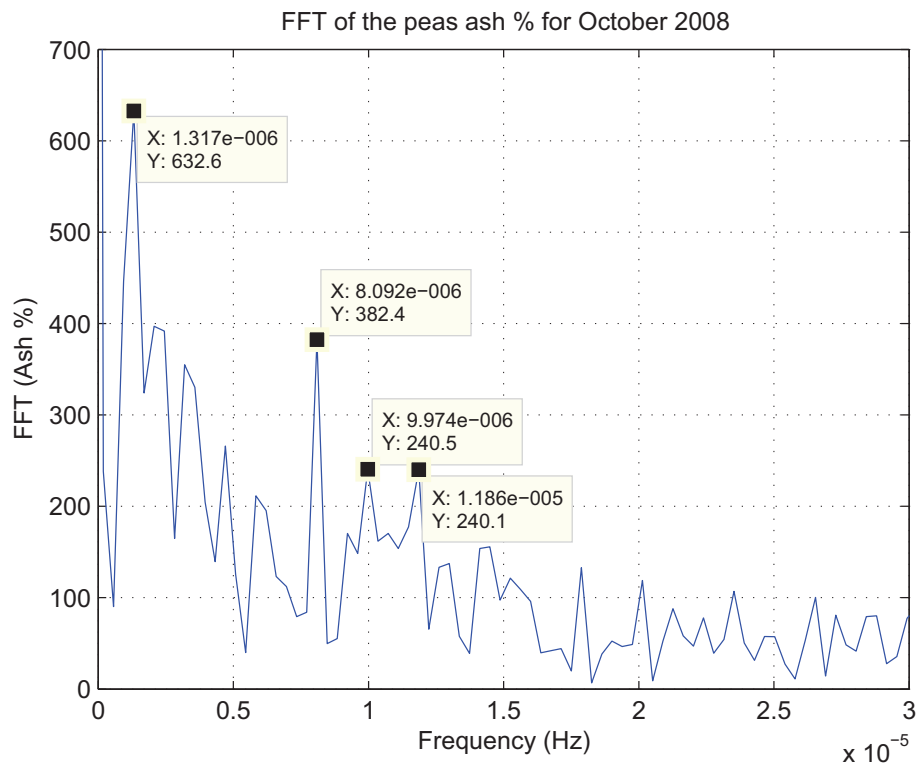


Figure 6.7: FFT of the peas ash percentage for October 2008.

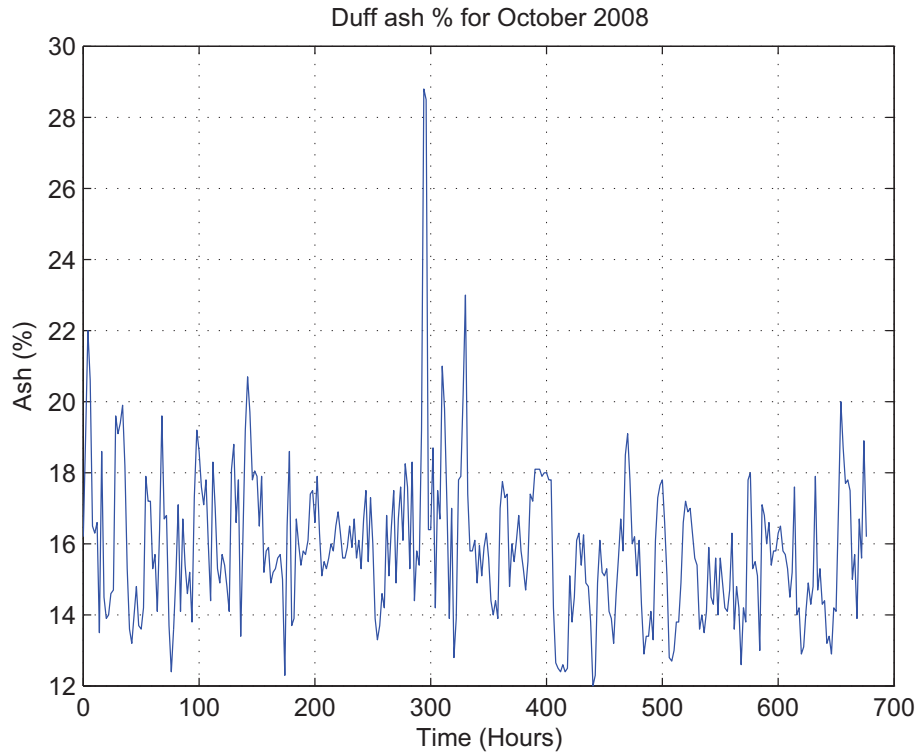


Figure 6.8: Ash percentage of the duff product during October 2008.

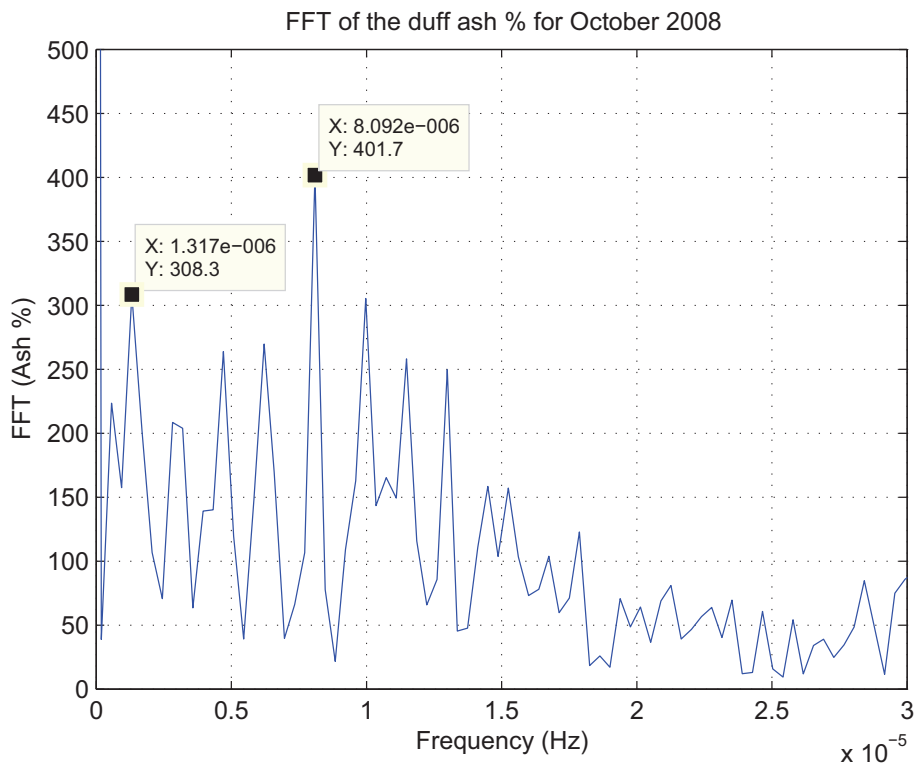


Figure 6.9: FFT of the duff ash percentage for October 2008.

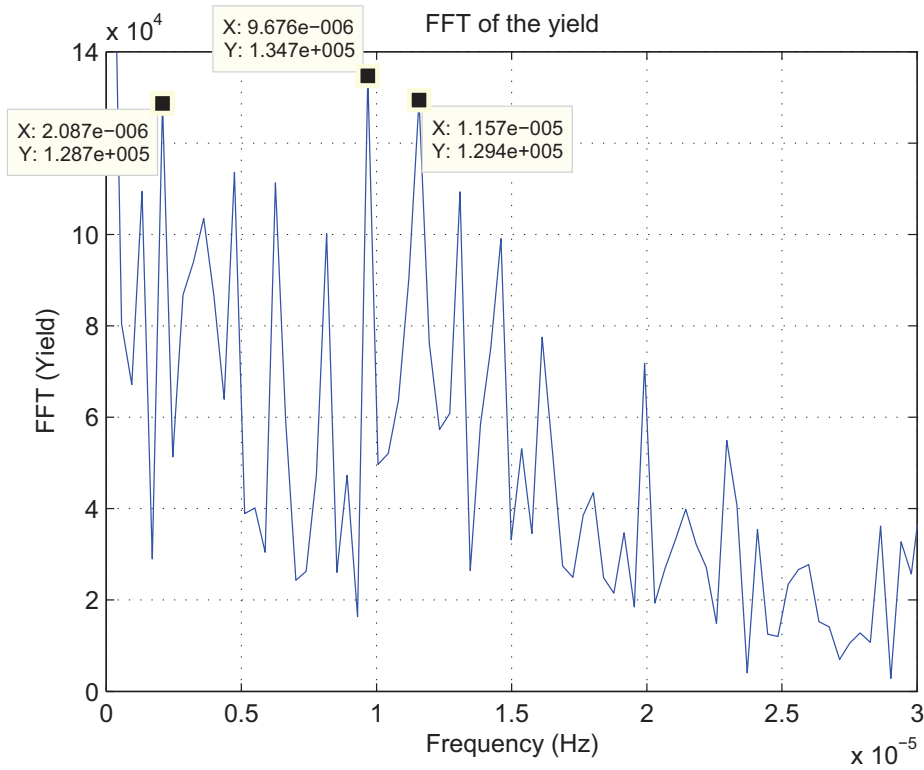


Figure 6.10: FFT of the yield for October 2008.

## 6.2.2 Industrial Experiment Test Case

In order to verify the model simulations it is necessary to perform a specific setpoint change on the Leeuwan DMS plant while taking measurements. The input measurements are then used for the model simulations. The output measurements are then compared to the model simulation outputs in order to validate the model.

The manipulated variable in the Leeuwan module one DMS plant is the medium density. Since it is difficult to take samples of the feed ore and product from the coarse and ultrafine cyclones, only the fine cyclone circuit was used. Figure 6.11 illustrates the change in density setpoint that was made for the step test and the measured feed rate into module one. During the step test, the feed rate of the ore into the plant dropped owing to the control system that is currently implemented. The reason for this occurring is to ensure that no spillages occur at the product conveyor belts.

During the step test representative samples were collected by a South African Bureau of Standards-approved laboratory every 5 minutes from the product washing screen of the fine cyclone. The laboratory results from the samples

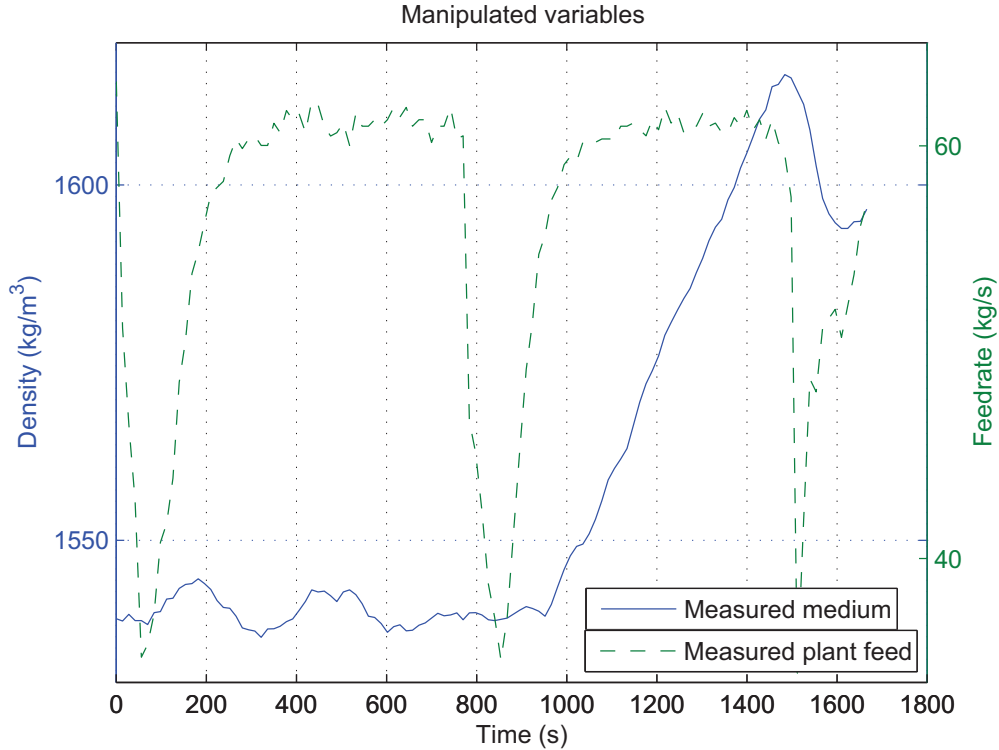


Figure 6.11: Step test for fine cyclone circuit from module 1 DMS plant.

can be found in table 6.1.

The author's involvement during the industrial step test was to oversee and supervise the sampling taken by the laboratory. The plant operators assisted the author in making the step changes to the plant control system. The data collected from the plant control system was obtained from the plant historian by the author himself.

Table 6.1: Laboratory results for fine cyclone circuit step test.

	Time	% Ash	% Moisture	% Volatiles	% Fixed carbon
Fine cyclone product screen (density step change)	12:15	14.5	0.9	11.8	72.8
	12:20	14.5	1.3	12.3	71.9
	12:25	15.6	1.5	11.1	71.8
	12:30	16.0	1.4	11.9	70.7
	12:35	15.8	1.5	12.3	70.4
	12:40	16.1	1.5	12.9	69.5
Average		15.4	1.4	12.1	71.2
Standard deviation		0.731	0.23	0.61	1.2

## 6.3 MODEL SIMULATIONS

### 6.3.1 Single- and double-deck screen models

Figure 6.12 illustrates the simulated feed rates of the oversize and coarse material of the double-deck screen model for over 2 hours. It also illustrates the fine material produced from the single-deck screen. By using this simulation, it is also possible to illustrate the mass states on top of each deck of the screens.

Figures 6.13 and 6.14 illustrate the mass states across the top and bottom deck oversize and coarse material of the double-deck screen over time during the simulation. Figure 6.15 illustrates this for the top deck of the single-deck screen fine material. It can be seen that the ore on the top deck in figure 6.13 decreases as it moves towards the overflow through each of the ten components. The bottom deck in figure 6.14 is initially empty and then quickly fills up with mass near the first few components. Thereafter it begins to decrease in mass as it nears the exit. The ore on the top deck of the single-deck screen reduces more slowly over time, as it is primarily used for washing and removal of ultrafine material.

In order to validate the model, the simulated output of the oversized material from the top deck of the double-deck screen can be compared to the actual measured output. This can be found in figure 6.16. The scalar-valued norm  $V_N(\theta, \mathbf{Z}^N)$  for this comparison as described by equation 5.14 is 0.03.

Figure 6.17 illustrates the scatterplot of the comparison between the simulated response and actual measured output of the top deck for the double-deck screen. The correlation of these data is 0.998.

In order to ensure the overall mass balance is met, it is possible to plot the sum of the outputs in figure 6.12 and compare this to the feed into the double-deck screen. Figure 6.18 illustrates this comparison. The difference between these two curves is related to the rates of change in the mass states on the decks of the double-deck screen.

The average yield for each particle-sized product can also be determined. The average yield for the oversized material at the top deck is 34% while for the coarse material it is 30%. The remaining 36% is collected and fed into the single-deck de-watering screen to separate the fine material from the ultrafine material. The yield of the fine material from the single-deck screen is 88%.

By using the same model parameters for the previous simulations, it is possible

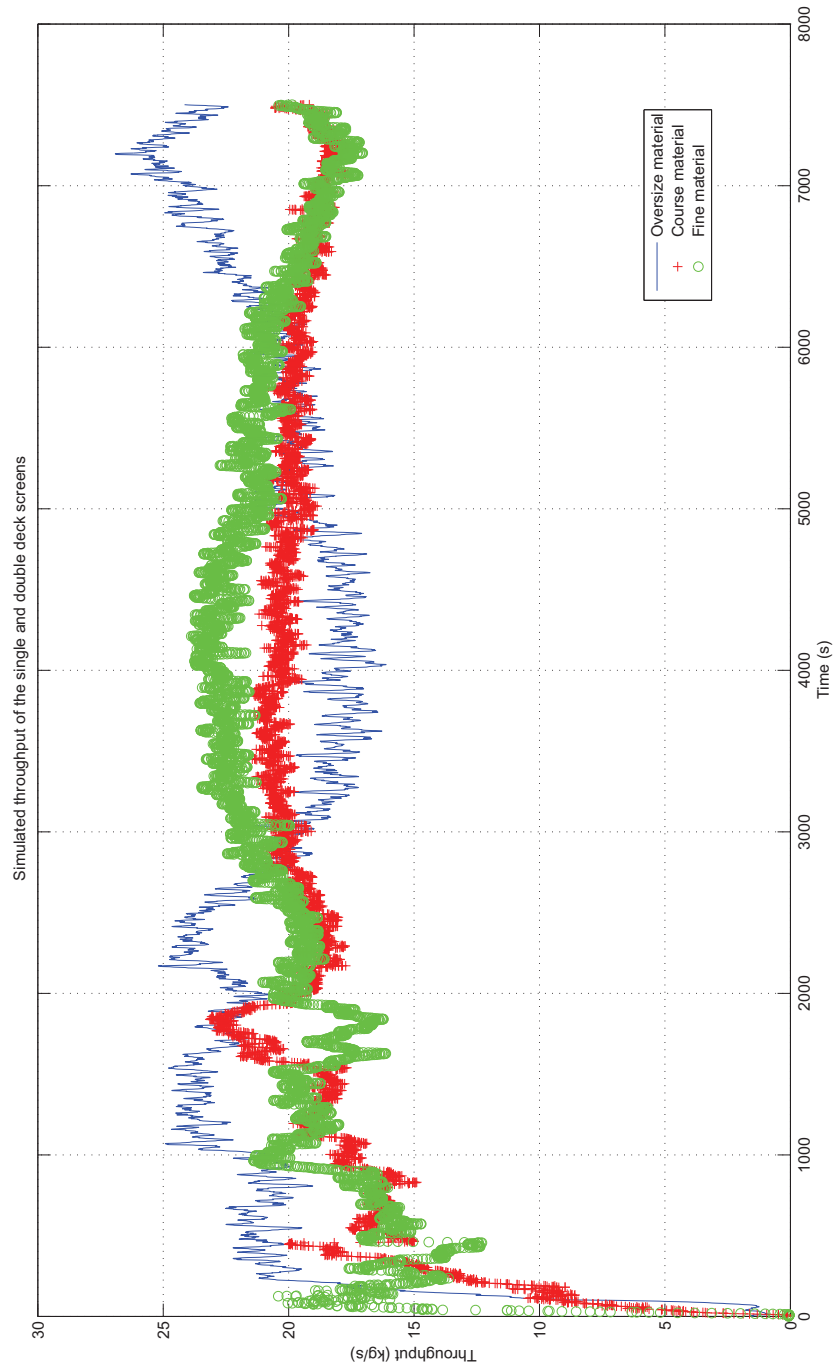


Figure 6.12: Simulation of the single- and double-deck screens.

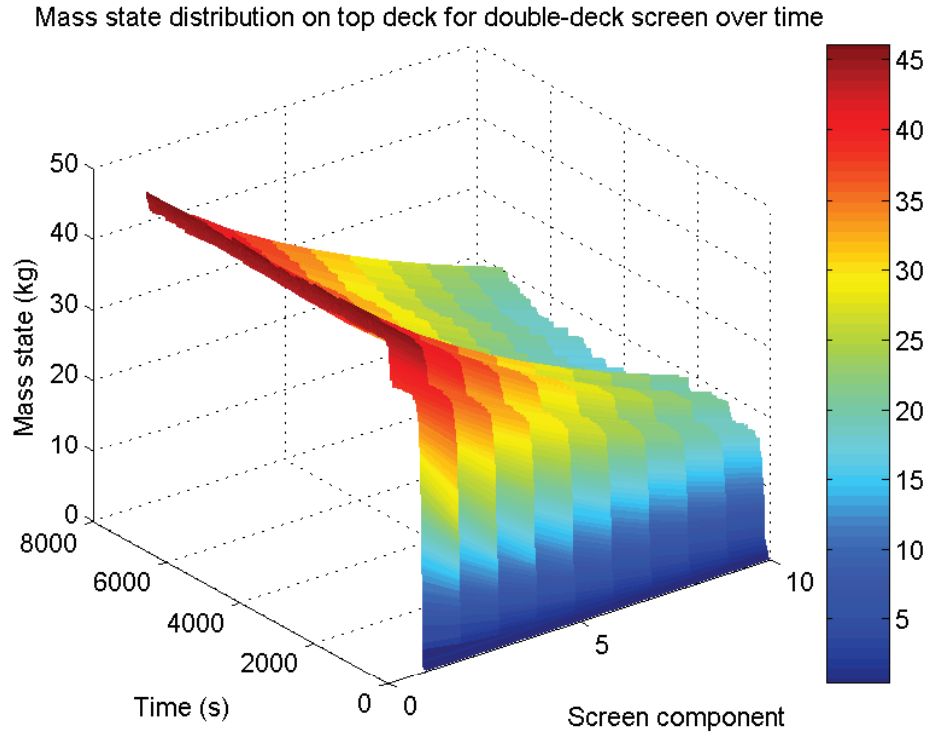


Figure 6.13: Mass state over top deck for double-deck screen.

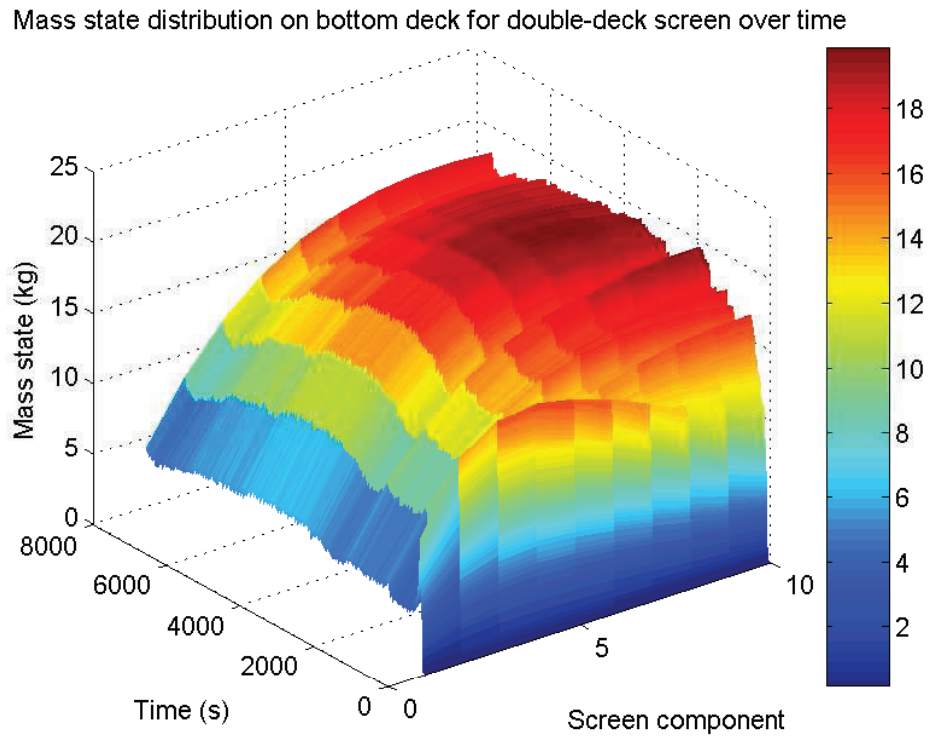


Figure 6.14: Mass state over bottom deck for double-deck screen.

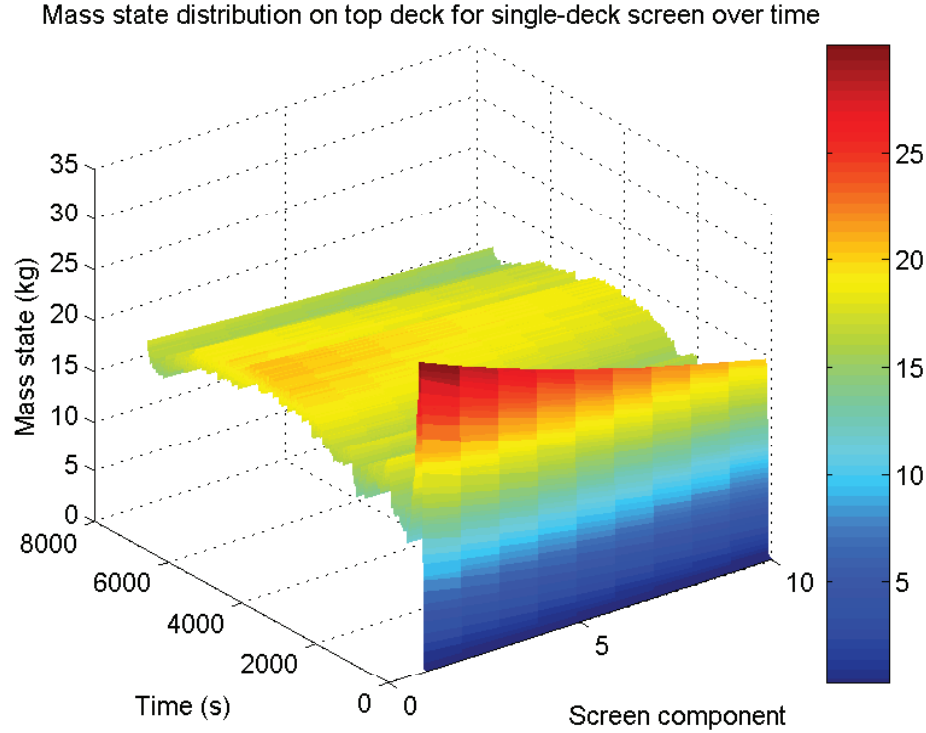


Figure 6.15: Mass state over top deck for single-deck screen.

to simulate the response of the screens over a shorter, more specific period where the density step test scenario was conducted (figure 6.19). The output of this simulation, specifically the fine material, is used for the remaining simulations through which the fine cyclone circuit is modelled and discussed later. The fine material simulation is used as a feed to the mixing box model (section 6.3.3). It is assumed that the feed ore measurement is delayed by 140 seconds before it reaches the screen. This transfer delay approximation was accepted by the plant metallurgist as a reasonable estimate (Lundt, 2008). The time delay can be determined experimentally by making use of a tracer and stop watch. The correlation of this simulation's oversized material to the actual oversize is 0.891. The scalar-valued norm  $V_N(\theta, \mathbf{Z}^N)$  for this comparison as described by equation 5.14 is 3.20. The average yield for this oversized material at the top deck is 41%, while for the coarse material it is 39%. The remaining 20% is collected and fed into the single-deck de-watering screen to separate the fine material from the ultrafine material. The yield of the fine material from the single-deck screen is 71%. This is achieved by using the same parameter settings as in the previous screening simulation.

The correlation between the simulated oversize material and actual oversize measurement is high. This high correlation means that the model predicts the

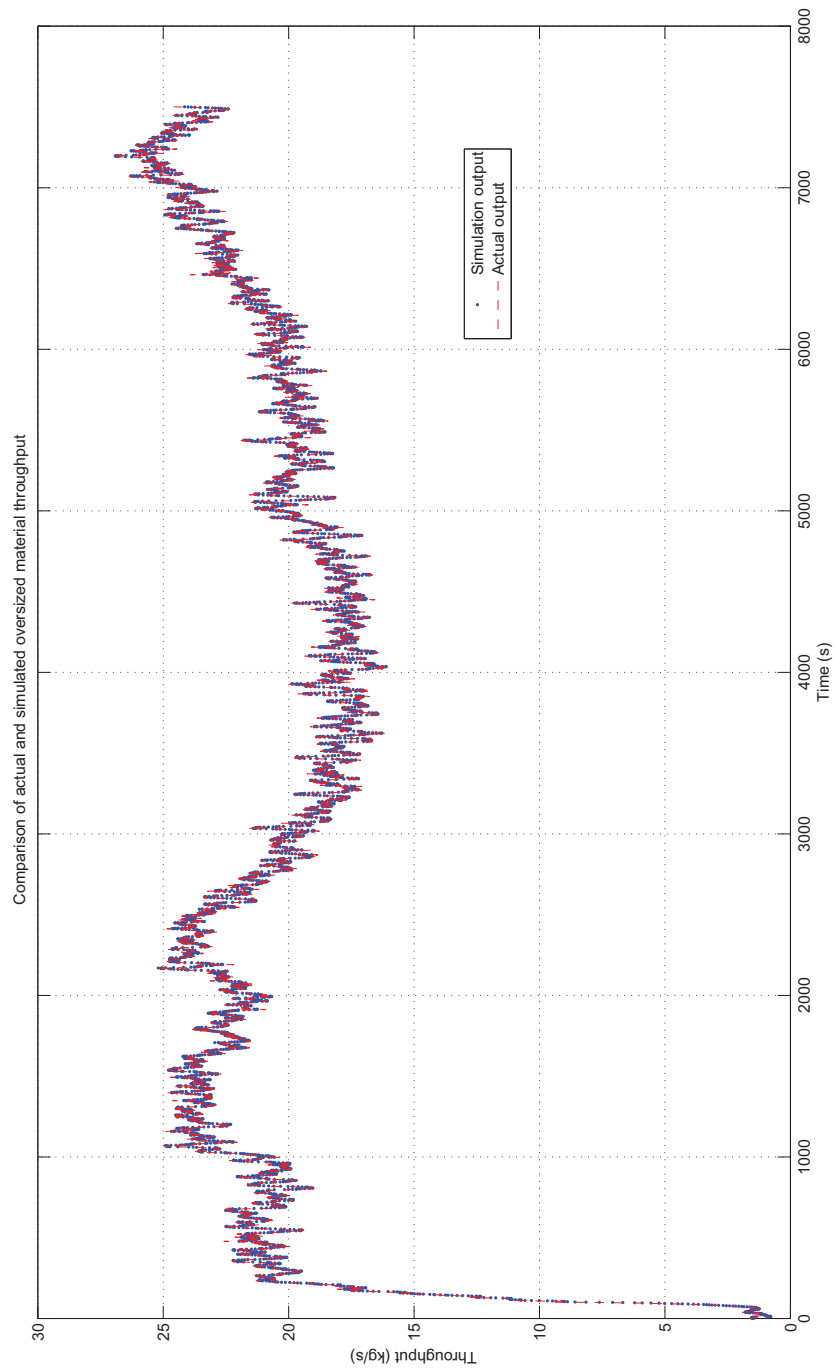


Figure 6.16: Simulated output versus actual output for the top deck of the double-deck screen.

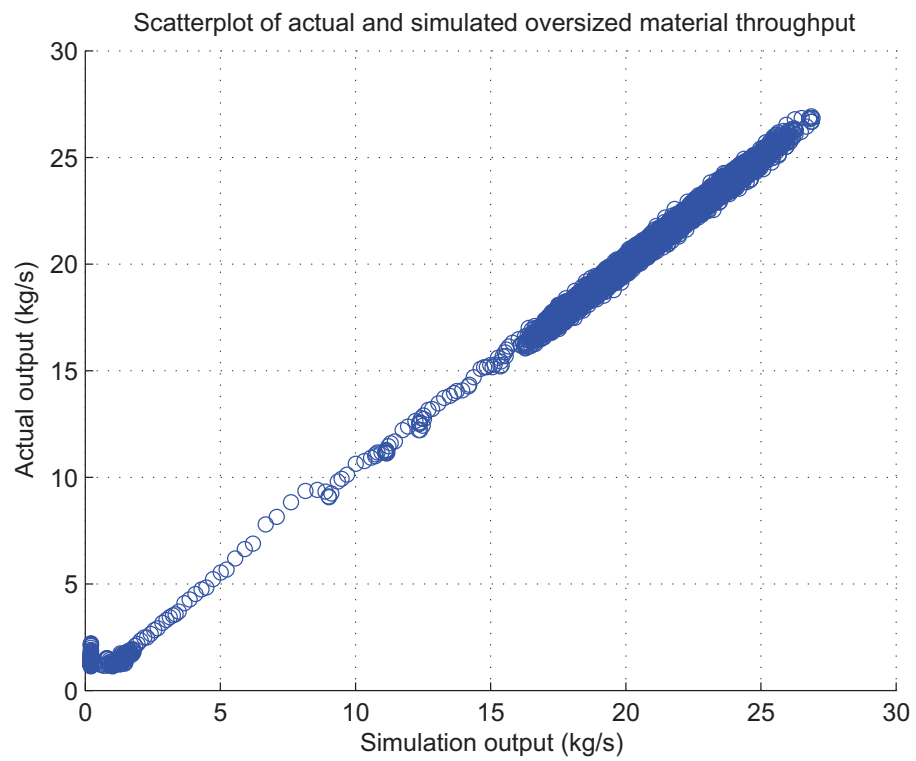


Figure 6.17: Scatterplot of the simulated output and actual output for the top deck.

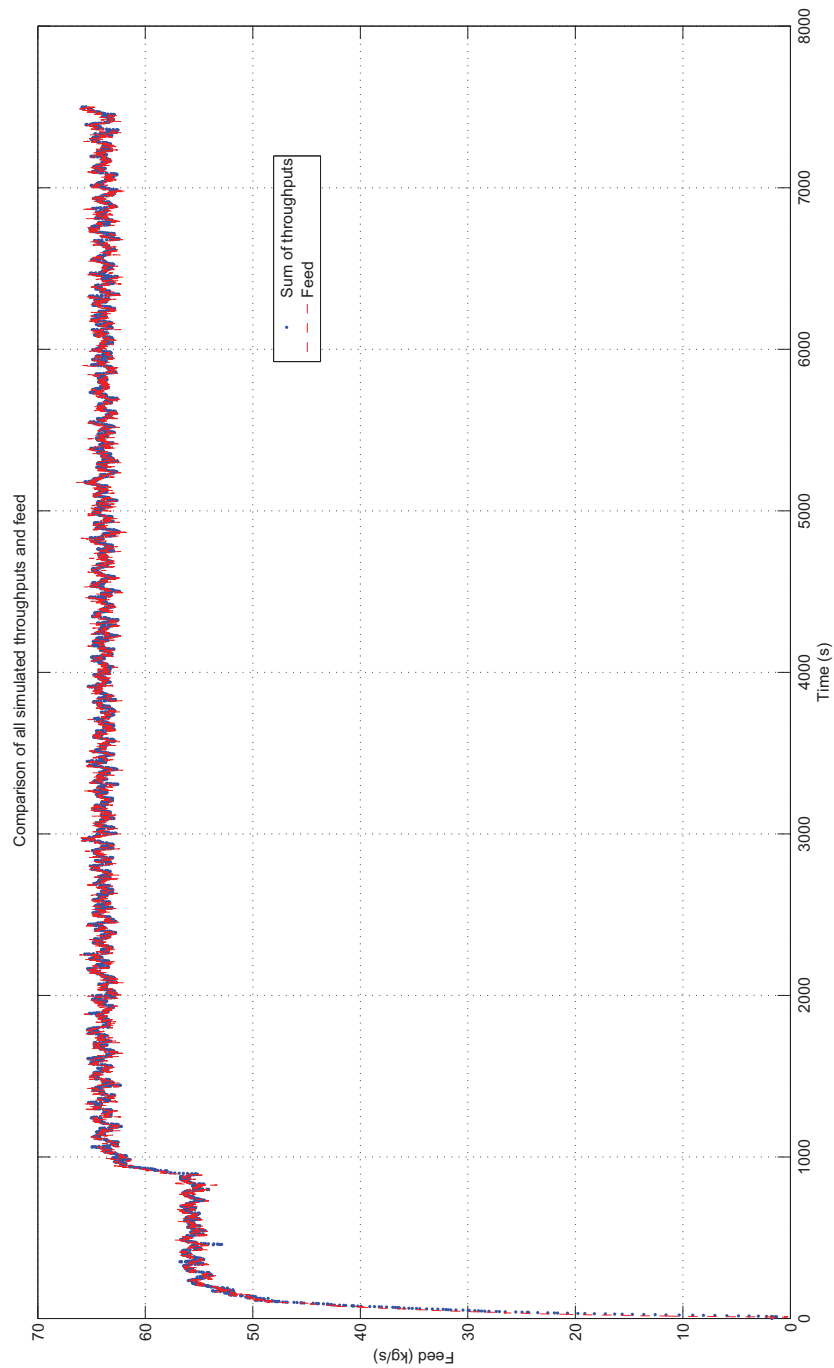


Figure 6.18: Comparison of feed into the double-deck screen and sum of feed rates exiting the screen.

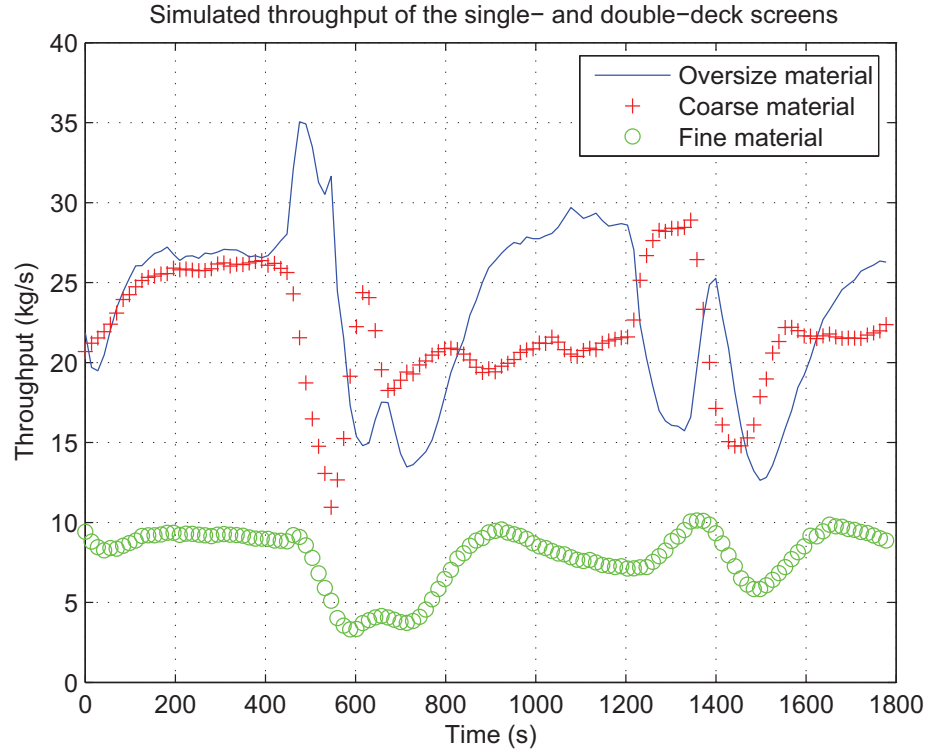


Figure 6.19: Simulated screen responses for the density step test scenario.

oversize material accurately. The yield for the different sized products is also comparable to that of what Leeuwan typically obtains.

### 6.3.2 Magnetite water-addition model

Figure 6.20 illustrates the simulation of the water-addition model. The medium-density measurement used as input into the water-addition model is not available, as it is not measured in the Leeuwan DMS operation. As a result, the simulated medium output from the DMC model (section 6.3.4) is used as input to the water-addition model. The simulated response is delayed by 14 seconds owing to the collection and recovery of the medium. This transfer delay approximation was accepted by the plant metallurgist as a reasonable estimate (Lundt, 2008). The time delay can be determined experimentally by making use of a tracer and stop watch. The other input that is used is the valve position. The scalar-valued norm  $V_N(\theta, \mathbf{Z}^N)$  for the simulated response and actual density measurement as described by equation 5.14 is 0.1698. The correlation between the simulated response and actual density measurement is 0.9998.

The residual for the water-addition model is given in figure 6.21. The fit

described by equation 5.17 is 97.8%. The whiteness and independence tests for the water-addition model are given in figures 6.22 and 6.23. The correlation for negative lags in the independence test indicates that “output feedback” occurs.

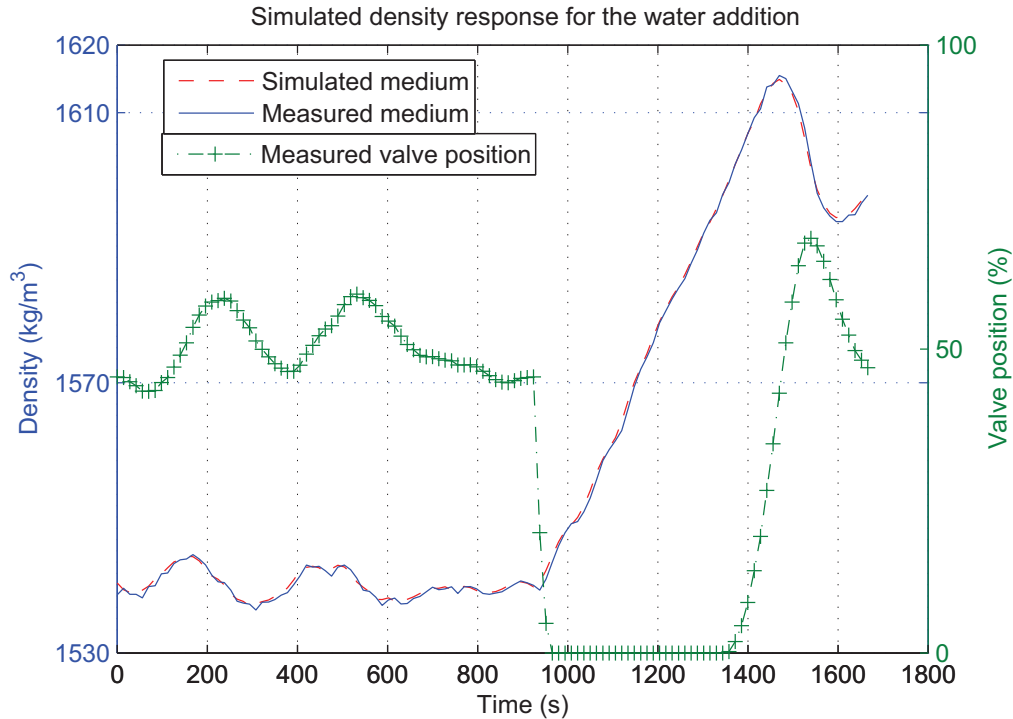


Figure 6.20: Simulated response of the water-addition model.

The high correlation in the water-addition comparison means that the model predicts the output accurately. The fit value indicates that the model explains the percentage of output variation well. The whiteness test in figure 6.22 shows that the residual does not contain information that can be encapsulated in the model. A correlation for the negative lags in the independence test (figure 6.23) is not necessarily an indication of an inaccurate model. The correlation at positive lags indicates that the time delay was estimated incorrectly. Since the sampling period of the data was 14 seconds, it was not possible to simulate the system with a smaller time delay.

### 6.3.3 Mixing box model

Figure 6.24 illustrates the simulation of the mixing box model.

The feed of the fine ore fed into the mixing box is not measured in the Leeuwpan DMS operation. As a result, the simulated response of the fine single-deck screen is used from section 6.3.1. Since the density of the mix is not measured as

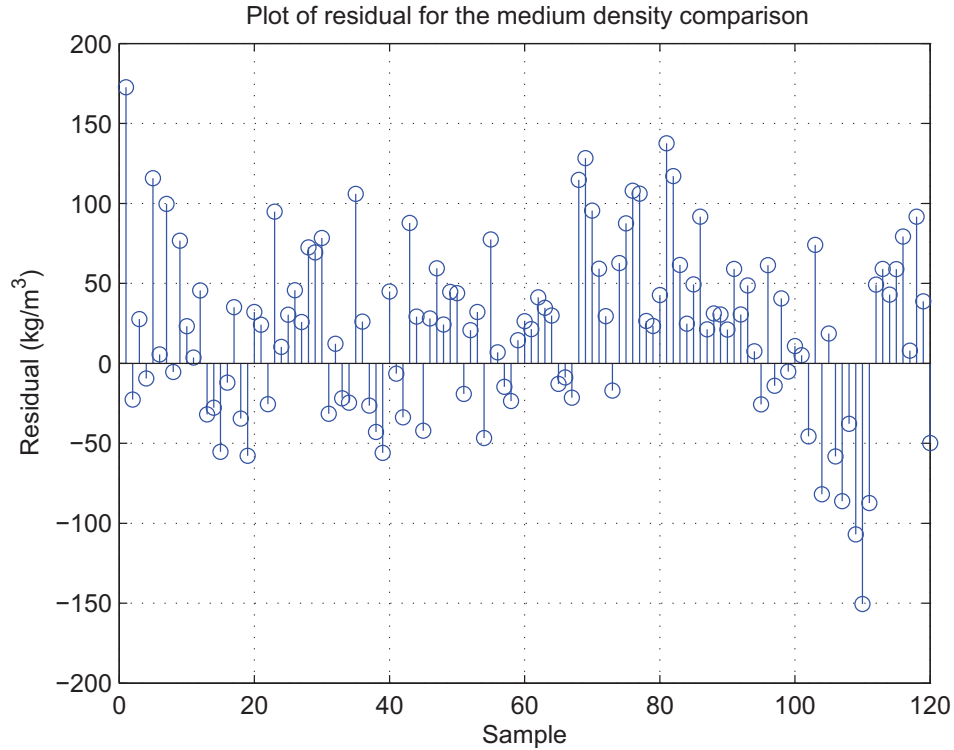


Figure 6.21: Water-addition residual plot.

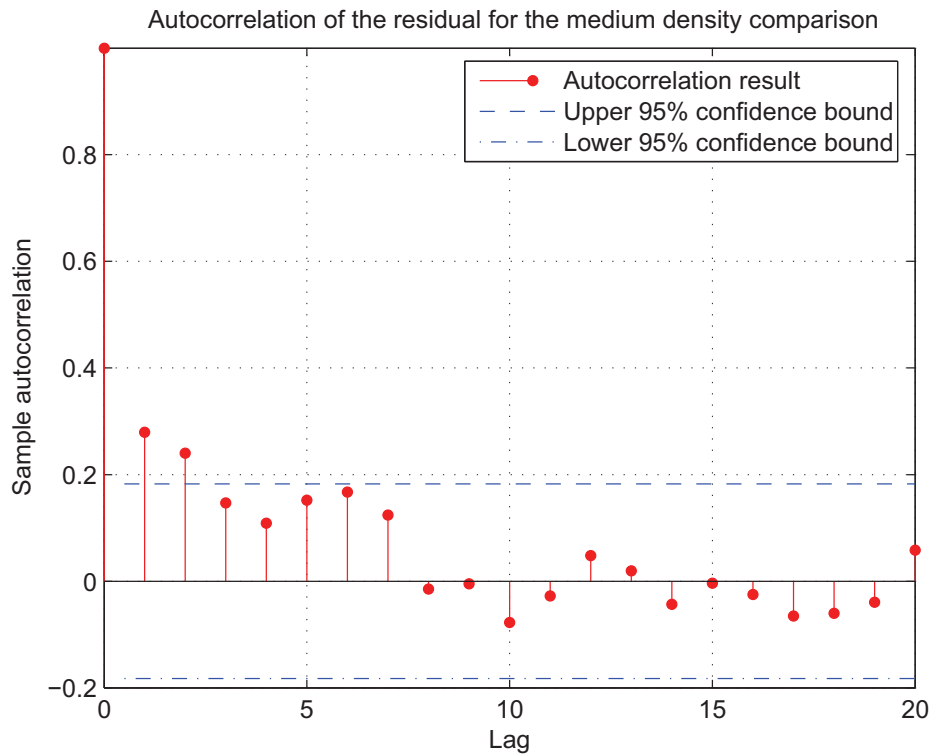


Figure 6.22: Whiteness test (95% confidence interval) for the water-addition model.

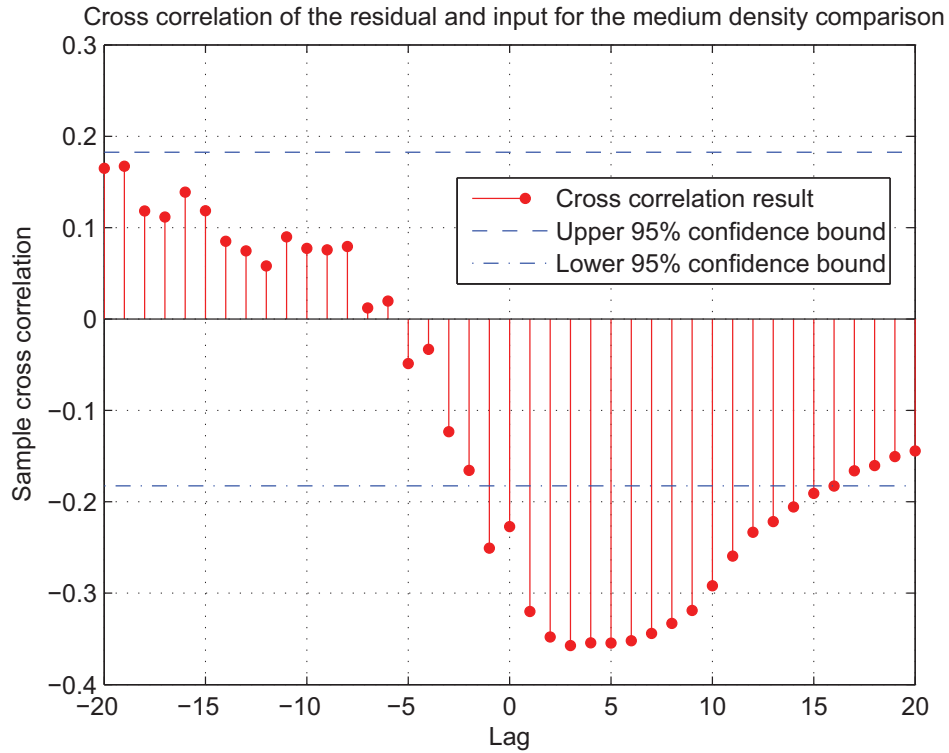


Figure 6.23: Independence test (95% confidence interval) for the water-addition model.

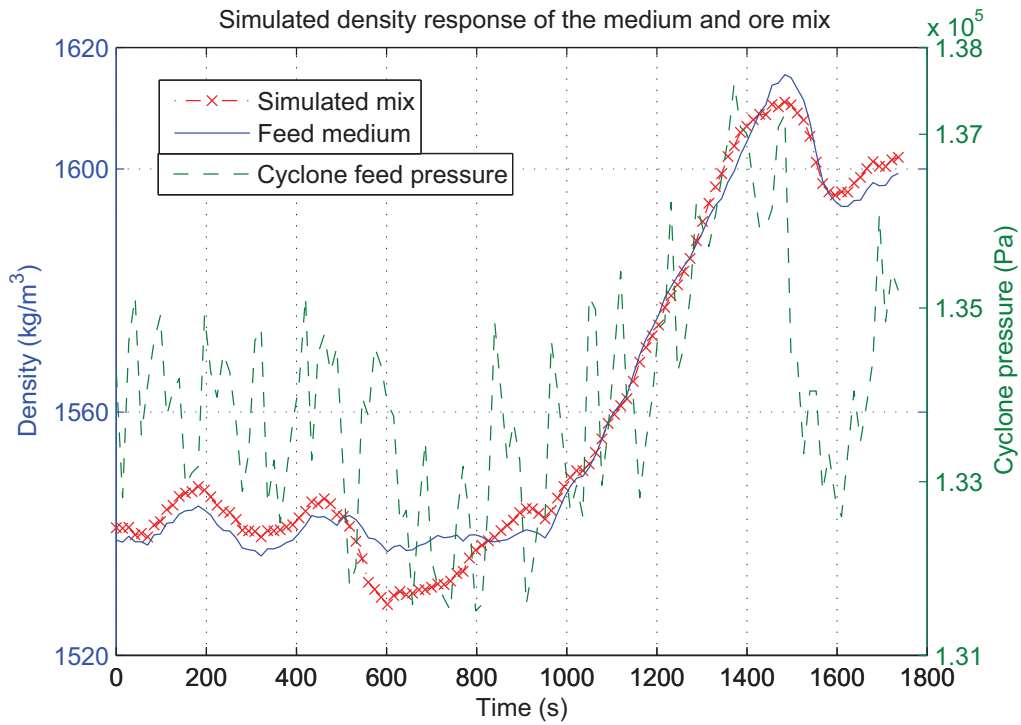


Figure 6.24: Simulated response of the mixing box output.

well, the pressure measurement at the cyclone inlet can be used to compare results. However, no correlation was made as the pressure measurement shows more oscillations than the density of the mix. These oscillations could be a result of the pump cavitating or the vibrations of the screens.

The density of the medium is, however, measured and is used as feed to be mixed with the ore. The feed medium is delayed by 28 seconds owing to the transport delay between the measurement point and feed. This transfer delay approximation was accepted by the plant metallurgist as a reasonable estimate (Lundt, 2008). The time delay can be determined experimentally by making use of a tracer and stop watch. Figure 6.25 illustrates the measured medium density and simulated fine ore feed rate used as input for the mixing box model.

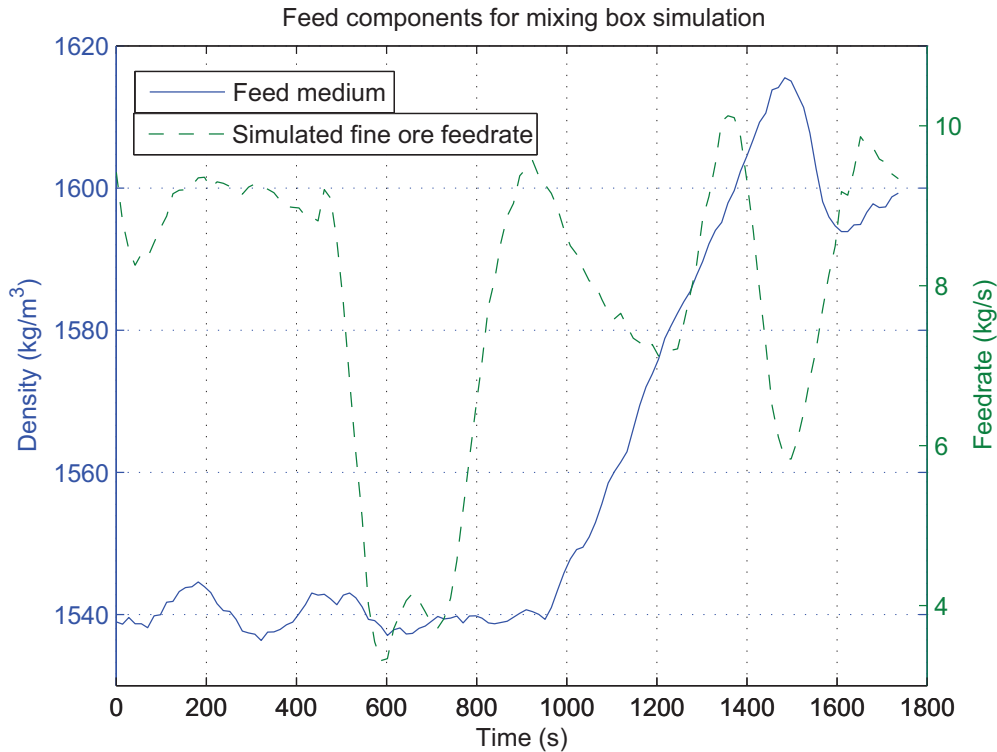


Figure 6.25: Feed components for the mixing box model.

#### 6.3.4 DMC model

In order to simulate the DMC model, the density of the feed into the DMC is estimated by using the simulation from the mixing box model. By ensuring the magnetite medium density is within the range of the feed mix density as illustrated in figure 6.24, it can be assumed that the mix density is at a reasonable degree of accuracy.

The simulation output for the overflow and underflow densities can be found in figure 6.26. This simulation gives a clear indication of how the underflow density is higher than the overflow density due to the separation process with ash and coal. Figure 6.27 illustrates what the simulated response is for the percentage magnetite in both products. These two curves remain close to each other, which indicate that the medium is distributed evenly between overflow and underflow. The increase in percentage over time indicates that the ore in the feed was reduced. A similar response occurs in the medium feed, which can be seen in figure 6.28.

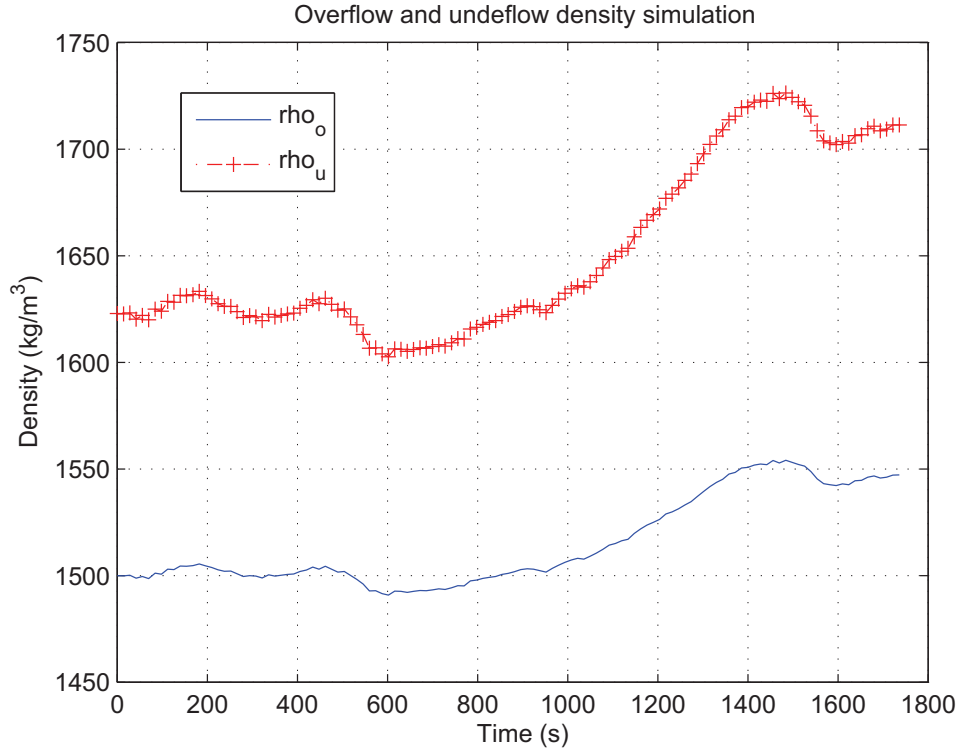


Figure 6.26: Simulated overflow and underflow densities.

By using the partition factor (equation 4.30) and process described at the end of section 4.2.4 an efficiency curve can be simulated for the DMC for a particular set of conditions. By using the DMC model parameters from table 5.5, the following float and sink equations can be computed:

$$W_{c,o,ore} = \frac{2055W_{c,i,ore}^2 - 0.9\rho_{c,i,med}^2 + 1857W_{c,i,ore}\rho_{c,i,med}}{5000W_{c,i,ore} + 2477\rho_{c,i,med}}, \quad (6.1)$$

$$W_{c,u,ore} = \frac{3836W_{c,i,ore}^2 - 1.1\rho_{c,i,med}^2 + 1065W_{c,i,ore}\rho_{c,i,med}}{5000W_{c,i,ore} + 2477\rho_{c,i,med}}, \quad (6.2)$$

where  $W_{c,i,ore} = Q_{c,i}\rho_{c,i}(1 - x_{c,i,med})$ . By computing the partition factor in decreasing density fractions and in increasing density fractions from 1500 kg/m<sup>3</sup> in 10 kg/m<sup>3</sup> increments, and using a yield of 65%, an efficiency curve for the

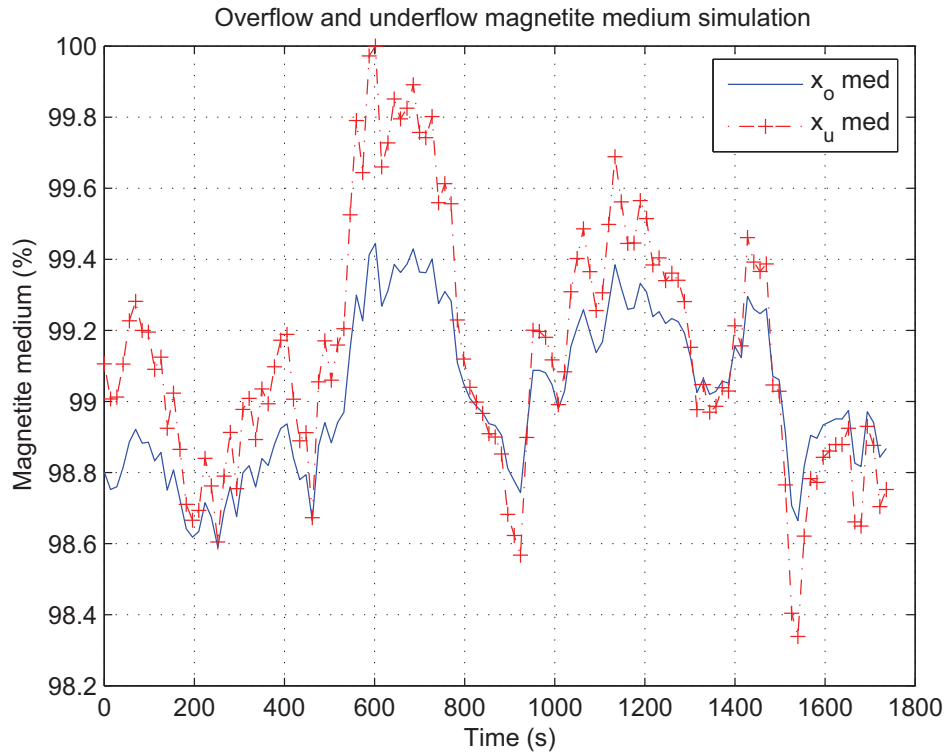


Figure 6.27: Simulated overflow and underflow medium percentages.

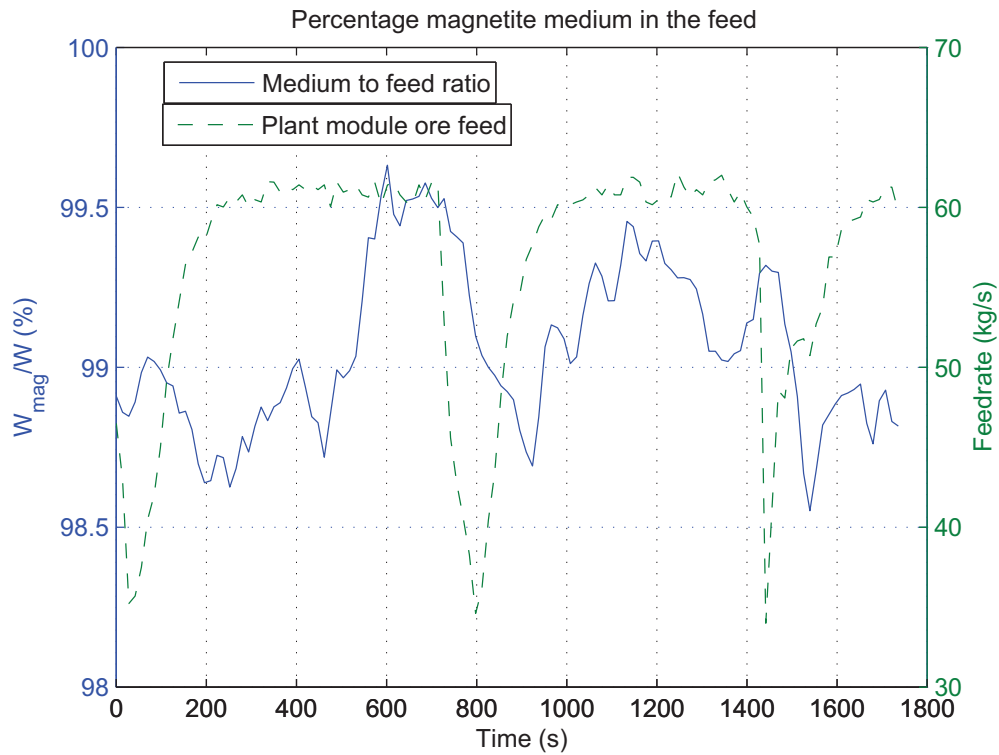


Figure 6.28: Percentage magnetite medium in the feed.

DMC was generated (figure 6.29). The resulting partition curve is similar to that described in section 2.4.2.1 where the predicted mass distributions to float and sink products at different densities in the feed ( $\rho_{c,i}$ ) are obtained.

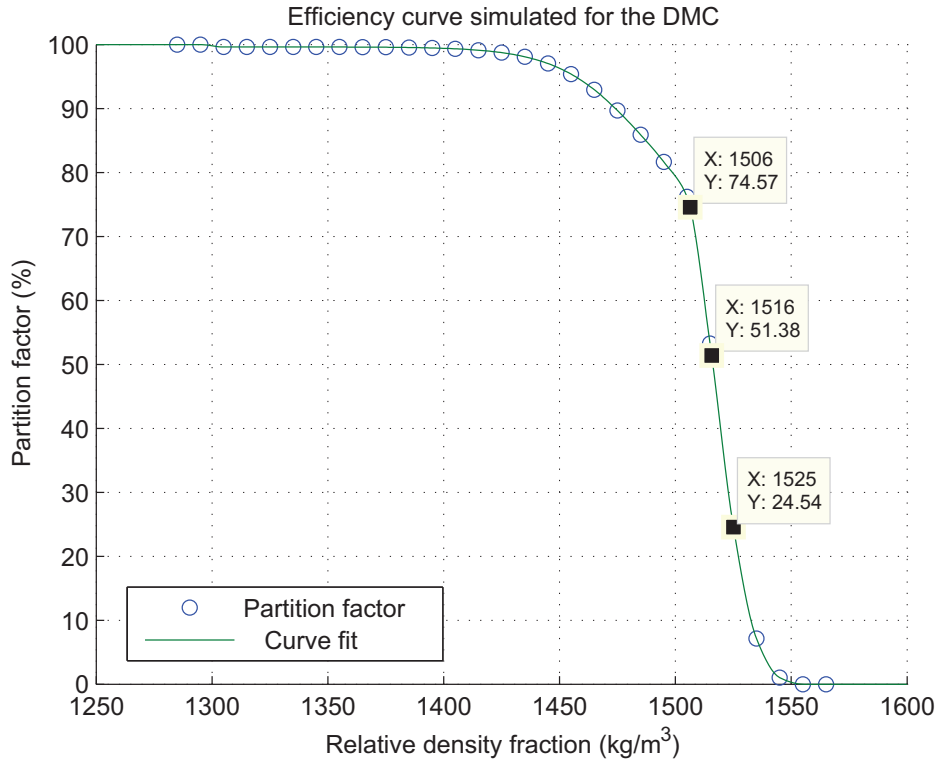


Figure 6.29: Simulated efficiency curve for the DMC using a theoretical steady-state model.

Using equation 2.2, the approximate separation efficiency for the DMC, based on the specific set of parameters used, is  $9.5 \text{ kg/m}^3$  with a  $\rho_{50}$  of approximately  $1516 \text{ kg/m}^3$ .

By measuring the feed mass components and overflow mass components of ash, sulphur, moisture and volatiles it is possible to obtain simulated responses for the overflow and underflow of each component, as illustrated in figures 6.30, 6.31, 6.32, 6.33 and 6.34.

Figure 6.35 illustrates the simulated response of the ash component in the overflow. This simulation can be compared to the actual measured response. The limitation in the measured response is that samples can only be obtained approximately every 5 minutes and then analysed in a laboratory, while the simulation makes use of online measurements such as feed rates and medium density to model the output. The scalar-valued norm  $V_N(\theta, \mathbf{Z}^N)$  for this comparison as described by equation 5.14 is  $29.3\text{E}-6$ . The correlation of this

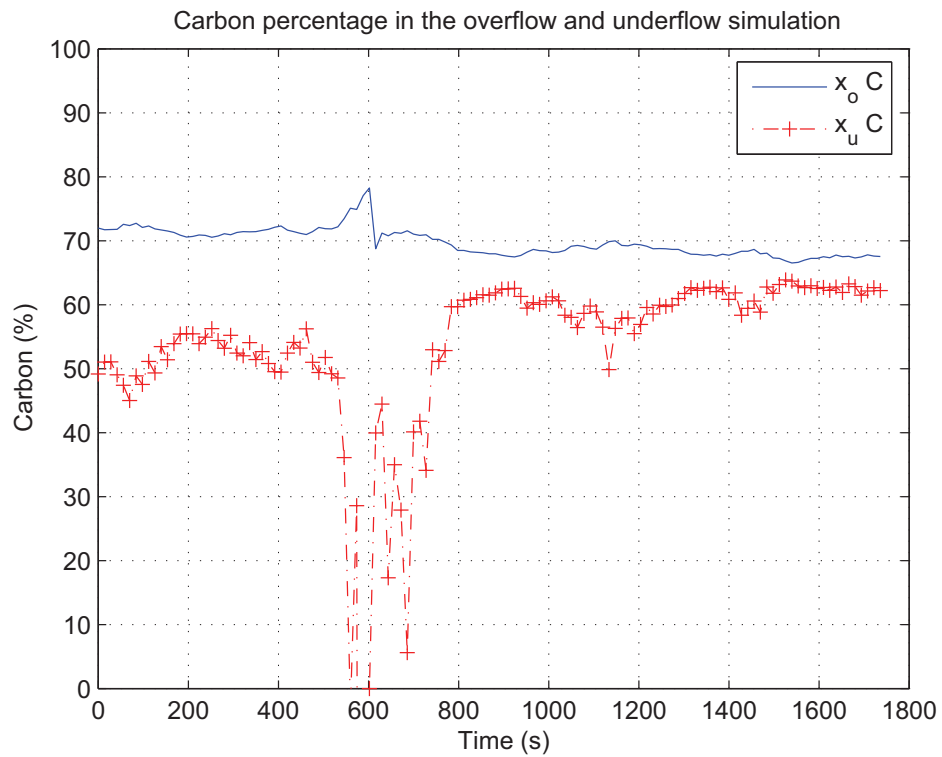


Figure 6.30: Simulated response of the overflow and underflow carbon mass component.

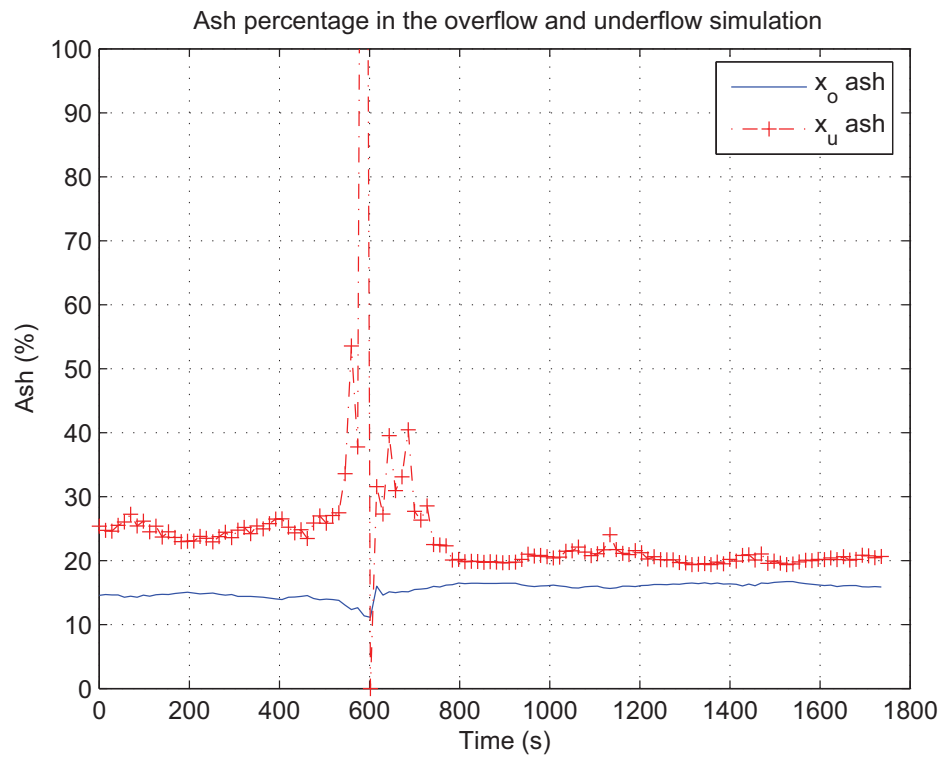


Figure 6.31: Simulated response of the overflow and underflow ash mass component.

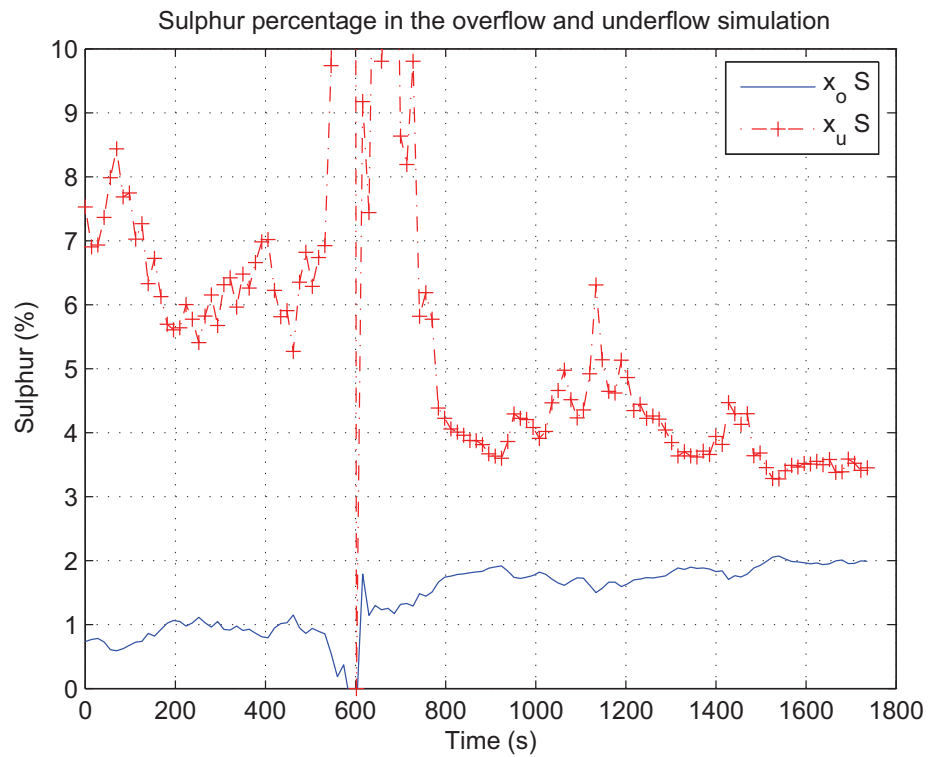


Figure 6.32: Simulated response of the overflow and underflow sulphur mass component.

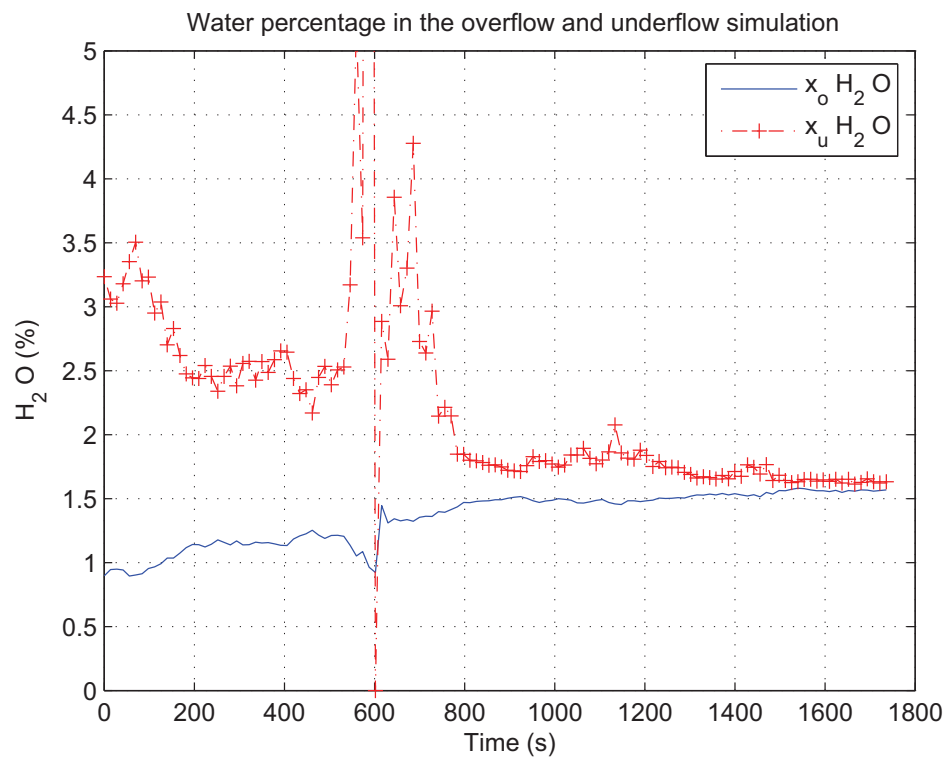


Figure 6.33: Simulated response of the overflow and underflow moisture mass component.

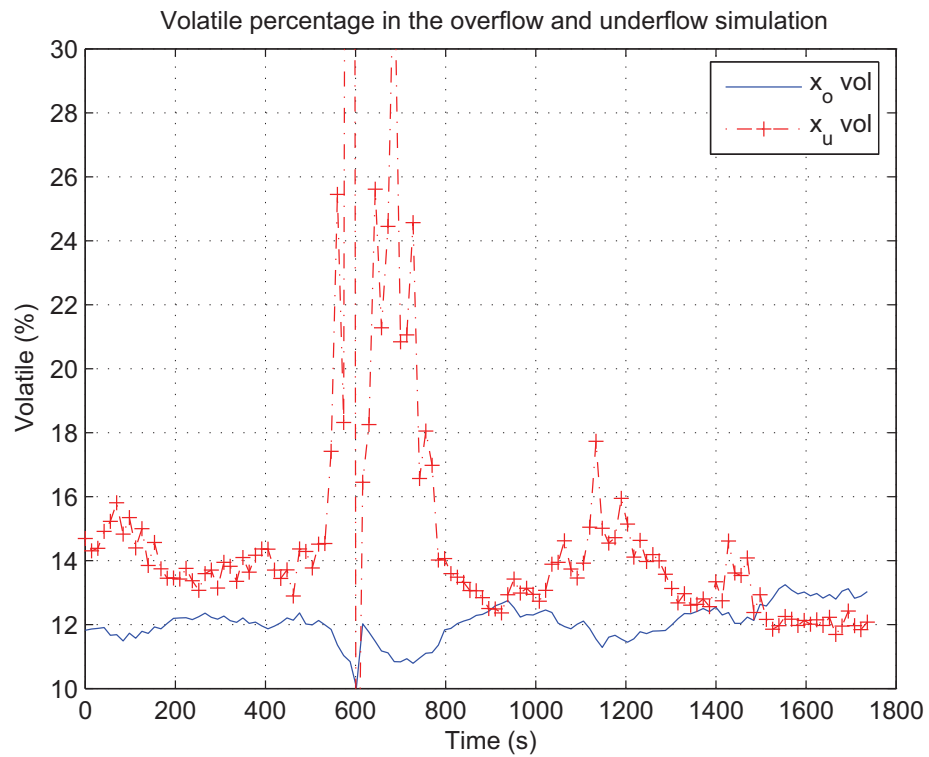


Figure 6.34: Simulated response of the overflow and underflow volatile mass component.

comparison is 0.7177. The average of the simulation output is also determined for every 5 minutes to illustrate its response when compared to the actual data.

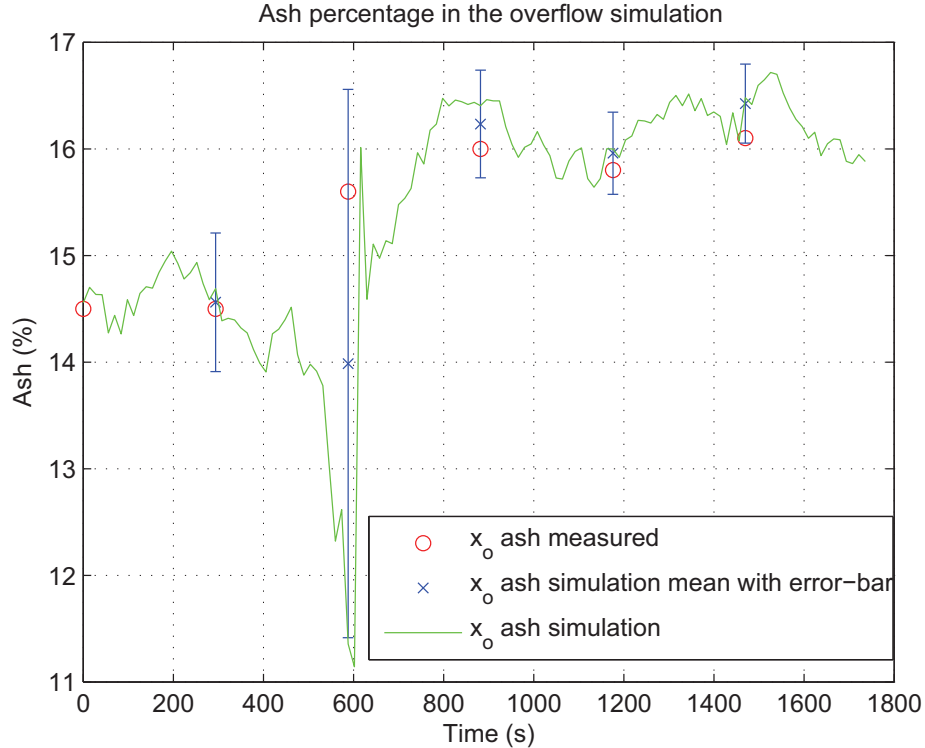


Figure 6.35: Comparison of simulated, simulated mean and measured ash percentage in overflow.

The residual for the ash comparison is given in figure 6.36. The fit for the ash simulation described by equation 5.17 is 59.5%. The whiteness and independence tests for the ash comparison are given in figures 6.37 and 6.38.

Similarly the moisture and volatile components are simulated and illustrated in figures 6.39 and 6.40. For the moisture comparison the scalar-valued norm  $V_N(\theta, \mathbf{Z}^N)$  is  $0.877\text{E}-6$  and its correlation is 0.801. For the volatile comparison the scalar-valued norm  $V_N(\theta, \mathbf{Z}^N)$  is  $8.80\text{E}-6$  and its correlation is 0.722.

The residual for the moisture comparison is given in figure 6.41. The fit for the moisture simulation described by equation 5.17 is 64.9%. The whiteness and independence tests for the moisture comparison are given in figures 6.42 and 6.43.

The residual for the volatile comparison is given in figure 6.44. The fit for the volatile simulation described by equation 5.17 is  $-12.4\%$ . The negative fit means that the model does not fully explain the variation in the output. The whiteness and independence tests for the volatile comparison are given in figures 6.45 and

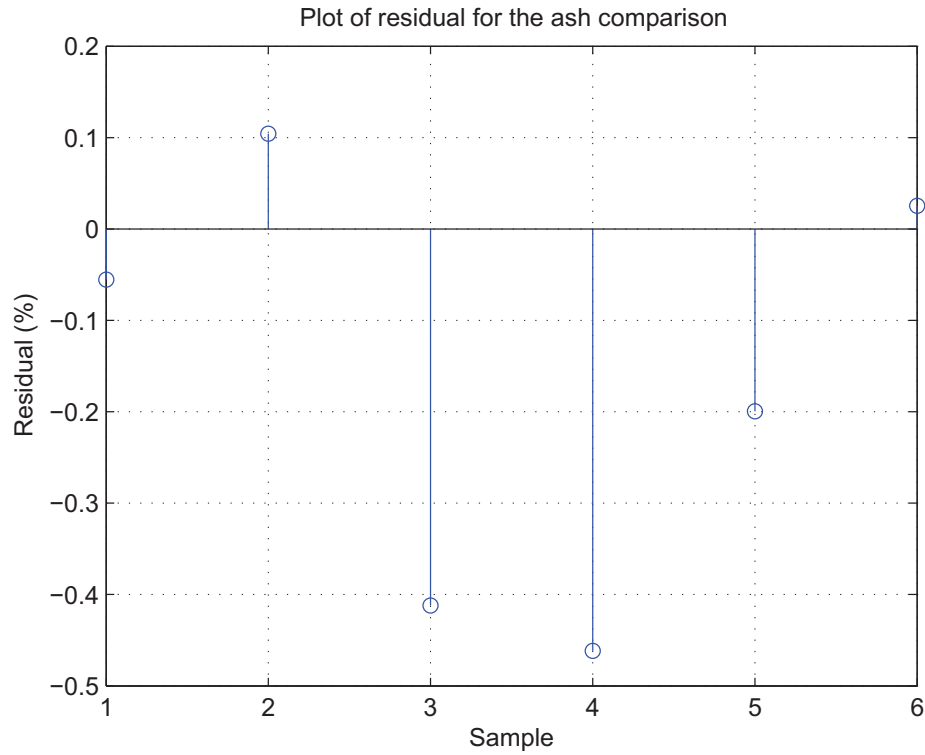


Figure 6.36: Ash comparison residual plot.

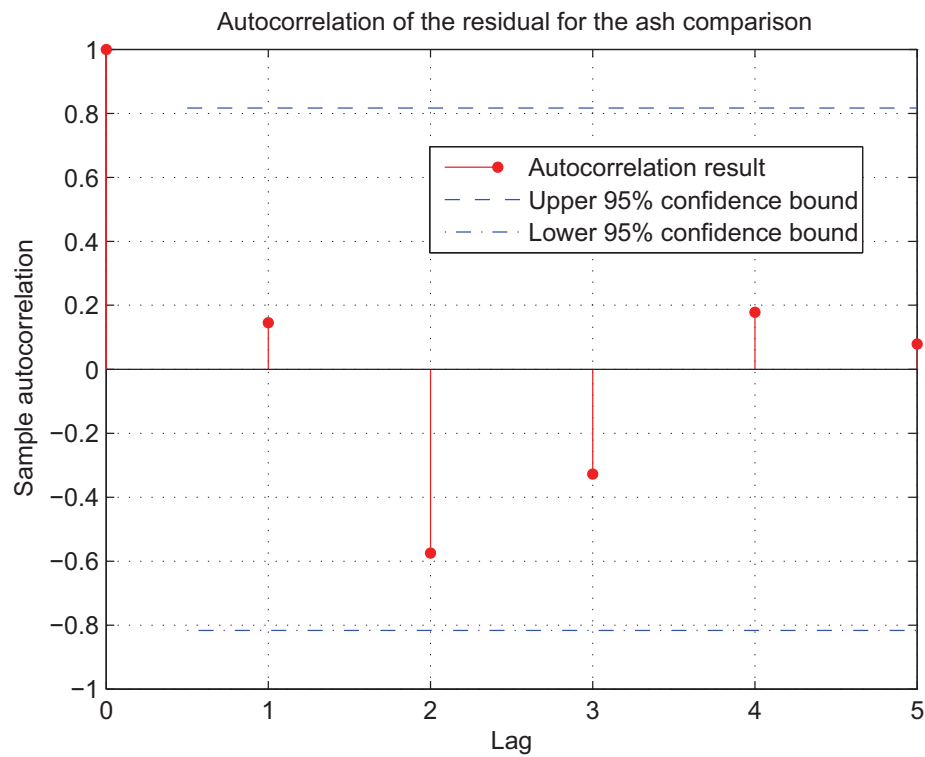


Figure 6.37: Whiteness test (95% confidence interval) for the ash comparison.

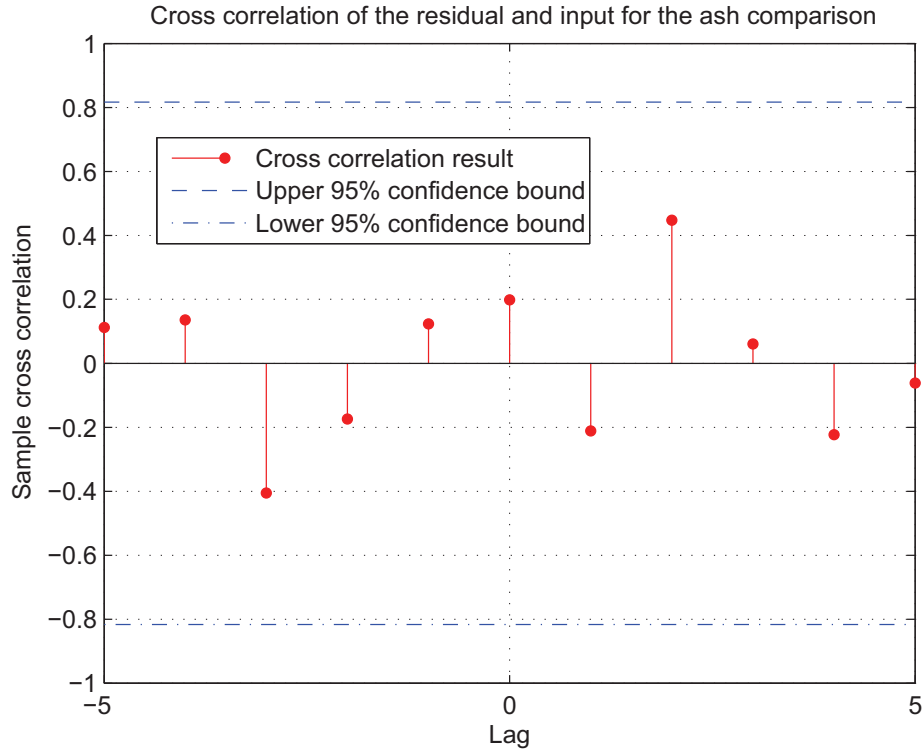


Figure 6.38: Independence test (95% confidence interval) for the ash comparison.

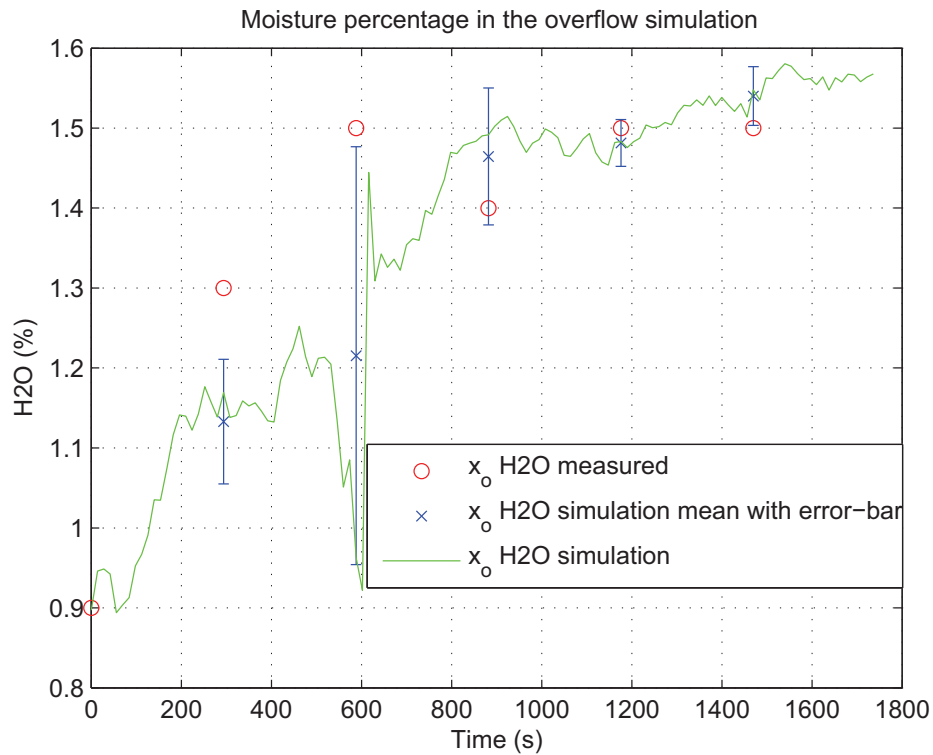


Figure 6.39: Comparison of simulated, simulated mean and measured moisture percentage in overflow.

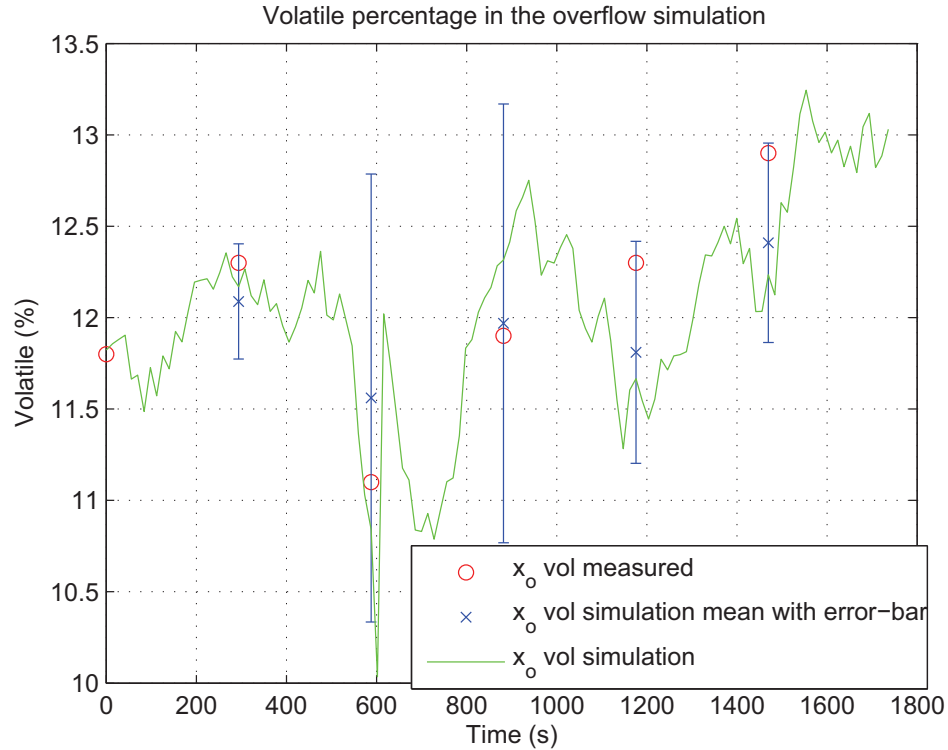


Figure 6.40: Comparison of simulated, simulated mean and measured volatile percentage in overflow.

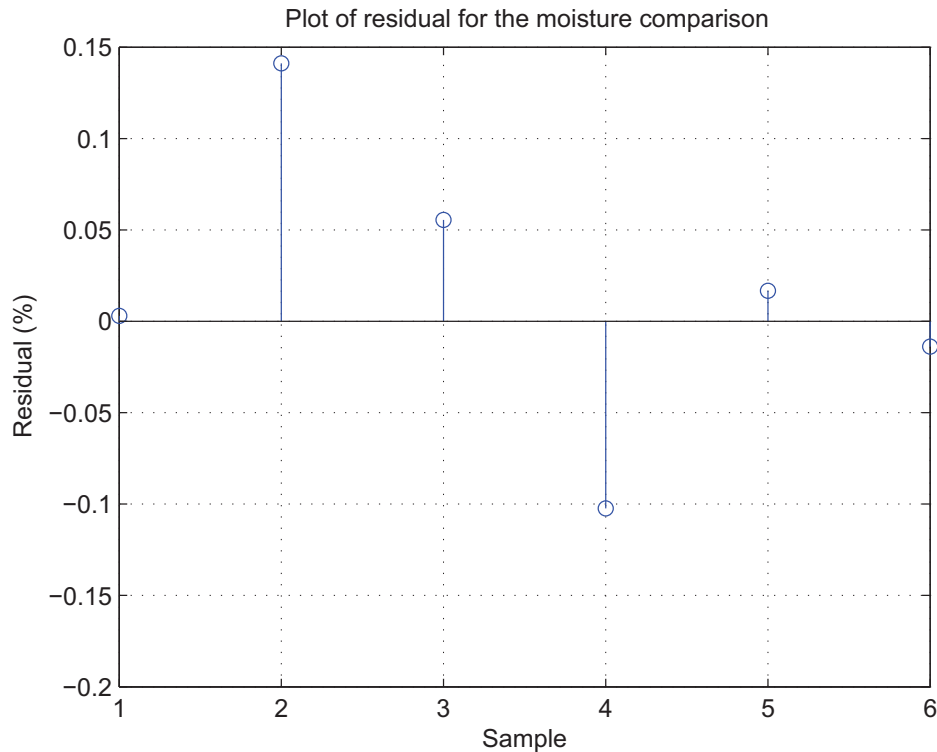


Figure 6.41: Moisture comparison residual plot.

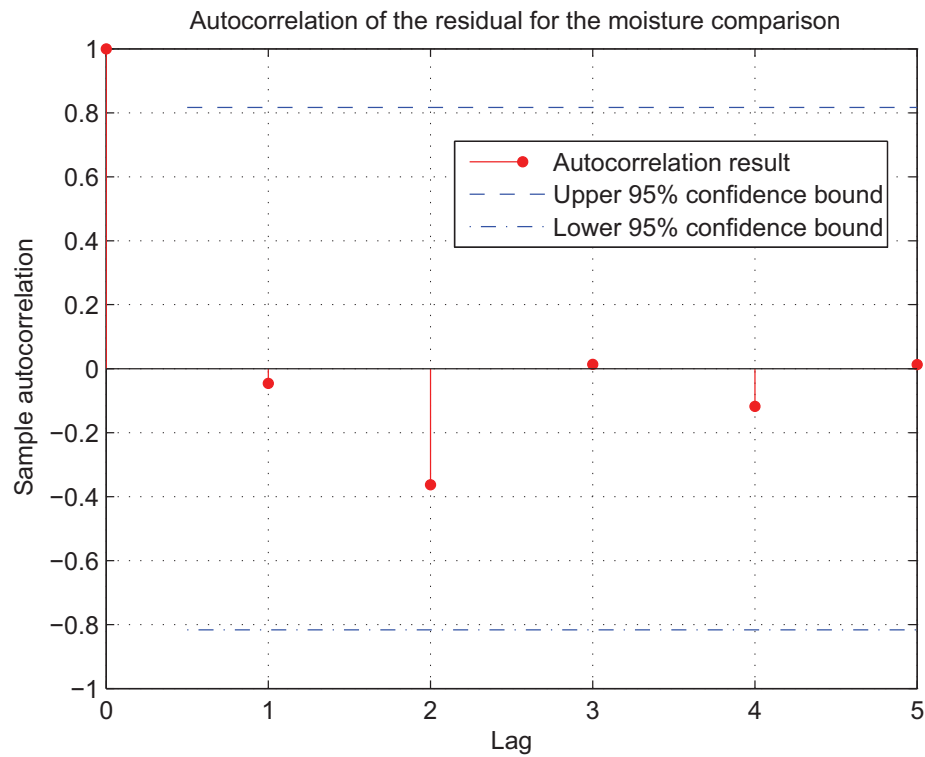


Figure 6.42: Whiteness test (95% confidence interval) for the moisture comparison.

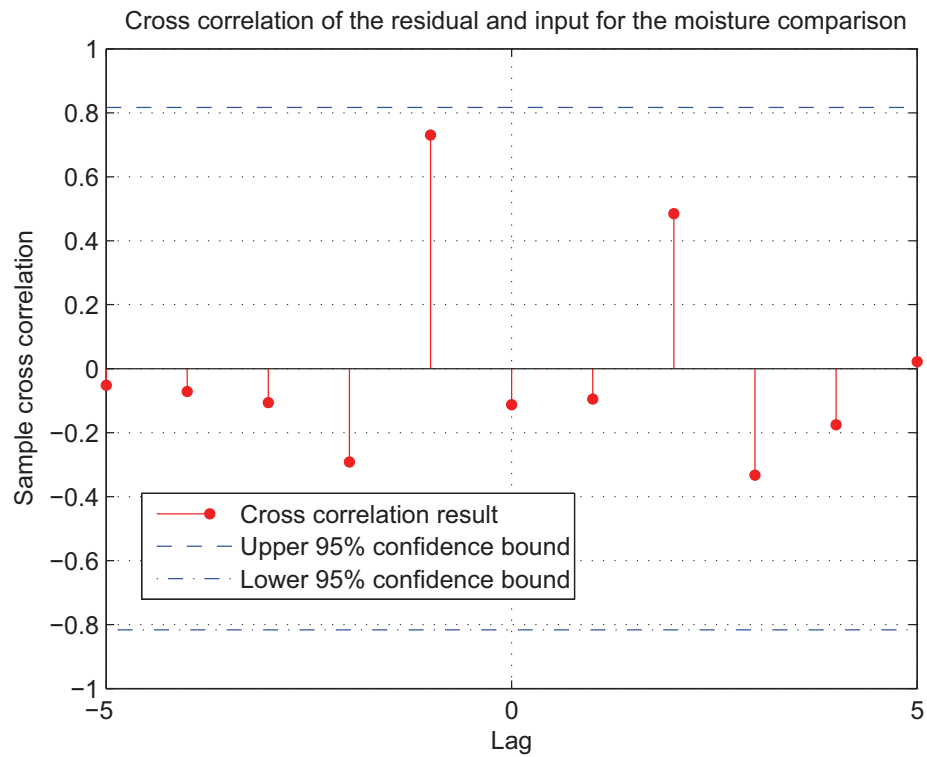


Figure 6.43: Independence test (95% confidence interval) for the moisture comparison.

6.46.

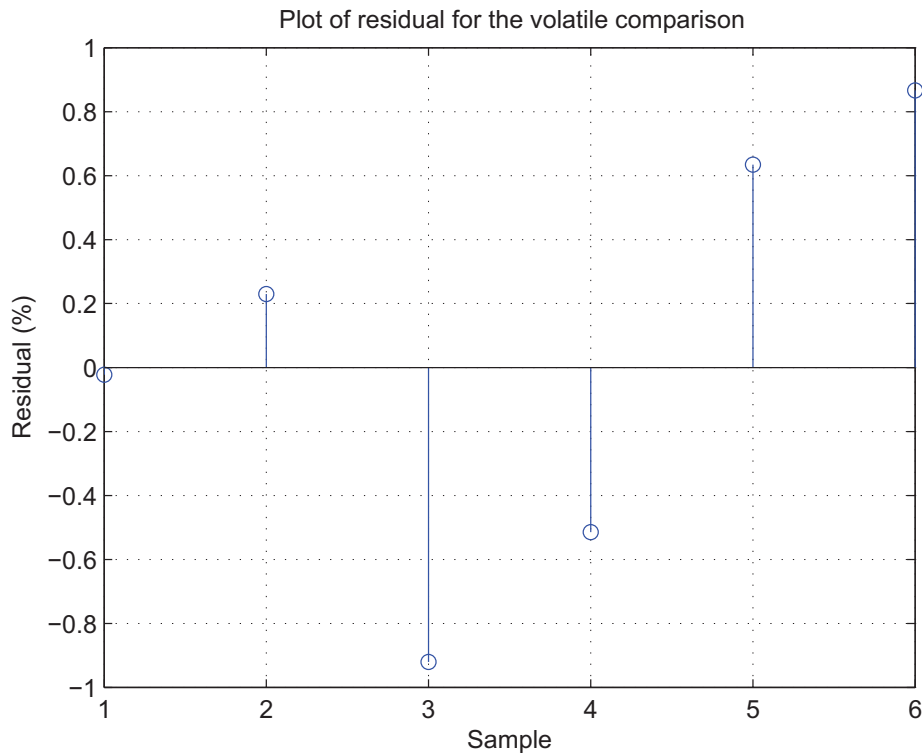


Figure 6.44: Volatile comparison residual plot.

The outliers near 600 seconds in figures 6.30, 6.31, 6.32, 6.33, 6.34, 6.35, 6.39 and 6.40 are due to the abrupt change in feed rate into the plant (figure 6.11).

### 6.3.5 Magnetite make-up corrected medium model

Figure 6.47 illustrates the simulated density response of the magnetite make-up corrected medium.

Since there is no measurement available from the Leeuwpan DMS plant for the corrected medium tank, there is no means of comparing the simulated output to an actual output. The simulated output is, however, used as input into the magnetite water-addition model (section 6.3.2). The results from this allow the accuracy of the model to be determined.

Figure 6.48 illustrates the simulated mass rate response of the magnetite make-up corrected medium with tank height measurement as an input into the model. This is achieved by making use of the fourth-order Runge-Kutta approximation method.

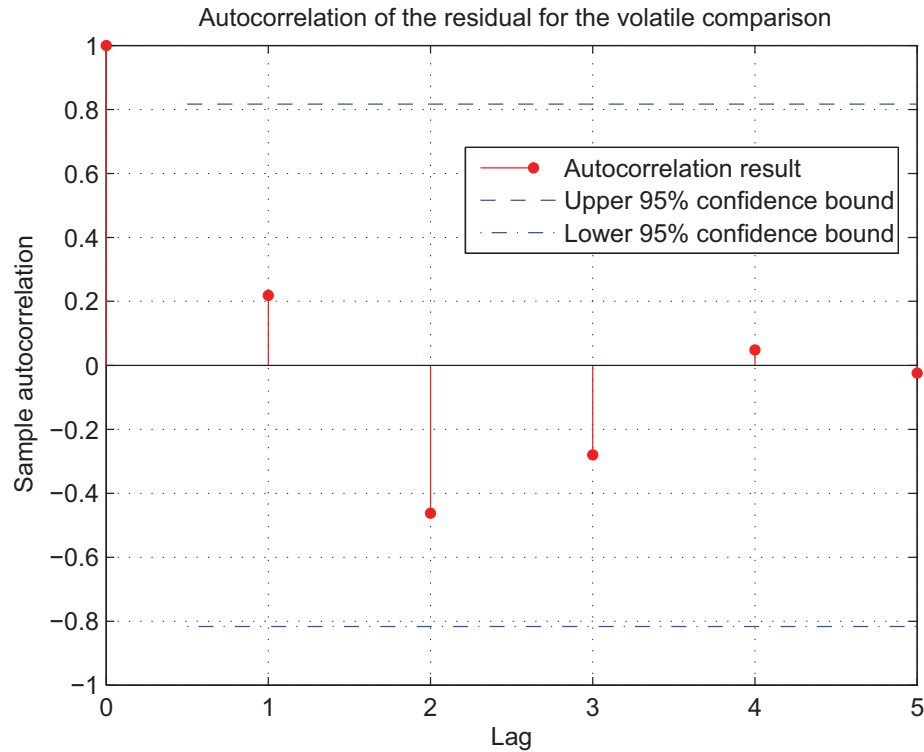


Figure 6.45: Whiteness test (95% confidence interval) for the volatile comparison.

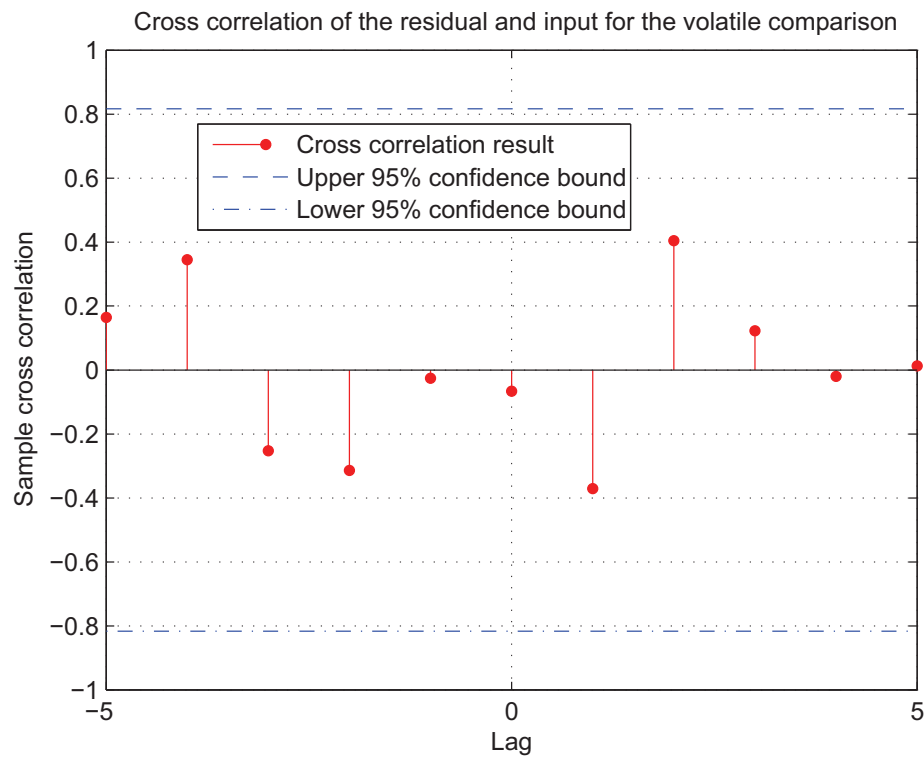


Figure 6.46: Independence test (95% confidence interval) for the volatile comparison.

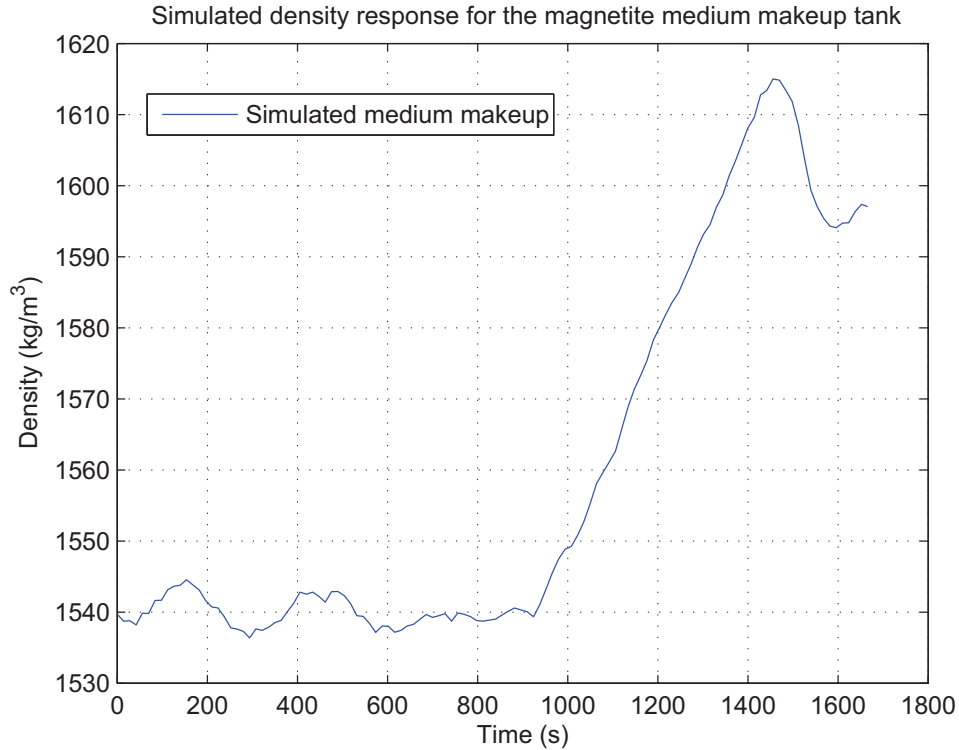


Figure 6.47: Simulated response of the medium make-up.

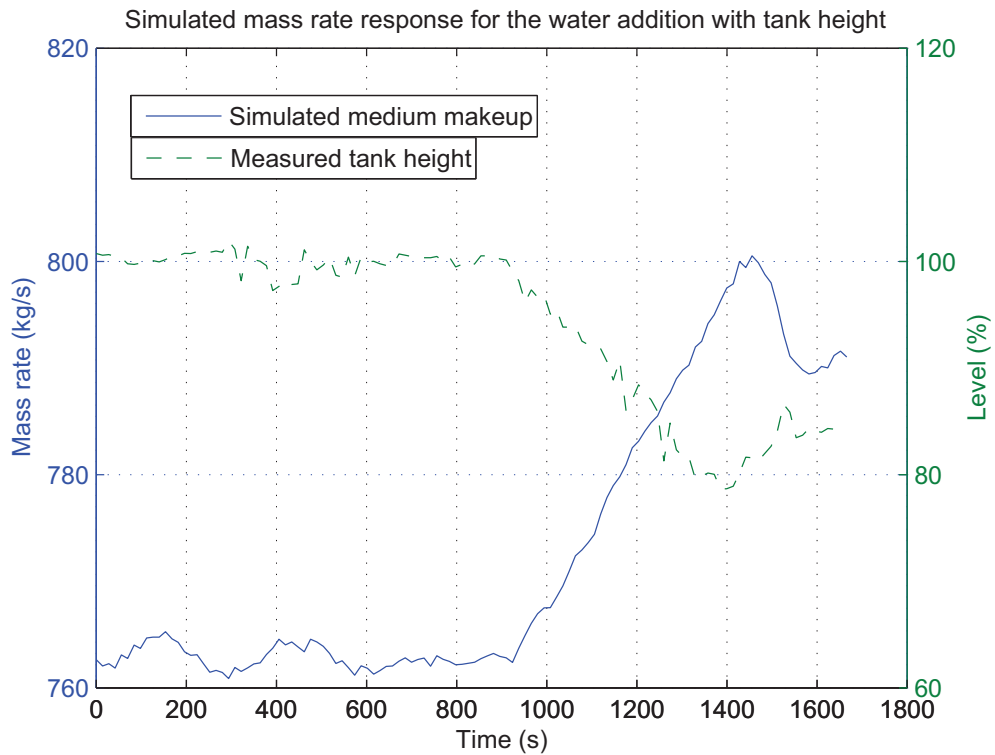


Figure 6.48: Simulated response of the medium make-up tank and tank height measurement.

## 6.4 MODEL SIMULATION

With the development and validation of each individual model, it is possible to integrate all models together into a graphical simulation environment called Simulink<sup>2</sup>. Figure 6.49 illustrates the Simulink model for the fines cyclone section in module one of the Leeuwpan DMS plant. The source code and sub-elements of the blocks can be found in addendum E.

Using the model developed in figure 6.49, the output can be simulated for a longer period of time, or possibly in near real time from the actual plant data. The secondary screen fines, the DMC outputs and the medium density outputs are indicated below. These simulations make use of actual plant data sampled every second over a period of 11 hours.

Figure 6.50 illustrates the simulated response of the fines product from the single-deck screen. Figure 6.51 illustrates the simulated medium and ore mix density response and the actual medium density feed for the mixing box. Figure 6.52 illustrates the density response for the overflow and underflow products of the fine cyclone. Figure 6.53 shows the simulated medium response in the overflow and underflow of the fine cyclone. Figures 6.54, 6.55, 6.56, 6.57 and 6.58 illustrate the simulated response of the mass components for ash, sulphur, moisture, volatiles and carbon for the overflow and underflow of the fine cyclone. Figure 6.59 illustrates the simulated density response of the medium after it has been collected and followed through the density controller. This is compared to the actual measured medium density for the fine cyclone.

It can be seen that the overflow and underflow ash contents deviate greatly in figure 6.54. This is a good indication that the model is accurately depicting the process of separation in the DMC, as the primary function of the DMC is to separate the coal from the ash in the ore and thus reduce the ash contents in the overflow product.

## 6.5 DISCUSSION

By performing an industrial experiment test case, the models developed in chapter 4 with parameters in chapter 5 can be validated to a certain degree of accuracy. This accuracy is measured by the scalar-valued norm between the simulated response of each equipment model and the actual measurements taken in the

---

<sup>2</sup>Simulink is a simulation and model-based design application for Matlab that is developed by The MathWorks, Inc. ([www.mathworks.com](http://www.mathworks.com)).

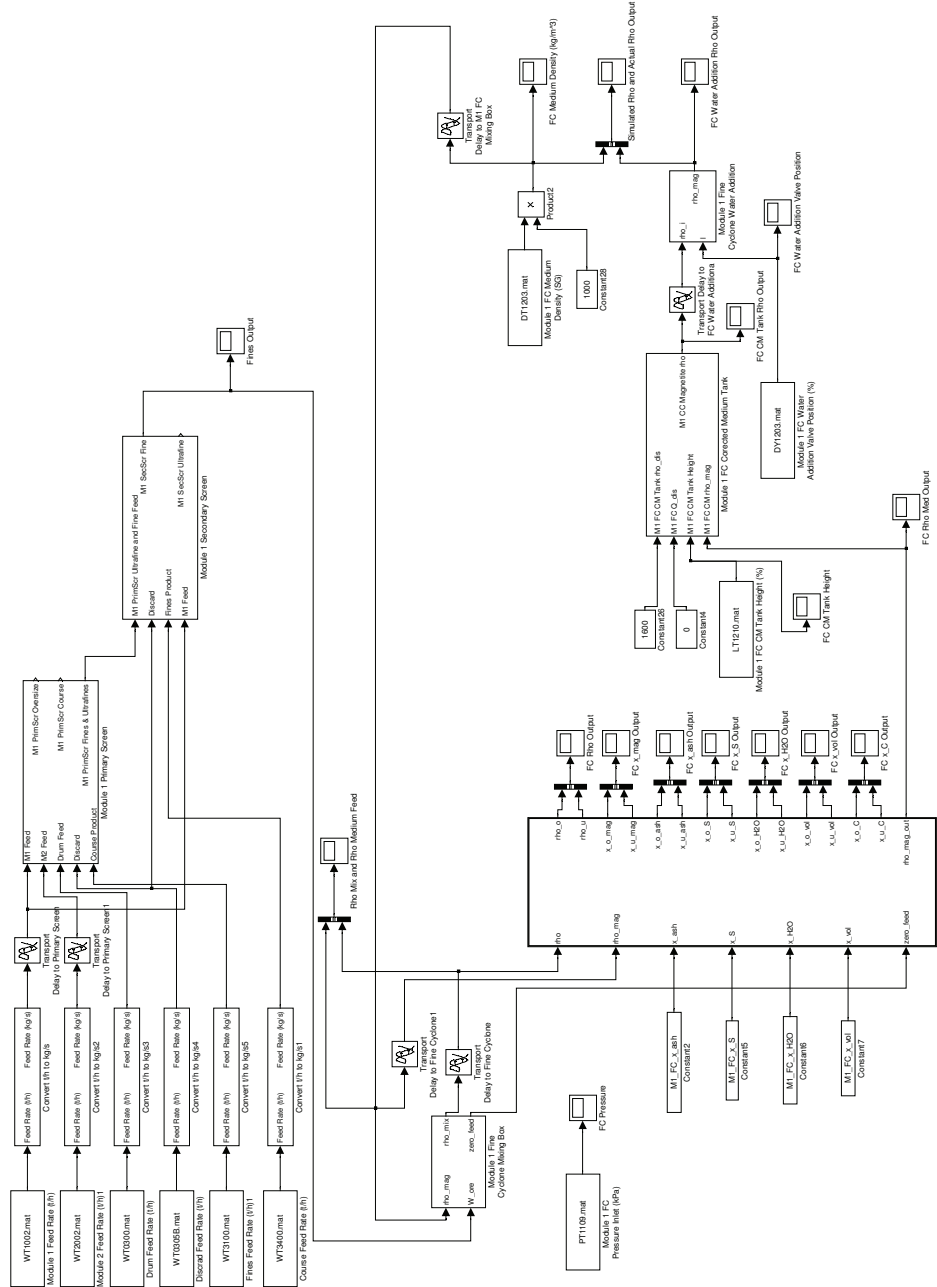


Figure 6.49: Simulink model of the fines cyclone DMS plant.

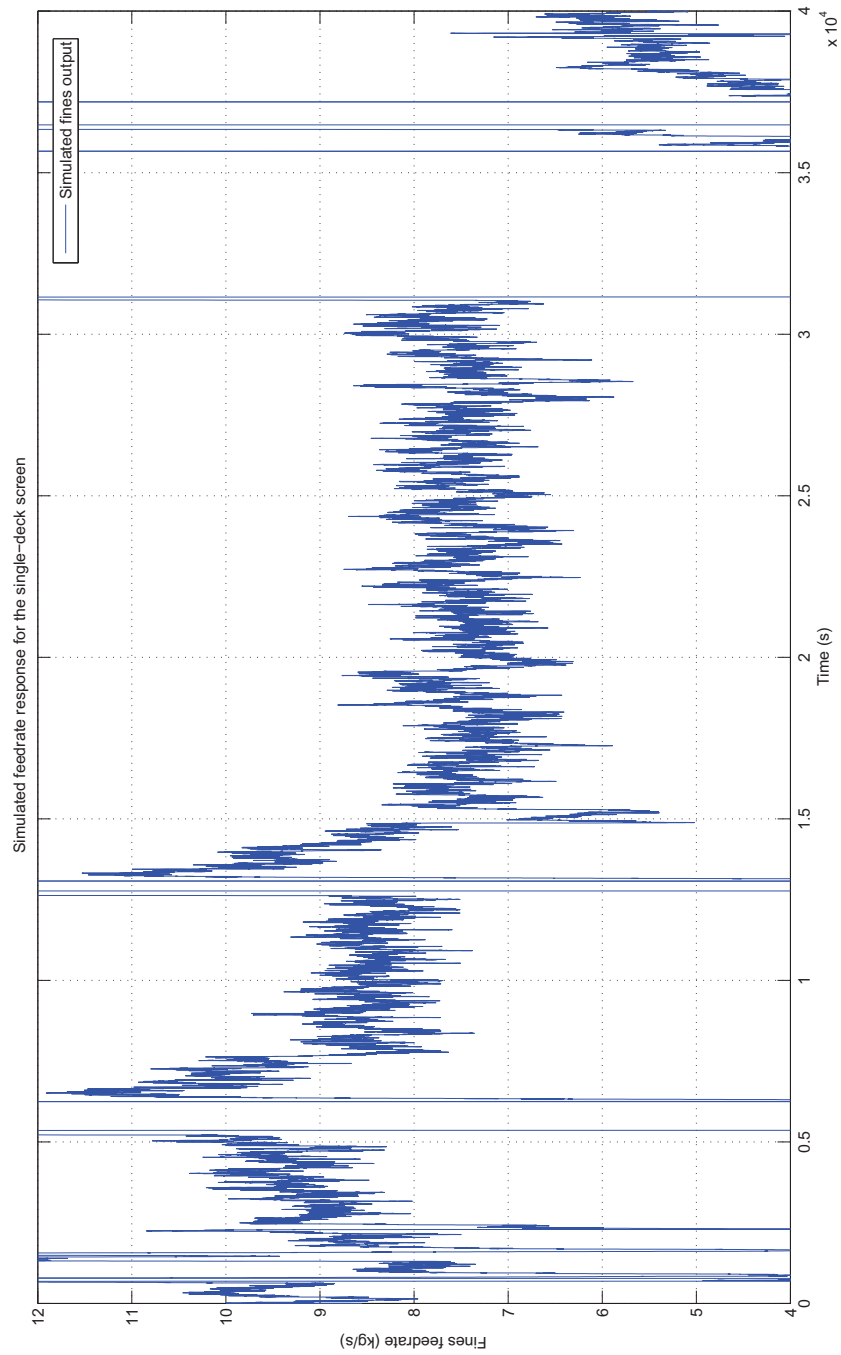


Figure 6.50: Simulated feed rate response for the single-deck screen.

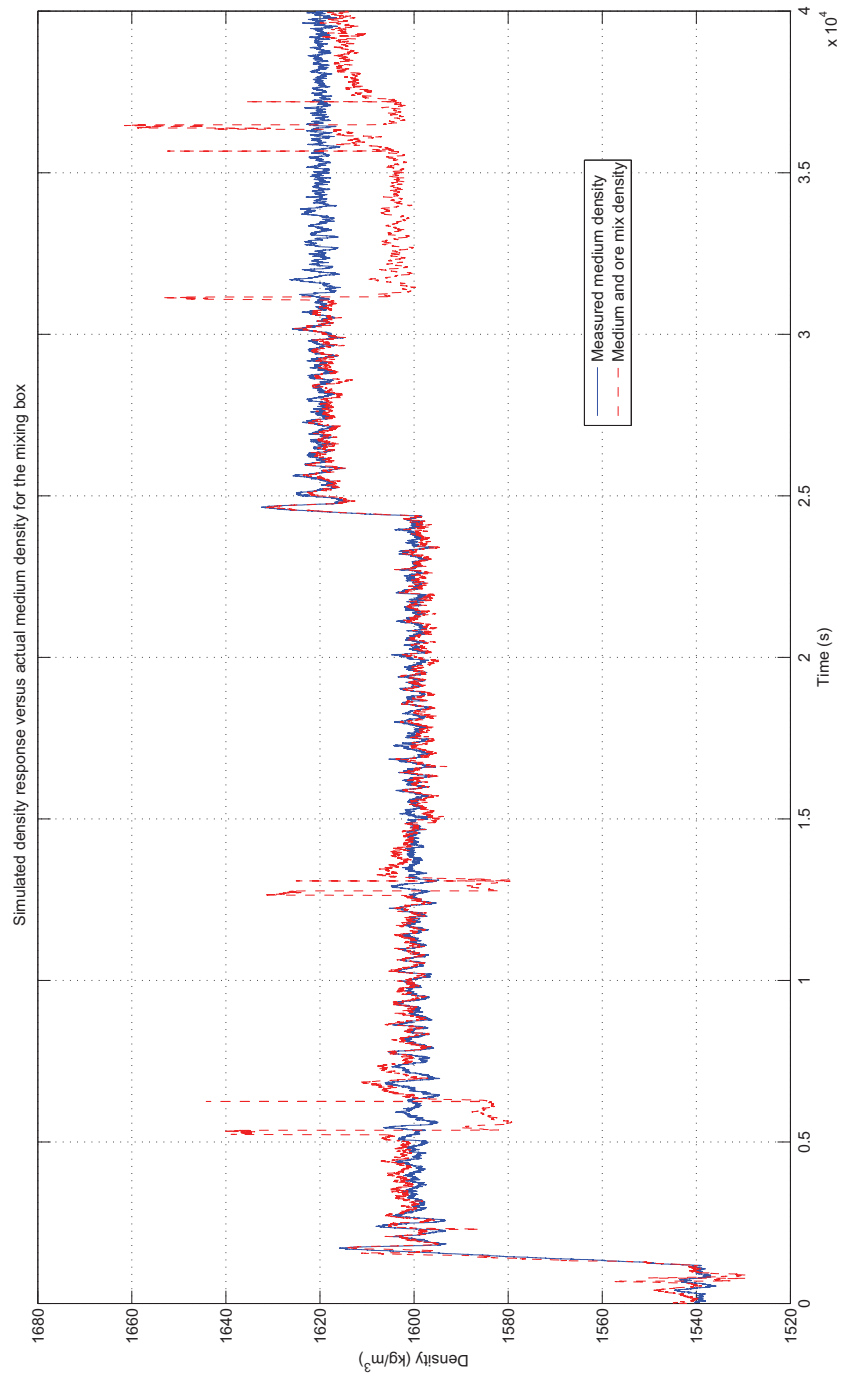


Figure 6.51: Simulated density response versus actual medium density for the mixing box.

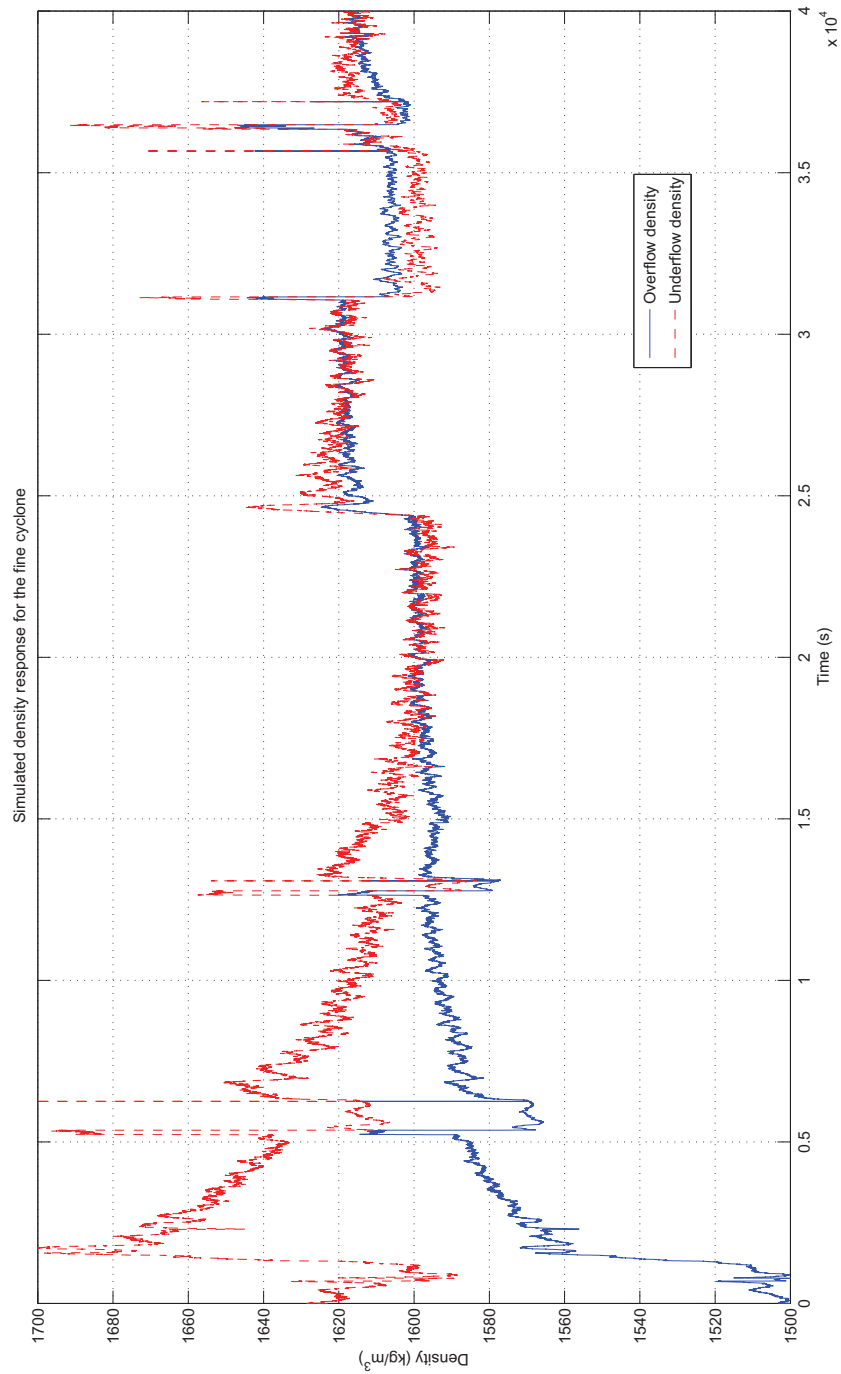


Figure 6.52: Simulated density response for the fine cyclone.

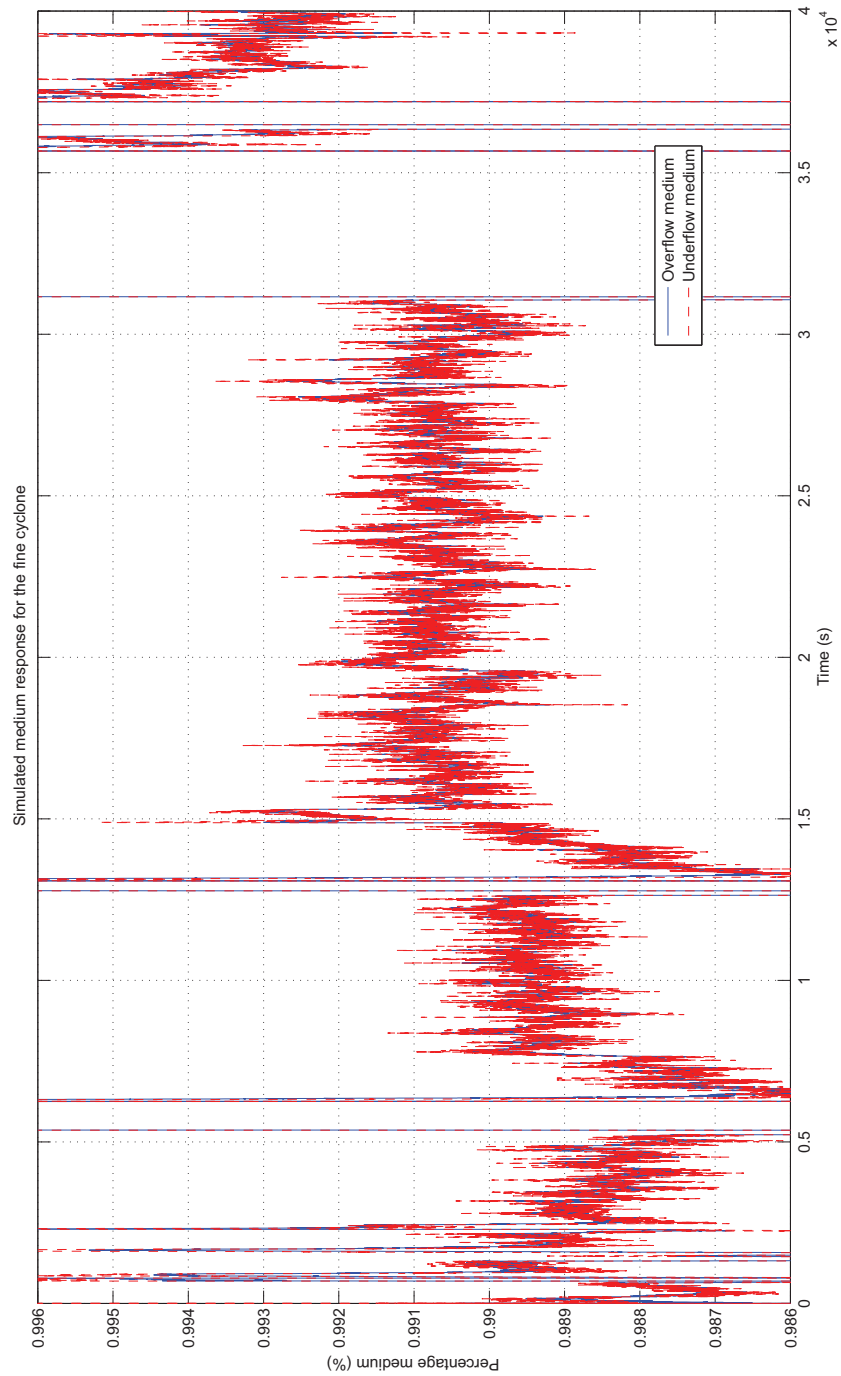


Figure 6.53: Simulated medium response for the fine cyclone.

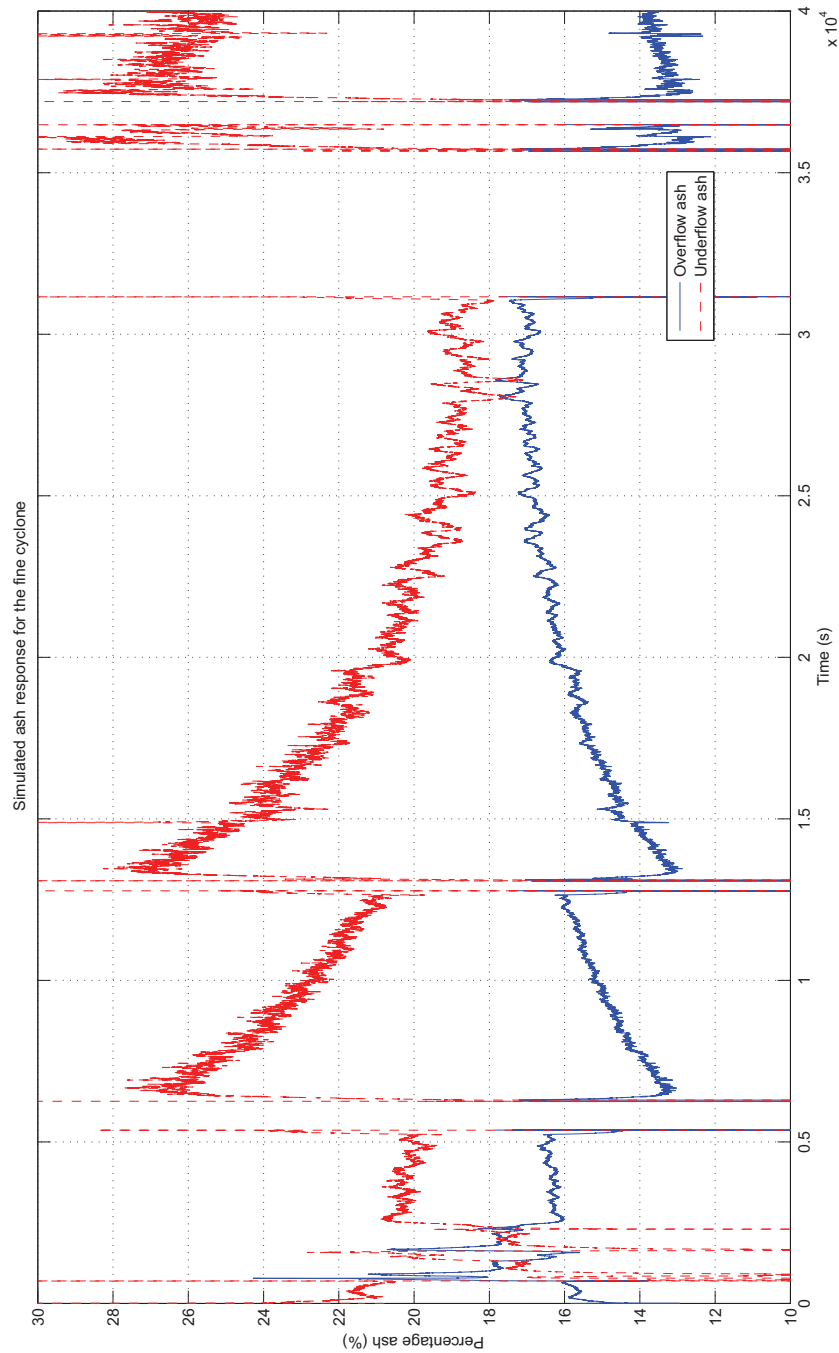


Figure 6.54: Simulated ash response for the fine cyclone.

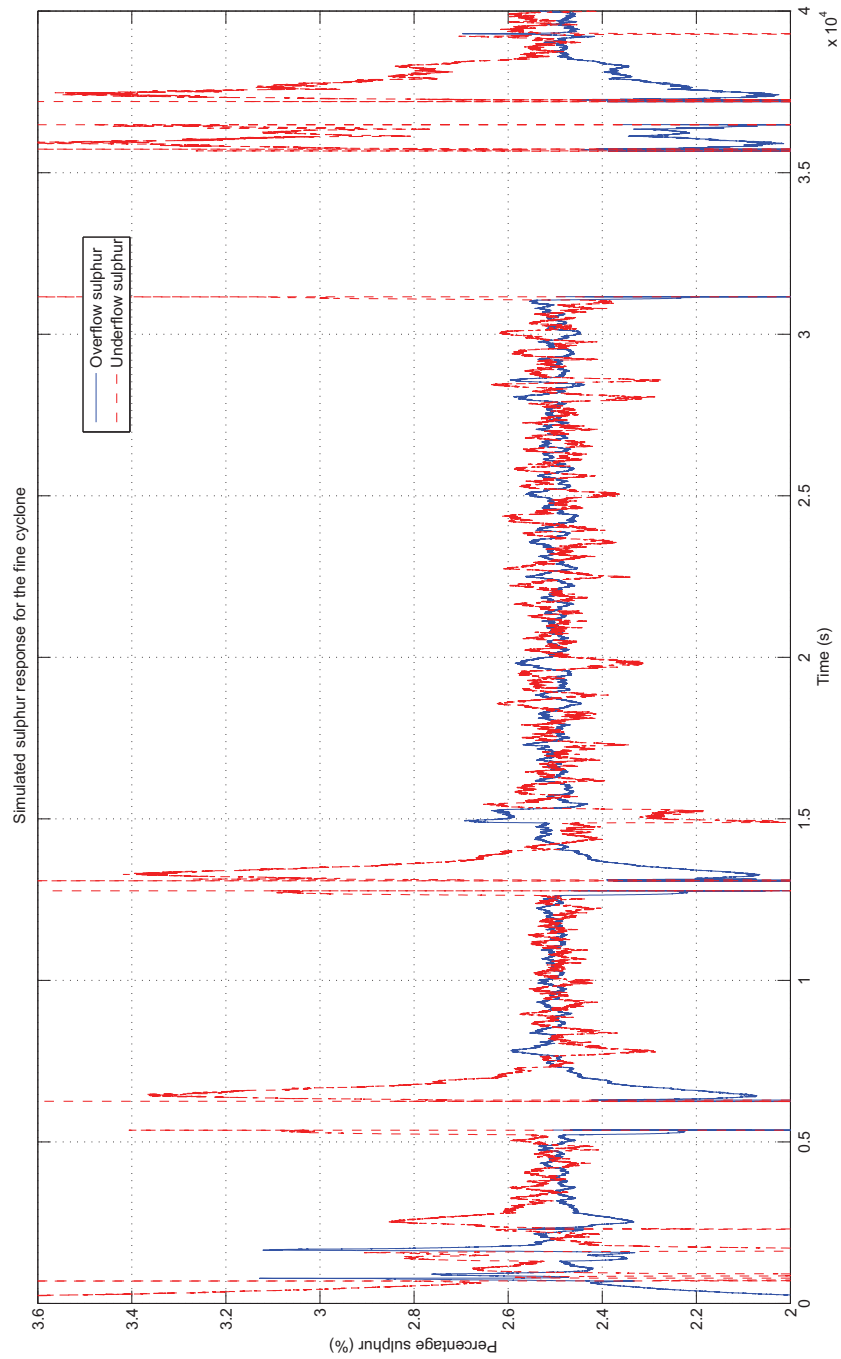


Figure 6.55: Simulated sulphur response for the fine cyclone.

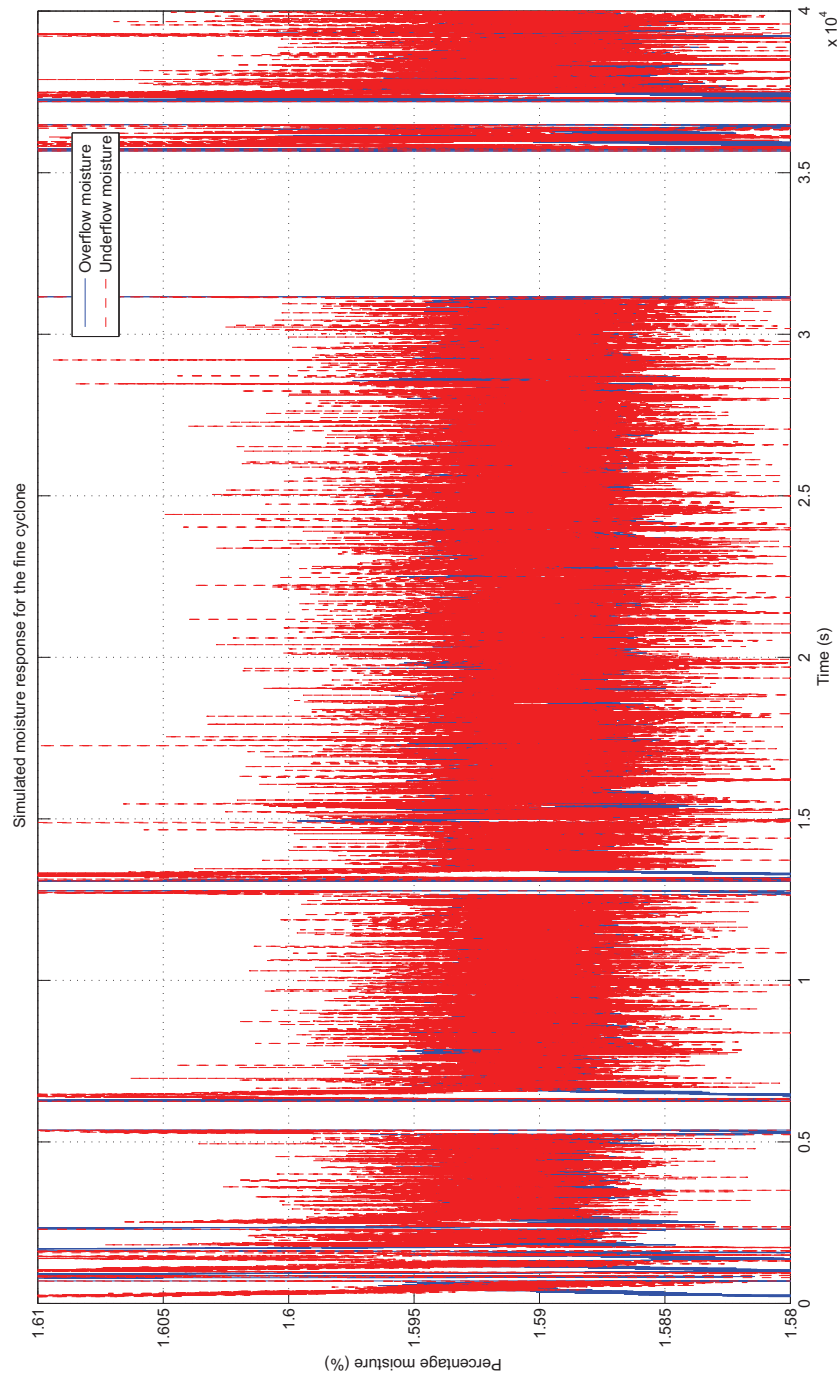


Figure 6.56: Simulated moisture response for the fine cyclone.

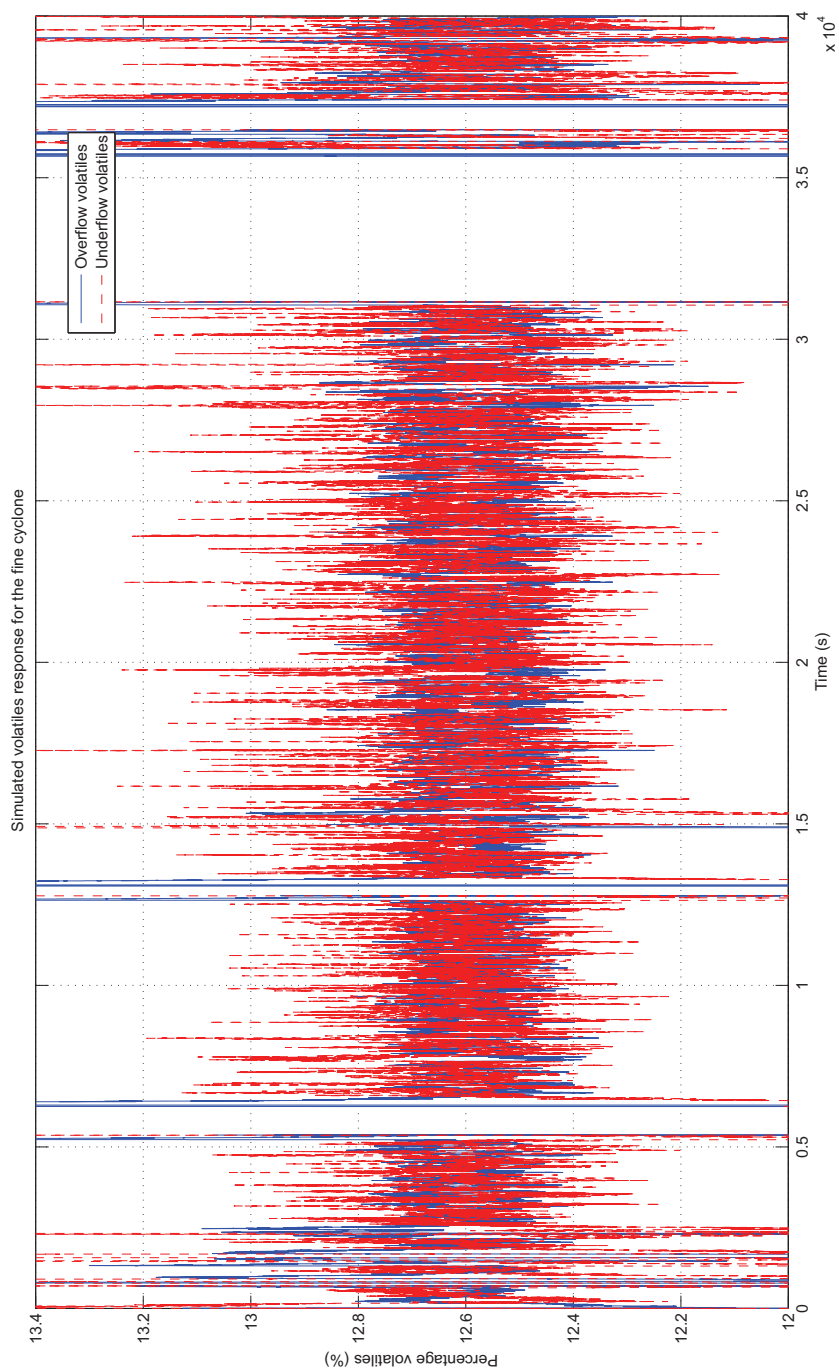


Figure 6.57: Simulated volatile response for the fine cyclone.

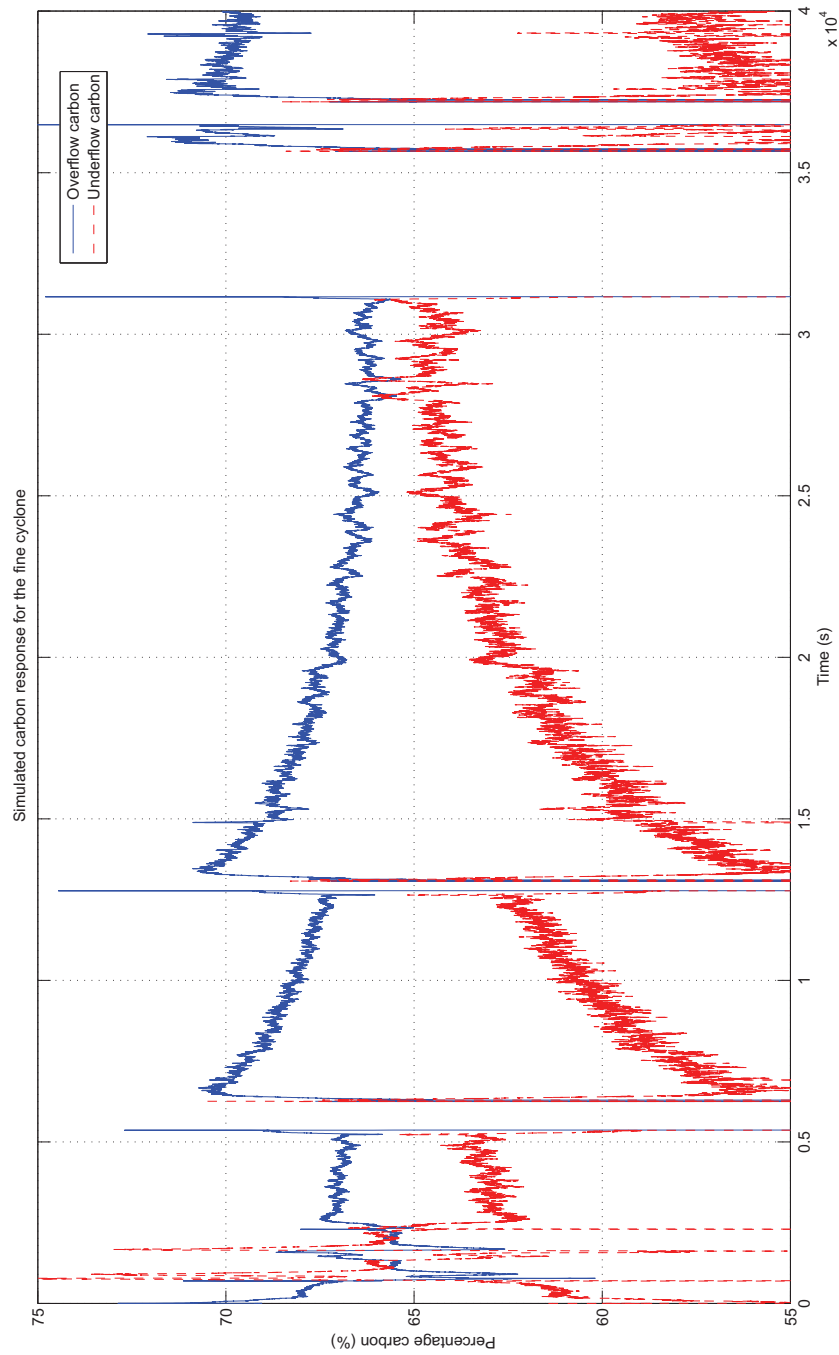


Figure 6.58: Simulated carbon response for the fine cyclone.

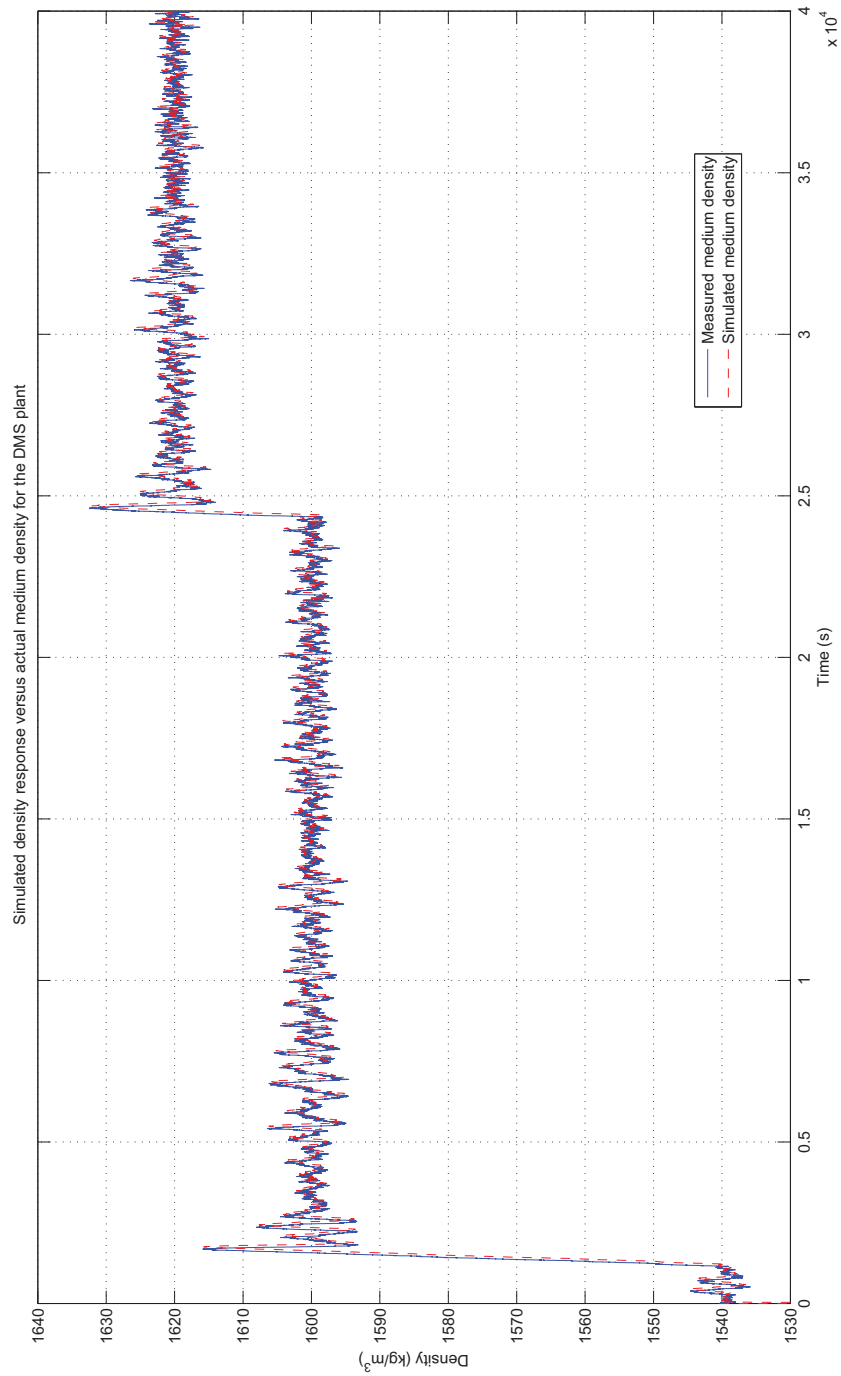


Figure 6.59: Simulated density response versus actual medium density for the DMS plant.

experiment. During the experiment the variables that could be manipulated (feed rate and medium density) were changed.

The response for the screen model (double-deck screen) can only be compared to the measured oversize material feed rate, as the other particle size product feed rates are not measured online. Because of the brittle nature of coal and its variability in particle size, it is necessary to make use of actual belt scale measurements available in the plant to simulate the screen mass split ratios. The crushing that takes place in the mining operation has an impact on the particle size distribution of the feed into the DMS plant. In order to accommodate this, the ratio between the oversize feed rate and initial feed is used. A comparison of this ratio over a long period of time showed that this varies dramatically. Since the undersize particles from the bottom deck of the double-deck screen are collected and fed into the single-deck screen, the response of the single-deck screen is similar to that of the double-deck screen. The yields achieved for the variously sized products are similar to that of the actual Leeuwpan operation.

By using the measured medium density, the response of the mixing box (with fine ore fed from the single-deck screen), DMC, medium tank and addition of water can be determined. It is determined that these responses match the actual process fairly accurately, based on the industrial experiment test case. The high correlations and small scalar-valued norms indicate the accuracy of the models. The steady-state simulation derived from the dynamic model equations of the DMC enables the construction of an efficiency curve for a specific set of conditions. This curve is similar to that presented in the literature study which indicates that the dynamic equations describing the DMC is legitimate for steady-state analysis as well. The DMC results for ash, moisture and volatile percentages correlate very well with small scalar-valued norms. The mass components are critical to the model validation, as this is ultimately what will be controlled by manipulating the feed rate and medium density.

The integrated model allows the simulation of the entire fine cyclone DMS plant. This model also allows the process to be simulated at a higher resolution over a longer period of time. It is also possible to use this model to perform a simulation in parallel to the actual process in real time.

## 6.6 CONCLUSION

This chapter describes and illustrates the results obtained for the model validations and simulations. By performing an industrial experiment test, the

equipment models developed can be validated. The scalar-valued norm between the simulated response and actual measured process output, where available, is determined per equipment model. The efficiency curve simulation of the DMC indicates the legitimacy of the DMC modelling approach presented in this dissertation.

Each equipment model output is illustrated graphically with associated variables. Once each equipment model is validated, an integrated model illustrating the interactions between all items is modelled. This allows for the fine cyclone DMS plant to be simulated for a longer duration at a higher resolution.

## CHAPTER 7: CONCLUSION

### 7.1 INTRODUCTION

This chapter provides a discussion and conclusion on the research that was conducted. The challenges involved in developing a DMS plant model, simulation and validation thereof are also described. Certain recommendations are made and future developments as a result of this research are then foreseen. Finally the work is summarised and the findings are presented.

### 7.2 DISCUSSION

This research required the author to develop a dynamic model of a DMS process in coal beneficiation. By conducting a detailed literature study on the status of the existing knowledge of metallurgical engineering for coal beneficiation and in control engineering for minerals processing, it is possible to determine what is required for the development of the model.

Because of the limitations in the findings with respect to practical applications of dynamic modelling of the DMS process in the literature study, the model was developed from first principles. The model developed consisted of individual equipment models integrated together. The parameters describing the equipment models have been identified, where non-linear, and estimated to a reasonable degree of accuracy. The validation of the model was performed using an industrial experiment test case where plant data were collected and samples were taken of the fine cyclone product and analysed. During the test case, the manipulated variables for the process were adjusted as required.

The limited information available from the literature study on applications of dynamic models in DMS processes and the validation of the model indicates that this research can contribute to the field of process control and mathematical modelling in minerals processing.

The challenges involved in validating the models that have been developed from first principles are ensuring that practical measurement points are used in the representation of the mathematical models. The other challenge experienced was to simulate the non-linear DMC model. The Runge-Kutta approximation provided a solution for simulating the non-linear DMC model. This approximation also allowed the use of process measurements as input to drive other equipment models.

The research methodology that was followed included the development of a problem statement and research questions, literature study, model development and model validation with an industrial experiment to answer the research questions. Although this approach allows research to be conducted in a structured manner, there were some deficiencies in the industrial experiment in that the amount of data points collected were limited. If more frequent data points were collected, the model could be validated for longer periods of time. The limitations of the model, in the model development, are that no equipment models of the drain and rinse screens or the drum separator were developed. The addition of water in the wet screening process should also have been included in the primary- and secondary-screen model. These deficiencies could be addressed by performing a number of industrial experiment tests, to allow for different experiments for system identification and model validation. The deficiencies in the model can be addressed by conducting a literature study on mathematical modelling of drain and rinse screens and drum separators. From this, it should be possible to develop dynamic models of the equipment from first principles, similar to what has been achieved in this dissertation.

### 7.3 RECOMMENDATION FOR FURTHER WORK

On the basis of the research process a number of recommendations can be made with regard to the Leeuwpan DMS plant process control environment and possible further research.

The medium make-up that is added to the corrected medium tank for the different cyclones is not currently being measured on-line at Leeuwpan. It is recommended that initially a flow switch be added to each medium make-up addition line. A density controller is also recommended to be used for the medium make-up section in the plant. This will allow the measurement of the disturbances experienced at the corrected medium tank due to medium loss.

In respect of the lag experienced in the sampling and laboratory analysis of the feed ore and product analyses, it is recommended that an online coal analyser (x-ray, gamma-ray or neutron) be used to measure these properties. If the feed mass components are measured, it is recommended that the DMC model feed mass components be used as inputs rather than parameters. This will also enable the model to be simulated in real time with the process.

Further research can be conducted to determine the dynamics involved in the recovery of magnetite medium. The losses involved for the medium and the

addition of non-magnetics to the medium could also be modelled to obtain a more accurate representation of the circulating medium. However, for the purposes of this study the measured medium density is sufficient to simulate the operation of the DMC. The variability in particle size distribution and possibly particle shape due to the brittle nature of coal in the crushing circuit can also influence the operation of the DMC. If this influences the dynamics of the DMC operation, it might be necessary to incorporate viscosity as a parameter or input to the DMC model.

It is also recommended that this research be continued so that the model is used in the development of a controller. The possible advantages of increasing product yield and quality with an automatic controller should also be investigated. The financial benefits of this should then be quantified and justified.

## REFERENCES

- Baguley, P. J. and Napier-Munn, T. J. (1996). Mathematical model of the dense medium drum, *Trans. Inst. Min. Met. (Section C)* **105**: C1–C8.
- Bauer, M. and Craig, I. K. (2008). Economic assessment of advanced process control - a survey and framework, *Journal of Process Control* **18**: 2–18.
- Borsaru, M., Dixon, R., Rojc, A., Stehle, R. and Jency, Z. (2001). Coal face and stockpile analyser for the coal mining industry, *Applied Radiation and Isotopes* **55**: 407–412.
- Bosman, J. and Engelbrecht, J. (1999). Dense medium separation: Does size really count. <http://www.sacoalprep.co.za/information.html>. Last accessed on 18 December 2008.
- Botha, B. W. (2008). *Management of the mineral resource risk associated with near-density material in the beneficiation plant at Leeuwan coal mine*, Master's thesis, University of Pretoria.
- Bradley, D. (1965). *The Hydrocyclone*, Pergamon Press, Oxford, England.
- Brennan, M. S. (2003). Multiphase CFD simulations of dense medium and classifying hydrocyclones, *Proceedings of the Third international Conference on CFD in the Minerals and Process Industries CSIRO, 10–12 December, 2003, Melbourne, Australia*, pp. 59–64.
- Brogan, W. L. (1991). *Modern Control Theory*, 3 edn, Prentice-Hall, Englewood Cliffs, NJ.
- Chen, W., Zydek, N. and Parma, F. (2000). Evaluation of hydrocyclone models for practical applications, *Chemical Engineering Journal* **80**: 295–303.
- Chen, X., Li, Q. and Fei, S. (2008). Constrained model predictive control in ball mill grinding process, *Powder Technology* **186**: 31–39.
- Cierpisz, S. (1998). Computer simulation of the control systems for heavy media coal preparation process, *Proceedings of the Third Regional APCOM Symposium, Kalgoorlie, Australia*, AusIMM, pp. 89–93.
- Cierpisz, S., Mironowicz, W. and Mirkowski, C. (1980). Instrumentation for coal preparation plants, *Proceedings of the IFAC Mining, Mineral and Metal Processing, 18–20 August, 1980, Montreal, Canada*, IFAC, pp. 375–387.
- Clarkson, C. J. (1983). A model of dense medium cyclones, *Proceedings of the Dense Medium Operators Conference, 1983, Brisbane, Australia*, pp. 235–245.

- Cortés, C. and Gil, A. (2007). Modelling the gas and particle flow inside cyclone separators, *Progress in Energy and Combustion Science* **33**: 409–452.
- Craig, I. K. and Henning, R. G. D. (2000). Evaluation of advanced industrial control projects: a framework for determining economic benefits, *Control Engineering Practice* **8**: 769–780.
- Craig, I. K. and MacLeod, I. M. (1995). Specification framework for robust control of a run-of-mine ore milling circuit, *Control Engineering Practice* **3**(5): 621–630.
- Craig, I. K. and MacLeod, I. M. (1996). Robust controller design and implementation for a run-of-mine ore milling circuit, *Control Engineering Practice* **4**(1): 1–12.
- Davis, J. J. and Napier-Munn, T. J. (1987). Influence of medium viscosity on the performance of dense medium cyclones in coal preparation, *Proceedings of the Third International Conference on Hydrocyclones, Oxford, BHRA*, pp. 147–154.
- de Korte, J. G. (2003a). Comments on the use of tracers to test dense-medium plant efficiency, *International Journal of Coal Preparation and Utilization* **23**(5): 251–266.
- de Korte, J. G. (2003b). Index of South African coal preparation plants. <http://www.sacoalprep.co.za/information.html>. Last accessed on 30 October 2008.
- de Korte, J. G. (2006). Determination and use of washability curves. [http://www.sacoalprep.co.za/papers/10\\_JdeKorte\\_Washability%20curves.pdf](http://www.sacoalprep.co.za/papers/10_JdeKorte_Washability%20curves.pdf). Last accessed on 30 November 2008.
- de Korte, J. G. (2008). The influence of near-dense material on the separation efficiency of dense-medium processes, *International Journal of Coal Preparation and Utilization* **28**(2): 69–93.
- England, T., Hand, P. E., Michael, D. C., Falcon, L. M. and Yell, A. D. (2002). *Coal Preparation in South Africa*, 4 edn, Natal Witness Commercial Printers, Pietermaritzburg, South Africa.
- Erasmus, T. C. (1973). The fitting of a smooth curve to the experimentally determined coordinates of a tromp curve, *Technical Report 4*, Fuel Research Institute of South Africa.
- Firth, B. A., Grice, C., Jenssen, E. and Weale, W. (1983). Computer simulation of coal preparation and its application at the Saxonvale mine, *Proceedings*

- of the Second Australian Coal Preparation Conference, 10–14 October, 1983, Rockhampton, Australia, Vol. 2, Australian Coal Preparation Society, pp. 421–443.
- Galán, O., Barton, G. W. and Romagnoli, J. A. (2002). Robust control of a sag mill, *Powder Technology* **124**: 264–271.
- Goodwin, G. C., Seron, M. M. and Mayne, D. Q. (2008). Optimization opportunities in mining, metal and mineral processing, *Annual Reviews in Control* **32**: 17–32.
- Gottfried, B. S. (1973). Computer simulation of coal preparation plants, *Technical Report Grant No. G0-155030*, U.S. Bureau of Mines.
- Gu, G., Cheng, D., Yin, J., Qiao, S., Liu, L. and Zhang, X. (2005). Rapid analysis of coal properties, *IEEE Instrumentation and Measurement Magazine* **12**: 22–27.
- Gupta, A. and Yan, D. (2006). *Mineral Processing Design and Operations: An Introduction*, 1 edn, Elsevier, Amsterdam, The Netherlands.
- Hayes, P. (2003). *Process principles in minerals and materials production*, 3 edn, Hayes Publishers, Brisbane, Australia.
- He, Y. B. and Laskowski, J. S. (1994). Effect of dense medium properties on the separation performance of a dense medium cyclone, *Minerals Engineering* **7**(2): 209–221.
- Herbst, J. A., Pate, W. T. and Oblad, A. E. (1992). Model-based control of mineral processing operations, *Powder Technology* **69**: 21–32.
- Honaker, R. Q. and Patwardhan, A. (2006). In-plant evaluation of dense medium process performances, *International Journal of Coal Preparation and Utilization* **26**(3): 149–164.
- Hucko, R. E. (1983). U.S. government research in physical coal cleaning, in R. L. Whitmore (ed.), *Proceedings of the Second Australian Coal Preparation Conference, 1983, Rockhampton, Australia*, Vol. 2 of *Density Separation*, Australian Coal Preparation Society, Australian Coal Preparation Society, pp. 63–82.
- Kalyani, V. K., Charan, T. G., Haldar, D. D., Sinah, A. and Suresh, N. (2008). Coal-fine beneficiation studies of a bench-scale water-only cyclone using artificial neural network, *International Journal of Coal Preparation and Utilization* **28**(2): 94–114.

- Keast-Jones, R., Smitham, J., Horrocks, K. and Ellison, J. (1991). Dense medium cyclone control by non-conventional means, *in* P. Lean (ed.), *Proceedings of the Fifth Australian Coal Preparation Conference, Newcastle, Australia*, Australian Coal Preparation Society, pp. 38–52.
- Keast-Jones, R., Smitham, J., Horrocks, K. R. S. and Ellison, J. (1993). Continuous control of dense medium cyclone separation density, *Proceedings of the XVIII International Mineral Processing Congress, Sydney, Australia*, AusIMM, pp. 349–356.
- King, R. P. (1999). Practical optimization strategies for coal-washing plants, *International Journal of Coal Preparation and Utilization* **20**(1): 13–34.
- King, R. P. and Juckes, A. H. (1984). Cleaning of fine coals by dense-medium hydrocyclones, *Powder Technology* **40**(1): 147–160.
- King, R. P. and Juckes, A. H. (1988). Performance of dense-medium cyclone when beneficiating fine coal, *Coal Preparation* **5**: 185–210.
- Lipták, B. G. (1995a). *Instrument engineers' handbook: Process control*, 3 edn, Butterworth-Heinemann Ltd, UK, Europe.
- Lipták, B. G. (1995b). *Instrument engineers' handbook: Process measurement and analysis*, 3 edn, Butterworth-Heinemann Ltd, UK, Europe.
- Ljung, L. (1987). *System Identification: Theory for the User*, 1 edn, Prentice-Hall, Inc, Englewood Cliffs, NJ.
- Ljung, L. (2005). *System identification toolbox user's guide*, 7 edn, The MathWorks, Inc, Natick, MA, USA.
- Lundt, M. (2008). DMS plant delay estimates, private communication.
- Lyman, G. J., Askew, H., Wood, C. J. and Davis, J. J. (1982). Dynamic modelling of dense medium cyclone washing circuits, *Proceedings of the Mill Operations Conference, NW Queensland, Australia*, AusIMM, pp. 369–381.
- Lyman, G. J., Denney, B., Wood, C. J., Askew, H. and Brenchley, R. (1983). Automatic control of product coal ash content using on-line coal ash gauge, *in* R. L. Whitmore (ed.), *Proceedings of the Second Australian Coal Preparation Conference, Rockhampton, Australia*, Vol. 2 of *Instrumentation and Control*, Australian Coal Preparation Society, pp. 291–309.
- Lynch, A. J. (1977). *Mineral Crushing and Grinding Circuits - Their Simulation, Optimisation, Design and Control*, Elsevier Scientific Pub. Co., Amsterdam.

- Magwai, M. and Bosman, J. (2007). The effect of cyclone geometry and operating conditions on spigot capacity of dense medium cyclones, *International Journal of Mineral Processing* **86**: 94–103.
- Majumder, A. K., Barnwal, J. P. and Ramakrishnan, N. (2004). A new approach to evaluate the performance of gravity-based coal washing equipment, *International Journal of Coal Preparation and Utilization* **24**(5): 277–284.
- Marlin, T. E. (1995). *Process control, Designing processes and control systems for dynamic performance*, 1 edn, McGraw-Hill Inc., USA.
- Mathews, J. H. and Fink, K. D. (1999). *Numerical methods using Matlab*, 3 edn, Prentice Hall Inc., USA.
- Mikhail, M. W. and Humeniuk, O. (1980). Automatic in-line ash monitor for coal slurries, *Proceedings of the IFAC Mining, Mineral and Metal Processing, 18–20 August, 1980, Montreal, Canada*, IFAC, pp. 389–400.
- Mukherjee, A. K., Sripriya, R., Rao, P. V. T. and Das, P. (2003). Effect of increase in feed inlet pressure on feed rate of dense medium cyclone, *International Journal of Mineral Processing* **69**: 259–274.
- Napier-Munn, T. J. (1991). Modelling and simulating dense medium separation processes - a progress report, *Minerals Engineering* **4**(3): 329–346.
- Page, C. and Meyer, D. (2003). *Applied research design for business management*, McGraw-Hill Australie Pty Ltd., Australia.
- Plitt, L. R. (1971). The analysis of solid-solid separations in classifiers, *The Can. Minerals Metallurgy, Bul.*, pp. 1–6.
- Preptech (2008). Preptech catalog. <http://www.preptech.com/assets/applets/PreptechCatalog.pdf>. Last accessed on 18 December 2008.
- Rao, B. V. (2004). Weibull partition surface representation for gravity concentrators, *Minerals Engineering* **17**: 953–956.
- Rao, B. V., Kapur, P. C. and Konnur, R. (2003). Modelling the size-density partition surface of dense-medium separators, *International Journal of Mineral Processing* **72**: 443–453.
- Rathaba, L. P. (2004). *Model fitting for electric arc furnace refining*, Master's thesis, University of Pretoria.
- Rayner, J. G. and Napier-Munn, T. J. (2003). A mathematical model of the recovery of dense medium magnetics in the wet drum magnetic separator, *International Journal of Mineral Processing* **69**: 157–173.

- Scott, I. A. and Lyman, G. J. (1987). Metallurgical evaluation of iron ore drum separators using density tracers, *Proceeding of the Australian Institute of Mining and Metallurgy, February, 1987*, Vol. 1, pp. 49–56.
- Scott, I. A. and Napier-Munn, T. J. (1992). Dense-medium cyclone model based on the pivot phenomenon, *Trans. Inst. Min. Metall. (Section C: Min. Proc. Extr. Metall.)* **101**: C61–C76.
- Seborg, D. E., Edgar, T. F. and Mellichamp, D. A. (1995). *Process dynamics and control*, 2 edn, John Wiley and Sons, Inc, USA.
- Skogestad, S. and Postlethwaite, I. (2005). *Multivariable feedback control analysis and design*, 2 edn, John Wiley and Sons, West Sussex, England.
- Stephanopoulos, G. (1984). *Chemical process control: an introduction to theory and practice*, 1 edn, Prentice-Hall, Inc., Englewood Cliffs, New Jersey.
- Suasnabar, D. J. and Fletcher, A. J. (1999). A CFD model for dense medium cyclones, *Proceedings of the Second international Conference on CFD in the Minerals and Process Industries CSIRO, 6–8 December, 1999, Melbourne, Australia*, pp. 199–204.
- Watt, J. S. and Sowerby, B. D. (1983). On-line determination of ash in coal using “siroash” gauges, *Proceedings of the Second Australian Coal Preparation Conference, 10–14 October, 1983, Rockhampton, Australia*, Vol. 2 of *Instrumentation and Control*, Australian Coal Preparation Society, Coal preparation Societies of New South Wales and Queensland AUSTRALIE (1983) (Monographie), pp. 263–290.
- Wilkes, K. D. (2006). The practical application of the wemco hms drum separator in the mining and metals recycling industries, *Proceedings of the SAIMM Present Status and Future for DMS Gravity Concentration in the South African Mining Industry Conference, 18–20 July, 2006*, SAIMM, pp. 179–190.
- Wood, C., Davis, J. and Lyman, G. (1987). Towards a medium behaviour based performance model for coal-washing dm cyclones, *Proceedings of the Dense Medium Operators Conference, Brisbane, Australia*, AusIMM, pp. 247–256.
- Xia, X. and Moog, C. H. (2003). Identifiability of nonlinear systems with applications to HIV/AIDS models, *IEEE Transactions on Automatic Control* **48**(2): 330–336.

## ADDENDUM A: WASHABILITY TABLES AND CURVES FOR BLOCKS OD, OH AND OM FOR SEAM 2

Wash tables for seam 2 for the various reserve blocks.

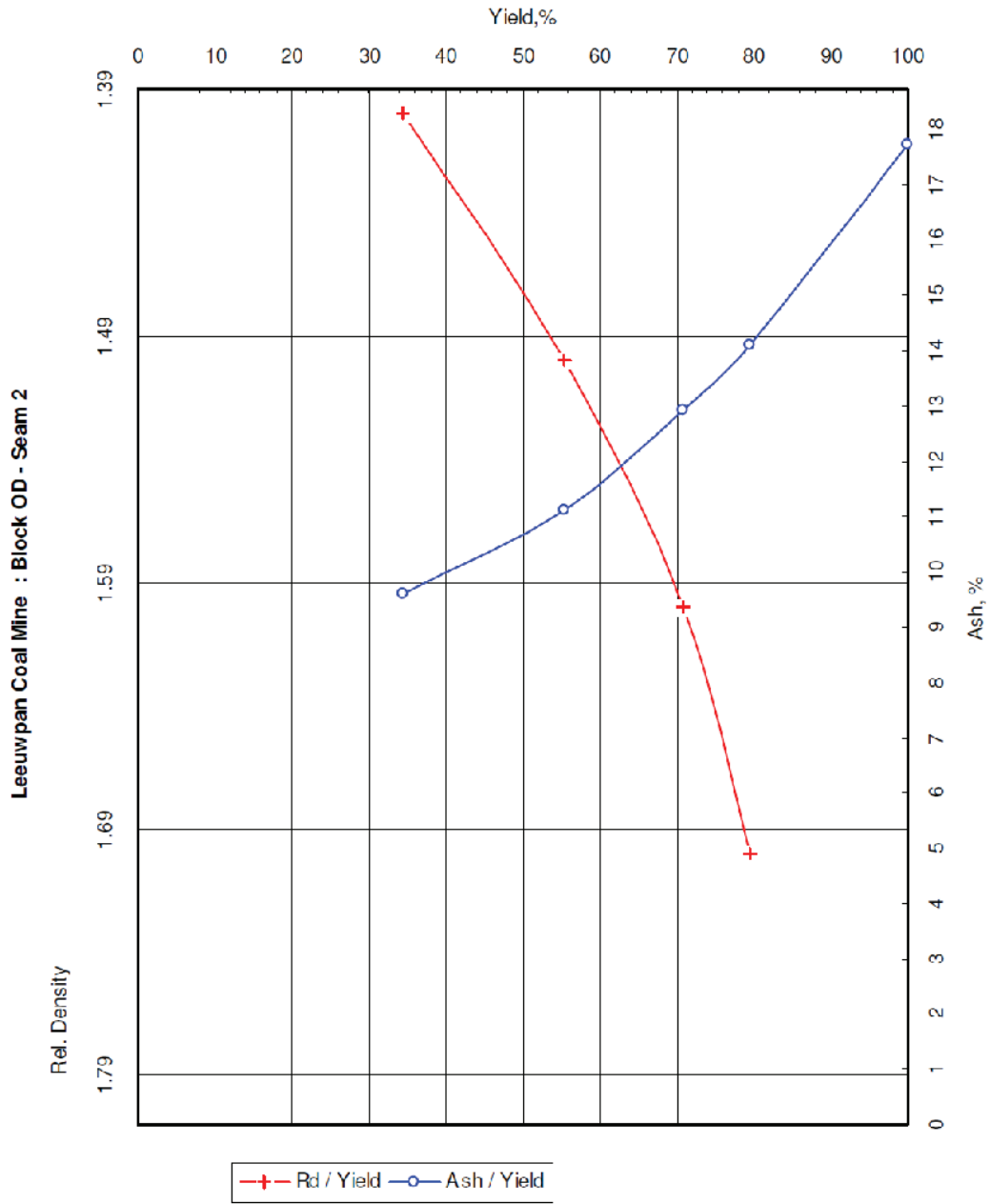
<b>Wash table for seam 2 for block OD</b>		
Relative Density	Yield(%)	Ash(%)
F@1.4	34.44	9.6
F@1.5	55.37	11.1
F@1.6	70.72	12.9
F@1.7	79.57	14.1
S@1.7	100	17.7

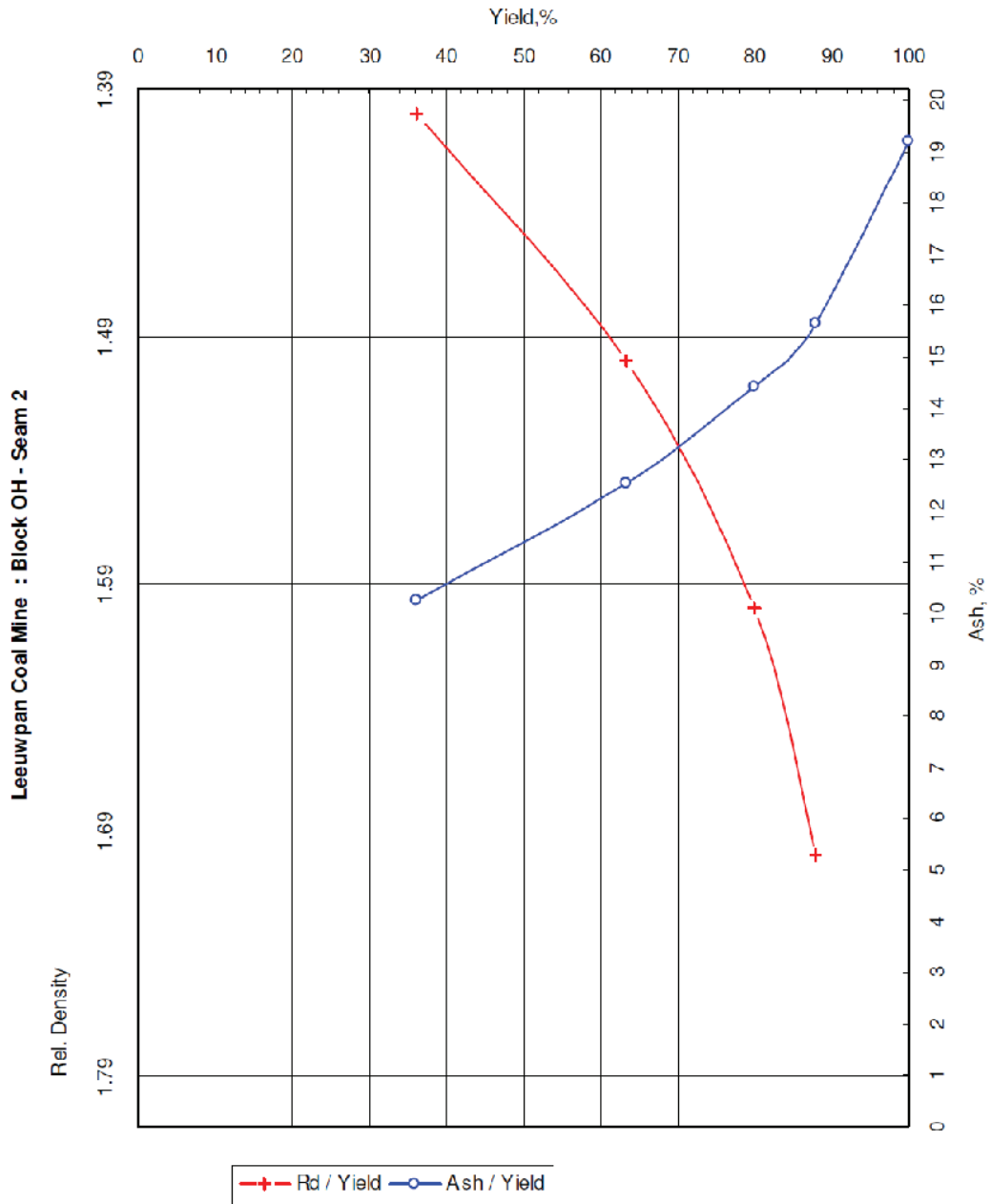
<b>Wash table for seam 2 for block OH</b>		
Relative Density	Yield(%)	Ash(%)
F@1.4	36.17	10.3
F@1.5	63.34	12.5
F@1.6	80.05	14.4
F@1.7	87.85	15.7
S@1.7	100	19.2

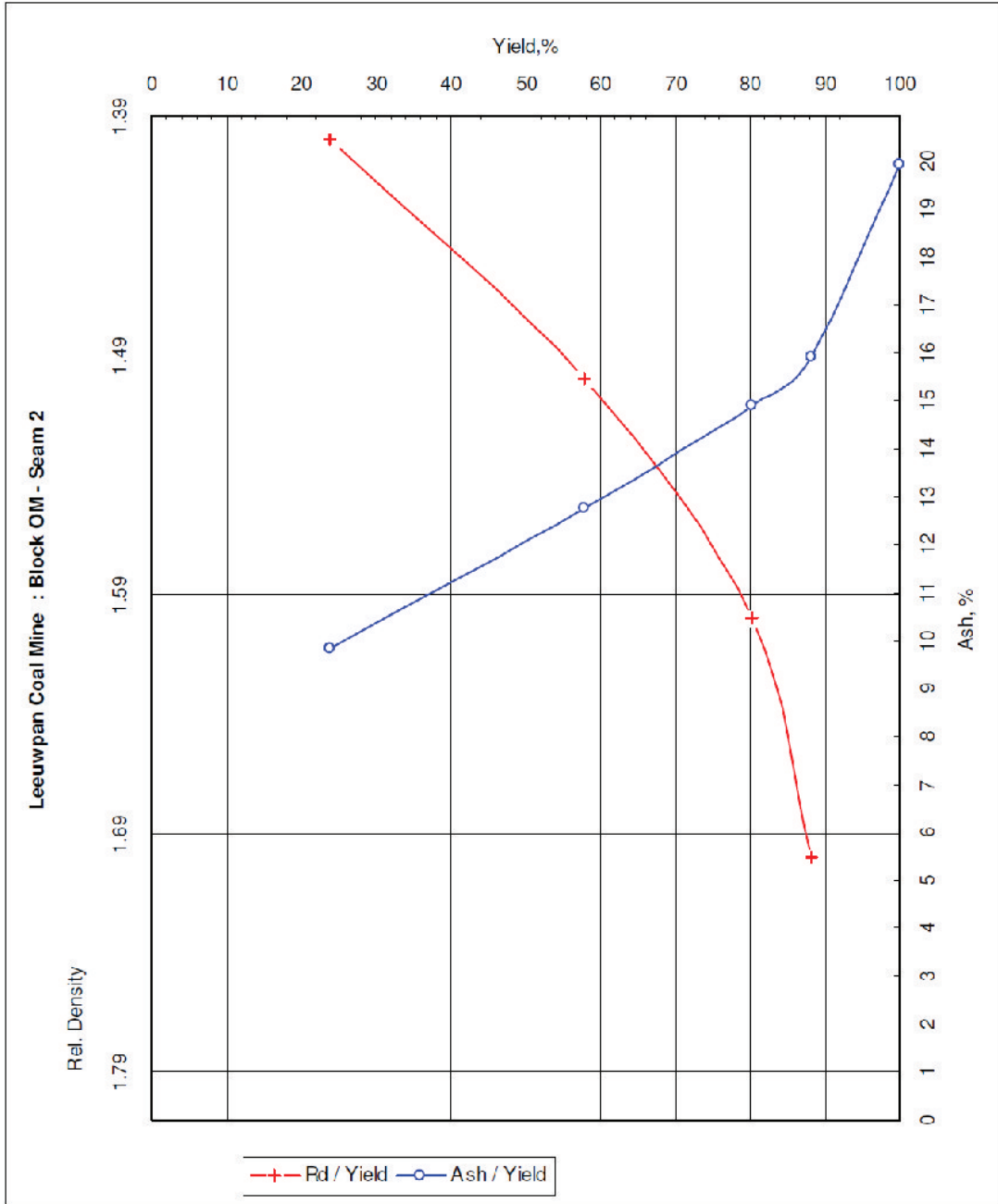
<b>Wash table for seam 2 for block OM</b>		
Relative Density	Yield(%)	Ash(%)
F@1.4	23.83	9.8
F@1.5	57.81	12.8
F@1.6	80.29	14.9
F@1.7	88.19	15.9
S@1.7	100	20

Note: Ash reporting base: air dry

Volatiles reporting base: absolute dry





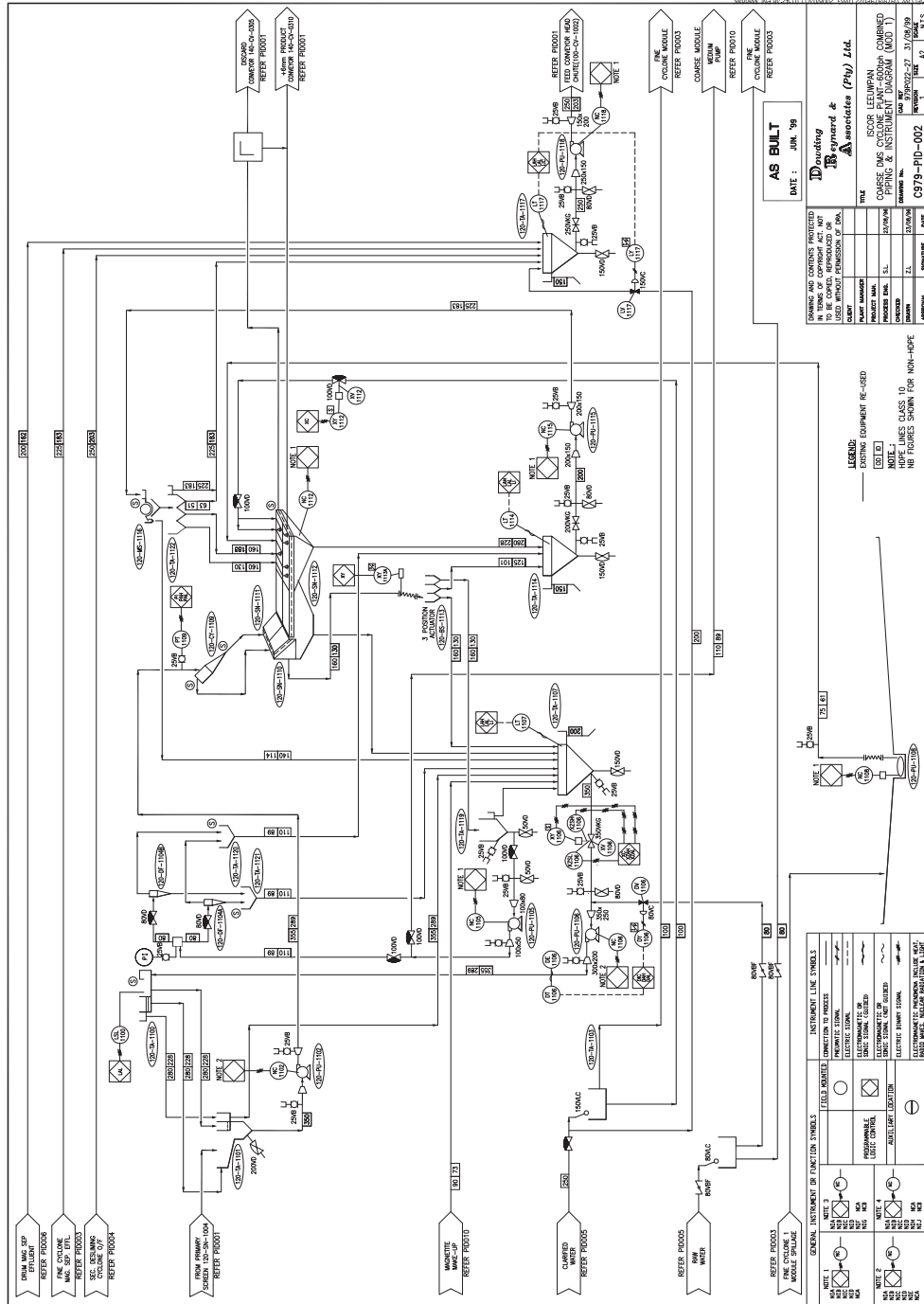




## ADDENDUM B: PROCESS AND INSTRUMENTATION DIAGRAMS FOR LEEUWPAN DMS PLANT







**AS BUILT**  
DATE: JUN. '99

**Drawings & Associates (Pty) Ltd.**

ISSOR: LEEMAN  
PROJECT: COARSE FINE CONTROL PIPING & INSTRUMENT DIAGRAM (MOD 1)

DATE: 27 JUN 99

NO: C979-PID-002

NO.	REVISION	DATE	BY	CHKD.
1				
2				
3				
4				
5				
6				
7				
8				
9				
10				
11				
12				
13				
14				
15				
16				
17				
18				
19				
20				
21				
22				
23				
24				
25				
26				
27				
28				
29				
30				
31				
32				
33				
34				
35				
36				
37				
38				
39				
40				
41				
42				
43				
44				
45				
46				
47				
48				
49				
50				
51				
52				
53				
54				
55				
56				
57				
58				
59				
60				
61				
62				
63				
64				
65				
66				
67				
68				
69				
70				
71				
72				
73				
74				
75				
76				
77				
78				
79				
80				
81				
82				
83				
84				
85				
86				
87				
88				
89				
90				
91				
92				
93				
94				
95				
96				
97				
98				
99				
100				

DRAWING AND CONTENTS PROTECTED BY PATENT RIGHTS AND IS NOT TO BE COPIED, REPRODUCED OR USED WITHOUT PERMISSION OF DWA.

ISSOR: LEEMAN  
PROJECT: COARSE FINE CONTROL PIPING & INSTRUMENT DIAGRAM (MOD 1)

DATE: 27 JUN 99

NO: C979-PID-002

AS BUILT  
DATE: JUN. '99

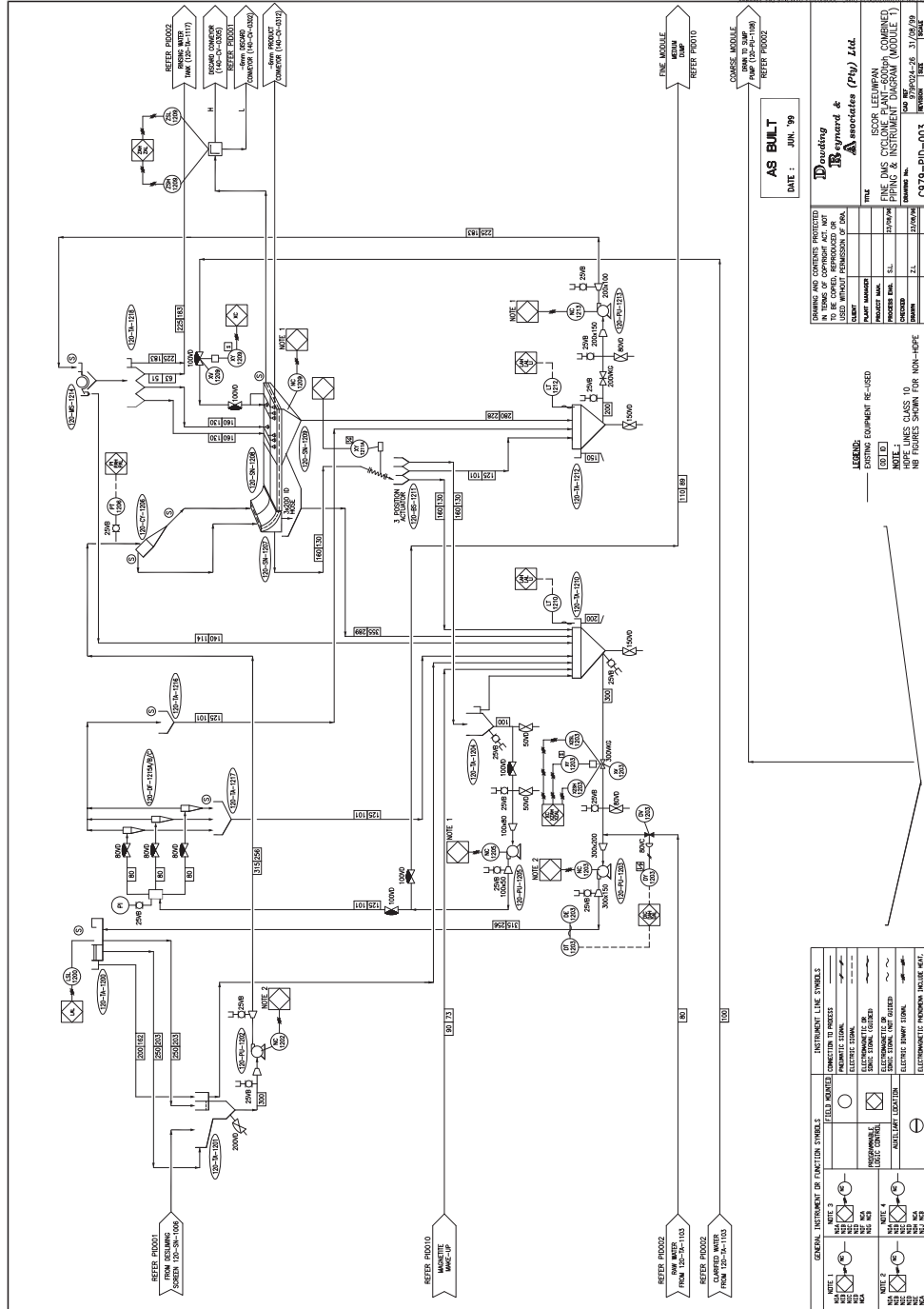
**Drawings & Associates (Pty) Ltd.**

ISSOR: LEEMAN  
PROJECT: COARSE FINE CONTROL PIPING & INSTRUMENT DIAGRAM (MOD 1)

DATE: 27 JUN 99

NO: C979-PID-002

NO.	REVISION	DATE	BY	CHKD.
1				
2				
3				
4				
5				
6				
7				
8				
9				
10				
11				
12				
13				
14				
15				
16				
17				
18				
19				
20				
21				
22				
23				
24				
25				
26				
27				
28				
29				
30				
31				
32				
33				
34				
35				
36				
37				
38				
39				
40				
41				
42				
43				
44				
45				
46				
47				
48				
49				
50				
51				
52				
53				
54				
55				
56				
57				
58				
59				
60				
61				
62				
63				
64				
65				
66				
67				
68				
69				
70				
71				
72				
73				
74				
75				
76				
77				
78				
79				
80				
81				
82				
83				
84				
85				
86				
87				
88				
89				
90				
91				
92				
93				
94				
95				
96				
97				
98				
99				
100				



**AS BUILT**  
DATE: JUN '99

DRIVING AND CONTENTS PROTECTED TO BE COVERED, REPRODUCED OR USED WITHOUT PERMISSION OF ISOR LEEMAN & ASSOCIATES (Pty) Ltd.

NO.	REVISION	DESCRIPTION	DATE
1	1	ISSUED FOR CONSTRUCTION	10/06/99
2	1	ISSUED FOR CONSTRUCTION	10/06/99
3	1	ISSUED FOR CONSTRUCTION	10/06/99
4	1	ISSUED FOR CONSTRUCTION	10/06/99
5	1	ISSUED FOR CONSTRUCTION	10/06/99
6	1	ISSUED FOR CONSTRUCTION	10/06/99
7	1	ISSUED FOR CONSTRUCTION	10/06/99
8	1	ISSUED FOR CONSTRUCTION	10/06/99
9	1	ISSUED FOR CONSTRUCTION	10/06/99
10	1	ISSUED FOR CONSTRUCTION	10/06/99

LEGEND: EQUIPMENT RE-USED  
NOTE: HOPE LINES CLASS 10  
HOPE LINES SHOWN FOR NON-HOPE

GENERAL INSTRUMENT OR FUNCTION SYMBOLS	FIELD SYMBOLS	INSTRUMENT LINE SYMBOLS
NOTE 1: [Symbol] FIELD SYMBOLS	[Symbol] FIELD SYMBOLS	[Symbol] INSTRUMENT LINE SYMBOLS
NOTE 2: [Symbol] FIELD SYMBOLS	[Symbol] FIELD SYMBOLS	[Symbol] INSTRUMENT LINE SYMBOLS
NOTE 3: [Symbol] FIELD SYMBOLS	[Symbol] FIELD SYMBOLS	[Symbol] INSTRUMENT LINE SYMBOLS
NOTE 4: [Symbol] FIELD SYMBOLS	[Symbol] FIELD SYMBOLS	[Symbol] INSTRUMENT LINE SYMBOLS
NOTE 5: [Symbol] FIELD SYMBOLS	[Symbol] FIELD SYMBOLS	[Symbol] INSTRUMENT LINE SYMBOLS
NOTE 6: [Symbol] FIELD SYMBOLS	[Symbol] FIELD SYMBOLS	[Symbol] INSTRUMENT LINE SYMBOLS
NOTE 7: [Symbol] FIELD SYMBOLS	[Symbol] FIELD SYMBOLS	[Symbol] INSTRUMENT LINE SYMBOLS
NOTE 8: [Symbol] FIELD SYMBOLS	[Symbol] FIELD SYMBOLS	[Symbol] INSTRUMENT LINE SYMBOLS
NOTE 9: [Symbol] FIELD SYMBOLS	[Symbol] FIELD SYMBOLS	[Symbol] INSTRUMENT LINE SYMBOLS
NOTE 10: [Symbol] FIELD SYMBOLS	[Symbol] FIELD SYMBOLS	[Symbol] INSTRUMENT LINE SYMBOLS

REFR. PRODUK FROM 100-0-008  
REFR. PRODUK FROM 100-0-103  
REFR. PRODUK FROM 100-0-103  
REFR. PRODUK FROM 100-0-103





**ADDENDUM C: PEA AND DUFF PRODUCT QUALITIES FOR  
OCTOBER 2008**

Oct-08		Peas			Duff		
Day	Time	H2O (%)	ASH (%)	VOLS (%)	H2O (%)	ASH (%)	VOLS (%)
1	07:00	2.0	16.2	6.6	1.1	16.2	5.9
1	09:00	2.3	17.7	12.3	1.8	19.0	12.1
1	11:00	2.6	18.5	21.2	2.2	22.0	19.8
1	13:00	3.4	17.2	21.8	2.4	20.6	20.7
1	15:00	2.7	17.0	21.2	1.5	16.5	21.4
1	17:00	2.7	14.8	21.2	1.5	16.3	21.4
1	19:00	4.5	15.1	21.7	2.4	16.6	21.7
1	21:00	2.2	14.1	19.9	1.7	13.5	19.8
1	23:00	3.0	13.4	18.8	3.3	18.6	18.7
2	01:00	3.0	14.2	18.7	2.6	14.5	18.8
2	03:00	3.0	14.6	18.1	2.4	13.9	19.1
2	05:00	5.3	13.9	18.7	3.2	14.0	19.7
2	07:00	4.2	14.0	19.0	2.3	14.6	19.6
2	09:00	3.1	14.6	19.1	2.1	14.7	18.8
2	11:00	3.9	17.0	22.1	3.3	19.6	20.6
2	13:00	3.4	18.5	22.0	2.4	19.1	21.1
2	15:00	2.7	18.5	23.1	2.7	19.4	21.9
2	17:00	3.5	16.9	21.2	1.2	19.9	21.9
2	19:00	3.9	15.8	21.4	1.6	18.2	21.2
2	21:00	4.0	15.8	20.7	3.9	15.3	19.6
2	23:00	2.9	14.6	20.6	2.7	13.6	19.6
3	01:00	4.5	13.7	18.6	4.1	13.2	19.0
3	03:00	4.7	12.7	19.1	3.4	14.0	18.7
3	05:00	3.0	14.6	19.2	2.4	14.8	18.1
3	07:00	2.3	13.4	20.0	1.9	13.7	18.8
3	09:00	2.5	12.8	21.0	3.6	13.6	18.6
3	11:00	2.6	15.2	17.2	1.6	14.2	17.2
3	13:00	1.4	15.7	11.1	1.3	17.9	7.8
3	15:00				0.9	17.2	9.1
3	17:00	2.4	14.7	7.9	2.2	17.2	8.5
3	19:00	2.2	15.3	8.1	3.5	15.3	6.0
3	21:00	3.9	13.7	7.1	1.9	15.7	7.6
3	23:00	4.7	13.8	7.4	7.3	14.1	6.5
4	01:00	5.2	14.1	7.0	1.8	16.4	7.5
4	03:00	5.6	17.1	8.8	2.4	19.6	8.6

Oct-08		Peas			Duff		
Day	Time	H2O (%)	ASH (%)	VOLS (%)	H2O (%)	ASH (%)	VOLS (%)
4	05:00	5.7	16.6	8.0	5.5	16.7	8.2
4	07:00	3.7	15.3	8.0	1.7	16.8	10.0
4	09:00	3.5	14.8	8.4	2.3	13.7	8.0
4	11:00	6.4	15.0	8.5	5.8	12.4	8.3
4	13:00	6.4	12.7	7.1	5.4	13.6	8.3
4	15:00	4.5	13.3	8.2	4.5	15.1	7.1
4	17:00	3.9	14.9	6.9	3.0	17.1	6.3
4	19:00	1.7	16.8	7.4	3.8	14.1	6.3
4	21:00	3.7	16.3	7.2	6.5	16.7	8.1
4	23:00	4.8	15.1	8.1	5.6	15.4	9.1
5	01:00	2.0	15.2	7.0	4.3	14.6	7.2
5	03:00	2.8	16.6	7.4	6.8	15.2	6.3
5	05:00	3.6	15.5	6.7	4.7	13.8	6.4
5	07:00	2.4	18.1	16.9	3.4	17.3	13.7
5	09:00	1.7	21.7	19.7	2.3	19.2	20.8
5	11:00	3.3	18.4	20.3	1.3	18.6	22.0
5	13:00	1.5	19.0	21.1	2.6	17.6	20.0
5	15:00	2.4	17.8	20.6	1.5	17.1	20.3
5	17:00	4.0	16.4	21.5	3.4	17.8	19.1
5	19:00	5.0	15.4	18.1	4.0	16.0	19.9
5	21:00	4.9	15.9	19.4	4.4	14.4	19.7
5	23:00	5.1	17.8	18.1	3.7	18.3	18.3
6	01:00	4.0	15.6	17.4	3.6	17.0	17.6
6	03:00	3.8	15.5	17.1	3.5	15.3	17.1
6	05:00	3.1	15.2	18.1	2.7	14.9	18.6
6	07:00	3.2	16.4	18.1	1.9	15.7	19.0
6	09:00	3.1	16.1	15.8	2.8	15.4	16.1
6	11:00						
6	13:00						
6	15:00						
6	17:00						
6	19:00	3.6	16.2	10.8	3.7	14.8	9.4
6	21:00	3.3	13.9	8.2	5.9	14.1	5.7
6	23:00	3.2	12.4	7.7	5.8	18.1	5.8
7	01:00	3.5	15.2	6.7	7.4	18.8	6.3
7	03:00	2.6	14.0	6.4	8.3	16.6	6.8
7	05:00	6.1	13.4	6.7	5.1	17.8	6.8

Oct-08		Peas			Duff		
Day	Time	H2O (%)	ASH (%)	VOLS (%)	H2O (%)	ASH (%)	VOLS (%)
7	07:00						
7	09:00						
7	11:00						
7	13:00						
7	15:00						
7	17:00	2.2	12.5	5.6	8.7	13.4	5.8
7	19:00	7.1	14.1	6.1	6.3	16.3	5.7
7	21:00	3.4	18.7	14.0	4.5	19.2	10.0
7	23:00	5.2	16.7	19.0	2.9	20.7	19.3
8	01:00	5.1	16.3	19.9	4.0	19.7	20.7
8	03:00	3.3	16.5	21.5	2.9	17.8	22.4
8	05:00	3.9	17.7	22.4	3.0	18.1	22.1
8	07:00	5.2	15.5	22.1	2.5	17.9	22.5
8	09:00	5.1	15.5	23.2	3.8	16.5	22.0
8	11:00	3.7	15.6	22.2	3.8	17.9	21.1
8	13:00						
8	15:00						
8	17:00	2.0	15.8	23.5	2.1	15.2	23.0
8	19:00	3.3	16.0	21.3	2.1	15.8	20.8
8	21:00						
8	23:00						
9	01:00	2.8	16.4	21.2	4.5	15.9	19.3
9	03:00	3.2	15.3	23.0	4.3	14.9	19.9
9	05:00						
9	07:00	2.8	16.1	21.7	1.7	15.2	22.9
9	09:00	1.8	15.2	23.6	1.9	15.3	21.3
9	11:00	2.0	17.5	23.1	2.9	15.6	19.6
9	13:00	2.2	15.8	23.6	3.4	15.7	21.7
9	15:00	3.8	16.3	22.8	3.2	15.0	22.1
9	17:00	4.7	14.2	22.0	4.2	12.3	20.4
9	19:00	3.0	15.5	23.2	4.1	16.5	21.2
9	21:00	4.1	14.8	23.1	3.0	18.6	22.5
9	23:00	4.5	14.6	22.7	3.3	13.7	22.8
10	01:00	4.2	15.2	23.4	3.5	13.9	22.9
10	03:00	4.3	15.5	23.4	3.6	16.7	23.2
10	05:00		15.2	23.0		16.0	23.4
10	07:00	5.6	14.6	21.9	4.0	15.4	22.4

Oct-08		Peas			Duff		
Day	Time	H2O (%)	ASH (%)	VOLS (%)	H2O (%)	ASH (%)	VOLS (%)
10	09:00	3.7	15.1	23.3	2.3	15.8	23.5
10	11:00	4.6	14.4	22.8	2.7	15.7	23.7
10	13:00	5.0	14.3	22.4	4.0	16.1	22.5
10	15:00	3.0	17.8	21.5	2.0	17.4	21.2
10	17:00	2.2	18.4	21.0	2.0	17.5	21.1
10	19:00	2.2	19.8	20.1	2.3	16.6	20.1
10	21:00	1.9	18.7	21.6	2.9	17.9	19.8
10	23:00	2.9	16.3	23.3	1.7	16.3	23.4
11	01:00	4.5	13.5	23.5	2.8	15.1	22.7
11	03:00	4.0	16.0	22.8	3.1	15.5	23.2
11	05:00	5.8	14.9	21.1	2.8	15.3	23.0
11	07:00	6.0	15.1	21.0	4.8	15.6	21.2
11	09:00	3.3	16.2	20.0	2.5	16.0	19.6
11	11:00	3.8	16.1	20.0	3.5	15.8	20.1
11	13:00	3.6	16.2	20.1	1.4	16.5	19.9
11	15:00	2.6	17.9	19.5	1.6	16.9	20.1
11	17:00	2.4	17.6	20.3	2.8	16.3	18.8
11	19:00	4.3	16.1	21.3	2.9	15.6	21.3
11	21:00	4.3	16.1	21.3	2.9	15.6	21.3
11	23:00	4.9	16.7	21.1	4.2	15.9	21.0
12	01:00	3.1	17.2	21.8	5.3	16.5	19.5
12	03:00	3.8	15.5	22.0	4.0	15.9	22.9
12	05:00	4.4	15.7	21.7	4.0	16.7	22.5
12	07:00	4.2	15.7	2.6	3.2	15.6	22.4
12	09:00	3.0	15.5	22.4	2.6	16.1	22.1
12	11:00	4.5	15.8	22.5	3.4	15.3	22.5
12	13:00	1.9	18.0	19.3	1.5	16.7	19.6
12	15:00	2.5	19.4	18.9	1.6	17.5	19.4
12	17:00	3.4	16.7	20.2	4.2	15.5	17.8
12	19:00	4.6	16.5	20.0	3.8	17.3	20.2
12	21:00	3.6	16.7	19.7	3.5	16.0	17.1
12	23:00	5.5	14.8	8.2	5.6	13.9	9.0
13	01:00	5.9	12.6	7.3	3.9	13.3	6.9
13	03:00	7.1	12.0	6.4	8.4	13.7	6.2
13	05:00	5.8	13.9	4.9	8.3	14.6	5.0
13	07:00	6.7	17.5	5.4	6.6	14.2	3.3
13	09:00	6.4	15.8	4.6	7.2	16.8	3.7

Oct-08		Peas			Duff		
Day	Time	H2O (%)	ASH (%)	VOLS (%)	H2O (%)	ASH (%)	VOLS (%)
13	11:00	7.0	15.8	5.2	8.0	15.1	3.4
13	13:00	7.0	15.3	4.9	6.8	16.5	5.6
13	15:00	5.7	13.9	4.4	6.5	17.5	4.0
13	17:00	7.1	13.6	7.2	4.7	14.9	7.7
13	19:00	5.1	15.8	6.6	3.2	16.7	5.6
13	21:00	1.4	16.5	6.1	2.8	17.6	5.2
13	23:00	1.2	16.0	5.8	3.7	16.1	4.8
14	01:00	1.2	15.7	5.6	3.4	18.3	4.8
14	03:00	2.8	14.9	5.0	1.4	17.6	5.1
14	05:00	2.2	14.6	4.1	2.5	15.3	4.4
14	07:00						
14	09:00						
14	11:00						
14	13:00						
14	15:00						
14	17:00						
14	19:00	2.5	14.7	6.1	3.7	18.3	5.8
14	21:00				2.1	14.4	6.1
14	23:00	2.7	15.8	9.5	2.2	15.8	9.4
15	01:00	5.9	16.1	8.2	5.5	15.4	7.6
15	03:00	3.8	14.7	7.9	2.7	19.2	7.6
15	05:00	6.8	12.9	5.1	5.6	28.8	5.4
15	07:00	5.7	19.0	5.5	2.9	28.5	8.7
15	09:00				3.4	16.4	12.4
15	11:00	2.7	15.1	21.7	4.1	16.4	20.1
15	13:00	3.7	12.5	23.1	3.1	18.7	21.8
15	15:00	1.3	14.8	24.4	3.8	14.2	23.4
15	17:00	3.4	13.7	23.1	1.4	17.5	22.4
15	19:00	1.5	12.9	23.2	2.7	16.7	22.7
15	21:00	4.0	17.2	21.3	2.1	21.0	20.8
15	23:00	4.5	14.7	23.7	2.6	19.8	22.3
16	01:00	4.2	15.0	23.4	4.4	17.0	23.2
16	03:00	5.2	15.1	20.2	4.4	13.9	20.7
16	05:00	4.7	14.8	21.4	4.2	17.0	21.5
16	07:00	3.2	14.7	20.7	3.7	12.8	22.2
16	09:00	3.2	15.7	20.3	3.0	13.9	20.1
16	11:00	3.8	18.2	22.0	1.6	17.8	23.1

Oct-08		Peas			Duff		
Day	Time	H2O (%)	ASH (%)	VOLS (%)	H2O (%)	ASH (%)	VOLS (%)
16	13:00	2.8	20.0	22.0	2.5	17.9	20.8
16	15:00	2.4	18.2	21.6	3.5	20.2	20.3
16	17:00	2.4	23.7	22.2	1.3	23.0	21.5
16	19:00	2.4	17.1	23.0	2.4	17.4	23.6
16	21:00	3.4	15.4	21.4	3.0	15.8	21.7
16	23:00	5.8	15.5	21.9	4.2	15.8	20.8
17	01:00	5.2	15.4	22.7	2.5	16.1	22.0
17	03:00	4.6	13.8	21.6	2.1	14.9	20.7
17	05:00	4.1	14.1	20.9	1.1	16.0	22.0
17	07:00	6.1	14.4	22.9	4.1	15.1	22.5
17	09:00	4.8	14.5	22.3	4.2	15.9	22.4
17	11:00	4.1	16.8	21.7	2.8	16.3	22.9
17	13:00	4.1	14.9	19.6	2.8	15.6	19.8
17	15:00	2.4	16.7	19.5	2.2	14.4	17.0
17	17:00	1.8	14.9	18.1	1.9	14.0	17.9
17	19:00	1.3	16.0	18.1	2.7	14.4	16.0
17	21:00	3.7	13.0	19.2	2.7	13.9	18.3
17	23:00	4.6	18.0	19.9	3.4	17.0	21.0
18	01:00	3.4	18.4	21.3	3.4	17.8	19.4
18	03:00	3.6	16.6	21.7	2.4	17.3	21.3
18	05:00	4.6	16.5	21.8	3.5	17.4	24.1
18	07:00	4.7	12.4	19.1	2.3	14.8	18.8
18	09:00	2.2	14.5	19.4	2.4	16.0	17.3
18	11:00	1.2	14.8	17.2	2.3	15.5	16.5
18	13:00	1.8	15.4	17.2	2.1	16.1	16.7
18	15:00	1.8	15.4	16.8	2.5	16.8	15.8
18	17:00	1.8	15.4	17.2	1.5	15.8	17.1
18	19:00	3.7	14.4	18.3	2.1	15.3	20.6
18	21:00	3.3	14.4	21.0	3.6	14.7	20.9
18	23:00	3.2	16.3	21.8	2.0	15.5	22.5
19	01:00	2.7	18.1	21.2	4.0	17.4	21.6
19	03:00	3.5	17.7	20.2	2.6	17.2	21.9
19	05:00	4.1	15.8	22.0	2.9	18.1	21.6
19	07:00	4.2	17.1	21.6	3.6	18.1	21.8
19	09:00	2.7	15.6	21.6	2.3	18.1	21.6
19	11:00	3.6	17.2	20.0	2.5	17.9	21.2
19	13:00	3.6	16.3	21.5	1.9	18.0	20.0

Oct-08		Peas			Duff		
Day	Time	H2O (%)	ASH (%)	VOLS (%)	H2O (%)	ASH (%)	VOLS (%)
19	15:00	3.7	15.8	21.1	2.5	18.0	20.8
19	17:00	2.5	17.4	21.5	3.3	17.8	19.9
19	19:00	2.9	17.4	21.5	3.3	17.8	19.9
19	21:00	2.6	11.4	14.0	3.1	14.2	13.7
19	23:00				3.4	12.7	11.8
20	01:00				3.5	12.5	12.5
20	03:00				2.2	12.4	13.2
20	05:00				3.2	12.6	11.1
20	07:00				3.4	12.4	11.8
20	09:00				3.9	12.5	13.1
20	11:00				2.5	15.1	13.3
20	13:00				4.5	13.8	13.2
20	15:00				2.7	14.5	13.2
20	17:00				2.5	16.1	13.5
20	19:00				3.0	16.3	13.9
20	21:00				2.6	15.4	
20	23:00				2.3	16.3	15.6
21	01:00				3.3	14.9	15.3
21	03:00				3.7	14.8	15.3
21	05:00				4.4	13.8	16.0
21	07:00				4.7	12.0	13.3
21	09:00						
21	11:00						
21	13:00						
21	15:00						
21	17:00						
21	19:00	3.1	12.4	15.9	2.5	12.3	15.5
21	21:00	2.3	12.2	12.7	2.4	14.9	12.5
21	23:00	1.9	14.0	12.6	2.4	16.1	12.6
22	01:00	2.8	13.4	1.3	3.9	15.2	11.8
22	03:00	1.4	15.8	13.4	2.7	15.1	13.3
22	05:00	3.2	17.5	12.0	3.2	15.3	13.7
22	07:00	3.4	15.0	13.3	3.6	14.1	13.2
22	09:00	1.8	20.6	11.6	2.2	13.9	12.1
22	11:00	1.6	20.5	13.0	3.6	13.2	14.1
22	13:00	1.1	13.6	16.2	1.9	14.6	13.0
22	15:00	1.9	13.4	17.4	1.1	15.6	19.3

Oct-08		Peas			Duff		
Day	Time	H2O (%)	ASH (%)	VOLS (%)	H2O (%)	ASH (%)	VOLS (%)
22	17:00	3.2	15.9	17.1	1.6	16.7	17.6
22	19:00	2.6	17.3	16.4	1.1	15.8	18.5
22	21:00	1.6	18.2	20.8	1.4	18.5	20.7
22	23:00	3.3	16.6	19.7	1.7	19.1	21.2
23	01:00	2.2	15.2	19.3	1.6	17.8	20.2
23	03:00	3.4	16.7	21.4	1.4	16.0	21.0
23	05:00	2.3	15.8	21.9	1.0	16.2	23.1
23	07:00	4.3	13.9	22.6	2.2	15.1	23.1
23	09:00	2.2	14.9	23.7	1.0	16.1	23.1
23	11:00	3.4	12.5	25.8	3.2	14.3	25.1
23	13:00	4.0	12.5	26.6	3.2	12.9	26.3
23	15:00	5.3	12.2	25.7	4.7	13.4	21.8
23	17:00	3.6	13.3	24.4	3.6	13.4	24.1
23	19:00	2.9	12.8	24.7	2.1	14.1	23.9
23	21:00	3.3	11.7	25.6	2.7	13.3	26.8
23	23:00	4.8	15.2	21.6	2.5	16.1	23.9
24	01:00	2.2	15.8	23.9	2.1	17.3	23.1
24	03:00	1.7	19.1	23.7	0.8	17.7	23.3
24	05:00	2.5	16.5	23.0	1.0	17.8	23.3
24	07:00	4.8	15.5	22.5	4.0	16.6	22.2
24	09:00	3.3	14.4	23.2	2.8	15.1	23.3
24	11:00	3.2	11.8	25.7	3.1	12.8	25.6
24	13:00	3.6	10.9	26.6	4.7	12.7	27.6
24	15:00	3.0	12.0	23.9	3.2	13.0	24.6
24	17:00	3.9	13.2	24.8	5.7	13.8	23.1
24	19:00	3.6	13.0	25.6	2.6	13.8	25.3
24	21:00	3.4	14.0	25.4	1.6	14.9	25.0
24	23:00	4.1	15.6	23.8	3.6	16.6	23.1
25	01:00	3.3	18.8		2.2	17.2	
25	03:00	5.4	14.9	21.7	3.9	16.9	22.0
25	05:00	3.1	15.5	22.1	2.4	17.0	22.0
25	07:00	4.5	16.4	21.2	2.9	16.3	21.5
25	09:00	4.0	14.4	23.3	3.3	15.6	21.5
25	11:00	3.7	14.9	21.7	3.9	15.4	21.4
25	13:00	3.9	13.9	24.4	4.0	13.6	24.7
25	15:00	3.7	12.1		2.7	14.0	
25	17:00	3.9	12.5	26.2	4.3	13.5	25.1

Oct-08		Peas			Duff		
Day	Time	H2O (%)	ASH (%)	VOLS (%)	H2O (%)	ASH (%)	VOLS (%)
25	19:00	4.6	10.7	27.7	3.3	14.1	27.1
25	21:00	3.5	11.2	20.2	2.5	15.9	17.0
25	23:00	4.6	16.1	12.1	2.6	14.5	15.7
26	01:00	4.6	12.9	11.5	4.5	14.3	13.0
26	03:00	2.6	15.8	12.5	2.5	15.6	14.0
26	05:00	2.8	16.9	11.6	2.5	14.0	15.2
26	07:00	2.8	13.9	12.4	3.1	15.6	13.2
26	09:00	3.1	16.2	14.3	2.7	14.9	15.7
26	11:00	2.7	14.7	13.0	3.6	14.2	14.1
26	13:00	2.1	13.5	13.6	3.8	14.1	13.1
26	15:00	2.7	16.8	13.5	2.2	14.7	14.5
26	17:00	3.1	15.3	14.1	3.5	16.3	16.2
26	19:00	2.8	12.3	15.7	4.9	13.6	15.1
26	21:00	4.0	12.0	25.9	3.4	14.8	25.2
26	23:00	5.5	11.6	25.1	1.9	14.2	26.3
27	01:00	4.3	13.1	25.6	4.0	12.6	25.9
27	03:00	5.9	12.5	25.0	3.7	14.2	25.3
27	05:00	6.3	12.1	24.5	4.7	13.8	24.4
27	07:00	4.6	16.3	24.2	3.4	17.8	24.2
27	09:00	4.2	16.7	23.3	3.3	18.0	23.4
27	11:00	4.8	13.4	24.3	5.6	15.3	22.8
27	13:00	3.5	14.0	25.1	3.1	15.5	25.0
27	15:00	5.7	14.4	23.0	3.3	15.1	23.7
27	17:00	3.5	12.5	23.7	3.5	13.0	20.0
27	19:00	3.4	17.8	23.6	2.0	17.1	23.7
27	21:00	4.3	16.2	23.7	4.9	16.8	21.4
27	23:00	5.3	15.9	23.3	3.0	16.0	22.9
28	01:00	3.4	17.6	22.5	2.3	16.6	21.5
28	03:00	4.4	16.1	22.3	2.5	15.4	21.2
28	05:00	4.0	15.4	21.6	3.0	15.8	21.5
28	07:00	4.0	15.4	21.6	3.0	15.8	21.5
28	09:00						
28	11:00						
28	13:00						
28	15:00						
28	17:00						
28	19:00	3.9	15.7	21.4	2.7	16.3	21.3

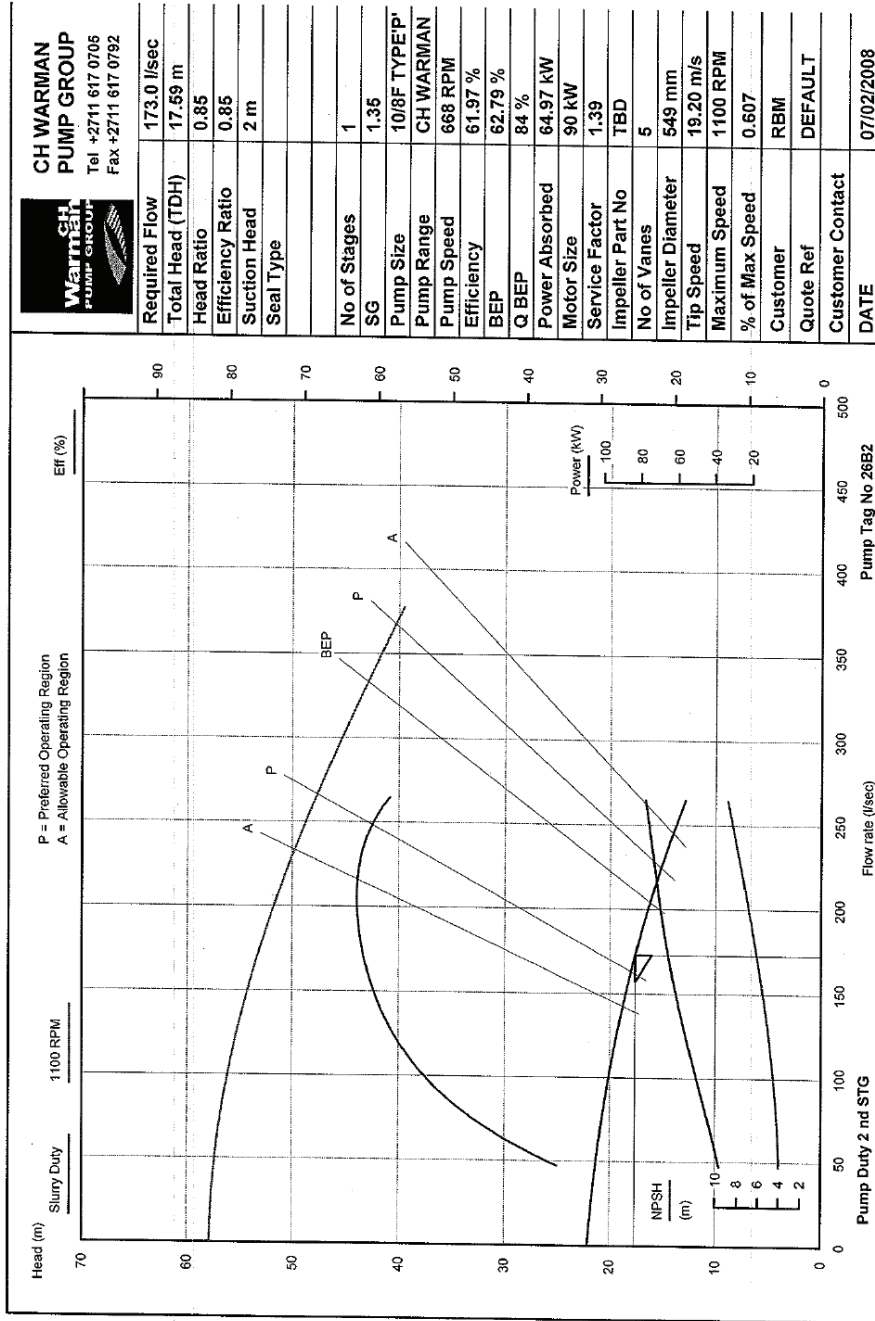
Oct-08		Peas			Duff		
Day	Time	H2O (%)	ASH (%)	VOLS (%)	H2O (%)	ASH (%)	VOLS (%)
28	21:00	3.9	17.1	20.4	4.1	16.5	19.2
28	23:00	4.4	17.2	19.6	3.3	15.8	20.0
29	01:00	4.5	15.4	21.5	4.2	15.7	20.5
29	03:00	3.9	17.1	20.7	3.7	15.3	21.0
29	05:00	2.8	14.6	22.0	2.6	14.5	20.8
29	07:00	3.1	15.4	21.2	3.1	15.2	20.3
29	09:00	2.7	16.1	22.8	3.2	17.6	22.4
29	11:00	2.3	15.2	20.5	2.6	14.0	14.8
29	13:00				2.4	14.2	15.9
29	15:00				2.6	12.9	12.4
29	17:00				3.3	13.1	13.1
29	19:00				3.4	14.1	12.4
29	21:00				3.2	14.9	12.1
29	23:00				5.0	14.3	14.1
30	01:00				5.8	14.8	14.4
30	03:00				4.5	17.9	13.4
30	05:00				4.2	14.7	14.2
30	07:00				2.5	15.3	16.6
30	09:00				1.3	14.3	16.7
30	11:00				3.4	14.4	14.6
30	13:00				3.2	13.2	16.2
30	15:00				3.4	13.4	16.7
30	17:00				3.9	12.9	15.9
30	19:00				4.2	14.2	14.8
30	21:00				4.6	14.1	13.7
30	23:00				5.1	17.1	5.4
31	01:00	9.0	21.4	5.2	8.1	20.0	4.8
31	03:00	8.1	19.4	5.6	6.8	18.7	6.4
31	05:00	4.8	15.9	7.2	6.8	17.7	5.3
31	07:00	6.1	15.7	3.4	9.6	17.8	4.0
31	09:00	6.1	15.6	7.5	6.7	17.5	6.9
31	11:00	4.8	15.2	10.0	8.1	15.0	6.5
31	13:00	4.9	12.2	26.7	1.8	15.7	26.7
31	15:00	5.9	10.8	26.1	3.3	13.9	25.6
31	17:00	4.6	11.4	28.8	5.5	16.7	25.8
31	19:00	4.3	11.7	28.6	3.1	15.6	28.1
31	21:00	4.7	14.3	24.1	3.1	18.9	22.4

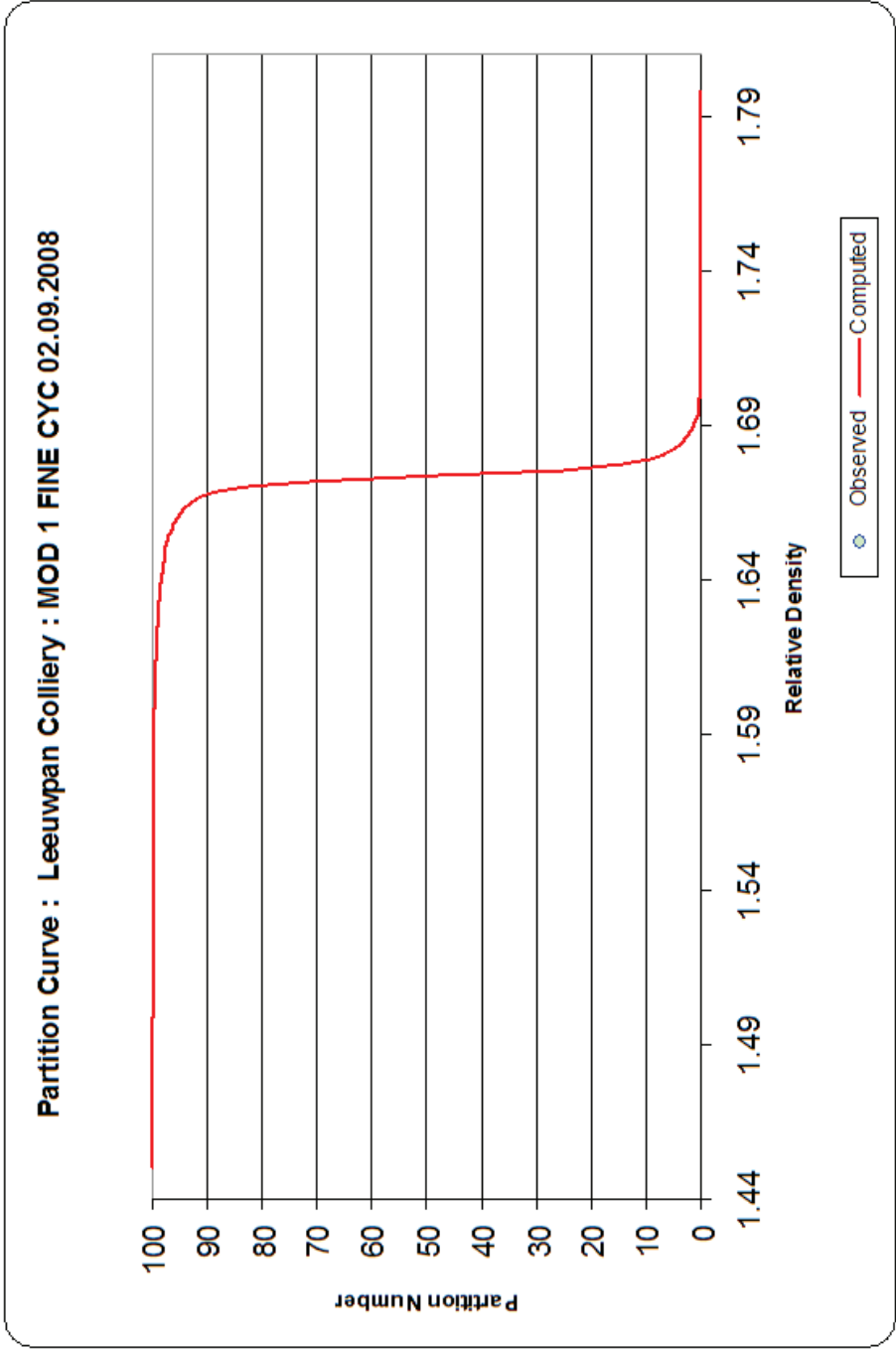


Oct-08		Peas			Duff		
Day	Time	H2O (%)	ASH (%)	VOLS (%)	H2O (%)	ASH (%)	VOLS (%)
31	23:00	4.2	18.0	20.0	2.8	16.2	19.6



## ADDENDUM D: LEEUWPAN PUMP AND FINE CYCLONE EQUIPMENT EFFICIENCIES





**ADDENDUM E: MATLAB SOURCE CODE FOR DMS PLANT  
SIMULATION**

```

1 clear;
2 %Load Data
3 tau = 10+32;
4 load WI1SCR;
5 W_i_1 = 1000.*WI1SCR(81-tau:208-tau)./3600;
6 load WI2SCR;
7 W_i_2 = 1000.*WI2SCR(81-tau:208-tau)./3600;
8 W_i = W_i_1;
9
10 load WOSCR;
11 W_o = 1000.*WOSCR(81-tau:208-tau)./3600./2;
12
13 load WDISSCR;
14 W_dis = 1000.*WDISSCR(81-tau:208-tau)./3600;
15
16 load WCSCR;
17 W_c = (1000.*WCSCR(81-tau:208-tau)./3600 + 0.33.*W_dis)./2;
18
19 load WFSCR;
20 W_f = (1000.*WFSCR(81-tau:208-tau)./3600 + 0.65.*0.33.*W_dis)./2;
21
22 %Set Variables and Constants for Double Deck Screen
23 t=0:14:127.*14;
24 ht=1;
25
26 tau_o = 0.7;
27 tau_c_o = 1.*tau_o;
28 tau_c = 0.7;
29 tau_f_c = 2.*tau_c;
30
31 alpha_o = (W_o./W_i).^(1./10);
32 alpha_c = (W_c./W_i).^(1./10);
33
34 M_o = zeros(1,10);
35 M_o_0 = ones(10,1).*21;
36 M_c = zeros(1,10);
37 M_c_0 = ones(10,1).*15;
38
39 W_o_sim = zeros(1,10);
40 W_c_sim = zeros(1,10);
41 W_ct_sim = zeros(1,10);
42 W_f_sim = zeros(1,10);
43
44 %Perform Simulation for Double Deck Screen
45
46 for I = 1:128,
47
48 for J = 1:10,
49
50     if W_o(I,1)./W_i(I,1) >= 1 && I > 1
51         alpha_o(I,1) = alpha_o(I-1,1);

```

```

52     end
53     if W_c(I,1)./W_i(I,1) >= 1 && I > 1
54         alpha_c(I,1) = alpha_c(I-1,1);
55     end
56
57     if I > 1
58         M_o_0(J,1) = M_o(I-1,J);
59         M_c_0(J,1) = M_c(I-1,J);
60     end
61
62     if J > 1
63         f1_M_o(J,1) = W_o_sim(I,J-1) - alpha_o(I,1).*M_o_0(J,1)./tau_o - (1 -
alpha_o(I,1)).*M_o_0(J,1)./tau_c_o;
64         f2_M_o(J,1) = W_o_sim(I,J-1) - alpha_o(I,1).*(M_o_0(J,1) + (ht./2).*f1_M_o
(J,1))./tau_o - (1 - alpha_o(I,1)).*(M_o_0(J,1) + (ht./2).*f1_M_o(J,1))./tau_c_o;
65         f3_M_o(J,1) = W_o_sim(I,J-1) - alpha_o(I,1).*(M_o_0(J,1) + (ht./2).*f2_M_o
(J,1))./tau_o - (1 - alpha_o(I,1)).*(M_o_0(J,1) + (ht./2).*f2_M_o(J,1))./tau_c_o;
66         f4_M_o(J,1) = W_o_sim(I,J-1) - alpha_o(I,1).*(M_o_0(J,1) + ht.*f3_M_o(J,1)).
/tau_o - (1 - alpha_o(I,1)).*(M_o_0(J,1) + ht.*f3_M_o(J,1))./tau_c_o;
67     else
68         f1_M_o(J,1) = W_i(I,1) - alpha_o(I,1).*M_o_0(J,1)./tau_o - (1 - alpha_o(I,
1)).*M_o_0(J,1)./tau_c_o;
69         f2_M_o(J,1) = W_i(I,1) - alpha_o(I,1).*(M_o_0(J,1) + (ht./2).*f1_M_o(J,1)).
/tau_o - (1 - alpha_o(I,1)).*(M_o_0(J,1) + (ht./2).*f1_M_o(J,1))./tau_c_o;
70         f3_M_o(J,1) = W_i(I,1) - alpha_o(I,1).*(M_o_0(J,1) + (ht./2).*f2_M_o(J,1)).
/tau_o - (1 - alpha_o(I,1)).*(M_o_0(J,1) + (ht./2).*f2_M_o(J,1))./tau_c_o;
71         f4_M_o(J,1) = W_i(I,1) - alpha_o(I,1).*(M_o_0(J,1) + ht.*f3_M_o(J,1))./tau_o
- (1 - alpha_o(I,1)).*(M_o_0(J,1) + ht.*f3_M_o(J,1))./tau_c_o;
72     end
73     M_o(I,J) = M_o_0(J,1) + ht.*(f1_M_o(J,1) + 2.*f2_M_o(J,1) + 2.*f3_M_o(J,1) +
f4_M_o(J,1))./6;
74
75     W_o_sim(I,J) = alpha_o(I,1).*M_o(I,J)./tau_o;
76     W_c_sim(I,J) = (1 - alpha_o(I,1)).*M_o(I,J)./tau_c_o;
77
78
79     if J > 1
80         f1_M_c(J,1) = W_ct_sim(I,J-1) + W_c_sim(I,J) - alpha_c(I,1).*M_c_0(J,1).
/tau_c - (1 - alpha_c(I,1)).*M_c_0(J,1)./tau_f_c;
81         f2_M_c(J,1) = W_ct_sim(I,J-1) + W_c_sim(I,J) - alpha_c(I,1).*(M_c_0(J,1) +
(ht./2).*f1_M_c(J,1))./tau_c - (1 - alpha_c(I,1)).*(M_c_0(J,1) + (ht./2).*f1_M_c(J,1)).
/tau_f_c;
82         f3_M_c(J,1) = W_ct_sim(I,J-1) + W_c_sim(I,J) - alpha_c(I,1).*(M_c_0(J,1) +
(ht./2).*f2_M_c(J,1))./tau_c - (1 - alpha_c(I,1)).*(M_c_0(J,1) + (ht./2).*f2_M_c(J,1)).
/tau_f_c;
83         f4_M_c(J,1) = W_ct_sim(I,J-1) + W_c_sim(I,J) - alpha_c(I,1).*(M_c_0(J,1) +
ht.*f3_M_c(J,1))./tau_c - (1 - alpha_c(I,1)).*(M_c_0(J,1) + ht.*f3_M_c(J,1))./tau_f_c;
84     else
85         f1_M_c(J,1) = W_c_sim(I,J) - alpha_c(I,1).*M_c_0(J,1)./tau_c - (1 - alpha_c
(I,1)).*M_c_0(J,1)./tau_f_c;
86         f2_M_c(J,1) = W_c_sim(I,J) - alpha_c(I,1).*(M_c_0(J,1) + (ht./2).*f1_M_c(J,

```



```
1)) ./tau_c - (1 - alpha_c(I,1)).*(M_c_0(J,1) + (ht./2).*f1_M_c(J,1))./tau_f_c;
87     f3_M_c(J,1) = W_c_sim(I,J) - alpha_c(I,1).*(M_c_0(J,1) + (ht./2).*f2_M_c(J,
1)) ./tau_c - (1 - alpha_c(I,1)).*(M_c_0(J,1) + (ht./2).*f2_M_c(J,1))./tau_f_c;
88     f4_M_c(J,1) = W_c_sim(I,J) - alpha_c(I,1).*(M_c_0(J,1) + ht.*f3_M_c(J,1)).
/tau_c - (1 - alpha_c(I,1)).*(M_c_0(J,1) + ht.*f3_M_c(J,1))./tau_f_c;
89     end
90     M_c(I,J) = M_c_0(J,1) + ht.*(f1_M_c(J,1) + 2.*f2_M_c(J,1) + 2.*f3_M_c(J,1) +
f4_M_c(J,1))./6;
91
92     W_ct_sim(I,J) = alpha_c(I,1).*M_c(I,J)./tau_c;
93     W_f_sim(I,J) = (1 - alpha_c(I,1)).*M_c(I,J)./tau_f_c;
94
95 end
96
97 end
98
99 W_c_sum = zeros(128,1);
100 W_f_sum = zeros(128,1);
101 for I=1:10,
102     W_c_sum = W_c_sum + W_c_sim(:,I);
103     W_f_sum = W_f_sum + W_f_sim(:,I);
104 end
105
106 %Set Variables and Constants for Single Deck Screen
107
108 tau_fo = 0.7;
109 tau_uf_o = 9.*tau_o;
110
111 alpha_f = (W_f./W_i).^(1./10);
112
113 M_fo = zeros(127,10);
114 M_fo_0 = ones(10,1).*10;
115
116 W_fo_sim = zeros(127,10);
117 W_uf_sim = zeros(127,10);
118
119 %Perform Simulation for Double Deck Screen
120
121 for I = 1:128,
122
123     for J = 1:10,
124
125         if W_f(I,1)./W_i(I,1) >= 1 && I > 1
126             alpha_f(I,1) = alpha_f(I-1,1);
127         end
128
129         if I > 1
130             M_fo_0(J,1) = M_fo(I-1,J);
131         end
132
133         if J > 1
```

```

134     f1_M_fo(J,1) = W_fo_sim(I,J-1) - alpha_f(I,1).*M_fo_0(J,1)./tau_fo - (1 -
alpha_f(I,1)).*M_fo_0(J,1)./tau_uf_o;
135     f2_M_fo(J,1) = W_fo_sim(I,J-1) - alpha_f(I,1).*(M_fo_0(J,1) + (ht./2)).
*f1_M_fo(J,1))./tau_fo - (1 - alpha_f(I,1)).*(M_fo_0(J,1) + (ht./2)).*f1_M_fo(J,1)).
/tau_uf_o;
136     f3_M_fo(J,1) = W_fo_sim(I,J-1) - alpha_f(I,1).*(M_fo_0(J,1) + (ht./2)).
*f2_M_fo(J,1))./tau_fo - (1 - alpha_f(I,1)).*(M_fo_0(J,1) + (ht./2)).*f2_M_fo(J,1)).
/tau_uf_o;
137     f4_M_fo(J,1) = W_fo_sim(I,J-1) - alpha_f(I,1).*(M_fo_0(J,1) + ht.*f3_M_fo(J,
1))./tau_fo - (1 - alpha_f(I,1)).*(M_fo_0(J,1) + ht.*f3_M_fo(J,1))./tau_uf_o;
138     else
139     f1_M_fo(J,1) = W_f_sum(I,1) - alpha_f(I,1).*M_fo_0(J,1)./tau_fo - (1 -
alpha_f(I,1)).*M_fo_0(J,1)./tau_uf_o;
140     f2_M_fo(J,1) = W_f_sum(I,1) - alpha_f(I,1).*(M_fo_0(J,1) + (ht./2)).*f1_M_fo
(J,1))./tau_fo - (1 - alpha_f(I,1)).*(M_fo_0(J,1) + (ht./2)).*f1_M_fo(J,1))./tau_uf_o;
141     f3_M_fo(J,1) = W_f_sum(I,1) - alpha_f(I,1).*(M_fo_0(J,1) + (ht./2)).*f2_M_fo
(J,1))./tau_fo - (1 - alpha_f(I,1)).*(M_fo_0(J,1) + (ht./2)).*f2_M_fo(J,1))./tau_uf_o;
142     f4_M_fo(J,1) = W_f_sum(I,1) - alpha_f(I,1).*(M_fo_0(J,1) + ht.*f3_M_fo(J,
1))./tau_fo - (1 - alpha_f(I,1)).*(M_fo_0(J,1) + ht.*f3_M_fo(J,1))./tau_uf_o;
143     end
144     M_fo(I,J) = M_fo_0(J,1) + ht.*(f1_M_fo(J,1) + 2.*f2_M_fo(J,1) + 2.*f3_M_fo(J,1)
+ f4_M_fo(J,1))./6;
145
146     W_fo_sim(I,J) = alpha_f(I,1).*M_fo(I,J)./tau_fo;
147     W_uf_sim(I,J) = (1 - alpha_f(I,1)).*M_fo(I,J)./tau_uf_o;
148
149 end
150
151 end
152
153 W_uf_sum = zeros(128,1);
154 for I=1:10,
155     W_uf_sum = W_uf_sum + W_uf_sim(:,I);
156 end
157
158 %Output Results
159
160 corr(W_o_sim(:,10),W_o)
161 sizeW_o=size(W_o);
162 VN=(1./sizeW_o(1,1)).*sum(0.5.*(W_o_sim(:,10)-W_o).^2)
163
164 figure
165 plot(t,W_o_sim(:,10),'.');
166 hold on;
167 plot(t,W_o,'-red');
168 xlabel('Time (s)');
169 ylabel('Throughput (kg/s)');
170 legend('Simulation output','Actual output');
171 title('Comparison of actual and simulated oversized material throughput');
172 grid on;
173

```

```
174 figure
175 plot(W_o_sim(:,10) + W_ct_sim(:,10) + W_f_sum, '.');
176 hold on;
177 plot(W_i, '-red');
178 xlabel('Time (s)');
179 ylabel('Feed (kg/s)');
180 legend('Sum of throughputs', 'Feed');
181 title('Comparison of all simulated throughputs and feed');
182 grid on;
183
184 figure
185 scatter(W_o_sim(:,10), W_o);
186 xlabel('Simulation output (kg/s)');
187 ylabel('Actual output (kg/s)');
188 title('Scatterplot of actual and simulated oversized material throughput');
189 grid on;
190
191 figure
192 surf(M_o);
193 ylabel('Time (s)');
194 xlabel('Screen component');
195 zlabel('Mass state (kg)');
196 title('Mass state distribution on top deck over time');
197 colorbar;
198
199 figure
200 surf(M_c);
201 ylabel('Time (s)');
202 xlabel('Screen component');
203 zlabel('Mass state (kg)');
204 title('Mass state distribution on bottom deck over time');
205 colorbar;
206
207 figure
208 plot(t, W_o_sim(:,10));
209 hold on;
210 plot(t, W_ct_sim(:,10), '+red');
211 hold on;
212 plot(t, W_fo_sim(:,10), 'ogreen');
213 xlabel('Time (s)');
214 ylabel('Throughput (kg/s)');
215 legend('Oversize material', 'Coarse material', 'Fine material');
216 title('Simulated throughput of the single- and double-deck screens');
217 grid on;
218
219 figure
220 surf(M_fo);
221 ylabel('Time (s)');
222 xlabel('Screen component');
223 zlabel('Mass state (kg)');
224 title('Mass state distribution on top deck over time');
```



```
225 colorbar;
226
227 mean(W_o_sim(:,10)./W_i)
228 mean(W_ct_sim(:,10)./W_i)
229 mean(W_f_sum./W_i)
230
231 mean(W_fo_sim(:,10)./W_f_sum)
232
233 fit = 100.*(1-norm(abs(W_o-W_o_sim(:,10)))/norm(abs(W_o-mean(W_o))))
234
235 %Save Fines Output for Mixing Box Simulation
236
237 WORE = W_fo_sim(:,10);
238 save WORE WORE
```



```
1 clear;
2 %Load Data
3 load WORE;
4 tau_W = 0;
5 W_ore = WORE(1-tau_W:125-tau_W);
6 load RHOMAGMIX;
7 tau_mag = 2+32;
8 rho_mag = RHOMAGMIX(81-tau_mag:205-tau_mag).*1000;
9 load PRESMIX;
10 tau_p = -1+32;
11 p = PRESMIX(81-tau_p:205-tau_p).*1000;
12
13 %Assign Variables and Constants
14 t = 0:14:124.*14;
15
16 Factor = 2./3.6;
17 Q = 0.278./Factor
18 Q_mag = 0.99.*Q
19 V = 0.3.*0.45.*0.65./Factor
20
21 rhomag_0 = 1523;
22 rhoWore_0 = 18;
23
24 A = -1.*Q./V;
25 Bmag = 1.*Q_mag./V;
26 BWore = 1./V;
27 C = 1;
28 D = 0;
29
30 %Perform Simulation
31 Gmag = ss(A,Bmag,C,D);
32 rhomag = lsim(Gmag,rho_mag,t,rhomag_0);
33 GWore = ss(A,BWore,C,D);
34 rhoWore = lsim(GWore,W_ore,t,rhoWore_0);
35
36 rho = rhomag+rhoWore;
37
38 %Output Results
39 figure;
40 plot(t,rho,'-.+r')
41 hold on
42 [AX, H1, H2] = plotyy(t,rho_mag,t,p);
43 xlabel('Time (s)');
44 set(get(AX(1),'Ylabel'),'String','Density (kg/m^3)');
45 set(get(AX(2),'Ylabel'),'String','Cyclone pressure (Pa)');
46 %legend('Simulated mix','Feed medium');
47 legend(H2,'Cyclone feed pressure');
48 title('Simulated density response of the medium and ore mix');
49 grid on;
50
51 figure;
```



```
52 [AX, H1, H2] = plotyy(t,rho_mag,t,W_ore)
53 xlabel('Time (s)');
54 set(get(AX(1),'Ylabel'),'String','Density (kg/m^3)');
55 set(get(AX(2),'Ylabel'),'String','Feedrate (kg/s)');
56 ylabel('Density (kg/m^3)');
57 legend('Feed Medium');
58 legend(H2,'Simulated fine ore feedrate');
59 title('Feed components for mixing box simulation');
60 grid on;
61
62 %Save Output for DMC Simulation
63 RHOSIM = rho;
64 save RHOSIM RHOSIM
```

```

1 %Module 1 Fine Cyclone
2 clear;
3 %Load Data
4 load RHOMAGMIX;
5 rho_mag = RHOMAGMIX(81-32:205-32).*1000;
6 load PRE;
7 p = PRE.*1000;
8 load ASH;
9 x_o_ash_meas = ASH./100;
10 load MOI;
11 x_o_H2O_meas = MOI./100;
12 load VOL;
13 x_o_vol_meas = VOL./100;
14 load FEED;
15 W_meas = FEED.*1000./3600;
16 load RHOSIM;
17 rho_sim = RHOSIM;
18
19 %Assign Variables and Constants
20 t=0:14:124.*14;
21 ht=1;
22
23 M1_FC_D = 0.71;
24 M1_FC_A_o = pi.*(0.43.*M1_FC_D).^2;
25 M1_FC_tau_o = 0.75;
26 M1_FC_A_u = pi.*(0.43.*M1_FC_D).^2;
27 M1_FC_tau_u = 1.*M1_FC_tau_o;
28
29 Q = 1.6069.*173./1000./2.*3.6;
30 V = Q.*(M1_FC_tau_o+M1_FC_tau_u)./2
31 alpha = 2;
32 rho_ash = 2000;
33 rho_S = 1920;
34 rho_vol = 1100;
35 rho_H2O = 1000;
36 delta_mag = 100;
37 Q_mag_ratio = 0.99;
38 Q_mag = Q_mag_ratio.*Q
39
40 K_o = M1_FC_A_o.*M1_FC_tau_o; %Module 1 fine cyclone↙
overflow proportional constant | A_o_eff.*tau_o
41 K_u = M1_FC_A_u.*M1_FC_tau_u; %Module 1 fine cyclone↙
undeflow proportional constant | A_u_eff.*tau_u
42
43 M1_FC_tau_o_mag = 0.75;
44 M1_FC_tau_u_mag = 0.8.*M1_FC_tau_o_mag;
45
46 M1_FC_tau_o_ash = 0.4;
47 M1_FC_tau_u_ash = 0.385.*M1_FC_tau_o_ash;
48
49 M1_FC_tau_o_H2O = 0.15;

```



```
50 M1_FC_tau_u_H2O = 0.2.*M1_FC_tau_o_H2O;
51
52 M1_FC_tau_o_vol = 0.98;
53 M1_FC_tau_u_vol = 0.01.*M1_FC_tau_o_vol;
54
55 K_o_mag = M1_FC_tau_o_mag./1550; %Module 1 fine cyclone✓
magnetite overflow proportional constant
56 K_u_mag = M1_FC_tau_u_mag./1550; %Module 1 fine cyclone✓
magnetite undeflow proportional constant
57 K_o_ash = M1_FC_tau_o_ash./rho_ash %Module 1 fine cyclone✓
ash overflow proportional constant
58 K_u_ash = M1_FC_tau_u_ash./rho_ash %Module 1 fine cyclone✓
ash undeflow proportional constant
59 K_o_S = M1_FC_tau_o./rho_S; %Module 1 fine cyclone✓
sulphur overflow proportional constant
60 K_u_S = M1_FC_tau_u./rho_S; %Module 1 fine cyclone✓
sulphur undeflow proportional constant
61 K_o_H2O = M1_FC_tau_o_H2O./rho_H2O; %Module 1 fine cyclone✓
water overflow proportional constant
62 K_u_H2O = M1_FC_tau_u_H2O./rho_H2O; %Module 1 fine cyclone✓
water undeflow proportional constant
63 K_o_vol = M1_FC_tau_o_vol./rho_vol; %Module 1 fine cyclone✓
volatiles overflow proportional constant
64 K_u_vol = M1_FC_tau_u_vol./rho_vol; %Module 1 fine cyclone✓
volatiles undeflow proportional constant
65
66
67 rho = rho_sim;
68 W = Q.*rho;
69 x_mag = rho_mag.*Q_mag./W;
70 x_ash = 17.6./100.*(1-x_mag);
71 x_S = 2.5./100.*(1-x_mag);
72 x_H2O = 1.59./100.*(1-x_mag);
73 x_vol = 12.6./100.*(1-x_mag);
74 x_C = 1 - x_ash - x_S - x_H2O - x_vol - x_mag;
75
76 Q_o = alpha.*Q./(1+alpha);
77 Q_u = Q./(1+alpha);
78 V_o = alpha.*V./(1+alpha);
79 V_u = V./(1+alpha);
80 W_mag = W.*x_mag;
81 Q_o_mag = alpha.*Q_mag./(1+alpha);
82 Q_u_mag = Q_mag./(1+alpha);
83
84 rho_o = zeros(125,1);
85 rho_o_0 = 1500;
86 rho_u = zeros(125,1);
87 rho_u_0 = (W(1,1)-rho_o_0.*Q_o)./Q_u;
88 x_o_mag = zeros(125,1);
89 x_o_mag_0 = Q_mag_ratio - 0.002;
90 x_u_mag = zeros(125,1);
```

```

91 x_u_mag_0 = (x_mag(1,1).*Q.*rho(1,1)-x_o_mag_0.*Q_o.*rho_o_0)./(Q_u.*rho_u_0);
92 x_o_ash = zeros(125,1);
93 x_o_ash_0 = 0.145.*(1-x_o_mag_0);
94 x_u_ash = zeros(125,1);
95 x_u_ash_0 = (x_ash(1,1).*Q.*rho(1,1)-x_o_ash_0.*Q_o.*rho_o_0)./(Q_u.*rho_u_0);
96 x_o_S = zeros(125,1);
97 x_o_S_0 = 0.006.*(1-x_o_mag_0);
98 x_u_S = zeros(125,1);
99 x_u_S_0 = (x_S(1,1).*Q.*rho(1,1)-x_o_S_0.*Q_o.*rho_o_0)./(Q_u.*rho_u_0);
100 x_o_H2O = zeros(125,1);
101 x_o_H2O_0 = 0.009.*(1-x_o_mag_0);
102 x_u_H2O = zeros(125,1);
103 x_u_H2O_0 = (x_H2O(1,1).*Q.*rho(1,1)-x_o_H2O_0.*Q_o.*rho_o_0)./(Q_u.*rho_u_0);
104 x_o_vol = zeros(125,1);
105 x_o_vol_0 = 0.118.*(1-x_o_mag_0);
106 x_u_vol = zeros(125,1);
107 x_u_vol_0 = (x_vol(1,1).*Q.*rho(1,1)-x_o_vol_0.*Q_o.*rho_o_0)./(Q_u.*rho_u_0);
108
109 %Perform Simulation
110 for I = 1:125,
111
112     if I > 1
113         rho_o_0 = rho_o(I-1,1);
114         rho_u_0 = rho_u(I-1,1);
115         x_o_ash_0 = x_o_ash(I-1,1);
116         x_u_ash_0 = x_u_ash(I-1,1);
117         x_o_S_0 = x_o_S(I-1,1);
118         x_u_S_0 = x_u_S(I-1,1);
119         x_o_H2O_0 = x_o_H2O(I-1,1);
120         x_u_H2O_0 = x_u_H2O(I-1,1);
121         x_o_vol_0 = x_o_vol(I-1,1);
122         x_u_vol_0 = x_u_vol(I-1,1);
123         x_o_mag_0 = x_o_mag(I-1,1);
124         x_u_mag_0 = x_u_mag(I-1,1);
125     end
126
127     f1_rho_o = (1./V_o).*((1 + K_u.*V_u.*x_mag(I,1).*x_ash(I,1)./Q_mag).*W(I,1) -
Q_o.*(rho_o_0) - (Q_u + K_u.*V_u.*x_ash(I,1)).*rho_u_0);
128     f1_rho_u = (1./V_u).*((1 - K_o.*V_o.*x_mag(I,1).*x_C(I,1)./Q_mag).*W(I,1) - (Q_o
- K_o.*V_o.*x_C(I,1)).*rho_o_0 - Q_u.*(rho_u_0));
129     f2_rho_o = (1./V_o).*((1 + K_u.*V_u.*x_mag(I,1).*x_ash(I,1)./Q_mag).*W(I,1) -
Q_o.*(rho_o_0 + (ht./2).*f1_rho_o) - (Q_u + K_u.*V_u.*x_ash(I,1)).*rho_u_0);
130     f2_rho_u = (1./V_u).*((1 - K_o.*V_o.*x_mag(I,1).*x_C(I,1)./Q_mag).*W(I,1) - (Q_o
- K_o.*V_o.*x_C(I,1)).*rho_o_0 - Q_u.*(rho_u_0 + (ht./2).*f1_rho_u));
131     f3_rho_o = (1./V_o).*((1 + K_u.*V_u.*x_mag(I,1).*x_ash(I,1)./Q_mag).*W(I,1) -
Q_o.*(rho_o_0 + (ht./2).*f2_rho_o) - (Q_u + K_u.*V_u.*x_ash(I,1)).*rho_u_0);
132     f3_rho_u = (1./V_u).*((1 - K_o.*V_o.*x_mag(I,1).*x_C(I,1)./Q_mag).*W(I,1) - (Q_o
- K_o.*V_o.*x_C(I,1)).*rho_o_0 - Q_u.*(rho_u_0 + (ht./2).*f2_rho_u));
133     f4_rho_o = (1./V_o).*((1 + K_u.*V_u.*x_mag(I,1).*x_ash(I,1)./Q_mag).*W(I,1) -
Q_o.*(rho_o_0 + ht.*f3_rho_o) - (Q_u + K_u.*V_u.*x_ash(I,1)).*rho_u_0);
134     f4_rho_u = (1./V_u).*((1 - K_o.*V_o.*x_mag(I,1).*x_C(I,1)./Q_mag).*W(I,1) - (Q_o

```

```

- K_o.*V_o.*x_C(I,1)).*rho_o_0 - Q_u.*(rho_u_0 + ht.*f3_rho_u));
135     rho_o(I,1) = rho_o_0 + ht.*(f1_rho_o + 2.*f2_rho_o + 2.*f3_rho_o + f4_rho_o)./6;
136     rho_u(I,1) = rho_u_0 + ht.*(f1_rho_u + 2.*f2_rho_u + 2.*f3_rho_u + f4_rho_u)./6;
137
138     if I > 1
139         d_rho_o = rho_o(I,1) - rho_o(I-1,1);
140         d_rho_u = rho_u(I,1) - rho_u(I-1,1);
141         f1_rho_o = d_rho_o;
142         f1_rho_u = d_rho_u;
143     else
144         f1_rho_o = 0;
145         f1_rho_u = 0;
146     end
147
148     f1_o_ash = (1./(V_o.*rho_o_0)).*(W(I,1).*x_ash(I,1) - Q_o.*rho_o_0.*x_o_ash_0 -
Q_u.*rho_u_0.*x_u_ash_0 - V_o.*x_o_ash_0.*f1_rho_o - V_u.*x_u_ash_0.*f1_rho_u - V_u.
.*rho_u_0.*(K_u_ash.*(rho_ash - rho_mag(I,1)).*(x_ash(I,1) - x_u_ash_0)));
149     f1_u_ash = (1./(V_u.*rho_u_0)).*(W(I,1).*x_ash(I,1) - Q_o.*rho_o_0.*x_o_ash_0 -
Q_u.*rho_u_0.*x_u_ash_0 - V_o.*x_o_ash_0.*f1_rho_o - V_o.*rho_o_0.*(K_o_ash.*(rho_mag(I,
1) - rho_ash).*(x_ash(I,1) - x_o_ash_0)) - V_u.*x_u_ash_0.*f1_rho_u);
150     f2_o_ash = (1./(V_o.*rho_o_0)).*(W(I,1).*x_ash(I,1) - Q_o.*rho_o_0.*(x_o_ash_0 +
(ht./2).*f1_o_ash) - Q_u.*rho_u_0.*x_u_ash_0 - V_o.*(x_o_ash_0 + (ht./2).*f1_o_ash).
.*f1_rho_o - V_u.*x_u_ash_0.*f1_rho_u - V_u.*rho_u_0.*(K_u_ash.*(rho_ash - rho_mag(I,1)).
*(x_ash(I,1) - x_u_ash_0)));
151     f2_u_ash = (1./(V_u.*rho_u_0)).*(W(I,1).*x_ash(I,1) - Q_o.*rho_o_0.*x_o_ash_0 -
Q_u.*rho_u_0.*(x_u_ash_0 + (ht./2).*f1_u_ash) - V_o.*x_o_ash_0.*f1_rho_o - V_o.*rho_o_0.
*(K_o_ash.*(rho_mag(I,1) - rho_ash).*(x_ash(I,1) - x_o_ash_0)) - V_u.*(x_u_ash_0 + (ht.
/2).*f1_u_ash).*f1_rho_u);
152     f3_o_ash = (1./(V_o.*rho_o_0)).*(W(I,1).*x_ash(I,1) - Q_o.*rho_o_0.*(x_o_ash_0 +
(ht./2).*f2_o_ash) - Q_u.*rho_u_0.*x_u_ash_0 - V_o.*(x_o_ash_0 + (ht./2).*f2_o_ash).
.*f1_rho_o - V_u.*x_u_ash_0.*f1_rho_u - V_u.*rho_u_0.*(K_u_ash.*(rho_ash - rho_mag(I,1)).
*(x_ash(I,1) - x_u_ash_0)));
153     f3_u_ash = (1./(V_u.*rho_u_0)).*(W(I,1).*x_ash(I,1) - Q_o.*rho_o_0.*x_o_ash_0 -
Q_u.*rho_u_0.*(x_u_ash_0 + (ht./2).*f2_u_ash) - V_o.*x_o_ash_0.*f1_rho_o - V_o.*rho_o_0.
*(K_o_ash.*(rho_mag(I,1) - rho_ash).*(x_ash(I,1) - x_o_ash_0)) - V_u.*(x_u_ash_0 + (ht.
/2).*f2_u_ash).*f1_rho_u);
154     f4_o_ash = (1./(V_o.*rho_o_0)).*(W(I,1).*x_ash(I,1) - Q_o.*rho_o_0.*(x_o_ash_0 +
ht.*f3_o_ash) - Q_u.*rho_u_0.*x_u_ash_0 - V_o.*(x_o_ash_0 + ht.*f3_o_ash).*f1_rho_o -
V_u.*x_u_ash_0.*f1_rho_u - V_u.*rho_u_0.*(K_u_ash.*(rho_ash - rho_mag(I,1)).*(x_ash(I,1)
- x_u_ash_0)));
155     f4_u_ash = (1./(V_u.*rho_u_0)).*(W(I,1).*x_ash(I,1) - Q_o.*rho_o_0.*x_o_ash_0 -
Q_u.*rho_u_0.*(x_u_ash_0 + ht.*f3_u_ash) - V_o.*x_o_ash_0.*f1_rho_o - V_o.*rho_o_0.*
(K_o_ash.*(rho_mag(I,1) - rho_ash).*(x_ash(I,1) - x_o_ash_0)) - V_u.*(x_u_ash_0 + ht.
*f3_u_ash).*f1_rho_u);
156     x_o_ash(I,1) = x_o_ash_0 + (ht.*(f1_o_ash + 2*f2_o_ash + 2*f3_o_ash + f4_o_ash))
/6;
157     x_u_ash(I,1) = x_u_ash_0 + (ht.*(f1_u_ash + 2*f2_u_ash + 2*f3_u_ash + f4_u_ash))
/6;
158
159     f1_o_S = (1./(V_o.*rho_o_0)).*(W(I,1).*x_S(I,1) - Q_o.*rho_o_0.*x_o_S_0 - Q_u.
.*rho_u_0.*x_u_S_0 - V_o.*x_o_S_0.*f1_rho_o - V_u.*x_u_S_0.*f1_rho_u - V_u.*rho_u_0.*

```

```

(K_u_S.*(rho_S - rho_mag(I,1)).*(x_S(I,1) - x_u_S_0)));
160    f1_u_S = (1./(V_u.*rho_u_0)).*(W(I,1).*x_S(I,1) - Q_o.*rho_o_0.*x_o_S_0 - Q_u.
*rho_u_0.*x_u_S_0 - V_o.*x_o_S_0.*f1_rho_o - V_o.*rho_o_0.*(K_o_S.*(rho_mag(I,1) -
rho_S)).*(x_S(I,1) - x_o_S_0)) - V_u.*x_u_S_0.*f1_rho_u);
161    f2_o_S = (1./(V_o.*rho_o_0)).*(W(I,1).*x_S(I,1) - Q_o.*rho_o_0.*(x_o_S_0 + (ht./
/2).*f1_o_S) - Q_u.*rho_u_0.*x_u_S_0 - V_o.*(x_o_S_0 + (ht./2).*f1_o_S).*f1_rho_o - V_u.
*x_u_S_0.*f1_rho_u - V_u.*rho_u_0.*(K_u_S.*(rho_S - rho_mag(I,1)).*(x_S(I,1) -
x_u_S_0)));
162    f2_u_S = (1./(V_u.*rho_u_0)).*(W(I,1).*x_S(I,1) - Q_o.*rho_o_0.*x_o_S_0 - Q_u.
*rho_u_0.*(x_u_S_0 + (ht./2).*f1_u_S) - V_o.*x_o_S_0.*f1_rho_o - V_o.*rho_o_0.*(K_o_S.
*(rho_mag(I,1) - rho_S)).*(x_S(I,1) - x_o_S_0)) - V_u.*(x_u_S_0 + (ht./2).*f1_u_S).
*f1_rho_u);
163    f3_o_S = (1./(V_o.*rho_o_0)).*(W(I,1).*x_S(I,1) - Q_o.*rho_o_0.*(x_o_S_0 + (ht./
/2).*f2_o_S) - Q_u.*rho_u_0.*x_u_S_0 - V_o.*(x_o_S_0 + (ht./2).*f2_o_S).*f1_rho_o - V_u.
*x_u_S_0.*f1_rho_u - V_u.*rho_u_0.*(K_u_S.*(rho_S - rho_mag(I,1)).*(x_S(I,1) -
x_u_S_0)));
164    f3_u_S = (1./(V_u.*rho_u_0)).*(W(I,1).*x_S(I,1) - Q_o.*rho_o_0.*x_o_S_0 - Q_u.
*rho_u_0.*(x_u_S_0 + (ht./2).*f2_u_S) - V_o.*x_o_S_0.*f1_rho_o - V_o.*rho_o_0.*(K_o_S.
*(rho_mag(I,1) - rho_S)).*(x_S(I,1) - x_o_S_0)) - V_u.*(x_u_S_0 + (ht./2).*f2_u_S).
*f1_rho_u);
165    f4_o_S = (1./(V_o.*rho_o_0)).*(W(I,1).*x_S(I,1) - Q_o.*rho_o_0.*(x_o_S_0 + ht.
*f3_o_S) - Q_u.*rho_u_0.*x_u_S_0 - V_o.*(x_o_S_0 + ht.*f3_o_S).*f1_rho_o - V_u.*x_u_S_0.
*f1_rho_u - V_u.*rho_u_0.*(K_u_S.*(rho_S - rho_mag(I,1)).*(x_S(I,1) - x_u_S_0)));
166    f4_u_S = (1./(V_u.*rho_u_0)).*(W(I,1).*x_S(I,1) - Q_o.*rho_o_0.*x_o_S_0 - Q_u.
*rho_u_0.*(x_u_S_0 + ht.*f3_u_S) - V_o.*x_o_S_0.*f1_rho_o - V_o.*rho_o_0.*(K_o_S.
*(rho_mag(I,1) - rho_S)).*(x_S(I,1) - x_o_S_0)) - V_u.*(x_u_S_0 + ht.*f3_u_S).*f1_rho_u);
167    x_o_S(I,1) = x_o_S_0 + (ht*(f1_o_S + 2*f2_o_S + 2*f3_o_S + f4_o_S))/6;
168    x_u_S(I,1) = x_u_S_0 + (ht*(f1_u_S + 2*f2_u_S + 2*f3_u_S + f4_u_S))/6;
169
170    f1_o_H2O = (1./(V_o.*rho_o_0)).*(W(I,1).*x_H2O(I,1) - Q_o.*rho_o_0.*x_o_H2O_0 -
Q_u.*rho_u_0.*x_u_H2O_0 - V_o.*x_o_H2O_0.*f1_rho_o - V_u.*x_u_H2O_0.*f1_rho_u - V_u.
*rho_u_0.*(K_u_H2O.*(rho_H2O - rho_mag(I,1)).*(x_H2O(I,1) - x_u_H2O_0)));
171    f1_u_H2O = (1./(V_u.*rho_u_0)).*(W(I,1).*x_H2O(I,1) - Q_o.*rho_o_0.*x_o_H2O_0 -
Q_u.*rho_u_0.*x_u_H2O_0 - V_o.*x_o_H2O_0.*f1_rho_o - V_o.*rho_o_0.*(K_o_H2O.*(rho_mag(I,
1) - rho_H2O)).*(x_H2O(I,1) - x_o_H2O_0)) - V_u.*x_u_H2O_0.*f1_rho_u);
172    f2_o_H2O = (1./(V_o.*rho_o_0)).*(W(I,1).*x_H2O(I,1) - Q_o.*rho_o_0.*(x_o_H2O_0 +
(ht./2).*f1_o_H2O) - Q_u.*rho_u_0.*x_u_H2O_0 - V_o.*(x_o_H2O_0 + (ht./2).*f1_o_H2O).
*f1_rho_o - V_u.*x_u_H2O_0.*f1_rho_u - V_u.*rho_u_0.*(K_u_H2O.*(rho_H2O - rho_mag(I,1)).
*(x_H2O(I,1) - x_u_H2O_0)));
173    f2_u_H2O = (1./(V_u.*rho_u_0)).*(W(I,1).*x_H2O(I,1) - Q_o.*rho_o_0.*x_o_H2O_0 -
Q_u.*rho_u_0.*(x_u_H2O_0 + (ht./2).*f1_u_H2O) - V_o.*x_o_H2O_0.*f1_rho_o - V_o.*rho_o_0.
*(K_o_H2O.*(rho_mag(I,1) - rho_H2O)).*(x_H2O(I,1) - x_o_H2O_0)) - V_u.*(x_u_H2O_0 + (ht.
/2).*f1_u_H2O).*f1_rho_u);
174    f3_o_H2O = (1./(V_o.*rho_o_0)).*(W(I,1).*x_H2O(I,1) - Q_o.*rho_o_0.*(x_o_H2O_0 +
(ht./2).*f2_o_H2O) - Q_u.*rho_u_0.*x_u_H2O_0 - V_o.*(x_o_H2O_0 + (ht./2).*f2_o_H2O).
*f1_rho_o - V_u.*x_u_H2O_0.*f1_rho_u - V_u.*rho_u_0.*(K_u_H2O.*(rho_H2O - rho_mag(I,1)).
*(x_H2O(I,1) - x_u_H2O_0)));
175    f3_u_H2O = (1./(V_u.*rho_u_0)).*(W(I,1).*x_H2O(I,1) - Q_o.*rho_o_0.*x_o_H2O_0 -
Q_u.*rho_u_0.*(x_u_H2O_0 + (ht./2).*f2_u_H2O) - V_o.*x_o_H2O_0.*f1_rho_o - V_o.*rho_o_0.
*(K_o_H2O.*(rho_mag(I,1) - rho_H2O)).*(x_H2O(I,1) - x_o_H2O_0)) - V_u.*(x_u_H2O_0 + (ht.
/2).*f2_u_H2O).*f1_rho_u);

```

```

176     f4_o_H2O = (1./(V_o.*rho_o_0)).*(W(I,1).*x_H2O(I,1) - Q_o.*rho_o_0.*(x_o_H2O_0 +
ht.*f3_o_H2O) - Q_u.*rho_u_0.*x_u_H2O_0 - V_o.*(x_o_H2O_0 + ht.*f3_o_H2O).*f1_rho_o -
V_u.*x_u_H2O_0.*f1_rho_u - V_u.*rho_u_0.*(K_u_H2O.*(rho_H2O - rho_mag(I,1)).*(x_H2O(I,1)
- x_u_H2O_0)));
177     f4_u_H2O = (1./(V_u.*rho_u_0)).*(W(I,1).*x_H2O(I,1) - Q_o.*rho_o_0.*x_o_H2O_0 -
Q_u.*rho_u_0.*(x_u_H2O_0 + ht.*f3_u_H2O) - V_o.*x_o_H2O_0.*f1_rho_o - V_o.*rho_o_0.*
(K_o_H2O.*(rho_mag(I,1) - rho_H2O)).*(x_H2O(I,1) - x_o_H2O_0)) - V_u.*(x_u_H2O_0 + ht.*
f3_u_H2O).*f1_rho_u);
178     x_o_H2O(I,1) = x_o_H2O_0 + (ht*(f1_o_H2O + 2*f2_o_H2O + 2*f3_o_H2O + f4_o_H2O))
/6;
179     x_u_H2O(I,1) = x_u_H2O_0 + (ht*(f1_u_H2O + 2*f2_u_H2O + 2*f3_u_H2O + f4_u_H2O))
/6;
180
181     f1_o_vol = (1./(V_o.*rho_o_0)).*(W(I,1).*x_vol(I,1) - Q_o.*rho_o_0.*x_o_vol_0 -
Q_u.*rho_u_0.*x_u_vol_0 - V_o.*x_o_vol_0.*f1_rho_o - V_u.*x_u_vol_0.*f1_rho_u - V_u.*
rho_u_0.*(K_u_vol.*(rho_vol - rho_mag(I,1)).*(x_vol(I,1) - x_u_vol_0)));
182     f1_u_vol = (1./(V_u.*rho_u_0)).*(W(I,1).*x_vol(I,1) - Q_o.*rho_o_0.*x_o_vol_0 -
Q_u.*rho_u_0.*x_u_vol_0 - V_o.*x_o_vol_0.*f1_rho_o - V_o.*rho_o_0.*(K_o_vol.*(rho_mag(I,
1) - rho_vol)).*(x_vol(I,1) - x_o_vol_0)) - V_u.*x_u_vol_0.*f1_rho_u);
183     f2_o_vol = (1./(V_o.*rho_o_0)).*(W(I,1).*x_vol(I,1) - Q_o.*rho_o_0.*(x_o_vol_0 +
(ht./2).*f1_o_vol) - Q_u.*rho_u_0.*x_u_vol_0 - V_o.*(x_o_vol_0 + (ht./2).*f1_o_vol).
f1_rho_o - V_u.*x_u_vol_0.*f1_rho_u - V_u.*rho_u_0.*(K_u_vol.*(rho_vol - rho_mag(I,1)).
*(x_vol(I,1) - x_u_vol_0)));
184     f2_u_vol = (1./(V_u.*rho_u_0)).*(W(I,1).*x_vol(I,1) - Q_o.*rho_o_0.*x_o_vol_0 -
Q_u.*rho_u_0.*(x_u_vol_0 + (ht./2).*f1_u_vol) - V_o.*x_o_vol_0.*f1_rho_o - V_o.*rho_o_0.*
(K_o_vol.*(rho_mag(I,1) - rho_vol)).*(x_vol(I,1) - x_o_vol_0)) - V_u.*(x_u_vol_0 + (ht.
/2).*f1_u_vol).*f1_rho_u);
185     f3_o_vol = (1./(V_o.*rho_o_0)).*(W(I,1).*x_vol(I,1) - Q_o.*rho_o_0.*(x_o_vol_0 +
(ht./2).*f2_o_vol) - Q_u.*rho_u_0.*x_u_vol_0 - V_o.*(x_o_vol_0 + (ht./2).*f2_o_vol).
f1_rho_o - V_u.*x_u_vol_0.*f1_rho_u - V_u.*rho_u_0.*(K_u_vol.*(rho_vol - rho_mag(I,1)).
*(x_vol(I,1) - x_u_vol_0)));
186     f3_u_vol = (1./(V_u.*rho_u_0)).*(W(I,1).*x_vol(I,1) - Q_o.*rho_o_0.*x_o_vol_0 -
Q_u.*rho_u_0.*(x_u_vol_0 + (ht./2).*f2_u_vol) - V_o.*x_o_vol_0.*f1_rho_o - V_o.*rho_o_0.*
(K_o_vol.*(rho_mag(I,1) - rho_vol)).*(x_vol(I,1) - x_o_vol_0)) - V_u.*(x_u_vol_0 + (ht.
/2).*f2_u_vol).*f1_rho_u);
187     f4_o_vol = (1./(V_o.*rho_o_0)).*(W(I,1).*x_vol(I,1) - Q_o.*rho_o_0.*(x_o_vol_0 +
ht.*f3_o_vol) - Q_u.*rho_u_0.*x_u_vol_0 - V_o.*(x_o_vol_0 + ht.*f3_o_vol).*f1_rho_o -
V_u.*x_u_vol_0.*f1_rho_u - V_u.*rho_u_0.*(K_u_vol.*(rho_vol - rho_mag(I,1)).*(x_vol(I,1)
- x_u_vol_0)));
188     f4_u_vol = (1./(V_u.*rho_u_0)).*(W(I,1).*x_vol(I,1) - Q_o.*rho_o_0.*x_o_vol_0 -
Q_u.*rho_u_0.*(x_u_vol_0 + ht.*f3_u_vol) - V_o.*x_o_vol_0.*f1_rho_o - V_o.*rho_o_0.*
(K_o_vol.*(rho_mag(I,1) - rho_vol)).*(x_vol(I,1) - x_o_vol_0)) - V_u.*(x_u_vol_0 + ht.*
f3_u_vol).*f1_rho_u);
189     x_o_vol(I,1) = x_o_vol_0 + (ht*(f1_o_vol + 2*f2_o_vol + 2*f3_o_vol + f4_o_vol))
/6;
190     x_u_vol(I,1) = x_u_vol_0 + (ht*(f1_u_vol + 2*f2_u_vol + 2*f3_u_vol + f4_u_vol))
/6;
191
192     f1_o_mag = (1./(V_o.*rho_o_0)).*(W(I,1).*x_mag(I,1) - Q_o.*rho_o_0.*x_o_mag_0 -
Q_u.*rho_u_0.*x_u_mag_0 - V_o.*x_o_mag_0.*f1_rho_o - V_u.*x_u_mag_0.*f1_rho_u - V_u.*
rho_u_0.*(K_u_mag.*(delta_mag).*(x_mag(I,1) - x_u_mag_0)));

```

```

193     f1_u_mag = (1./(V_u.*rho_u_0)).*(W(I,1).*x_mag(I,1) - Q_o.*rho_o_0.*x_o_mag_0 -
Q_u.*rho_u_0.*x_u_mag_0 - V_o.*x_o_mag_0.*f1_rho_o - V_o.*rho_o_0.*(K_o_mag.*(
(delta_mag).*(x_mag(I,1) - x_o_mag_0)) - V_u.*x_u_mag_0.*f1_rho_u);
194     f2_o_mag = (1./(V_o.*rho_o_0)).*(W(I,1).*x_mag(I,1) - Q_o.*rho_o_0.*(x_o_mag_0
+ (ht./2).*f1_o_mag) - Q_u.*rho_u_0.*x_u_mag_0 - V_o.*(x_o_mag_0 + (ht./2).*f1_o_mag).
*f1_rho_o - V_u.*x_u_mag_0.*f1_rho_u - V_u.*rho_u_0.*(K_u_mag.*(delta_mag).*(x_mag(I,1)
- x_u_mag_0)));
195     f2_u_mag = (1./(V_u.*rho_u_0)).*(W(I,1).*x_mag(I,1) - Q_o.*rho_o_0.*x_o_mag_0 -
Q_u.*rho_u_0.*(x_u_mag_0 + (ht./2).*f1_u_mag) - V_o.*x_o_mag_0.*f1_rho_o - V_o.
*rho_o_0.*(K_o_mag.*(delta_mag).*(x_mag(I,1) - x_o_mag_0)) - V_u.*(x_u_mag_0 + (ht./2).
*f1_u_mag).*f1_rho_u);
196     f3_o_mag = (1./(V_o.*rho_o_0)).*(W(I,1).*x_mag(I,1) - Q_o.*rho_o_0.*(x_o_mag_0
+ (ht./2).*f2_o_mag) - Q_u.*rho_u_0.*x_u_mag_0 - V_o.*(x_o_mag_0 + (ht./2).*f2_o_mag).
*f1_rho_o - V_u.*x_u_mag_0.*f1_rho_u - V_u.*rho_u_0.*(K_u_mag.*(delta_mag).*(x_mag(I,1)
- x_u_mag_0)));
197     f3_u_mag = (1./(V_u.*rho_u_0)).*(W(I,1).*x_mag(I,1) - Q_o.*rho_o_0.*x_o_mag_0 -
Q_u.*rho_u_0.*(x_u_mag_0 + (ht./2).*f2_u_mag) - V_o.*x_o_mag_0.*f1_rho_o - V_o.
*rho_o_0.*(K_o_mag.*(delta_mag).*(x_mag(I,1) - x_o_mag_0)) - V_u.*(x_u_mag_0 + (ht./2).
*f2_u_mag).*f1_rho_u);
198     f4_o_mag = (1./(V_o.*rho_o_0)).*(W(I,1).*x_mag(I,1) - Q_o.*rho_o_0.*(x_o_mag_0
+ ht.*f3_o_mag) - Q_u.*rho_u_0.*x_u_mag_0 - V_o.*(x_o_mag_0 + ht.*f3_o_mag).*f1_rho_o -
V_u.*x_u_mag_0.*f1_rho_u - V_u.*rho_u_0.*(K_u_mag.*(delta_mag).*(x_mag(I,1) -
x_u_mag_0)));
199     f4_u_mag = (1./(V_u.*rho_u_0)).*(W(I,1).*x_mag(I,1) - Q_o.*rho_o_0.*x_o_mag_0 -
Q_u.*rho_u_0.*(x_u_mag_0 + ht.*f3_u_mag) - V_o.*x_o_mag_0.*f1_rho_o - V_o.*rho_o_0.*
(K_o_mag.*(delta_mag).*(x_mag(I,1) - x_o_mag_0)) - V_u.*(x_u_mag_0 + ht.*f3_u_mag).
*f1_rho_u);
200     x_o_mag(I,1) = x_o_mag_0 + (ht*(f1_o_mag + 2*f2_o_mag + 2*f3_o_mag + f4_o_mag))
/6;
201     x_u_mag(I,1) = x_u_mag_0 + (ht*(f1_u_mag + 2*f2_u_mag + 2*f3_u_mag + f4_u_mag))
/6;
202
203     if x_o_mag(I,1) > 1
204         x_o_mag(I,1) = 1;
205         x_o_ash(I,1) = 0;
206         x_o_S(I,1) = 0;
207         x_o_H2O(I,1) = 0;
208         x_o_vol(I,1) = 0;
209     end
210     if x_u_mag(I,1) > 1
211         x_u_mag(I,1) = 1;
212         x_u_ash(I,1) = 0;
213         x_u_S(I,1) = 0;
214         x_u_H2O(I,1) = 0;
215         x_u_vol(I,1) = 0;
216     end
217
218     if x_o_mag(I,1) < 0
219         x_o_mag(I,1) = 0;
220         x_o_ash(I,1) = 0;
221         x_o_S(I,1) = 0;

```



```
222     x_o_H2O(I,1) = 0;
223     x_o_vol(I,1) = 0;
224 end
225 if x_u_mag(I,1) < 0
226     x_u_mag(I,1) = 0;
227     x_u_ash(I,1) = 0;
228     x_u_S(I,1) = 0;
229     x_u_H2O(I,1) = 0;
230     x_u_vol(I,1) = 0;
231 end
232
233 end
234
235 %Cleanup Simulation
236 for I=1:125,
237     if x_o_mag(I,1) == 1
238         x_o_ash(I,1) = 0;
239         x_o_S(I,1) = 0;
240         x_o_H2O(I,1) = 0;
241         x_o_vol(I,1) = 0;
242         x_o_C(I,1) = 0;
243     else
244         x_o_ash(I,1) = x_o_ash(I,1) ./ (1-x_o_mag(I,1));
245         x_o_S(I,1) = x_o_S(I,1) ./ (1-x_o_mag(I,1));
246         x_o_H2O(I,1) = x_o_H2O(I,1) ./ (1-x_o_mag(I,1));
247         x_o_vol(I,1) = x_o_vol(I,1) ./ (1-x_o_mag(I,1));
248         x_o_C(I,1) = 1-x_o_ash(I,1)-x_o_S(I,1)-x_o_H2O(I,1)-x_o_vol(I,1);
249     end
250     if x_u_mag(I,1) == 1
251         x_u_ash(I,1) = 0;
252         x_u_S(I,1) = 0;
253         x_u_H2O(I,1) = 0;
254         x_u_vol(I,1) = 0;
255         x_u_C(I,1) = 0;
256     else
257         x_u_ash(I,1) = x_u_ash(I,1) ./ (1-x_u_mag(I,1));
258         x_u_S(I,1) = x_u_S(I,1) ./ (1-x_u_mag(I,1));
259         x_u_H2O(I,1) = x_u_H2O(I,1) ./ (1-x_u_mag(I,1));
260         x_u_vol(I,1) = x_u_vol(I,1) ./ (1-x_u_mag(I,1));
261         x_u_C(I,1) = 1-x_u_ash(I,1)-x_u_S(I,1)-x_u_H2O(I,1)-x_u_vol(I,1);
262     end
263 end
264
265 figure
266 plot(t, (rho_o.*Q_o.*(1-x_o_mag))./(W.*(1-x_mag)))
267
268 %Output Results
269 figure
270 plot(t,rho_mag,'-r')
271 hold on;
272 plot(t,rho,':g')
```



```
273 legend('rho mag','rho meas');
274 grid on;
275 xlabel('Time (s)');
276 ylabel('Density (kg/m^3)');
277 title('Comparison of magnetite medium density and simulated feed density');
278
279 figure
280 plot(t,rho_o)
281 hold on
282 plot(t,rho_u,'+- .r')
283 legend('rho_o','rho_u');
284 grid on;
285 xlabel('Time (s)');
286 ylabel('Density (kg/m^3)');
287 title('Overflow and underflow density simulation');
288
289 figure
290 plot(t,100.*x_o_mag)
291 hold on
292 plot(t,100.*x_u_mag,'+- .r')
293 legend('x_o med','x_u med');
294 grid on;
295 xlabel('Time (s)');
296 ylabel('Magnetite medium (%)');
297 title('Overflow and underflow magnetite medium simulation');
298
299 figure
300 [AX, H1, H2] = plotyy(t,100.*W_mag./W,t,W_meas)
301 %legend('Medium to feed ratio');
302 legend(H2,'Plant module ore feed');
303 grid on;
304 xlabel('Time (s)');
305 set(get(AX(1),'Ylabel'),'String','W_{mag}/W (%)');
306 set(get(AX(2),'Ylabel'),'String','Feedrate (kg/s)');
307 %ylabel('W_{mag}/W (%)');
308 title('Percentage magnetite medium in the feed');
309
310 figure
311 plot(t,100.*x_o_C)
312 hold on
313 plot(t,100.*x_u_C,'+- .r')
314 legend('x_o C','x_u C');
315 grid on;
316 xlabel('Time (s)');
317 ylabel('Carbon (%)');
318 title('Carbon percentage in the overflow and underflow simulation');
319
320
321 figure
322 plot(t,100.*x_o_ash)
323 hold on
```



```
324 plot(t,100.*x_u_ash,'+-r')
325 legend('x_o ash','x_u ash');
326 grid on;
327 xlabel('Time (s)');
328 ylabel('Ash (%)');
329 title('Ash percentage in the overflow and underflow simulation');
330
331 figure
332 plot(t,100.*x_o_S);
333 hold on
334 plot(t,100.*x_u_S,'+-r');
335 legend('x_o S','x_u S');
336 grid on;
337 xlabel('Time (s)');
338 ylabel('Sulphur (%)');
339 title('Sulphur percentage in the overflow and underflow simulation');
340
341 figure
342 plot(t,100.*x_o_H2O)
343 hold on
344 plot(t,100.*x_u_H2O,'+-r')
345 legend('x_o H_2 O','x_u H_2 O');
346 grid on;
347 xlabel('Time (s)');
348 ylabel('H_2 O (%)');
349 title('Water percentage in the overflow and underflow simulation');
350
351 figure
352 plot(t,100.*x_o_vol)
353 hold on
354 plot(t,100.*x_u_vol,'+-r')
355 legend('x_o vol','x_u vol');
356 grid on;
357 xlabel('Time (s)');
358 ylabel('Volatile (%)');
359 title('Volatile percentage in the overflow and underflow simulation');
360
361 figure
362 plot(t,100.*x_o_C)
363 hold on
364 plot(t,100.*x_o_ash,'Vr')
365 hold on
366 plot(t,100.*x_o_S,':g');
367 hold on
368 plot(t,100.*x_o_H2O,'-.c')
369 hold on
370 plot(t,100.*x_o_vol,'--m')
371 legend('x_o C','x_o ash','x_o S','x_o H_2 O','x_o vol');
372 grid on;
373 xlabel('Time (s)');
374 ylabel('Component (%)');
```



```
375 title('Component percentage in the overflow simulation');
376
377
378 figure
379 plot(t,100.*x_u_C)
380 hold on
381 plot(t,100.*x_u_ash,'Vr')
382 hold on
383 plot(t,100.*x_u_S,':g');
384 hold on
385 plot(t,100.*x_u_H2O,'-c')
386 hold on
387 plot(t,100.*x_u_vol,'-m')
388 legend('x_u C','x_u ash','x_u S','x_u H_2 O','x_u vol');
389 grid on;
390 xlabel('Time (s)');
391 ylabel('Component (%)');
392 title('Component percentages in the underflow simulation');
393
394
395 x_o_ash_mean = ones(5,1);
396 x_o_ash_std = ones(5,1);
397 for I = 1:5,
398     x_o_ash_mean((I-1)+1:(I),1) = mean(100.*x_o_ash((I-1).*20+10+I:(I.*20)+11,1));
399     x_o_ash_std((I-1)+1:(I),1) = 1.96.*std(100.*x_o_ash((I-1).*20+10+I:(I.*20)+11,
400 1));
401 end
402 figure
403 ts=14.*21.*(0:5);
404 tt=14.*21.*(1:5);
405 plot(ts,100.*[x_o_ash_meas(1,1); x_o_ash_meas(25,1); x_o_ash_meas(45,1);
x_o_ash_meas(65,1); x_o_ash_meas(85,1); x_o_ash_meas(105,1)],'or')
406 hold on
407 %plot(t,100.*x_o_ash_mean,'vm')
408 errorbar(tt,x_o_ash_mean,x_o_ash_std,'x');
409 hold on
410 plot(t,100.*x_o_ash,'g')
411 legend('x_o ash measured','x_o ash simulation mean with error-bar','x_o ash
simulation');
412 grid on;
413 xlabel('Time (s)');
414 ylabel('Ash (%)');
415 title('Ash percentage in the overflow simulation');
416
417
418 x_o_H2O_mean = ones(5,1);
419 x_o_H2O_std = ones(5,1);
420 for I = 1:5,
421     x_o_H2O_mean((I-1)+1:(I),1) = mean(100.*x_o_H2O((I-1).*20+10+I:(I).*20+11,1));
422     x_o_H2O_std((I-1)+1:(I),1) = 1.96.*std(100.*x_o_H2O((I-1).*20+10+I:(I).*20+11,
423 1));
```



```
422 end
423 figure
424 %plot(ts,100.*x_o_H2O_meas,'og')
425 plot(ts,100.*[x_o_H2O_meas(1,1); x_o_H2O_meas(25,1); x_o_H2O_meas(45,1);
x_o_H2O_meas(65,1); x_o_H2O_meas(85,1); x_o_H2O_meas(105,1)], 'or')
426 hold on
427 errorbar(tt,x_o_H2O_mean,x_o_H2O_std,'x')
428 hold on
429 plot(t,100.*x_o_H2O,'g')
430 legend('x_o H2O measured','x_o H2O simulation mean with error-bar','x_o H2O
simulation');
431 grid on;
432 xlabel('Time (s)');
433 ylabel('H2O (%)');
434 title('Moisture percentage in the overflow simulation');
435
436 x_o_vol_mean = ones(5,1);
437 x_o_vol_std = ones(5,1);
438 for I = 1:5,
439     x_o_vol_mean((I-1)+1:(I),1) = mean(100.*x_o_vol((I-1).*20+10+I:(I).*20+11,1));
440     x_o_vol_std((I-1)+1:(I),1) = 1.96.*std(100.*x_o_vol((I-1).*20+10+I:(I).*20+11,
1));
441 end
442 figure
443 %plot(ts,100.*x_o_vol_meas,'og')
444 plot(ts,100.*[x_o_vol_meas(1,1); x_o_vol_meas(25,1); x_o_vol_meas(45,1);
x_o_vol_meas(65,1); x_o_vol_meas(85,1); x_o_vol_meas(105,1)], 'or')
445 hold on
446 errorbar(tt,x_o_vol_mean,x_o_vol_std,'x')
447 hold on
448 plot(t,100.*x_o_vol,'g')
449 legend('x_o vol measured','x_o vol simulation mean with error-bar','x_o vol
simulation');
450 grid on;
451 xlabel('Time (s)');
452 ylabel('Volatile (%)');
453 title('Volatile percentage in the overflow simulation');
454
455 cor_ash = corr(x_o_ash_meas,x_o_ash)
456 y=[x_o_ash_meas(1,1); x_o_ash_meas(25,1); x_o_ash_meas(45,1); x_o_ash_meas(65,1);
x_o_ash_meas(85,1); x_o_ash_meas(105,1)];
457 yh=[x_o_ash(1,1); x_o_ash(25,1); x_o_ash(45,1); x_o_ash(65,1); x_o_ash(85,1);
x_o_ash(105,1)];
458 fit_ash=100*(1 - norm(yh - y)/norm(y-mean(y)))
459 e=y-yh;
460 figure
461 stem(100.*e)
462 title('Plot of residual for the ash comparison')
463 ylabel('Residual (%)')
464 xlabel('Sample')
465 grid on
```



```
466 u=[x_ash(1,1); x_ash(25,1); x_ash(45,1); x_ash(65,1); x_ash(85,1); x_ash(105,1)];
467 figure
468 autocorr(e)
469 title('Autocorrelation of the residual for the ash comparison')
470 ylabel('Sample autocorrelation')
471 xlabel('Lag')
472 legend('Autocorrelation result','Upper 95% confidence bound','Lower 95% confidence
bound','');
473 figure
474 crosscorr(e,u)
475 title('Cross correlation of the residual and input for the ash comparison')
476 ylabel('Sample cross correlation')
477 xlabel('Lag')
478 legend('Cross correlation result','Upper 95% confidence bound','Lower 95% confidence
bound','');
479 size_x_o_ash=size(x_o_ash);
480 VN_ash = (1./size_x_o_ash(1,1)).*sum(0.5.*(x_o_ash_meas - x_o_ash).^2)
481
482 cor_H2O = corr(x_o_H2O_meas,x_o_H2O)
483 y=[x_o_H2O_meas(1,1); x_o_H2O_meas(25,1); x_o_H2O_meas(45,1); x_o_H2O_meas(65,1);
x_o_H2O_meas(85,1); x_o_H2O_meas(105,1)];
484 yh=[x_o_H2O(1,1); x_o_H2O(25,1); x_o_H2O(45,1); x_o_H2O(65,1); x_o_H2O(85,1);
x_o_H2O(105,1)];
485 fit_H2O=100*(1 - norm(yh - y)/norm(y-mean(y)))
486 e=y-yh;
487 figure
488 stem(100.*e)
489 title('Plot of residual for the moisture comparison')
490 ylabel('Residual (%)')
491 xlabel('Sample')
492 grid on;
493 u=[x_H2O(1,1); x_H2O(25,1); x_H2O(45,1); x_H2O(65,1); x_H2O(85,1); x_H2O(105,1)];
494 figure
495 autocorr(e)
496 title('Autocorrelation of the residual for the moisture comparison')
497 ylabel('Sample autocorrelation')
498 xlabel('Lag')
499 legend('Autocorrelation result','Upper 95% confidence bound','Lower 95% confidence
bound','');
500 figure
501 crosscorr(e,u)
502 title('Cross correlation of the residual and input for the moisture comparison')
503 ylabel('Sample cross correlation')
504 xlabel('Lag')
505 legend('Cross correlation result','Upper 95% confidence bound','Lower 95% confidence
bound','');
506 size_x_o_H2O = size(x_o_H2O);
507 VN_H2O = (1./size_x_o_H2O(1,1)).*sum(0.5.*(x_o_H2O_meas - x_o_H2O).^2)
508
509 cor_vol = corr(x_o_vol_meas,x_o_vol)
510 y=[x_o_vol_meas(1,1); x_o_vol_meas(25,1); x_o_vol_meas(45,1); x_o_vol_meas(65,1);
```



```
x_o_vol_meas(85,1); x_o_vol_meas(105,1)];
511 yh=[x_o_vol(1,1); x_o_vol(25,1); x_o_vol(45,1); x_o_vol(65,1); x_o_vol(85,1);
x_o_vol(105,1)];
512 fit_vol=100*(1 - norm(yh - y)/norm(y-mean(y)))
513 e=y-yh;
514 figure
515 stem(100.*e)
516 title('Plot of residual for the volatile comparison')
517 ylabel('Residual (%)')
518 xlabel('Sample')
519 grid on;
520 u=[x_vol(1,1); x_vol(25,1); x_vol(45,1); x_vol(65,1); x_vol(85,1); x_vol(105,1)];
521 figure
522 autocorr(e)
523 title('Autocorrelation of the residual for the volatile comparison')
524 ylabel('Sample autocorrelation')
525 xlabel('Lag')
526 legend('Autocorrelation result','Upper 95% confidence bound','Lower 95% confidence
bound','');
527 figure
528 crosscorr(e,u)
529 title('Cross correlation of the residual and input for the volatile comparison')
530 ylabel('Sample cross correlation')
531 xlabel('Lag')
532 legend('Cross correlation result','Upper 95% confidence bound','Lower 95% confidence
bound','');
533 size_x_o_vol=size(x_o_vol);
534 VN_vol = (1./size_x_o_vol(1,1)).*sum(0.5.*(x_o_vol_meas - x_o_vol).^2)
535
536 W_o = rho_o.*Q_o;
537 W_u = rho_u.*Q_u;
538 W_o_mag = W_o.*x_o_mag;
539 W_u_mag = W_u.*x_u_mag;
540 rho_mag_out = (W_o_mag+W_u_mag)./(Q_o_mag+Q_u_mag);
541
542 %Save Output for Magnetite Medium Makeup Tank
543 RHOMAGIN = rho_mag_out;
544 save RHOMAGIN RHOMAGIN;
```



```
1 clear;
2 %Load Data
3 load RHOMAGIN;
4 rho_mag = RHOMAGIN(1:125-5);
5 load HGT;
6 height = HGT(81+5-32:205-32)./100;
7
8 %Assign Variables and Constants
9 t=0:14:119.*14;
10 ht=1;
11 hmax = 1.5;
12 height = hmax.*height;
13 area = pi.*(0.3).^2;
14
15 Q_mag = 0.1376.*3.6;
16 Q = Q_mag;
17 Q_dis = 0;
18 rho_dis = 1600.*ones(120,1);
19 rho = zeros(120,1);
20 rho_0 = 1540;
21
22 W_mag = Q_mag.*rho_mag;
23
24 for I = 1:120,
25
26
27     if I > 1
28         rho_0 = rho(I-1,1);
29     end
30
31     f1_rho = (1./(area.*height(I,1)).*(W_mag(I,1) + Q_dis.*rho_dis(I,1) - (Q_mag + Q_dis).*(rho_0)));
32     f2_rho = (1./(area.*height(I,1)).*(W_mag(I,1) + Q_dis.*rho_dis(I,1) - (Q_mag + Q_dis).*(rho_0 + (ht./2).*f1_rho)));
33     f3_rho = (1./(area.*height(I,1)).*(W_mag(I,1) + Q_dis.*rho_dis(I,1) - (Q_mag + Q_dis).*(rho_0 + (ht./2).*f2_rho)));
34     f4_rho = (1./(area.*height(I,1)).*(W_mag(I,1) + Q_dis.*rho_dis(I,1) - (Q_mag + Q_dis).*(rho_0 + ht.*f3_rho)));
35     rho(I,1) = rho_0 + ht.*(f1_rho + 2.*f2_rho + 2.*f3_rho + f4_rho)./6;
36
37 end
38
39 %Output Results
40 figure;
41 plot(t,rho);
42 xlabel('Time (s)');
43 ylabel('Density (kg/m^3)');
44 legend('Simulated medium makeup');
45 title('Simulated density response for the magnetite medium makeup tank');
46 grid on;
47
```



```
48 figure;
49 [AX, H1, H2] = plotyy(t,W_mag,t,100.*height)
50 xlabel('Time (s)');
51 ylabel('Mass rate (kg/s)');
52 set(get(AX(1),'Ylabel'),'String','Mass rate (kg/s)');
53 set(get(AX(2),'Ylabel'),'String','Level (%)');
54 legend('Simulated medium makeup');
55 legend(H2,'Measured tank height');
56 title('Simulated mass rate response for the water addition with tank height');
57 grid on;
58
59 %Save Output for Water Addition Model
60 rho_mag_out = rho;
61 save rho_mag_out rho_mag_out;
```



```
1 clear;
2 %Load Data
3 load rho_mag_out;
4 rho_i = rho_mag_out;
5 load RHOMAG;
6 tau = 1;
7 rho_mag_meas = RHOMAG(81-32-tau:200-32-tau).*1000;
8 load VALVEL;
9 l = VALVEL(81-32-tau:200-32-tau)./100;
10
11 %Assign Variables and Constants
12 t = 0:14:119.*14;
13
14 Q_mag = 0.1376.*3.6;
15 V = 72.*pi.*(0.025.*10).^2./4.*1;
16 K = 0.01.*0.05.*sqrt(100./1000);
17 Q_i = Q_mag;
18
19 rho1_0 = 0.36;
20 rho_i_0 = 1540;
21
22 A = -1.*Q_mag./V;
23 B1 = 1000.*K./V;
24 Brho = Q_i./V;
25 C = 1;
26 D = 0;
27
28 %Perform Simulation
29 G1 = ss(A,B1,C,D);
30 rho1 = lsim(G1,l,t,rho1_0);
31 Grho = ss(A,Brho,C,D);
32 rhorho = lsim(Grho,rho_i,t,rho_i_0);
33
34 rho_mag = rho1+rhorho;
35
36 %Output Results
37 plot(t,rho_mag,'--r')
38 hold on;
39 [AX, H1, H2] = plotyy(t,rho_mag_meas,t,100.*1);
40 xlabel('Time (s)');
41 ylabel('Density (kg/m^3)');
42 set(get(AX(1),'Ylabel'),'String','Density (kg/m^3)');
43 set(get(AX(2),'Ylabel'),'String','Valve position (%)');
44 legend(H1,'Simulated medium','Measured medium');
45 legend(H2,'Measured valve position');
46 title('Simulated density response for the water addition');
47 grid on;
48
49 figure
50 load WI1SCR;
51 W_i_1 = 1000.*WI1SCR(81-tau:200-tau)./3600;
```



```
52 W_i = W_i_1;
53
54 [AX, H1, H2] = plotyy(t,rho_mag_meas,t,W_i);
55 xlabel('Time (s)');
56 ylabel('Density (kg/m^3)');
57 set(get(AX(1), 'Ylabel'), 'String', 'Density (kg/m^3)');
58 set(get(AX(2), 'Ylabel'), 'String', 'Feedrate (kg/s)');
59 legend(H1, 'Measured medium');
60 legend(H2, 'Measured plant feed');
61 title('Manipulated variables');
62 grid on;
63
64 corr(rho_mag_meas, rho_mag)
65 sizerho_mag = size(rho_mag);
66 VN=(1./sizerho_mag(1,1)).*sum(.5.*(rho_mag_meas-rho_mag).^2)
67
68 fit = 100.*(1-norm(abs(rho_mag_meas-rho_mag))./norm(abs(rho_mag_meas-mean(
(rho_mag_meas))))
69 e=rho_mag-rho_mag_meas;
70 figure
71 stem(100.*e)
72 title('Plot of residual for the medium density comparison')
73 ylabel('Residual (kg/m^3)')
74 xlabel('Sample')
75 grid on;
76 u=rhol;
77 figure
78 autocorr(e)
79 title('Autocorrelation of the residual for the medium density comparison')
80 ylabel('Sample autocorrelation')
81 xlabel('Lag')
82 legend('Autocorrelation result', 'Upper 95% confidence bound', 'Lower 95% confidence
bound', '');
83 figure
84 crosscorr(e,u)
85 title('Cross correlation of the residual and input for the medium density
comparison')
86 ylabel('Sample cross correlation')
87 xlabel('Lag')
88 legend('Cross correlation result', 'Upper 95% confidence bound', 'Lower 95% confidence
bound', '');
```

```

1 clear
2 %Load Data
3 t1 = 448;
4 deltat = 72000;
5 load PlantData;
6
7 %Create Files for DMS Plant Simulation
8 WT1002 = [1:deltat;data(t1:t1+deltat-1,1)'];
9 save WT1002 WT1002
10
11 WT2002 = [1:deltat;data(t1:t1+deltat-1,2)'];
12 save WT2002 WT2002
13
14 WT0300 = [1:deltat;data(t1:t1+deltat-1,7)'];
15 save WT0300 WT0300
16
17 WT0305B = [1:deltat;data(t1:t1+deltat-1,8)'];
18 save WT0305B WT0305B
19
20 WT3100 = [1:deltat;data(t1:t1+deltat-1,9)'];
21 save WT3100 WT3100
22
23 WT3400 = [1:deltat;data(t1:t1+deltat-1,10)'];
24 save WT3400 WT3400
25
26 LT1210 = [1:deltat;data(t1:t1+deltat-1,5)'];
27 save LT1210 LT1210
28
29 DY1203 = [1:deltat;data(t1:t1+deltat-1,4)'];
30 save DY1203 DY1203
31
32 DT1203 = [1:deltat;data(t1:t1+deltat-1,3)'];
33 save DT1203 DT1203
34
35 PT1109 = [1:deltat;data(t1:t1+deltat-1,6)'];
36 save PT1109 PT1109
37
38 clear;
39 %Defining the parameters for the model
40
41 %Module 1 Transport to Primary Screen
42 M1_Feed_Delay = 140; %Module 1 ore feed delay to
primary screen
43
44 %Module 1 Primary Screen (Double Deck)
45 M1_PrimScr_Time_Increment = 1; %Module 1 primary screen time
increment for Runge-Kutta approximation
46 M1_PrimScr_tau_o = 0.7; %Module 1 primary screen top deck
oversize time delay
47 M1_PrimScr_tau_c_o = 0.7; %Module 1 primary screen top deck
undersize time delay

```



```
48 M1_PrimScr_tau_c = 0.7; %Module 1 primary screen bottom✓  
deck oversize time delay  
49 M1_PrimScr_tau_f_c = 1.4; %Module 1 primary screen bottom✓  
deck undersize time delay  
50  
51 %Module 1 Secondary Screen (Single Deck)  
52 M1_SecScr_Time_Increment = 1; %Module 1 secondary screen time✓  
increment for Runge-Kutta approximation  
53 M1_SecScr_tau_f_o = 0.7; %Module 1 secondary screen oversize✓  
time delay  
54 M1_SecScr_tau_uf_o = 6.3; %Module 1 secondary screen✓  
undersize time delay  
55  
56 %Module 1 Fine Cyclone Mixing Box  
57 M1_MixBox_Q = 0.278./(2./3.6); %Module 1 mixing box for fine✓  
cyclone flow rate  
58 M1_MixBox_Q_mag = 0.99.*M1_MixBox_Q; %Module 1 mixing box for fine✓  
cyclone magnetite feed flow rate  
59 M1_MixBox_V = 0.3.*0.45.*0.65./(2./3.6); %Module 1 mixing box for fine✓  
cyclone volume  
60  
61 %Module 1 Transport to Fine Cyclone  
62 M1_FC_Feed_Delay = 5; %Module 1 transport delay from✓  
mixing box to fine cyclone  
63 M1_FC_Feed_Delay1 = 5+M1_MixBox_V./M1_MixBox_Q_mag; %Module 1 transport delay from✓  
mixing box to fine cyclone  
64  
65 %Module 1 Fine Cyclone  
66 M1_FC_Diameter = 0.71; %Module 1 fine cyclone diameter  
67 M1_FC_Time_Increment = 1; %Module 1 fine cyclone time✓  
increment for runge kutta approximation  
68 M1_FC_Feed_Flow_Rate = M1_MixBox_Q; %Module 1 fine cyclone feed flow✓  
rate  
69 M1_FC_alpha = 2; %Module 1 fine cyclone volume ratio✓  
between overflow and underflow  
70  
71 M1_FC_x_ash = 0.176; %Module 1 fine cyclone ore feed ash✓  
percentage  
72 M1_FC_x_S = 0.025; %Module 1 fine cyclone ore feed✓  
sulphur percentage  
73 M1_FC_x_H2O = 0.0159; %Module 1 fine cyclone ore feed✓  
water percentage  
74 M1_FC_x_vol = 0.126; %Module 1 fine cyclone ore feed✓  
volatile percentage  
75  
76 M1_FC_A_o = pi.*(0.43.*M1_FC_Diameter).^2;  
77 M1_FC_tau_o = 0.75;  
78 M1_FC_A_u = pi.*(0.43.*M1_FC_Diameter).^2;  
79 M1_FC_tau_u = M1_FC_tau_o;  
80  
81 M1_FC_tau_o_mag = 0.75;
```



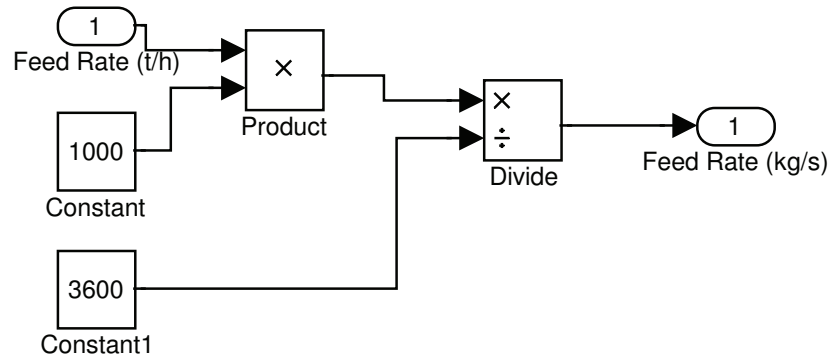
```
82 M1_FC_tau_u_mag = 0.8.*M1_FC_tau_o_mag;
83 M1_FC_tau_o_ash = 0.4;
84 M1_FC_tau_u_ash = 0.95.*M1_FC_tau_o_ash;
85 M1_FC_tau_o_H2O = 0.15;
86 M1_FC_tau_u_H2O = 0.2.*M1_FC_tau_o_H2O;
87 M1_FC_tau_o_vol = 0.98;
88 M1_FC_tau_u_vol = 0.01.*M1_FC_tau_o_vol;
89
90 M1_FC_Volume = M1_FC_Feed_Flow_Rate.*(M1_FC_tau_o+M1_FC_tau_u)./2;; %Module 1 fine
cyclone volume
91
92 M1_FC_rho_ash = 2000;
93 M1_FC_rho_S = 1920;
94 M1_FC_rho_vol = 1100;
95 M1_FC_rho_H2O = 1000;
96 M1_FC_delta_mag = 100; %Module 1 fine cyclone magnetite
differential density to feed magnetite density
97 M1_FC_Q_mag_ratio = 0.99;
98 M1_FC_Q_mag = M1_FC_Q_mag_ratio.*M1_FC_Feed_Flow_Rate; %Module 1 fine cyclone feed
magnetite flow rate
99
100 %M1_CC_d_o = 0.0025;
101 %M1_CC_d_u = 0.0025;
102 M1_FC_K_o = M1_FC_A_o.*M1_FC_tau_o; %Module 1 fine cyclone overflow
proportional constant | A_o_eff.*tau_o
103 M1_FC_K_u = M1_FC_A_u.*M1_FC_tau_u; %Module 1 fine cyclone undeflow
proportional constant | A_u_eff.*tau_u
104 M1_FC_K_o_mag = M1_FC_tau_o_mag./1550; %Module 1 fine cyclone magnetite
overflow proportional constant
105 M1_FC_K_u_mag = M1_FC_tau_u_mag./1550; %Module 1 fine cyclone magnetite
undeflow proportional constant
106 M1_FC_K_o_ash = M1_FC_tau_o_ash./M1_FC_rho_ash; %Module 1 fine cyclone ash overflow
proportional constant
107 M1_FC_K_u_ash = M1_FC_tau_u_ash./M1_FC_rho_ash; %Module 1 fine cyclone ash undeflow
proportional constant
108 M1_FC_K_o_S = M1_FC_tau_o./M1_FC_rho_S; %Module 1 fine cyclone sulphur
overflow proportional constant
109 M1_FC_K_u_S = M1_FC_tau_u./M1_FC_rho_S; %Module 1 fine cyclone sulphur
undeflow proportional constant
110 M1_FC_K_o_H2O = M1_FC_tau_o_H2O./M1_FC_rho_H2O; %Module 1 fine cyclone water
overflow proportional constant
111 M1_FC_K_u_H2O = M1_FC_tau_u_H2O./M1_FC_rho_H2O; %Module 1 fine cyclone water
undeflow proportional constant
112 M1_FC_K_o_vol = M1_FC_tau_o_vol./M1_FC_rho_vol; %Module 1 fine cyclone volatiles
overflow proportional constant
113 M1_FC_K_u_vol = M1_FC_tau_u_vol./M1_FC_rho_vol; %Module 1 fine cyclone volatiles
undeflow proportional constant
114
115 %Module 1 Fine Cyclone Magnetite Medium Makeup Tank
116 M1_FC_MagTank_Area = pi.*(0.3).^2; %Module 1 fine cyclone magnetite
makeup tank effective surface area
```



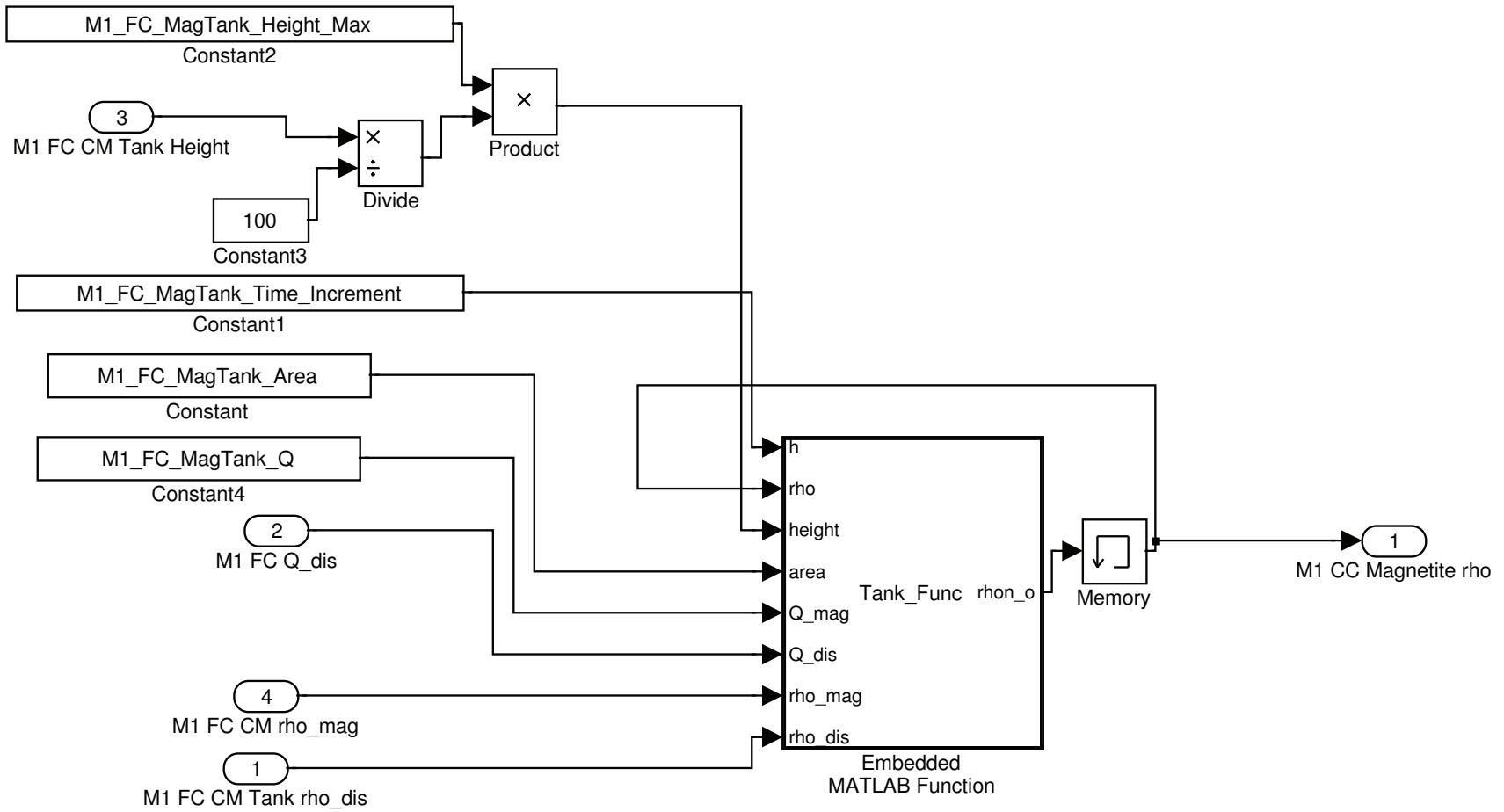
```
117 M1_FC_MagTank_Time_Increment = 1;           %Module 1 fine cyclone magnetite✓  
makeup time increment for runge kutta approximation  
118 M1_FC_MagTank_Height_Max = 1.5;           %Module 1 fine cyclone magnetite✓  
makeup tank maximum height  
119 M1_FC_MagTank_Q = M1_FC_Q_mag;           %Module 1 fine cyclone magnetite✓  
makeup tank volumetric flow rate of product  
120  
121 %Module 1 Transport Delay to Fine Cyclone Water Addition  
122 M1_FC_WaterAdd_Delay = 28;  
123  
124 %Module 1 Fine Cyclone Water Addition  
125 M1_FC_WaterAdd_K = 0.01.*0.05.*sqrt(100./1000); %Module 1 fine cyclone water✓  
addition valve Cv  
126 M1_FC_WaterAdd_V = 72.*pi.*(0.025.*10).^2./4.*1; %Module 1 fine cyclone water✓  
addition mixing volume  
127 M1_FC_WaterAdd_Q_mag = M1_FC_MagTank_Q;%0.1376; %Module 1 fine cyclone water✓  
addition volumetric flow rate of magnetite product  
128 M1_FC_WaterAdd_Q_i = M1_FC_MagTank_Q;     %Module 1 fine cyclone water✓  
addition volumetric flow rate of feed magnetite  
129  
130 %Module 1 Transport to Fine Cyclone Mixing Box  
131 M1_FC_MixBox_Feed_Delay = 28;             %Module 1 transport delay from✓  
corrected magnetite tank to Fine cyclone mixing box  
132
```



DMSPlantVer2Print/Convert t/h to kg/s



**DMSPlantVer2Print/Module 1 FC Corected Medium Tank**



C:\MATLAB701\work\DMS Plant\Final\DMSPlantVer2Print.mdl



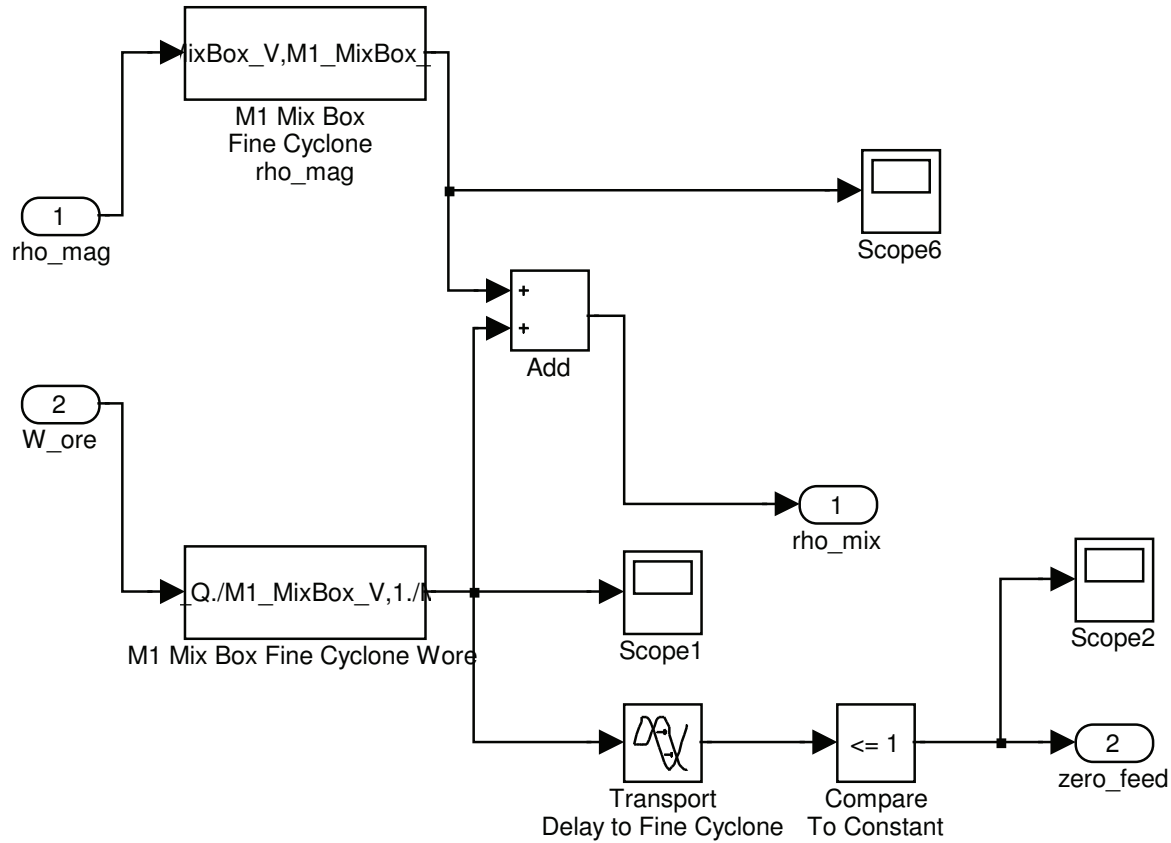
%<fullsystem>

DMSPlantVer2Print/Module 1 FC Corected Medium Tank/Embedded MATLAB Function.eML\_blk\_kernel

```
1: function rhon_o = Tank_Func(h, rho, height, area, Q_mag, Q_dis, rho_mag, rho_dis )
2: %Tank_Func Computes the magnetite density of the makeup tank product
3: %using fourth-order runge kutta approximation
4: W_mag = Q_mag.*rho_mag;
5:
6: f1_rho = (1./(area.*height)).*(W_mag + Q_dis.*rho_dis - (Q_mag + Q_dis).*(rho));
7: f2_rho = (1./(area.*height)).*(W_mag + Q_dis.*rho_dis - (Q_mag + Q_dis).*(rho + (h./2).*f1_rho));
8: f3_rho = (1./(area.*height)).*(W_mag + Q_dis.*rho_dis - (Q_mag + Q_dis).*(rho + (h./2).*f2_rho));
9: f4_rho = (1./(area.*height)).*(W_mag + Q_dis.*rho_dis - (Q_mag + Q_dis).*(rho + h.*f3_rho));
10: rhon_o = rho + h.*(f1_rho + 2.*f2_rho + 2.*f3_rho + f4_rho)./6;
```

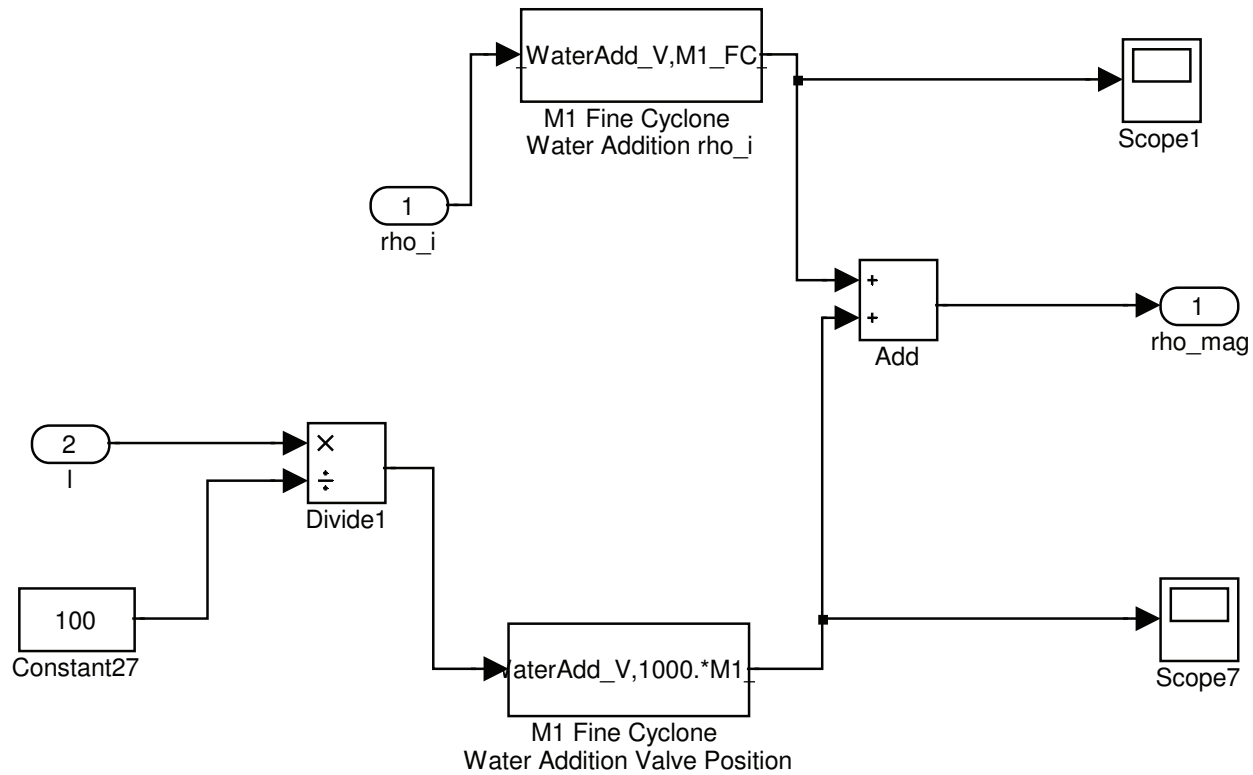
%<fullfilename>

DMSPlantVer2Print/Module 1 Fine Cyclone Mixing Box



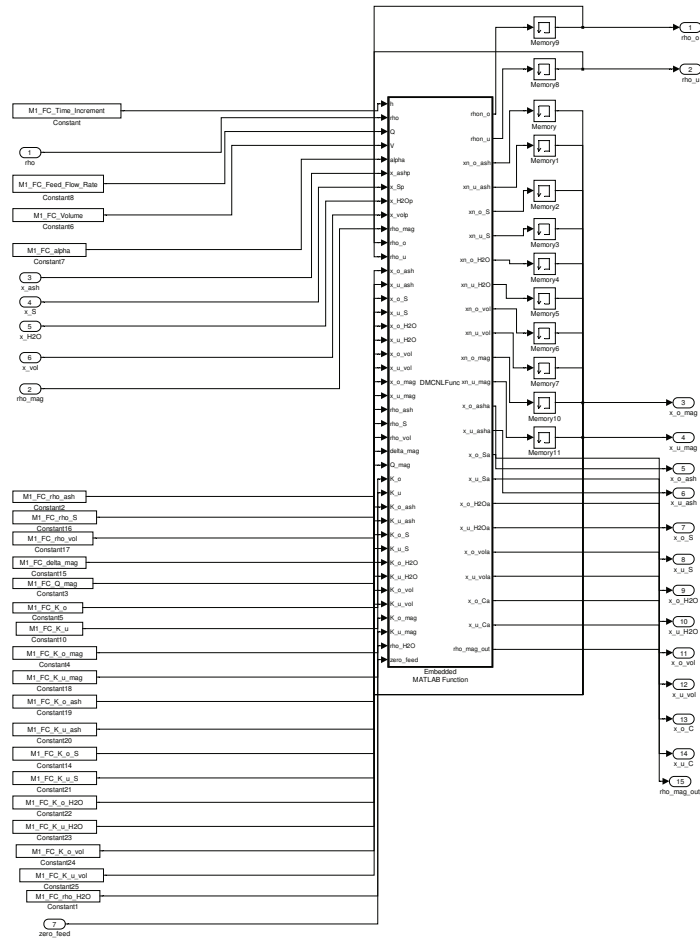
C:\MATLAB701\work\DMS Plant\Final\DMSPlantVer2Print.mdl

DMSPlantVer2Print/Module 1 Fine Cyclone Water Addition



C:\MATLAB701\work\DMS Plant\Final\DMSPlantVer2Print.mdl

**DMSPlantVer2Print/Module 1 Fine Cyclone**



C:\MATLAB701\work\DMS Plant\Final\DMSPlantVer2Print.mdl

```

1 function [ rhon_o, rhon_u, xn_o_ash, xn_u_ash, xn_o_S, xn_u_S, xn_o_H2O, xn_u_H2O,
xn_o_vol, xn_u_vol, xn_o_mag, xn_u_mag, x_o_asha, x_u_asha, x_o_Sa, x_u_Sa, x_o_H2Oa,
x_u_H2Oa, x_o_vola, x_u_vola, x_o_Ca, x_u_Ca, rho_mag_out ] = DMCNLFunc( h, rho, Q, V,
alpha, x_ashp, x_Sp, x_H2Op, x_volp, rho_mag, rho_o, rho_u, x_o_ash, x_u_ash, x_o_S,
x_u_S, x_o_H2O, x_u_H2O, x_o_vol, x_u_vol, x_o_mag, x_u_mag, rho_ash, rho_S, rho_vol,
delta_mag, Q_mag, K_o, K_u, K_o_ash, K_u_ash, K_o_S, K_u_S, K_o_H2O, K_u_H2O, K_o_vol,
K_u_vol, K_o_mag, K_u_mag, rho_H2O, zero_feed )
2 %DMCNLFunc Computes the fourth-order runge kutta approximation for a DMC
3 W = Q.*rho;
4 if zero_feed == 1
5     %W = 0;
6     x_mag = 1;
7     x_ash = 0;
8     x_S = 0;
9     x_H2O = 0;
10    x_vol = 0;
11    x_C = 1 - x_ash - x_S - x_H2O - x_vol - x_mag;
12 else
13    x_mag = rho_mag.*Q_mag./W;
14    x_ash = x_ashp.*(1-x_mag);
15    x_S = x_Sp.*(1-x_mag);
16    x_H2O = x_H2Op.*(1-x_mag);
17    x_vol = x_volp.*(1-x_mag);
18    x_C = 1 - x_ash - x_S - x_H2O - x_vol - x_mag;
19 end
20
21 Q_o = alpha.*Q./(1+alpha);
22 Q_u = Q./(1+alpha);
23 V_o = alpha.*V./(1+alpha);
24 V_u = V./(1+alpha);
25 W_mag = W.*x_mag;
26 Q_o_mag = alpha.*Q_mag./(1+alpha);
27 Q_u_mag = Q_mag./(1+alpha);
28
29 f1_rho_o = (1./V_o).*((1 + K_u.*V_u.*x_mag.*x_ash./Q_mag).*W - Q_o.*(rho_o) - (Q_u +
K_u.*V_u.*x_ash).*rho_u);
30 f1_rho_u = (1./V_u).*((1 - K_o.*V_o.*x_mag.*x_C./Q_mag).*W - (Q_o - K_o.*V_o.*x_C).
*rho_o - Q_u.*(rho_u));
31 f2_rho_o = (1./V_o).*((1 + K_u.*V_u.*x_mag.*x_ash./Q_mag).*W - Q_o.*(rho_o + (h./2).
*f1_rho_o) - (Q_u + K_u.*V_u.*x_ash).*rho_u);
32 f2_rho_u = (1./V_u).*((1 - K_o.*V_o.*x_mag.*x_C./Q_mag).*W - (Q_o - K_o.*V_o.*x_C).
*rho_o - Q_u.*(rho_u + (h./2).*f1_rho_u));
33 f3_rho_o = (1./V_o).*((1 + K_u.*V_u.*x_mag.*x_ash./Q_mag).*W - Q_o.*(rho_o + (h./2).
*f2_rho_o) - (Q_u + K_u.*V_u.*x_ash).*rho_u);
34 f3_rho_u = (1./V_u).*((1 - K_o.*V_o.*x_mag.*x_C./Q_mag).*W - (Q_o - K_o.*V_o.*x_C).
*rho_o - Q_u.*(rho_u + (h./2).*f2_rho_u));
35 f4_rho_o = (1./V_o).*((1 + K_u.*V_u.*x_mag.*x_ash./Q_mag).*W - Q_o.*(rho_o + h.
*f3_rho_o) - (Q_u + K_u.*V_u.*x_ash).*rho_u);
36 f4_rho_u = (1./V_u).*((1 - K_o.*V_o.*x_mag.*x_C./Q_mag).*W - (Q_o - K_o.*V_o.*x_C).
*rho_o - Q_u.*(rho_u + h.*f3_rho_u));
37 rhon_o = rho_o + h.*(f1_rho_o + 2.*f2_rho_o + 2.*f3_rho_o + f4_rho_o)./6;

```

```

38 rhon_u = rho_u + h.*(f1_rho_u + 2.*f2_rho_u + 2.*f3_rho_u + f4_rho_u)./6;
39
40 f1_rho_o = rhon_o - rho_o;
41 f1_rho_u = rhon_u - rho_u;
42
43 f1_o_ash = (1./(V_o.*rho_o)).*(W.*x_ash - Q_o.*rho_o.*x_o_ash - Q_u.*rho_u.*x_u_ash
- V_o.*x_o_ash.*f1_rho_o - V_u.*x_u_ash.*f1_rho_u - V_u.*rho_u.*(K_u_ash.*(rho_ash -
rho_mag).*(x_ash - x_u_ash)));
44 f1_u_ash = (1./(V_u.*rho_u)).*(W.*x_ash - Q_o.*rho_o.*x_o_ash - Q_u.*rho_u.*x_u_ash
- V_o.*x_o_ash.*f1_rho_o - V_o.*rho_o.*(K_o_ash.*(rho_mag - rho_ash).*(x_ash - x_o_ash))
- V_u.*x_u_ash.*f1_rho_u);
45 f2_o_ash = (1./(V_o.*rho_o)).*(W.*x_ash - Q_o.*rho_o.*(x_o_ash + (h./2).*f1_o_ash) -
Q_u.*rho_u.*x_u_ash - V_o.*(x_o_ash + (h./2).*f1_o_ash).*f1_rho_o - V_u.*x_u_ash.*
*f1_rho_u - V_u.*rho_u.*(K_u_ash.*(rho_ash - rho_mag).*(x_ash - x_u_ash)));
46 f2_u_ash = (1./(V_u.*rho_u)).*(W.*x_ash - Q_o.*rho_o.*x_o_ash - Q_u.*rho_u.*(x_u_ash
+ (h./2).*f1_u_ash) - V_o.*x_o_ash.*f1_rho_o - V_o.*rho_o.*(K_o_ash.*(rho_mag -
rho_ash).*(x_ash - x_o_ash)) - V_u.*(x_u_ash + (h./2).*f1_u_ash).*f1_rho_u);
47 f3_o_ash = (1./(V_o.*rho_o)).*(W.*x_ash - Q_o.*rho_o.*(x_o_ash + (h./2).*f2_o_ash) -
Q_u.*rho_u.*x_u_ash - V_o.*(x_o_ash + (h./2).*f2_o_ash).*f1_rho_o - V_u.*x_u_ash.*
*f1_rho_u - V_u.*rho_u.*(K_u_ash.*(rho_ash - rho_mag).*(x_ash - x_u_ash)));
48 f3_u_ash = (1./(V_u.*rho_u)).*(W.*x_ash - Q_o.*rho_o.*x_o_ash - Q_u.*rho_u.*(x_u_ash
+ (h./2).*f2_u_ash) - V_o.*x_o_ash.*f1_rho_o - V_o.*rho_o.*(K_o_ash.*(rho_mag -
rho_ash).*(x_ash - x_o_ash)) - V_u.*(x_u_ash + (h./2).*f2_u_ash).*f1_rho_u);
49 f4_o_ash = (1./(V_o.*rho_o)).*(W.*x_ash - Q_o.*rho_o.*(x_o_ash + h.*f3_o_ash) - Q_u.*
rho_u.*x_u_ash - V_o.*(x_o_ash + h.*f3_o_ash).*f1_rho_o - V_u.*x_u_ash.*f1_rho_u - V_u.*
rho_u.*(K_u_ash.*(rho_ash - rho_mag).*(x_ash - x_u_ash)));
50 f4_u_ash = (1./(V_u.*rho_u)).*(W.*x_ash - Q_o.*rho_o.*x_o_ash - Q_u.*rho_u.*(x_u_ash
+ h.*f3_u_ash) - V_o.*x_o_ash.*f1_rho_o - V_o.*rho_o.*(K_o_ash.*(rho_mag - rho_ash).*(
x_ash - x_o_ash)) - V_u.*(x_u_ash + h.*f3_u_ash).*f1_rho_u);
51 xn_o_ash = x_o_ash + (h.*(f1_o_ash + 2*f2_o_ash + 2*f3_o_ash + f4_o_ash))/6;
52 xn_u_ash = x_u_ash + (h.*(f1_u_ash + 2*f2_u_ash + 2*f3_u_ash + f4_u_ash))/6;
53
54 f1_o_S = (1./(V_o.*rho_o)).*(W.*x_S - Q_o.*rho_o.*x_o_S - Q_u.*rho_u.*x_u_S - V_o.*
x_o_S.*f1_rho_o - V_u.*x_u_S.*f1_rho_u - V_u.*rho_u.*(K_u_S.*(rho_S - rho_mag).*(x_S -
x_u_S)));
55 f1_u_S = (1./(V_u.*rho_u)).*(W.*x_S - Q_o.*rho_o.*x_o_S - Q_u.*rho_u.*x_u_S - V_o.*
x_o_S.*f1_rho_o - V_o.*rho_o.*(K_o_S.*(rho_mag - rho_S).*(x_S - x_o_S)) - V_u.*x_u_S.*
*f1_rho_u);
56 f2_o_S = (1./(V_o.*rho_o)).*(W.*x_S - Q_o.*rho_o.*(x_o_S + (h./2).*f1_o_S) - Q_u.*
rho_u.*x_u_S - V_o.*(x_o_S + (h./2).*f1_o_S).*f1_rho_o - V_u.*x_u_S.*f1_rho_u - V_u.*
rho_u.*(K_u_S.*(rho_S - rho_mag).*(x_S - x_u_S)));
57 f2_u_S = (1./(V_u.*rho_u)).*(W.*x_S - Q_o.*rho_o.*x_o_S - Q_u.*rho_u.*(x_u_S + (h.
/2).*f1_u_S) - V_o.*x_o_S.*f1_rho_o - V_o.*rho_o.*(K_o_S.*(rho_mag - rho_S).*(x_S -
x_o_S)) - V_u.*(x_u_S + (h./2).*f1_u_S).*f1_rho_u);
58 f3_o_S = (1./(V_o.*rho_o)).*(W.*x_S - Q_o.*rho_o.*(x_o_S + (h./2).*f2_o_S) - Q_u.*
rho_u.*x_u_S - V_o.*(x_o_S + (h./2).*f2_o_S).*f1_rho_o - V_u.*x_u_S.*f1_rho_u - V_u.*
rho_u.*(K_u_S.*(rho_S - rho_mag).*(x_S - x_u_S)));
59 f3_u_S = (1./(V_u.*rho_u)).*(W.*x_S - Q_o.*rho_o.*x_o_S - Q_u.*rho_u.*(x_u_S + (h.
/2).*f2_u_S) - V_o.*x_o_S.*f1_rho_o - V_o.*rho_o.*(K_o_S.*(rho_mag - rho_S).*(x_S -
x_o_S)) - V_u.*(x_u_S + (h./2).*f2_u_S).*f1_rho_u);
60 f4_o_S = (1./(V_o.*rho_o)).*(W.*x_S - Q_o.*rho_o.*(x_o_S + h.*f3_o_S) - Q_u.*rho_u.*

```

```

*x_u_S - V_o.*(x_o_S + h.*f3_o_S).*f1_rho_o - V_u.*x_u_S.*f1_rho_u - V_u.*rho_u.*(K_u_S.*
*(rho_S - rho_mag).*(x_S - x_u_S)));
61 f4_u_S = (1./(V_u.*rho_u)).*(W.*x_S - Q_o.*rho_o.*x_o_S - Q_u.*rho_u.*(x_u_S + h.*
*f3_u_S) - V_o.*x_o_S.*f1_rho_o - V_o.*rho_o.*(K_o_S.*(rho_mag - rho_S).*(x_S - x_o_S))
- V_u.*(x_u_S + h.*f3_u_S).*f1_rho_u);
62 xn_o_S = x_o_S + (h*(f1_o_S + 2*f2_o_S + 2*f3_o_S + f4_o_S))/6;
63 xn_u_S = x_u_S + (h*(f1_u_S + 2*f2_u_S + 2*f3_u_S + f4_u_S))/6;
64
65 f1_o_H2O = (1./(V_o.*rho_o)).*(W.*x_H2O - Q_o.*rho_o.*x_o_H2O - Q_u.*rho_u.*x_u_H2O
- V_o.*x_o_H2O.*f1_rho_o - V_u.*x_u_H2O.*f1_rho_u - V_u.*rho_u.*(K_u_H2O.*(rho_H2O -
rho_mag).*(x_H2O - x_u_H2O)));
66 f1_u_H2O = (1./(V_u.*rho_u)).*(W.*x_H2O - Q_o.*rho_o.*x_o_H2O - Q_u.*rho_u.*x_u_H2O
- V_o.*x_o_H2O.*f1_rho_o - V_o.*rho_o.*(K_o_H2O.*(rho_mag - rho_H2O).*(x_H2O - x_o_H2O))
- V_u.*x_u_H2O.*f1_rho_u);
67 f2_o_H2O = (1./(V_o.*rho_o)).*(W.*x_H2O - Q_o.*rho_o.*(x_o_H2O + (h./2).*f1_o_H2O) -
Q_u.*rho_u.*x_u_H2O - V_o.*(x_o_H2O + (h./2).*f1_o_H2O).*f1_rho_o - V_u.*x_u_H2O.*
*f1_rho_u - V_u.*rho_u.*(K_u_H2O.*(rho_H2O - rho_mag).*(x_H2O - x_u_H2O)));
68 f2_u_H2O = (1./(V_u.*rho_u)).*(W.*x_H2O - Q_o.*rho_o.*x_o_H2O - Q_u.*rho_u.*(x_u_H2O
+ (h./2).*f1_u_H2O) - V_o.*x_o_H2O.*f1_rho_o - V_o.*rho_o.*(K_o_H2O.*(rho_mag -
rho_H2O).*(x_H2O - x_o_H2O)) - V_u.*(x_u_H2O + (h./2).*f1_u_H2O).*f1_rho_u);
69 f3_o_H2O = (1./(V_o.*rho_o)).*(W.*x_H2O - Q_o.*rho_o.*(x_o_H2O + (h./2).*f2_o_H2O) -
Q_u.*rho_u.*x_u_H2O - V_o.*(x_o_H2O + (h./2).*f2_o_H2O).*f1_rho_o - V_u.*x_u_H2O.*
*f1_rho_u - V_u.*rho_u.*(K_u_H2O.*(rho_H2O - rho_mag).*(x_H2O - x_u_H2O)));
70 f3_u_H2O = (1./(V_u.*rho_u)).*(W.*x_H2O - Q_o.*rho_o.*x_o_H2O - Q_u.*rho_u.*(x_u_H2O
+ (h./2).*f2_u_H2O) - V_o.*x_o_H2O.*f1_rho_o - V_o.*rho_o.*(K_o_H2O.*(rho_mag -
rho_H2O).*(x_H2O - x_o_H2O)) - V_u.*(x_u_H2O + (h./2).*f2_u_H2O).*f1_rho_u);
71 f4_o_H2O = (1./(V_o.*rho_o)).*(W.*x_H2O - Q_o.*rho_o.*(x_o_H2O + h.*f3_o_H2O) - Q_u.*
rho_u.*x_u_H2O - V_o.*(x_o_H2O + h.*f3_o_H2O).*f1_rho_o - V_u.*x_u_H2O.*f1_rho_u - V_u.*
rho_u.*(K_u_H2O.*(rho_H2O - rho_mag).*(x_H2O - x_u_H2O)));
72 f4_u_H2O = (1./(V_u.*rho_u)).*(W.*x_H2O - Q_o.*rho_o.*x_o_H2O - Q_u.*rho_u.*(x_u_H2O
+ h.*f3_u_H2O) - V_o.*x_o_H2O.*f1_rho_o - V_o.*rho_o.*(K_o_H2O.*(rho_mag - rho_H2O).*(
x_H2O - x_o_H2O)) - V_u.*(x_u_H2O + h.*f3_u_H2O).*f1_rho_u);
73 xn_o_H2O = x_o_H2O + (h*(f1_o_H2O + 2*f2_o_H2O + 2*f3_o_H2O + f4_o_H2O))/6;
74 xn_u_H2O = x_u_H2O + (h*(f1_u_H2O + 2*f2_u_H2O + 2*f3_u_H2O + f4_u_H2O))/6;
75
76 f1_o_vol = (1./(V_o.*rho_o)).*(W.*x_vol - Q_o.*rho_o.*x_o_vol - Q_u.*rho_u.*x_u_vol
- V_o.*x_o_vol.*f1_rho_o - V_u.*x_u_vol.*f1_rho_u - V_u.*rho_u.*(K_u_vol.*(rho_vol -
rho_mag).*(x_vol - x_u_vol)));
77 f1_u_vol = (1./(V_u.*rho_u)).*(W.*x_vol - Q_o.*rho_o.*x_o_vol - Q_u.*rho_u.*x_u_vol
- V_o.*x_o_vol.*f1_rho_o - V_o.*rho_o.*(K_o_vol.*(rho_mag - rho_vol).*(x_vol - x_o_vol))
- V_u.*x_u_vol.*f1_rho_u);
78 f2_o_vol = (1./(V_o.*rho_o)).*(W.*x_vol - Q_o.*rho_o.*(x_o_vol + (h./2).*f1_o_vol) -
Q_u.*rho_u.*x_u_vol - V_o.*(x_o_vol + (h./2).*f1_o_vol).*f1_rho_o - V_u.*x_u_vol.*
*f1_rho_u - V_u.*rho_u.*(K_u_vol.*(rho_vol - rho_mag).*(x_vol - x_u_vol)));
79 f2_u_vol = (1./(V_u.*rho_u)).*(W.*x_vol - Q_o.*rho_o.*x_o_vol - Q_u.*rho_u.*(x_u_vol
+ (h./2).*f1_u_vol) - V_o.*x_o_vol.*f1_rho_o - V_o.*rho_o.*(K_o_vol.*(rho_mag -
rho_vol).*(x_vol - x_o_vol)) - V_u.*(x_u_vol + (h./2).*f1_u_vol).*f1_rho_u);
80 f3_o_vol = (1./(V_o.*rho_o)).*(W.*x_vol - Q_o.*rho_o.*(x_o_vol + (h./2).*f2_o_vol) -
Q_u.*rho_u.*x_u_vol - V_o.*(x_o_vol + (h./2).*f2_o_vol).*f1_rho_o - V_u.*x_u_vol.*
*f1_rho_u - V_u.*rho_u.*(K_u_vol.*(rho_vol - rho_mag).*(x_vol - x_u_vol)));
81 f3_u_vol = (1./(V_u.*rho_u)).*(W.*x_vol - Q_o.*rho_o.*x_o_vol - Q_u.*rho_u.*(x_u_vol

```

```

+ (h./2).*f2_u_vol) - V_o.*x_o_vol.*f1_rho_o - V_o.*rho_o.*(K_o_vol.*(rho_mag -
rho_vol).*(x_vol - x_o_vol)) - V_u.*(x_u_vol + (h./2).*f2_u_vol).*f1_rho_u);
82 f4_o_vol = (1./(V_o.*rho_o)).*(W.*x_vol - Q_o.*rho_o.*(x_o_vol + h.*f3_o_vol) - Q_u.
*rho_u.*x_u_vol - V_o.*(x_o_vol + h.*f3_o_vol).*f1_rho_o - V_u.*x_u_vol.*f1_rho_u - V_u.
*rho_u.*(K_u_vol.*(rho_vol - rho_mag).*(x_vol - x_u_vol)));
83 f4_u_vol = (1./(V_u.*rho_u)).*(W.*x_vol - Q_o.*rho_o.*x_o_vol - Q_u.*rho_u.*(x_u_vol
+ h.*f3_u_vol) - V_o.*x_o_vol.*f1_rho_o - V_o.*rho_o.*(K_o_vol.*(rho_mag - rho_vol).*(
x_vol - x_o_vol)) - V_u.*(x_u_vol + h.*f3_u_vol).*f1_rho_u);
84 xn_o_vol = x_o_vol + (h*(f1_o_vol + 2*f2_o_vol + 2*f3_o_vol + f4_o_vol))/6;
85 xn_u_vol = x_u_vol + (h*(f1_u_vol + 2*f2_u_vol + 2*f3_u_vol + f4_u_vol))/6;
86
87 f1_o_mag = (1./(V_o.*rho_o)).*(W.*x_mag - Q_o.*rho_o.*x_o_mag - Q_u.*rho_u.*x_u_mag
- V_o.*x_o_mag.*f1_rho_o - V_u.*x_u_mag.*f1_rho_u - V_u.*rho_u.*(K_u_mag.*(delta_mag).*(
x_mag - x_u_mag)));
88 f1_u_mag = (1./(V_u.*rho_u)).*(W.*x_mag - Q_o.*rho_o.*x_o_mag - Q_u.*rho_u.*x_u_mag
- V_o.*x_o_mag.*f1_rho_o - V_o.*rho_o.*(K_o_mag.*(delta_mag).*(x_mag - x_o_mag)) - V_u.
*x_u_mag.*f1_rho_u);
89 f2_o_mag = (1./(V_o.*rho_o)).*(W.*x_mag - Q_o.*rho_o.*(x_o_mag + (h./2).*f1_o_mag)
- Q_u.*rho_u.*x_u_mag - V_o.*(x_o_mag + (h./2).*f1_o_mag).*f1_rho_o - V_u.*x_u_mag.
*f1_rho_u - V_u.*rho_u.*(K_u_mag.*(delta_mag).*(x_mag - x_u_mag)));
90 f2_u_mag = (1./(V_u.*rho_u)).*(W.*x_mag - Q_o.*rho_o.*x_o_mag - Q_u.*rho_u.*(x_u_mag
+ (h./2).*f1_u_mag) - V_o.*x_o_mag.*f1_rho_o - V_o.*rho_o.*(K_o_mag.*(delta_mag).*(x_mag
- x_o_mag)) - V_u.*(x_u_mag + (h./2).*f1_u_mag).*f1_rho_u);
91 f3_o_mag = (1./(V_o.*rho_o)).*(W.*x_mag - Q_o.*rho_o.*(x_o_mag + (h./2).*f2_o_mag)
- Q_u.*rho_u.*x_u_mag - V_o.*(x_o_mag + (h./2).*f2_o_mag).*f1_rho_o - V_u.*x_u_mag.
*f1_rho_u - V_u.*rho_u.*(K_u_mag.*(delta_mag).*(x_mag - x_u_mag)));
92 f3_u_mag = (1./(V_u.*rho_u)).*(W.*x_mag - Q_o.*rho_o.*x_o_mag - Q_u.*rho_u.*(x_u_mag
+ (h./2).*f2_u_mag) - V_o.*x_o_mag.*f1_rho_o - V_o.*rho_o.*(K_o_mag.*(delta_mag).*(x_mag
- x_o_mag)) - V_u.*(x_u_mag + (h./2).*f2_u_mag).*f1_rho_u);
93 f4_o_mag = (1./(V_o.*rho_o)).*(W.*x_mag - Q_o.*rho_o.*(x_o_mag + h.*f3_o_mag) -
Q_u.*rho_u.*x_u_mag - V_o.*(x_o_mag + h.*f3_o_mag).*f1_rho_o - V_u.*x_u_mag.*f1_rho_u -
V_u.*rho_u.*(K_u_mag.*(delta_mag).*(x_mag - x_u_mag)));
94 f4_u_mag = (1./(V_u.*rho_u)).*(W.*x_mag - Q_o.*rho_o.*x_o_mag - Q_u.*rho_u.*(x_u_mag
+ h.*f3_u_mag) - V_o.*x_o_mag.*f1_rho_o - V_o.*rho_o.*(K_o_mag.*(delta_mag).*(x_mag -
x_o_mag)) - V_u.*(x_u_mag + h.*f3_u_mag).*f1_rho_u);
95 xn_o_mag = x_o_mag + (h*(f1_o_mag + 2*f2_o_mag + 2*f3_o_mag + f4_o_mag))/6;
96 xn_u_mag = x_u_mag + (h*(f1_u_mag + 2*f2_u_mag + 2*f3_u_mag + f4_u_mag))/6;
97
98 W_o = rhon_o.*Q_o;
99 W_u = rhon_u.*Q_u;
100 W_o_mag = W_o.*xn_o_mag;
101 W_u_mag = W_u.*xn_u_mag;
102 rho_mag_out = (W_o_mag+W_u_mag)./(Q_o_mag+Q_u_mag);
103
104 if xn_o_mag > 1
105     xn_o_mag = 1;
106     xn_o_ash = 0;
107     xn_o_S = 0;
108     xn_o_H2O = 0;
109     xn_o_vol = 0;
110

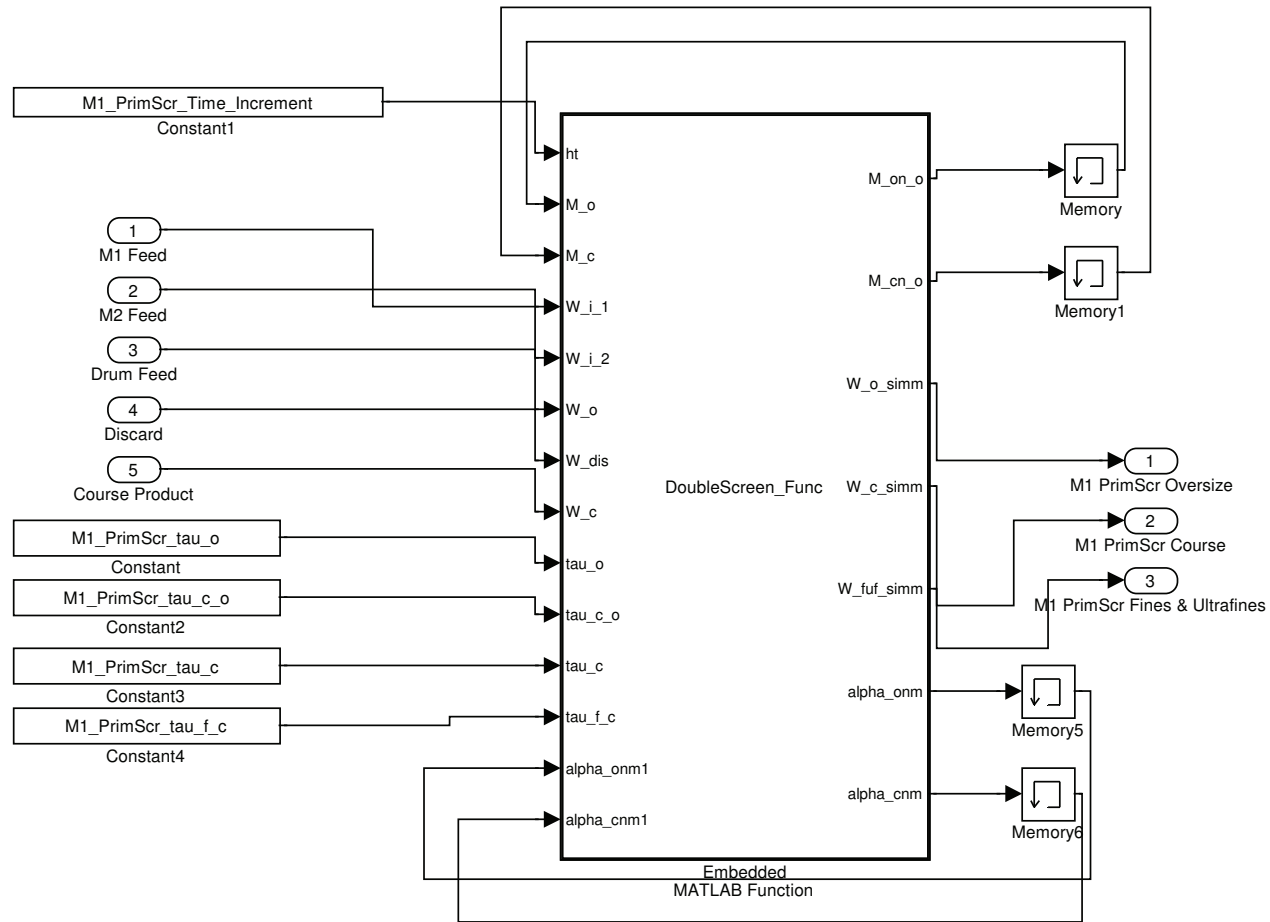
```

```
111     x_o_asha = 0;
112     x_o_Sa = 0;
113     x_o_H2Oa = 0;
114     x_o_vola = 0;
115     x_o_Ca = 0;
116 elseif xn_o_mag < 0
117     xn_o_mag = 0;
118     xn_o_ash = 0;
119     xn_o_S = 0;
120     xn_o_H2O = 0;
121     xn_o_vol = 0;
122
123     x_o_asha = 0;
124     x_o_Sa = 0;
125     x_o_H2Oa = 0;
126     x_o_vola = 0;
127     x_o_Ca = 0;
128 else
129     x_o_asha = 100.*xn_o_ash./(1-xn_o_mag);
130     x_o_Sa = 100.*xn_o_S./(1-xn_o_mag);
131     x_o_H2Oa = 100.*xn_o_H2O./(1-xn_o_mag);
132     x_o_vola = 100.*xn_o_vol./(1-xn_o_mag);
133     x_o_Ca = 100-x_o_asha-x_o_Sa-x_o_H2Oa-x_o_vola;
134 end
135
136 if xn_u_mag > 1
137     xn_u_mag = 1;
138     xn_u_ash = 0;
139     xn_u_S = 0;
140     xn_u_H2O = 0;
141     xn_u_vol = 0;
142
143     x_u_asha = 0;
144     x_u_Sa = 0;
145     x_u_H2Oa = 0;
146     x_u_vola = 0;
147     x_u_Ca = 0;
148 elseif xn_u_mag < 0
149     xn_u_mag = 0;
150     xn_u_ash = 0;
151     xn_u_S = 0;
152     xn_u_H2O = 0;
153     xn_u_vol = 0;
154
155     x_u_asha = 0;
156     x_u_Sa = 0;
157     x_u_H2Oa = 0;
158     x_u_vola = 0;
159     x_u_Ca = 0;
160 else
161     x_u_asha = 100.*xn_u_ash./(1-xn_u_mag);
```



```
162     x_u_Sa = 100.*xn_u_S./(1-xn_u_mag);
163     x_u_H2Oa = 100.*xn_u_H2O./(1-xn_u_mag);
164     x_u_vola = 100.*xn_u_vol./(1-xn_u_mag);
165     x_u_Ca = 100-x_u_asha-x_u_Sa-x_u_H2Oa-x_u_vola;
166 end
167
168 if zero_feed == 1
169     xn_o_mag = 1;
170     xn_o_ash = 0;
171     xn_o_S = 0;
172     xn_o_H2O = 0;
173     xn_o_vol = 0;
174
175     x_o_asha = 0;
176     x_o_Sa = 0;
177     x_o_H2Oa = 0;
178     x_o_vola = 0;
179     x_o_Ca = 0;
180
181     xn_u_mag = 1;
182     xn_u_ash = 0;
183     xn_u_S = 0;
184     xn_u_H2O = 0;
185     xn_u_vol = 0;
186
187     x_u_asha = 0;
188     x_u_Sa = 0;
189     x_u_H2Oa = 0;
190     x_u_vola = 0;
191     x_u_Ca = 0;
192 end
```

### DMSPlantVer2Print/Module 1 Primary Screen



C:\MATLAB701\work\DMS Plant\Final\DMSPlantVer2Print.mdl

```

1 function [M_on_o, M_cn_o, W_o_simm, W_c_simm, W_fuf_simm, alpha_onm, alpha_cnm]
= DoubleScreen_Func(ht, M_o, M_c, W_i_1, W_i_2, W_o, W_dis, W_c, tau_o, tau_c_o, tau_c,
tau_f_c, alpha_onm1, alpha_cnm1 )
2 %DoubleScreen_Func Computes the particle sized product feed rates for a double deck
screen
3 %using fourth-order runge kutta approximation
4 W_i = W_i_1;
5 alpha_o = (W_o./2./W_i).^(1./10);
6 if alpha_o > 1
7     alpha_o = alpha_onm1;
8 end
9 alpha_onm = alpha_o;
10
11 alpha_c = ((W_c+0.33.*W_dis)./2./W_i).^(1./10);
12 if alpha_c > 1
13     alpha_c = alpha_cnm1;
14 end
15 alpha_cnm = alpha_c;
16
17 W_o_sim = zeros(10,1);
18 W_c_sim = zeros(10,1);
19 W_ct_sim = zeros(10,1);
20 W_f_sim = zeros(10,1);
21 f1_M_o = zeros(10,1);
22 f2_M_o = zeros(10,1);
23 f3_M_o = zeros(10,1);
24 f4_M_o = zeros(10,1);
25 f1_M_c = zeros(10,1);
26 f2_M_c = zeros(10,1);
27 f3_M_c = zeros(10,1);
28 f4_M_c = zeros(10,1);
29 M_on_o = zeros(10,1);
30 M_cn_o = zeros(10,1);
31
32 for J = 1:10,
33
34     if J > 1
35         f1_M_o(J,1) = W_o_sim(J-1,1) - alpha_o.*M_o(J,1)./tau_o - (1 - alpha_o).*M_o
(J,1)./tau_c_o;
36         f2_M_o(J,1) = W_o_sim(J-1,1) - alpha_o.*(M_o(J,1) + (ht./2).*f1_M_o(J,1)).
/tau_o - (1 - alpha_o).(M_o(J,1) + (ht./2).*f1_M_o(J,1))./tau_c_o;
37         f3_M_o(J,1) = W_o_sim(J-1,1) - alpha_o.*(M_o(J,1) + (ht./2).*f2_M_o(J,1)).
/tau_o - (1 - alpha_o).(M_o(J,1) + (ht./2).*f2_M_o(J,1))./tau_c_o;
38         f4_M_o(J,1) = W_o_sim(J-1,1) - alpha_o.*(M_o(J,1) + ht.*f3_M_o(J,1))./tau_o -
(1 - alpha_o).(M_o(J,1) + ht.*f3_M_o(J,1))./tau_c_o;
39     else
40         f1_M_o(J,1) = W_i - alpha_o.*M_o(J,1)./tau_o - (1 - alpha_o).*M_o(J,1).
/tau_c_o;
41         f2_M_o(J,1) = W_i - alpha_o.*(M_o(J,1) + (ht./2).*f1_M_o(J,1))./tau_o - (1 -
alpha_o).(M_o(J,1) + (ht./2).*f1_M_o(J,1))./tau_c_o;
42         f3_M_o(J,1) = W_i - alpha_o.*(M_o(J,1) + (ht./2).*f2_M_o(J,1))./tau_o - (1 -

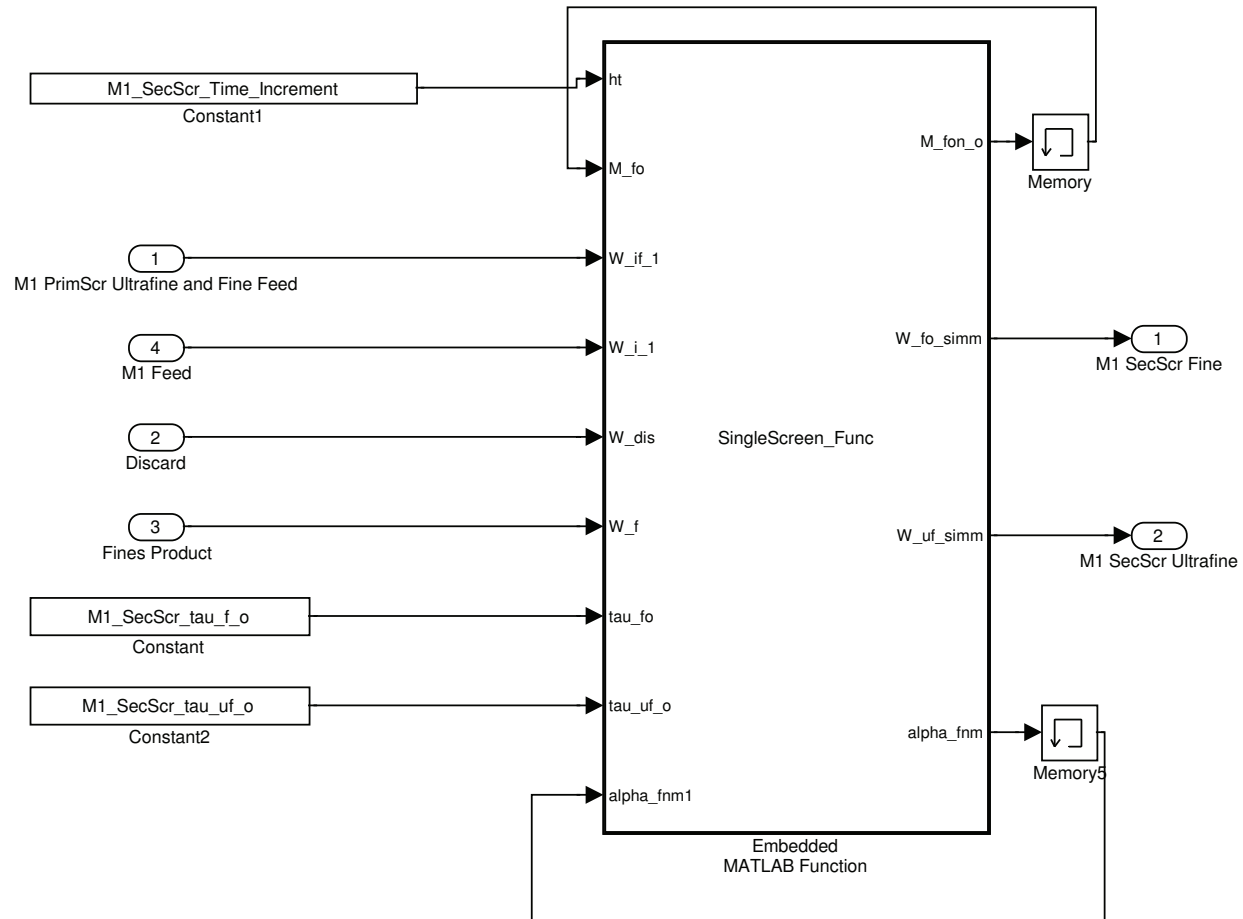
```

```

alpha_o).(M_o(J,1) + (ht./2).*f2_M_o(J,1))./tau_c_o;
43     f4_M_o(J,1) = W_i - alpha_o.*(M_o(J,1) + ht.*f3_M_o(J,1))./tau_o - (1 -
alpha_o).(M_o(J,1) + ht.*f3_M_o(J,1))./tau_c_o;
44     end
45     M_on_o(J,1) = M_o(J,1) + ht.*(f1_M_o(J,1) + 2.*f2_M_o(J,1) + 2.*f3_M_o(J,1) +
f4_M_o(J,1))./6;
46
47     W_o_sim(J,1) = alpha_o.*M_on_o(J,1)./tau_o;
48     W_c_sim(J,1) = (1 - alpha_o).*M_on_o(J,1)./tau_c_o;
49
50
51     if J > 1
52         f1_M_c(J,1) = W_ct_sim(J-1,1) + W_c_sim(J-1,1) - alpha_c.*M_c(J,1)./tau_c -
(1 - alpha_c).*M_c(J,1)./tau_f_c;
53         f2_M_c(J,1) = W_ct_sim(J-1,1) + W_c_sim(J-1,1) - alpha_c.*(M_c(J,1) + (ht.
/2).*f1_M_c(J,1))./tau_c - (1 - alpha_c).(M_c(J,1) + (ht./2).*f1_M_c(J,1))./tau_f_c;
54         f3_M_c(J,1) = W_ct_sim(J-1,1) + W_c_sim(J-1,1) - alpha_c.*(M_c(J,1) + (ht.
/2).*f2_M_c(J,1))./tau_c - (1 - alpha_c).(M_c(J,1) + (ht./2).*f2_M_c(J,1))./tau_f_c;
55         f4_M_c(J,1) = W_ct_sim(J-1,1) + W_c_sim(J-1,1) - alpha_c.*(M_c(J,1) + ht.
*f3_M_c(J,1))./tau_c - (1 - alpha_c).(M_c(J,1) + ht.*f3_M_c(J,1))./tau_f_c;
56     else
57         f1_M_c(J,1) = W_c_sim(J,1) - alpha_c.*M_c(J,1)./tau_c - (1 - alpha_c).*M_c(J,
1)./tau_f_c;
58         f2_M_c(J,1) = W_c_sim(J,1) - alpha_c.*(M_c(J,1) + (ht./2).*f1_M_c(J,1)).
/tau_c - (1 - alpha_c).(M_c(J,1) + (ht./2).*f1_M_c(J,1))./tau_f_c;
59         f3_M_c(J,1) = W_c_sim(J,1) - alpha_c.*(M_c(J,1) + (ht./2).*f2_M_c(J,1)).
/tau_c - (1 - alpha_c).(M_c(J,1) + (ht./2).*f2_M_c(J,1))./tau_f_c;
60         f4_M_c(J,1) = W_c_sim(J,1) - alpha_c.*(M_c(J,1) + ht.*f3_M_c(J,1))./tau_c -
(1 - alpha_c).(M_c(J,1) + ht.*f3_M_c(J,1))./tau_f_c;
61     end
62     M_cn_o(J,1) = M_c(J,1) + ht.*(f1_M_c(J,1) + 2.*f2_M_c(J,1) + 2.*f3_M_c(J,1) +
f4_M_c(J,1))./6;
63
64     W_ct_sim(J,1) = alpha_c.*M_cn_o(J,1)./tau_c;
65     W_f_sim(J,1) = (1 - alpha_c).*M_cn_o(J,1)./tau_f_c;
66
67 end
68
69 W_c_sum = 0;
70 W_f_sum = 0;
71 for J=1:10,
72     W_c_sum = W_c_sum + W_c_sim(J,1);
73     W_f_sum = W_f_sum + W_f_sim(J,1);
74 end
75
76 W_o_simm = W_o_sim(10,1);
77 W_c_simm = W_ct_sim(10,1);
78 W_fuf_simm = W_f_sum;

```

DMSPlantVer2Print/Module 1 Secondary Screen



C:\MATLAB701\work\DMS Plant\Final\DMSPlantVer2Print.mdl

```

1 function [M_fon_o, W_fo_simm, W_uf_simm, alpha_fnm] = SingleScreen_Func(ht,
M_fo, W_if_1, W_i_1, W_dis, W_f, tau_fo, tau_uf_o, alpha_fnm1 )
2 %SingleScreen_Func Computes the particle sized product feed rates for a single deck
screen
3 %using fourth-order runge kutta approximation
4 W_i = W_i_1;
5 alpha_f = ((W_f+0.65.*0.4.*W_dis)./2./W_i).^(1./10);
6 if alpha_f > 1
7     alpha_f = alpha_fnm1;
8 end
9 alpha_fnm = alpha_f;
10
11 W_fo_sim = zeros(10,1);
12 W_uf_sim = zeros(10,1);
13 f1_M_fo = zeros(10,1);
14 f2_M_fo = zeros(10,1);
15 f3_M_fo = zeros(10,1);
16 f4_M_fo = zeros(10,1);
17 M_fon_o = zeros(10,1);
18
19 for J = 1:10,
20
21     if J > 1
22         f1_M_fo(J,1) = W_fo_sim(J-1,1) - alpha_f.*M_fo(J,1)./tau_fo - (1 - alpha_f).
*M_fo(J,1)./tau_uf_o;
23         f2_M_fo(J,1) = W_fo_sim(J-1,1) - alpha_f.*(M_fo(J,1) + (ht./2).*f1_M_fo(J,
1)).)/tau_fo - (1 - alpha_f).*(M_fo(J,1) + (ht./2).*f1_M_fo(J,1)).)/tau_uf_o;
24         f3_M_fo(J,1) = W_fo_sim(J-1,1) - alpha_f.*(M_fo(J,1) + (ht./2).*f2_M_fo(J,
1)).)/tau_fo - (1 - alpha_f).*(M_fo(J,1) + (ht./2).*f2_M_fo(J,1)).)/tau_uf_o;
25         f4_M_fo(J,1) = W_fo_sim(J-1,1) - alpha_f.*(M_fo(J,1) + ht.*f3_M_fo(J,1)).
/tau_fo - (1 - alpha_f).*(M_fo(J,1) + ht.*f3_M_fo(J,1)).)/tau_uf_o;
26     else
27         f1_M_fo(J,1) = W_if_1 - alpha_f.*M_fo(J,1)./tau_fo - (1 - alpha_f).*M_fo(J,
1)).)/tau_uf_o;
28         f2_M_fo(J,1) = W_if_1 - alpha_f.*(M_fo(J,1) + (ht./2).*f1_M_fo(J,1)).)/tau_fo
- (1 - alpha_f).*(M_fo(J,1) + (ht./2).*f1_M_fo(J,1)).)/tau_uf_o;
29         f3_M_fo(J,1) = W_if_1 - alpha_f.*(M_fo(J,1) + (ht./2).*f2_M_fo(J,1)).)/tau_fo
- (1 - alpha_f).*(M_fo(J,1) + (ht./2).*f2_M_fo(J,1)).)/tau_uf_o;
30         f4_M_fo(J,1) = W_if_1 - alpha_f.*(M_fo(J,1) + ht.*f3_M_fo(J,1)).)/tau_fo - (1
- alpha_f).*(M_fo(J,1) + ht.*f3_M_fo(J,1)).)/tau_uf_o;
31     end
32     M_fon_o(J,1) = M_fo(J,1) + ht.*(f1_M_fo(J,1) + 2.*f2_M_fo(J,1) + 2.*f3_M_fo(J,1)
+ f4_M_fo(J,1)).)/6;
33
34     W_fo_sim(J,1) = alpha_f.*M_fon_o(J,1)./tau_fo;
35     W_uf_sim(J,1) = (1 - alpha_f).*M_fon_o(J,1)./tau_uf_o;
36
37 end
38
39 W_uf_sum = 0;
40 for J=1:10,

```



```
41     W_uf_sum = W_uf_sum + W_uf_sim(J,1);  
42 end  
43  
44 W_fo_simm = W_fo_sim(10,1);  
45 W_uf_simm = W_uf_sum;
```

```
1 figure;
2 plot(FinesOutput(:,1),FinesOutput(:,2));
3 xlabel('Time (s)');
4 ylabel('Fines feedrate (kg/s)');
5 legend('Simulated fines output');
6 title('Simulated feedrate response for the single-deck screen');
7 grid on;
8
9 figure;
10 plot(MixMediumOutput(:,1),MixMediumOutput(:,2));
11 hold on
12 plot(MixMediumOutput(:,1),MixMediumOutput(:,3),'--r');
13 xlabel('Time (s)');
14 ylabel('Density (kg/m^3)');
15 legend('Measured medium density','Medium and ore mix density');
16 title('Simulated density response versus actual medium density for the mixing box');
17 grid on;
18
19 figure;
20 plot(FCRhoOutput(:,1),FCRhoOutput(:,2));
21 hold on
22 plot(FCRhoOutput(:,1),FCRhoOutput(:,3),'--r');
23 xlabel('Time (s)');
24 ylabel('Density (kg/m^3)');
25 legend('Overflow density','Underflow density');
26 title('Simulated density response for the fine cyclone');
27 grid on;
28
29 figure;
30 plot(FCxMagOutput(:,1),FCxMagOutput(:,2));
31 hold on
32 plot(FCxMagOutput(:,1),FCxMagOutput(:,3),'--r');
33 xlabel('Time (s)');
34 ylabel('Percentage medium (%)');
35 legend('Overflow medium','Underflow medium');
36 title('Simulated medium response for the fine cyclone');
37 grid on;
38
39 figure;
40 plot(FCxAshOutput(:,1),FCxAshOutput(:,2));
41 hold on
42 plot(FCxAshOutput(:,1),FCxAshOutput(:,3),'--r');
43 xlabel('Time (s)');
44 ylabel('Percentage ash (%)');
45 legend('Overflow ash','Underflow ash');
46 title('Simulated ash response for the fine cyclone');
47 grid on;
48
49 figure;
50 plot(FCxSOutput(:,1),FCxSOutput(:,2));
51 hold on
```



```
52 plot(FCxSOutput(:,1),FCxSOutput(:,3),'--r');
53 xlabel('Time (s)');
54 ylabel('Percentage sulphur (%)');
55 legend('Overflow sulphur','Underflow sulphur');
56 title('Simulated sulphur response for the fine cyclone');
57 grid on;
58
59 figure;
60 plot(FCxH2OOutput(:,1),FCxH2OOutput(:,2));
61 hold on
62 plot(FCxH2OOutput(:,1),FCxH2OOutput(:,3),'--r');
63 xlabel('Time (s)');
64 ylabel('Percentage moisture (%)');
65 legend('Overflow moisture','Underflow moisture');
66 title('Simulated moisture response for the fine cyclone');
67 grid on;
68
69 figure;
70 plot(FCxVolOutput(:,1),FCxVolOutput(:,2));
71 hold on
72 plot(FCxVolOutput(:,1),FCxVolOutput(:,3),'--r');
73 xlabel('Time (s)');
74 ylabel('Percentage volatiles (%)');
75 legend('Overflow volatiles','Underflow volatiles');
76 title('Simulated volatiles response for the fine cyclone');
77 grid on;
78
79 figure;
80 plot(FCxCOutput(:,1),FCxCOutput(:,2));
81 hold on
82 plot(FCxCOutput(:,1),FCxCOutput(:,3),'--r');
83 xlabel('Time (s)');
84 ylabel('Percentage carbon (%)');
85 legend('Overflow carbon','Underflow carbon');
86 title('Simulated carbon response for the fine cyclone');
87 grid on;
88
89 figure;
90 plot(SimulatedActualOutput(:,1),SimulatedActualOutput(:,2));
91 hold on
92 plot(SimulatedActualOutput(:,1),SimulatedActualOutput(:,3),'--r');
93 xlabel('Time (s)');
94 ylabel('Density (kg/m^3)');
95 legend('Measured medium density','Simulated medium density');
96 title('Simulated density response versus actual medium density for the DMS plant');
97 grid on;
```

## LIST OF TABLES

2.1	Measurements used to describe coal (Hayes, 2003:28). . . . .	6
2.2	Leeuwpan normal ash distributions per block (taken from Botha (2008:40)). . . . .	7
2.3	Various forces acting on a particle in motion through a liquid. . .	11
2.4	Example of details and calculations required for a partition curve (England <i>et al.</i> , 2002:51). . . . .	13
2.5	Different DMC equipment available from Multotec (Preptech, 2008:5). . . . .	26
2.6	DMC capacity table (England <i>et al.</i> , 2002:164). . . . .	26
4.1	Table indicating the description of the tag names taken from the production supervisory control and data acquisition system used for Leeuwpan DMS plant measurements. . . . .	81
5.1	Table showing single-deck screen parameter estimates. . . . .	93
5.2	Table showing double-deck screen parameter estimates. . . . .	93
5.3	Table showing magnetite water-addition parameter estimates. . .	95
5.4	Table showing mixing box parameter estimates. . . . .	95
5.5	Table showing DMC parameter estimates. . . . .	96
5.6	Table showing magnetite make-up corrected medium parameter estimates. . . . .	97
6.1	Laboratory results for fine cyclone circuit step test. . . . .	107

## LIST OF FIGURES

2.1	The influence of oxygen and hydrogen in coal transformation (Hayes, 2003:27). . . . .	5
2.2	Low volatile and medium volatile nuts and peas product specifications. . . . .	7
2.3	Lean coal product specifications. . . . .	8
2.4	LV and MV duff product specifications. . . . .	8
2.5	Nuts product specifications. . . . .	9
2.6	Steam power station coal specifications. . . . .	9
2.7	Free body diagram illustrating the different forces acting on a particle moving in a relative motion in a liquid. . . . .	10
2.8	Float and sink analysis illustration. . . . .	12
2.9	Example of a partition curve plotted from table 2.4. . . . .	14
2.10	Example of a washability curve (de Korte, 2006:16). . . . .	16
2.11	Diagram illustrating the geometry of a cyclone (Magwai and Bosman, 2007:95). . . . .	19
2.12	Spiral flow within a cyclone (England <i>et al.</i> , 2002:165). . . . .	19
2.13	Overflow and underflow medium relative density versus feed medium relative density (He and Laskowski, 1994:214). . . . .	21
2.14	Effect of feed inlet pressure on separation efficiency in a DMC (Mukherjee <i>et al.</i> , 2003:265). . . . .	22
2.15	Effect of feed pressure on magnetite relative density differential between the overflow and underflow (Mukherjee, Sripriya, Rao and Das, 2003:267). . . . .	22
2.16	Feed overflow to underflow flow rate ratio and its effect on separation efficiency and cutpoint shift (He and Laskowski, 1994:213). . . . .	23
2.17	Medium relative density and its effect on medium flow rate and overflow to underflow flow rate ratio (He and Laskowski, 1994:213). . . . .	24
2.18	The relationship between cutpoint shift ratio, particle size and medium-to-coal ratio (King and Juckes, 1984:153). . . . .	25
2.19	DMC diameter (represented as horizontal lines) and EPM versus ore particle size (Bosman and Engelbrecht, 1999:5). . . . .	27
2.20	Typical modern process flow diagram to treat a variety of size-spectrum coal feeds (King, 1999:16). . . . .	27
2.21	Dense medium drum with circulating medium circuit (Adapted from England <i>et al.</i> (2002:157)). . . . .	28
2.22	DMC with circulating medium circuit (Adapted from England <i>et al.</i> (2002:166)). . . . .	29

2.23	Relationship of screen efficiency and feed rate ((England <i>et al.</i> , 2002:66). . . . .	31
2.24	Typical operation of the Wemco drum (Wilkes, 2006:180). . . . .	32
2.25	Illustration of a Teska drum (England <i>et al.</i> , 2002:161). . . . .	33
2.26	Wet drum magnetic separator operating in co-current configuration (Rayner and Napier-Munn, 2003:163). . . . .	34
2.27	Illustration depicting the principle of density measurement by using gamma radiation (Lipták, 1995a:631). . . . .	35
2.28	Example of a pneumatic control valve (Lipták, 1995b:422). . . . .	36
2.29	Graphical representation of a differential pressure cell (Lipták, 1995a:553). . . . .	37
2.30	Illustration of on-line coal analysis (Lipták, 1995a:957). . . . .	38
2.31	Low-energy gamma-based radiation directed through a conveyor belt to determine ash content in coal (Watt and Sowerby, 1983:265). . . . .	39
2.32	Illustration of a pair production gauge (Watt and Sowerby, 1983:278). . . . .	39
2.33	Principles of a neutron-based coal analyser (Lipták, 1995a:957). . . . .	40
2.34	Measurement points for in-line ash monitor using a linear coal relative density to ash relationship (Mikhailm and Humeniuk, 1980:398). . . . .	41
2.35	Head making use of capacitance to measure moisture in solids (Lipták, 1995a:1082). . . . .	42
2.36	Moisture analyser using the microwave principle (Lipták, 1995a:1082). . . . .	42
2.37	Example of a size-by-size partition curve for a DMC (Napier-Munn, 1991:341). . . . .	44
2.38	Example of a DMC partitioned surface (Rao <i>et al.</i> , 2003:444). . . . .	45
3.1	General control framework (Craig and Henning, 2000:770). . . . .	50
3.2	Classes of system equations used for modelling for control (Brogan, 1991:13). . . . .	52
3.3	The system identification procedure (Ljung, 1987:9). . . . .	53
3.4	Model-based control strategy (Herbst <i>et al.</i> , 1992:22). . . . .	56
3.5	Illustration of the dynamic matrix control used by Chen <i>et al.</i> (2008:35). . . . .	57
3.6	APC survey results indicating main profit contributors for APC (Bauer and Craig, 2008:8). . . . .	60
3.7	Effect of APC on throughput and quality (Bauer and Craig, 2008:8). . . . .	60
4.1	Simplified representation of a single-deck screen. . . . .	63
4.2	Simplified representation of the mass distribution for a single-deck screen. . . . .	63

4.3	Simplified representation of a double-deck screen. . . . .	65
4.4	Simplified representation of the mass distribution for a double-deck screen. . . . .	67
4.5	Simplified representation of water-magnetite in-line mixing. . . . .	68
4.6	Simplified representation of a mixing box. . . . .	70
4.7	Simplified representation of a DMC. . . . .	71
4.8	Simplified representation of a corrected medium make-up tank. . . . .	79
4.9	Diagram combining different models of equipment for the fine section for module one DMS plant at Leeuwan. . . . .	82
5.1	Parameter estimation iteration (Adapted from Rathaba (2004:88))	91
5.2	Comparison of a plant model to an actual plant output . . . . .	92
5.3	Scatterplot illustrating relationship between double-deck screen feed and oversized material. . . . .	94
6.1	Leeuwan plant process flow diagram. . . . .	100
6.2	Yield over the month of October 2008. . . . .	101
6.3	FFT of the yield for October 2008. . . . .	101
6.4	Yield for an hour during October 2008. . . . .	102
6.5	FFT of the yield for an hour during October 2008. . . . .	103
6.6	Ash percentage of the peas product during October 2008. . . . .	104
6.7	FFT of the peas ash percentage for October 2008. . . . .	104
6.8	Ash percentage of the duff product during October 2008. . . . .	105
6.9	FFT of the duff ash percentage for October 2008. . . . .	105
6.10	FFT of the yield for October 2008. . . . .	106
6.11	Step test for fine cyclone circuit from module 1 DMS plant. . . . .	107
6.12	Simulation of the single- and double-deck screens. . . . .	109
6.13	Mass state over top deck for double-deck screen. . . . .	110
6.14	Mass state over bottom deck for double-deck screen. . . . .	110
6.15	Mass state over top deck for single-deck screen. . . . .	111
6.16	Simulated output versus actual output for the top deck of the double-deck screen. . . . .	112
6.17	Scatterplot of the simulated output and actual output for the top deck. . . . .	113
6.18	Comparison of feed into the double-deck screen and sum of feed rates exiting the screen. . . . .	114
6.19	Simulated screen responses for the density step test scenario. . . . .	115
6.20	Simulated response of the water-addition model. . . . .	116
6.21	Water-addition residual plot. . . . .	117
6.22	Whiteness test (95% confidence interval) for the water-addition model. . . . .	117

6.23 Independence test (95% confidence interval) for the water-addition model. . . . .	118
6.24 Simulated response of the mixing box output. . . . .	118
6.25 Feed components for the mixing box model. . . . .	119
6.26 Simulated overflow and underflow densities. . . . .	120
6.27 Simulated overflow and underflow medium percentages. . . . .	121
6.28 Percentage magnetite medium in the feed. . . . .	121
6.29 Simulated efficiency curve for the DMC using a theoretical steady-state model. . . . .	122
6.30 Simulated response of the overflow and underflow carbon mass component. . . . .	123
6.31 Simulated response of the overflow and underflow ash mass component. . . . .	124
6.32 Simulated response of the overflow and underflow sulphur mass component. . . . .	125
6.33 Simulated response of the overflow and underflow moisture mass component. . . . .	126
6.34 Simulated response of the overflow and underflow volatile mass component. . . . .	127
6.35 Comparison of simulated, simulated mean and measured ash percentage in overflow. . . . .	128
6.36 Ash comparison residual plot. . . . .	129
6.37 Whiteness test (95% confidence interval) for the ash comparison. .	129
6.38 Independence test (95% confidence interval) for the ash comparison.	130
6.39 Comparison of simulated, simulated mean and measured moisture percentage in overflow. . . . .	130
6.40 Comparison of simulated, simulated mean and measured volatile percentage in overflow. . . . .	131
6.41 Moisture comparison residual plot. . . . .	131
6.42 Whiteness test (95% confidence interval) for the moisture comparison. . . . .	132
6.43 Independence test (95% confidence interval) for the moisture comparison. . . . .	133
6.44 Volatile comparison residual plot. . . . .	134
6.45 Whiteness test (95% confidence interval) for the volatile comparison.	135
6.46 Independence test (95% confidence interval) for the volatile comparison. . . . .	135
6.47 Simulated response of the medium make-up. . . . .	136
6.48 Simulated response of the medium make-up tank and tank height measurement. . . . .	136

6.49	Simulink model of the fines cyclone DMS plant. . . . .	138
6.50	Simulated feed rate response for the single-deck screen. . . . .	139
6.51	Simulated density response versus actual medium density for the mixing box. . . . .	140
6.52	Simulated density response for the fine cyclone. . . . .	141
6.53	Simulated medium response for the fine cyclone. . . . .	142
6.54	Simulated ash response for the fine cyclone. . . . .	143
6.55	Simulated sulphur response for the fine cyclone. . . . .	144
6.56	Simulated moisture response for the fine cyclone. . . . .	145
6.57	Simulated volatile response for the fine cyclone. . . . .	146
6.58	Simulated carbon response for the fine cyclone. . . . .	147
6.59	Simulated density response versus actual medium density for the DMS plant. . . . .	148